

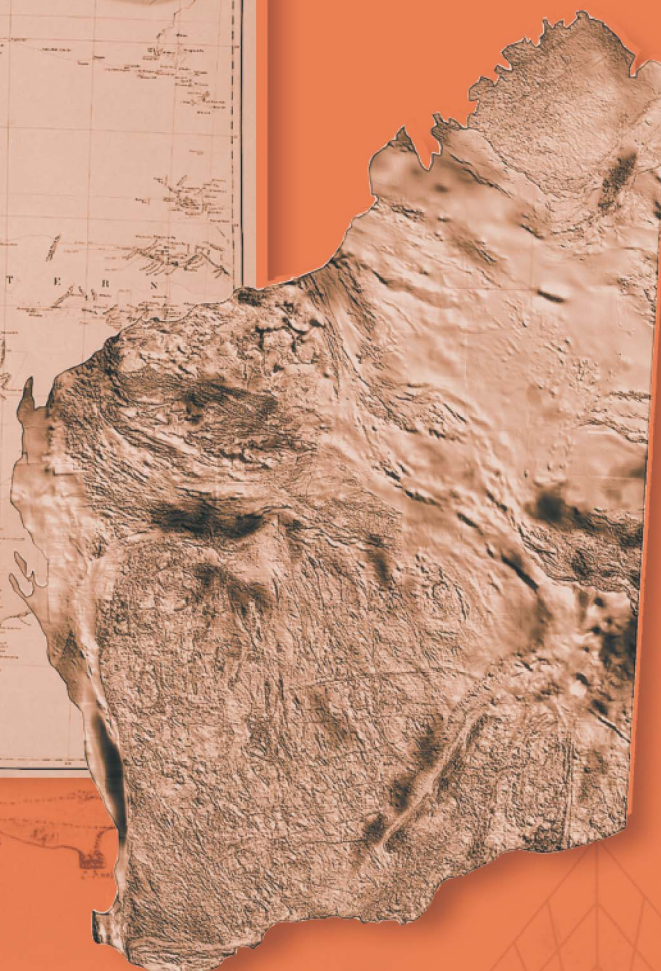


Department of Mineral and  
Petroleum Resources

**RECORD  
2001/6**

**GSWA WOODLEIGH 1, 2, AND 2A  
WELL COMPLETION REPORT  
WOODLEIGH IMPACT STRUCTURE  
SOUTHERN CARNARVON BASIN  
WESTERN AUSTRALIA**

**compiled by A. J. Mory, F. Pirajno, A. Y. Glikson, and J. Coker**



Geological Survey of Western Australia



**GEOLOGICAL SURVEY OF WESTERN AUSTRALIA**

**Record 2001/6**

# **GSWA WOODLEIGH 1, 2, AND 2A WELL COMPLETION REPORT**

## **Woodleigh impact structure, Southern Carnarvon Basin, Western Australia**

**compiled by**

**A. J. Mory, F. Pirajno, A. Y. Glikson<sup>1</sup>, and J. Coker**

**with contributions by**

**J. Backhouse<sup>2</sup>, K. A. R. Ghorri, S. Kelley<sup>3</sup>, B. P. Kohn<sup>4</sup>, R. S. Nicoll<sup>5</sup>,  
A. Raza<sup>4</sup>, P. W. Schmidt<sup>6</sup>, T. Uysal<sup>7</sup>, and U. D. Weber<sup>4</sup>**

<sup>1</sup> Research School of Earth Sciences, Australian National University

<sup>2</sup> Backhouse Biostrat Pty Ltd, Perth, Western Australia

<sup>3</sup> Department of Earth Science, Open University, Milton Keynes, U.K.

<sup>4</sup> School of Earth Sciences, University of Melbourne

<sup>5</sup> Department of Geology, Australian National University

<sup>6</sup> CSIRO Exploration and Mining, North Ryde, New South Wales

<sup>7</sup> Department of Earth Sciences, University of Queensland

**Perth 2001**

**MINISTER FOR STATE DEVELOPMENT  
Hon. Clive Brown MLA**

**DIRECTOR GENERAL  
DEPARTMENT OF MINERAL AND PETROLEUM RESOURCES  
Jim Limerick**

**DIRECTOR, GEOLOGICAL SURVEY OF WESTERN AUSTRALIA  
Tim Griffin**

**REFERENCE**

**The recommended reference for this publication is:**

MORY, A. J., PIRAJNO, F., GLIKSON, A. Y., and COKER, J., (compilers), 2001, GSWA Woodleigh 1, 2, and 2A well completion report, Woodleigh impact structure, Southern Carnarvon Basin, Western Australia: Western Australia Geological Survey, Record 2001/6, 147p.

**National Library of Australia Card Number and ISBN 0 7307 5686 6**

**Grid references in this publication refer to the Geocentric Datum of Australia 1994 (GDA94). Locations mentioned in the text are referenced using Map Grid Australia (MGA) coordinates, Zone 50. All locations are quoted to at least the nearest 100 m.**

Printed by Image Source, Perth, Western Australia

**Published 2001 by Geological Survey of Western Australia**

**Copies available from:**

Information Centre  
Department of Mineral and Petroleum Resources  
100 Plain Street  
EAST PERTH, WESTERN AUSTRALIA 6004  
Telephone: (08) 9222 3459 Facsimile: (08) 9222 3444

**This and other publications of the Geological Survey of Western Australia are available online through dme.bookshop at [www.dme.wa.gov.au](http://www.dme.wa.gov.au)**

## Contents

Abstract .....	1
Introduction .....	2
Well histories .....	4
Woodleigh 1 .....	4
General data .....	4
Drilling data .....	5
Logging data .....	5
Woodleigh 2 .....	5
General data .....	5
Drilling data .....	5
Woodleigh 2A .....	6
General data .....	6
Drilling data .....	6
Logging data .....	6
Regional structural setting .....	6
Stratigraphy .....	10
Quaternary sediments .....	14
Toolonga Calcilutite .....	14
Winning Group .....	14
Gearle Siltstone .....	14
Windalia Radiolarite .....	14
Muderong Shale .....	14
Birdrong Sandstone .....	15
Woodleigh Formation .....	15
Unnamed paraconglomerate .....	16
Unnamed breccia .....	18
Dirk Hartog Group .....	19
Coburn Formation .....	19
Granitoid basement .....	20
Petroleum geology .....	22
Source potential .....	22
Maturation .....	22
Reservoir characteristics .....	23
Seals .....	23
Shows .....	23
Mineral potential .....	23
Contribution to geological knowledge .....	25
Acknowledgements .....	27
References .....	28

## Appendices

1. Operations report .....	30
2. Impact terminology .....	38
3. Petrology .....	41
4. Electron microscopy and energy dispersive spectrometry probe investigation .....	65
5. Palynology .....	80
6. Conodonts .....	91
7. Apatite fission-track analysis of basement samples .....	93
8. UV laser Ar–Ar analysis .....	97
9. K–Ar dating .....	100
10. Petroleum geochemistry .....	106
11. Core analyses .....	136
12. Palaeomagnetism .....	141
13. Well index sheets .....	146

## Plates

1. Woodleigh 1 composite well log
2. Woodleigh 2A composite well log



## Figures

1. Well location and access map .....	2
2. Tectonic elements map showing location of wells .....	3
3. Seismic lines W65G-003 and W65T-003 across the Woodleigh impact structure .....	7
4. Isometric view of the first vertical derivative of the Bouguer gravity .....	8
5. East–west correlation of Yaringa 1 with Woodleigh 1 and 2A; datum: base Cretaceous .....	9
6. Magnetic image showing surface drainage .....	10
7. Regional stratigraphy of the Gascoyne Platform .....	11
8. Woodleigh 1 stratigraphy .....	12
9. Woodleigh 2A stratigraphy .....	13
10. Core photograph of Woodleigh Formation, Woodleigh 2A (386.1 – 391.9 m) .....	16
11. Core (slabbed) photographs of unnamed paraconglomerate, Woodleigh 2A .....	17
12. Core (slabbed) photographs of unnamed breccia, Woodleigh 2A .....	19
13. Core (slabbed) photographs of Coburn Formation, Woodleigh 2A .....	20
14. Photomicrographs showing post-impact minerals .....	24

## Tables

1. Bedding dips in Woodleigh 2A .....	18
2. Ages obtained from granitoid basement in Woodleigh 1 .....	21

## Digital data

CD-ROM containing Woodleigh text and well-log information

# GSWA Woodleigh 1, 2, and 2A well completion report, Woodleigh impact structure, Southern Carnarvon Basin, Western Australia

compiled by

A. J. Mory, F. Pirajno, A. Y. Glikson<sup>1</sup>, and J. Coker

with contributions by

J. Backhouse<sup>2</sup>, K. A. R. Ghorri, S. Kelley<sup>3</sup>, B. P. Kohn<sup>4</sup>, R. S. Nicoll<sup>5</sup>,  
A. Raza<sup>4</sup>, P. W., Schmidt<sup>6</sup>, T. Uysal<sup>7</sup>, and U. D. Weber<sup>4</sup>

## Abstract

Woodleigh 1, 2, and 2A are stratigraphic wells within the circular Woodleigh impact structure, on the Gascoyne Platform in the Southern Carnarvon Basin. Woodleigh 1 is located at latitude 26°03'19.3"S and longitude 114°39'56.3"E, at the centre of the structure due east of Hamelin Pool and penetrated shock-metamorphosed granitoid basement (171 – 333.1 m) below the Cretaceous Toolonga Calcilutite and Winning Group. Woodleigh 2A, 15 km to the west at latitude 26°03'28"S and longitude 114°31'33"E, penetrated a Cretaceous section similar to Woodleigh 1 followed by lacustrine Lower Jurassic Woodleigh Formation (223 – 521.3 m), unnamed paraconglomerate (521.3 – 587.2 m), unnamed breccia (587.2 – 600.85 m), and Silurian carbonate and gypsum (Coburn Formation, 600.85 – 618.3 m), in which the well was terminated. Woodleigh 1 and Woodleigh 2A were continuously diamond cored from 190.5 m to total depth (TD), and 270 m to TD respectively.

An impact origin for the structure is indicated by the central uplifted granitoid core, which in Woodleigh 1 displays shock-induced planar deformation features in quartz, pervasive diaplectic vitrification of feldspar, and penetrative pseudotachylite veining. Pseudotachylite vein systems within the shocked granitoid are strongly enriched in Al, Ca, Mg, Ni, Co, Cr, V, and S, and depleted in K and Si relative to an average granite, suggesting chemical fractionation attendant on shock volatilization, enrichment by an injected and volatilized meteoritic component, and potential sulfide mineralization. The age of impact is regionally constrained by overlying Lower Jurassic strata and deformed Lower Devonian and older units. K–Ar dating of clay minerals from the granitoid core indicates a Late Devonian age, but this conflicts with the mid-Carboniferous to ?Early Triassic age indicated by a palaeomagnetic study of mafic sections of the same core.

The petroleum potential of the Woodleigh impact structure is limited by the immaturity of the otherwise good to excellent source-rock characteristics of the Mesozoic section and low maturity of the Silurian section in Woodleigh 2A, the paucity of potential sealing sections, and the uncertainty of the age of the impact relative to peak hydrocarbon generation. However, good quality source rock is evident in Silurian clasts reworked into the unnamed breccia (up to 2.24% TOC and S<sub>1</sub> + S<sub>2</sub> up to 8.45 mg/g rock).

**KEYWORDS:** impact structures, Cretaceous, Jurassic, Silurian, stratigraphy, stable isotopes, palynology, conodonts, petroleum potential, diamond drilling, palaeomagnetism

<sup>1</sup> Research School of Earth Sciences, Australian National University

<sup>2</sup> Backhouse Biostrat, Perth, Western Australia

<sup>3</sup> Department of Earth Science, Open University, Milton Keynes, U.K.

<sup>4</sup> School of Earth Sciences, University of Melbourne

<sup>5</sup> Department of Geology, Australian National University

<sup>6</sup> CSIRO Exploration and Mining, North Ryde

<sup>7</sup> Department of Earth Sciences, University of Queensland

## Introduction

The Geological Survey of Western Australia's (GSWA) Woodleigh 1, 2, and 2A are stratigraphic wells drilled on Woodleigh Station about 170 km south-southeast of Carnarvon and 190 km north-northeast of Kalbarri. Woodleigh 1 (latitude 26°03'19.3"S and longitude 114°39'56.3"E) is located adjacent to a station track 8.5 km due west of the homestead, and Woodleigh 2 (latitude 26°03'28"S and longitude 114°31'34"E) and 2A (latitude 26°03'28"S and longitude 114°31'33"E) are located a further 15 km to the west. Access is from the Woodleigh–Byro road 25 km north of the Overlander Roadhouse on the North West Coastal Highway (Fig. 1). The nearest petroleum wells are Yaringa 1, 30 km to the west of Woodleigh 1; Yaringa East 1, 32 km west-northwest; and Hamelin Pool 2, 32 km west-southwest (Fig. 2). Although Woodleigh 1, 2, and 2A were located on an east–west seismic section line (Fig. 3), the structural position of the holes was determined from gravity data as the quality of the seismic is poor. No hydrocarbons were found in the wells.

The primary objective of Woodleigh 1 was to test the impact origin of the circular gravity anomaly in the south of the Gascoyne Platform, named the 'Woodleigh structure' by Mory et al. (2000a), by recovering core samples from the central-most gravity peak (Fig. 4). The impact origin of the structure, which may be 120 km in diameter, was first suspected from possible impact deformation of quartz in an exploration drillhole (Woodleigh 1981/2) at the centre of the gravity anomaly (Mory

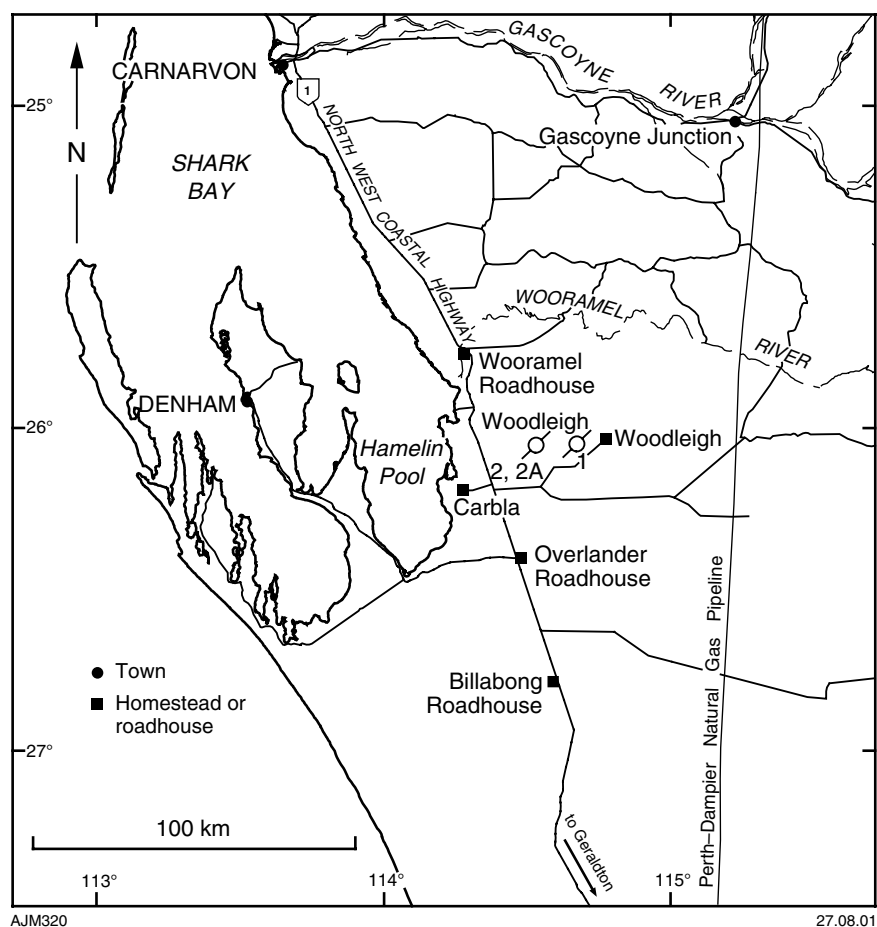


Figure 1. Well location and access map

et al., 2000a; Iasky et al., 2001). The well was drilled in the centre of the structure by re-entering that drill hole, which was terminated at 189 m in granitoid rocks below a Lower Cretaceous section (Layton and Associates, 1981). As none of the samples from the original hole could be located, Woodleigh 1 was continuously cored from 190.5 m to total depth (TD) at 333.1 m. Woodleigh 1981/2 was spudded into unconsolidated Quaternary sand and intersected Cretaceous strata at 17 m (Toolonga Calcilutite and Winning Group) and, at 171 m, a section of granitoid rock. Woodleigh 1 was

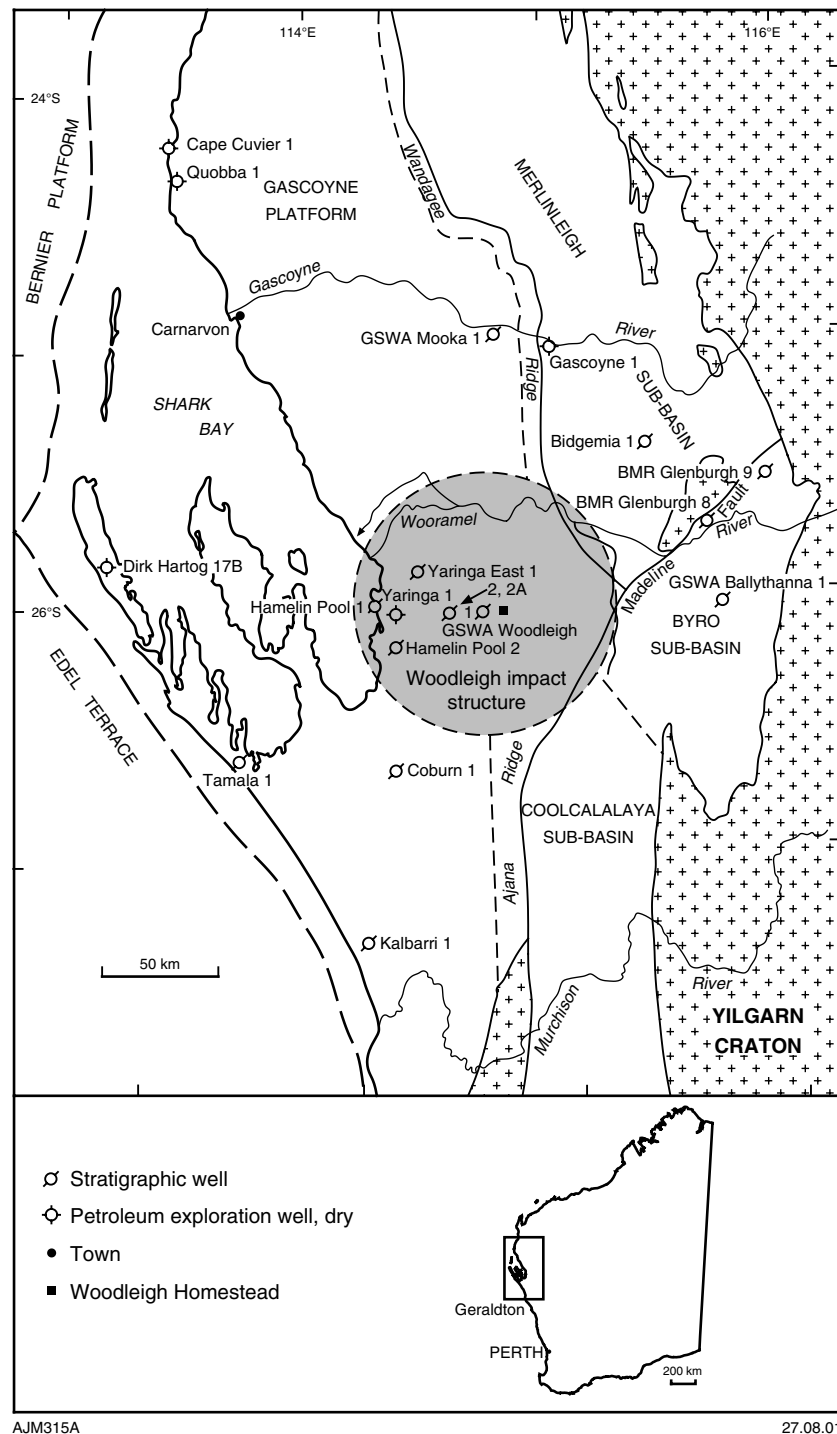


Figure 2. Tectonic elements map showing location of wells

abandoned for possible future use as a waterbore by the station. The hole was not re-logged at the time of abandonment as the section above the granitoid had been logged previously.

The positive evidence of an impact origin provided from thin sections of the granitoid in Woodleigh 1 justified the drilling of a second hole, Woodleigh 2, a further 15 km to the west to investigate the nature and hydrocarbon potential of the crater-fill succession. Woodleigh 2 and 2A lie on Carbla Station next to a mineral exploration hole (Carpentaria CB4), which was terminated at 285 m in the Jurassic Woodleigh Formation (Fewster, 1991). This location was chosen as it is on the edge of the central uplift of the Woodleigh impact structure, as interpreted from gravity data (Iasky et al., 2001), and was the most distant, proven occurrence of the Woodleigh Formation from the centre of the structure. Other wells that penetrated below the Cretaceous within the Woodleigh impact structure are listed in Iasky et al. (2001, appendix 1). In addition, the Carpentaria hole could be converted to a waterbore for the drilling operations. Woodleigh 2 was spudded into unconsolidated Quaternary sand and intersected Cretaceous strata at 14 m (Toolonga Calcilutite and Winning Group), but was abandoned at 198 m because of lost circulation and running sands in the Cretaceous Birdrong Sandstone. The rig was relocated 25 m to the east and Woodleigh 2A was commenced. This well intersected a virtually identical section to Woodleigh 2, as well as the Jurassic Woodleigh Formation at 223 m, unnamed paraconglomerate or matrix-supported conglomerate at 521.3 m, unnamed breccia at 587.2 m, and the Upper Silurian Coburn Formation at 600.85 m. Drilling was terminated at 618.3 m in the latter unit. Woodleigh 2A was rotary drilled to 270 m and then followed by continuous wireline coring to TD. Because of hole instability, only gamma-density and neutron-neutron logging tools could be run (from within the drill string) prior to abandonment of the hole. Further details of the drilling operation are given in Appendix 1. A summary of impact terminology, as used in this report, is given in Appendix 2.

## Well histories

### Woodleigh 1

#### General data

Permit:	vacant
Location:	Latitude 26°03'19.3"S, Longitude 114°39'56.3"E (GDA94) 7116095N, 266452E (MGA Zone 50), determined from Differential Global Positioning System (DGPS) Drilled by re-entering Woodleigh 1981/2 (TD 189 m; Layton and Associates, 1981)
Derivation of name:	Woodleigh Station
Total depth (TD):	333.1 m (driller)
Date re-entered:	9 March 1999
Reached TD:	15 March 1999
Logging:	27 March 1999
Date completed:	15 March 1999
Elevation:	108 m Australian Height Datum (AHD) from DGPS
Drill floor:	Ground level
Status:	Abandoned for possible use as a waterbore



**Drilling data**

Drilling contractor:	Mt Magnet Drilling, 33 Paramount Drive, Wangara, W.A. 6065	
Rig:	Hydco SD 1000	
Rig datum:	Ground level	
Hole size:	0–30 m	215 mm with 178 mm conductor pipe to 10 m
	30 – 190.5 m	96 mm with HQ casing
	190.5 – 333.1 m	76 mm open hole
Mud:	Polymer based (Aqua-Pac)	
Core recovery:	190.5 – 333.1 m	(HQ) 63.5 mm diameter (97.9% recovery)
Hole deviation:	Not measured	
Plugs:	None	

**Logging data**

Logging contractor:	Geophysical Logging Technologies, 3 Barnard St, Bunbury W.A. 6230	
Logs run:	Gamma ray, temperature, caliper	1–92 m
	Gamma and density	2 – 187.5 m
	(from Woodleigh 1981/1)	

**Woodleigh 2****General data**

Permit:	vacant
Location:	Latitude 26°03'27.5"S, Longitude 114°31'33"E (GDA94) 7115587N, 252468E (MGA Zone 50) from DGPS
Derivation of name:	Woodleigh Station
Total depth (TD):	198 m (driller)
Date spudded:	16 March 1999
Reached TD:	20 March 1999
Logging:	Not logged
Date completed:	20 March 1999
Elevation:	67 m AHD from DGPS
Drill Floor:	Ground level
Status:	Abandoned

**Drilling data**

Drilling contractor:	Mt Magnet Drilling, 33 Paramount Drive, Wangara, W.A. 6065	
Rig:	Hydco SD 1000	
Rig datum:	Ground level	
Hole size:	0–6 m	159 mm with conductor pipe
	6–156 m	76 mm with NQ casing
	156–198 m	76 mm open hole
Mud:	Polymer based (Aqua-Pac)	
Core recovery:	193–198 m	(NQ) 48 mm diameter (46% recovery)
Hole deviation:	Not measured	
Plugs:	None	

## Woodleigh 2A

### General data

Permit:	vacant
Location:	Latitude 26°03'27.5"S, Longitude 114°31'34"E (GDA94) 7115587N, 252493E (MGA Zone 50) from DGPS
Derivation of name:	Woodleigh Station
Total depth (TD):	618.3 m (driller)
Date spudded:	21 March 1999
Reached TD:	27 March 1999
Logging:	27 March 1999
Date completed:	28 March 1999
Elevation:	67 m AHD from DGPS
Drill Floor:	Ground level
Status:	Abandoned

### Drilling data

Drilling contractor:	Mt Magnet Drilling, 33 Paramount Drive, Wangara, W.A. 6065	
Rig:	Hydco SD 1000	
Rig datum:	Ground level	
Hole size:	0–6 m	159 mm with conductor pipe
	6–270 m	89 mm with HQ casing
	270 – 618.3 m	76 mm open hole
Mud:	Polymer based (Aqua-Pac)	
Core recovery:	270–618.3 m	(NQ) 48 mm diameter (91.2% recovery)
Hole deviation:	Not measured	
Plugs:	None	

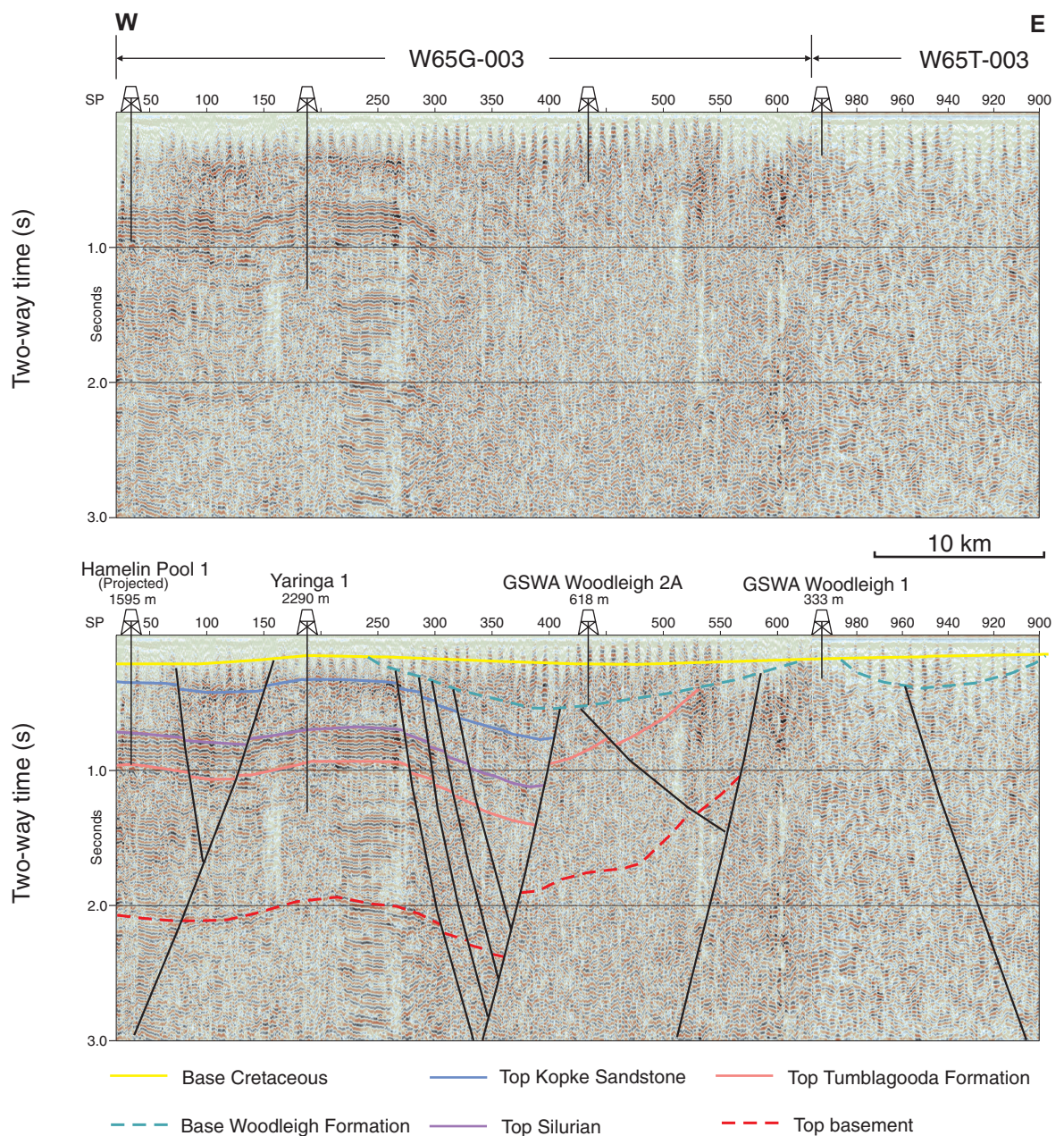
### Logging data

Logging contractor:	Geophysical Logging Technologies, 3 Barnard St, Bunbury W.A. 6230	
Log runs	Gamma and density	2–612 m
	Gamma, neutron-neutron, caliper	2–612 m

## Regional structural setting

Woodleigh 1, 2, and 2A were drilled within the ‘Woodleigh structure’ of Mory et al. (2000a), delineated by a circular gravity anomaly within the southwestern part of the Ordovician to Quaternary Southern Carnarvon Basin (Hocking et al., 1994). The feature has a proven impact origin (Mory et al., 2000a,b; Appendices 3 and 4) and has been renamed the ‘Woodleigh impact structure’ (Iasky et al., 2001). It lies largely within the Gascoyne Platform, a structurally high area between the Merlinleigh, Byro, and Coolcalalaya Sub-basins to the east, and the Bernier Platform and Edel Terrace to the west (Fig. 2; Iasky and Mory, 1999; Hocking et al., 1987), and is covered by flat-lying Cretaceous and Lower Jurassic strata. The former sub-basins form a prominent Carboniferous–Permian depocentre. The Wandagee and Ajana Ridges mark the raised eastern rim of the Gascoyne Platform, which contains a thin cover of mostly subhorizontal Cretaceous strata unconformably overlying up to 5000 m of faulted and

folded Ordovician–Devonian strata (Iasky and Mory, 1999, fig. 4) and, in the central part of the Woodleigh impact structure, flat-lying Jurassic strata. As seismic control in the region is sparse and of poor quality (Fig. 3), the wells were located primarily on the basis of gravity data. Woodleigh 1, 2, and 2A are located over the central gravity anomaly of the Woodleigh impact structure and on the margin of the central uplift (Figs 4 and 5). The Woodleigh impact structure is a multi-ring feature, possibly as much as 120 km in diameter, determined from gravity and aeromagnetic data. Subtle drainage features along the margin of the structure probably post-date Miocene reactivation of the outermost ring faults (Fig. 6; Mory et al., 2000a,b; Iasky et al., 1998, 2001; Iasky and Mory, 1999).



AJM364

28.08.01

**Figure 3. Seismic lines W65G-003 and W65T-003 across the Woodleigh impact structure (from Iasky et al., 2001)**



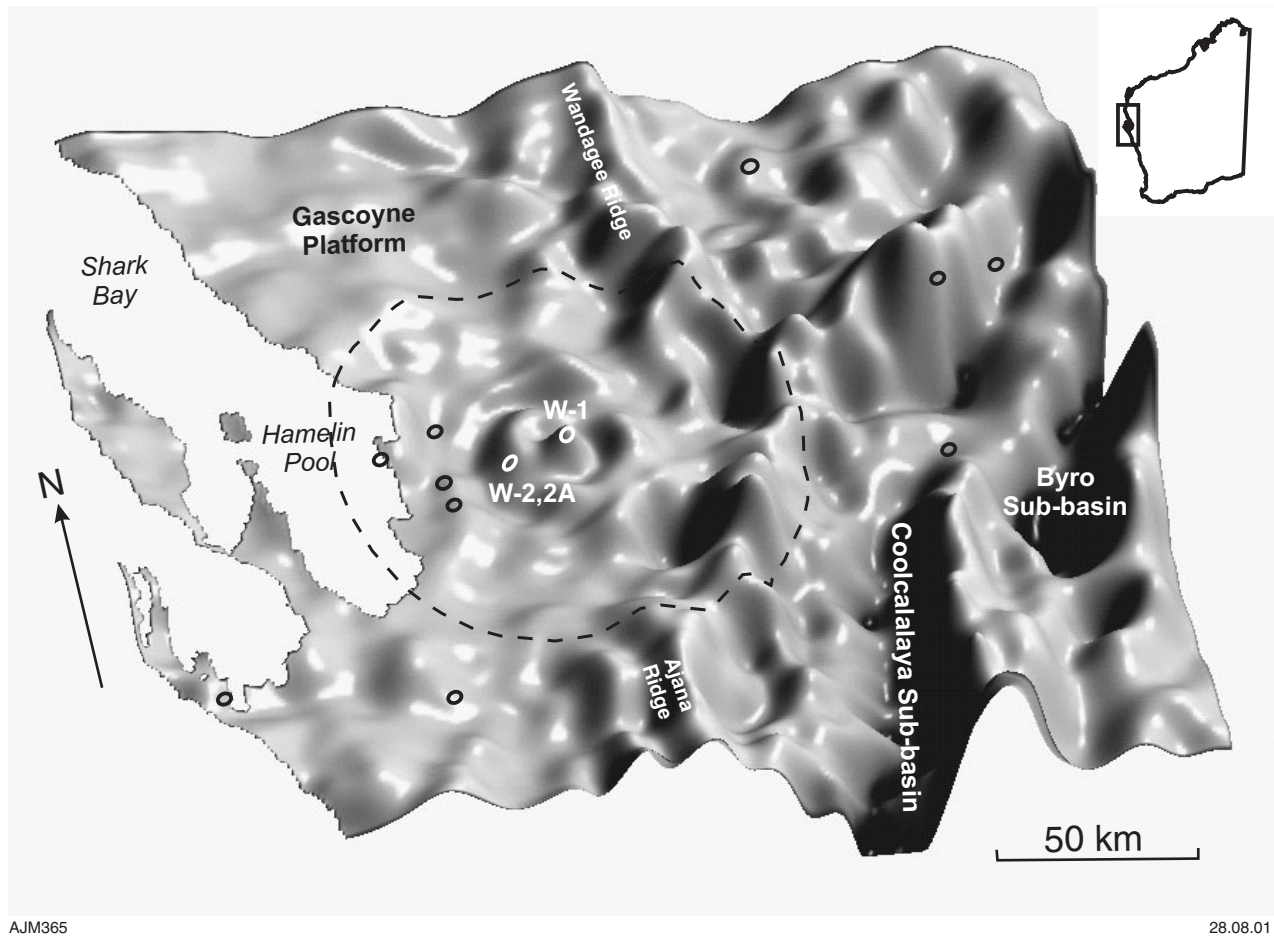


**Figure 4.** Isometric view of the first vertical derivative of the Bouguer gravity (area shown corresponds exactly to that shown in Fig. 6). Small circles indicate well locations, dashed line shows the extent of the Woodleigh impact structure. Details of surveys are in Iasky et al. (2001)

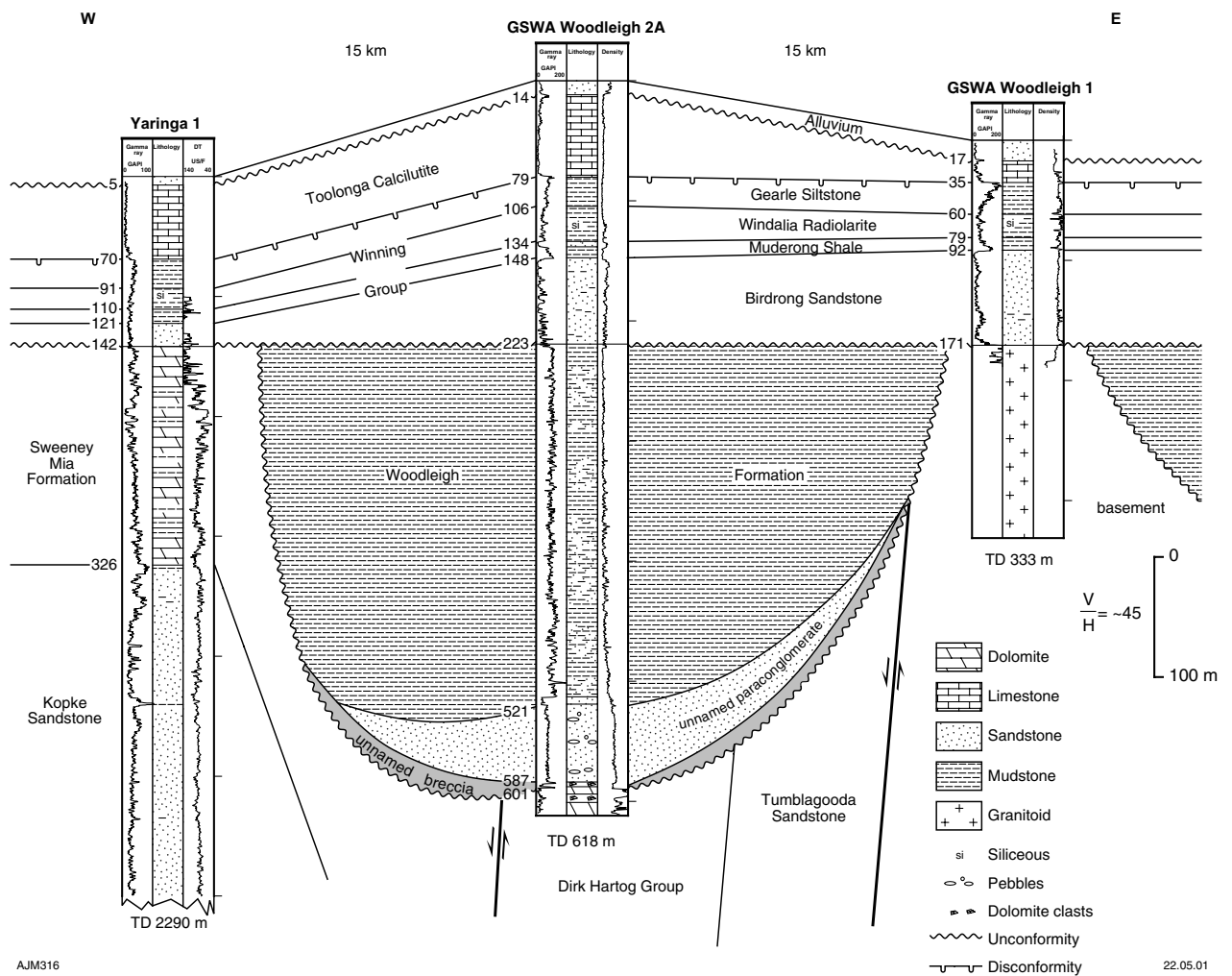


Figure 5. East-west correlation of Yaringa 1 with Woodleigh 1 and 2A; datum: base Cretaceous



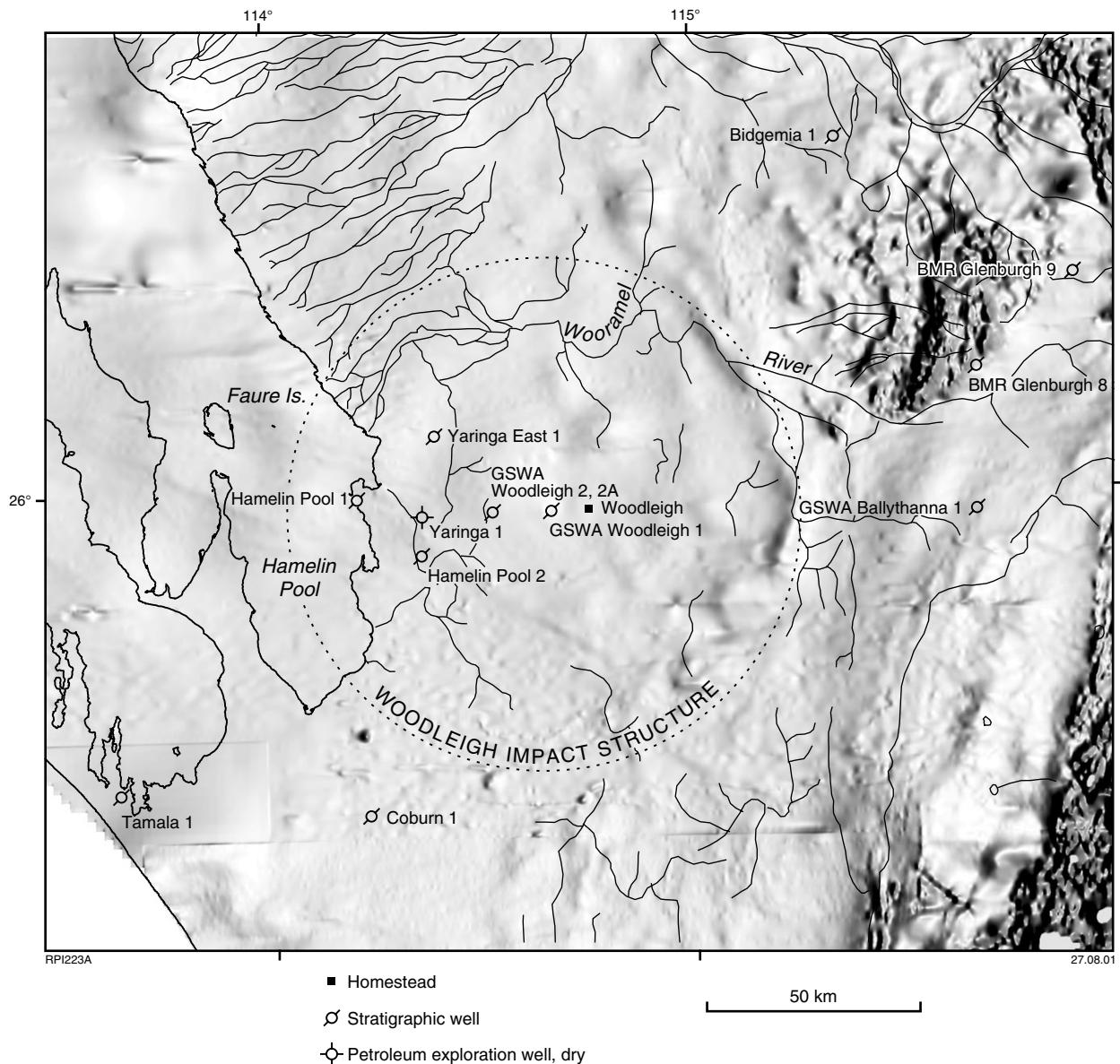


Figure 6. Magnetic image showing surface drainage (dashed line shows the extent of Woodleigh impact structure, after Mory et al., 2000a, details of surveys given by Iasky et al., 2001)

## Stratigraphy

The southern Gascoyne Platform contains Ordovician – Lower Devonian and Cretaceous units (Fig. 7). The wells were spudded into Quaternary sand, below which the Cretaceous Toolonga Calcilutite and the Winning Group overlie severely deformed, Proterozoic granitoid basement in Woodleigh 1 (Fig. 8). In Woodleigh 2A, the Cretaceous overlies the Lower Jurassic Woodleigh Formation, which in turn overlies two unnamed units (paraconglomerate and breccia) and the Upper Silurian Coburn Formation (Dirk Hartog Group), in which this well was terminated (Fig. 9).

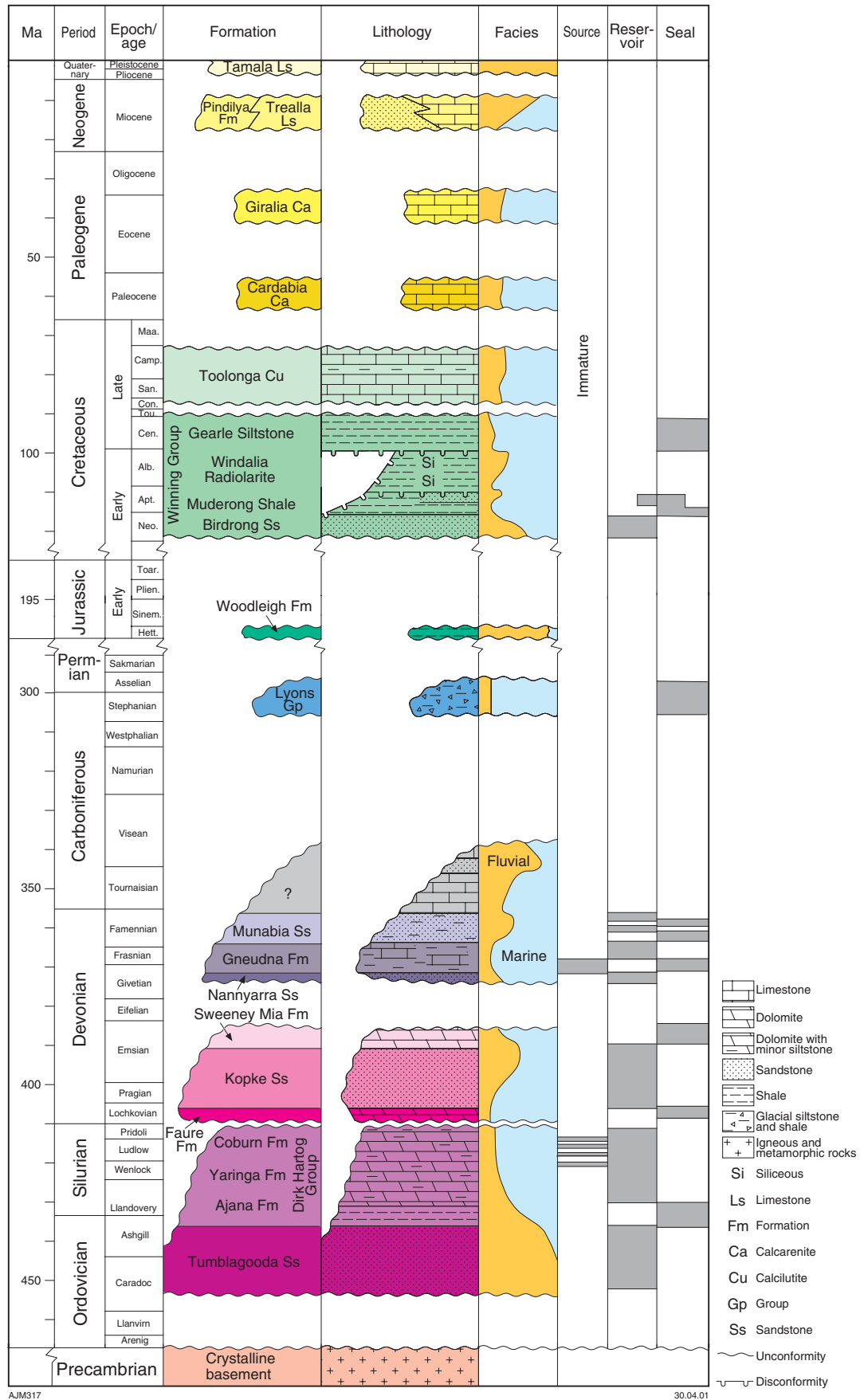
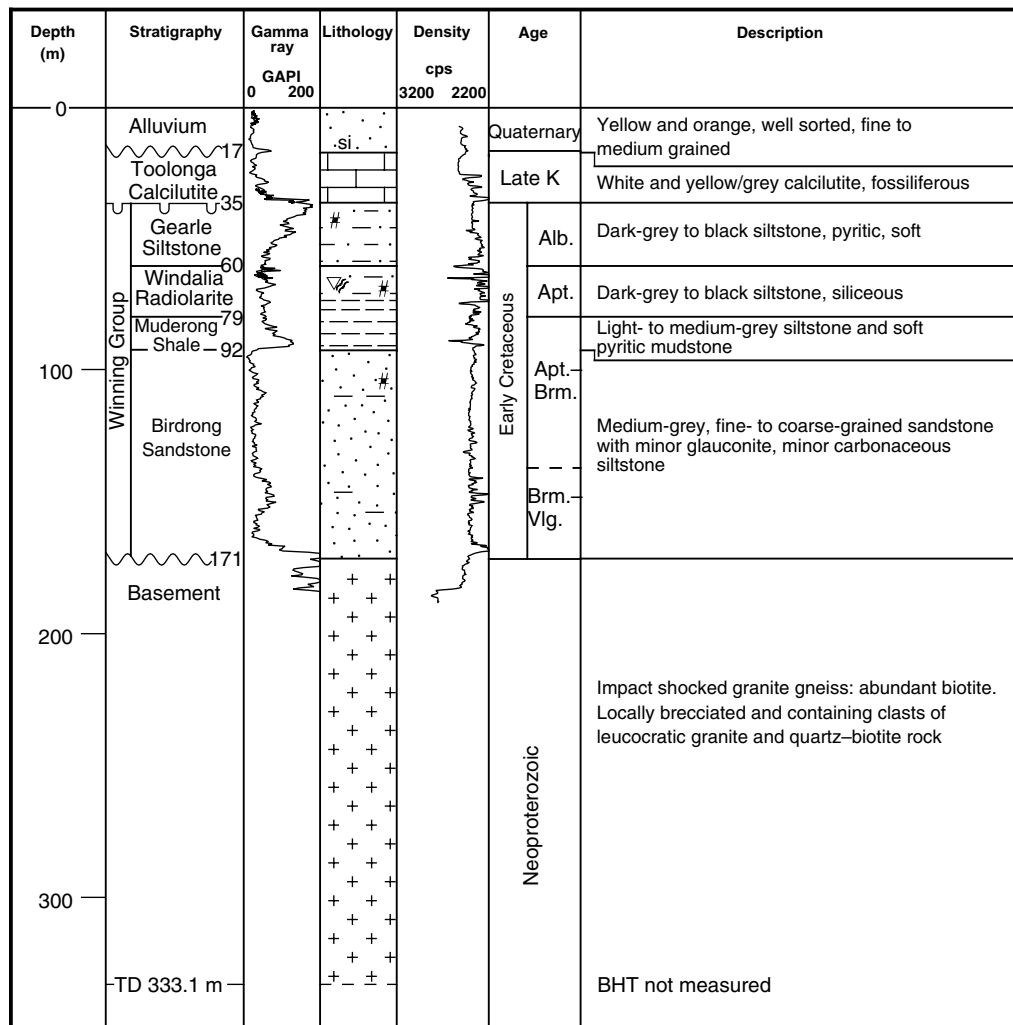


Figure 7. Regional stratigraphy of the Gascoyne Platform (after Iasky and Mory, 1999)



AJM319

11.06.01

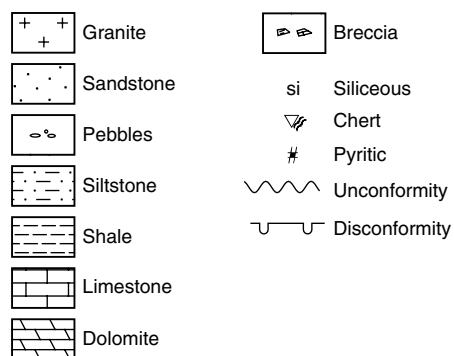
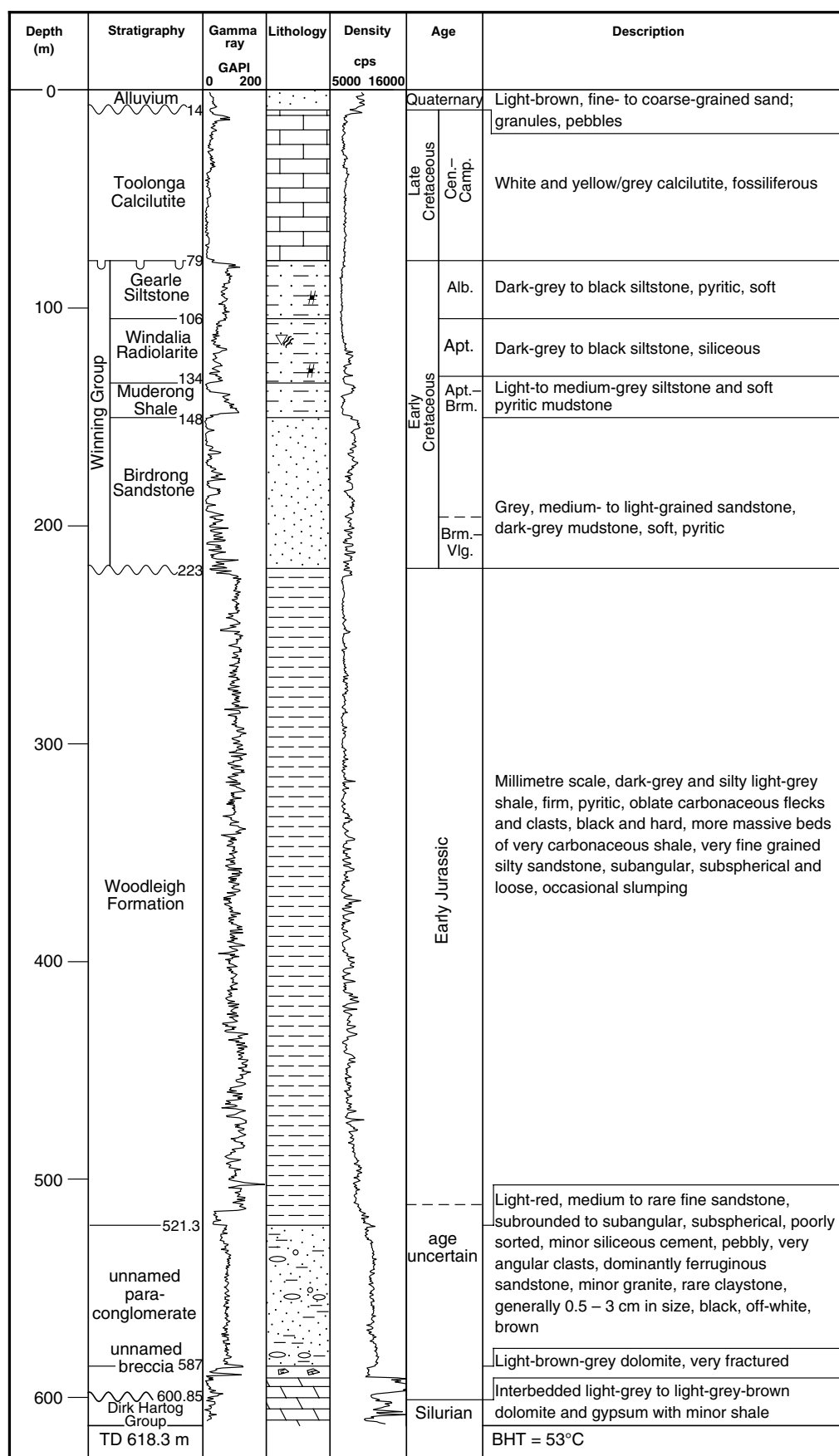


Figure 8. Woodleigh 1 stratigraphy



AJM318

25.07.01

Figure 9. Woodleigh 2A stratigraphy (legend on Fig. 8)

## Quaternary sediments

Red to brown, medium- to coarse-grained, loose, dune sand was intersected from 0 to 17 m in Woodleigh 1, and 0 to 14 m in Woodleigh 2 and 2A.

## Toolonga Calcilutite

The Cenomanian to Campanian (Late Cretaceous) Toolonga Calcilutite is present over the interval 17–35 m in Woodleigh 1 and 14–79 m in Woodleigh 2 and 2A. The unit consists of richly fossiliferous, bluish-grey to bluish-white wackestone–packstone and calcareous siltstone. Planktonic foraminifera and *Inoceramus* prisms are evident in the cuttings samples. The lower contact with the Gearle Siltstone (Winning Group) is a regional disconformity.

## Winning Group

In Woodleigh 1, 2, and 2A, the Winning Group consists of the Gearle Siltstone, Windalia Radiolarite, Muderong Shale (possibly including the Windalia Sandstone Member), and Birdrong Sandstone. These units are separated by minor breaks that are well documented in GSWA Barrabiddy 1 and 1A (Mory and Yasin, 1999) and Coburn 1 (Yasin and Mory, 1999a). The lack of core from this group in the Woodleigh wells hinders the precise identification of not only these breaks, but also the constituent formations. Therefore, most formation picks have been made from the electric logs. However, even though the two wells are just 15 km apart, internal correlation between them on this basis is difficult.

## Gearle Siltstone

The Gearle Siltstone is present over the interval 35–60 m in Woodleigh 1 and 79–106 m in Woodleigh 2 and 2A, and consists of dark-grey to black, pyritic mudstone and siltstone. In Woodleigh 2A, the *Canninginopsis denticulata* spore-pollen zone of Albian age is tentatively identified from the base of this unit (Appendix 5).

## Windalia Radiolarite

The Windalia Radiolarite (60–79 m in Woodleigh 1, 106–134 m in Woodleigh 2 and 2A) is characterized by distinctly siliceous, radiolarian-rich, dark-grey to black siltstone. The upper contact of the unit is identified on the overall character of the gamma-ray log where there is a general decrease in gamma values. The base of the unit in Woodleigh 1 is picked somewhat arbitrarily above a high gamma interval marking a general increase in gamma readings at 79 m. In Woodleigh 2A, the base of the unit is placed at the top of a prominent sandstone bed at 134 m. In Woodleigh 2A, the *Diconodinium davidii* dinoflagellate zone of late Aptian age is present in cuttings samples from 120 to 133 m (Appendix 5). The unit extends to a waterbore next to Woodleigh Homestead on the basis of palynomorphs of this zone (Backhouse, 2000). Previous wells in the region that intersected the unit and in which the *D. davidii* dinoflagellate zone has been identified, include Barrabiddy 1 and 1A (Mory and Yasin, 1999), Mooka 1 (Mory and Yasin, 1998), and Yaringa East 1 (Yasin and Mory, 1999b).

## Muderong Shale

In Woodleigh 1, the Muderong Shale (79–92 m) consists of a light- to medium-grey mudstone, possibly grading up to a sandy siltstone. In Woodleigh 2 and 2A



(134–148 m), it shows a distinct sandstone interval at the top (134–139 m), which is tentatively correlated with the Windalia Sandstone Member, which overlies a dark-grey, pyritic basal mudstone. In Woodleigh 2 and 2A, palynomorphs from cuttings samples belong to the mid-Albian *C. denticulata*, late Aptian *D. davidii*, and early Aptian – Barremian *Muderongia australis* Zones, but the former two zones are probably from caved material. The basal mudstone interval was deposited in a low-energy, shallow-marine environment.

### Birdrong Sandstone

The intervals 92–171 m in Woodleigh 1 and 148–223 m in Woodleigh 2 and 2A are correlated with the Birdrong Sandstone. In these wells the unit consists of grey, fine- to medium-grained sandstone with interbedded, dark-grey silty clay and minor pyrite. The unit overlies an erosional surface ('Breakup Unconformity') cut into Precambrian granitoid rocks in Woodleigh 1 and the Lower Jurassic Woodleigh Formation in Woodleigh 2 and 2A.

In Woodleigh 1, the Birdrong Sandstone contains palynomorphs of the *M. australis* Zone, which is early Aptian – Barremian in age, whereas in Woodleigh 2, the basal part of the unit contains undifferentiated *Balmeiopsis limata* Zone of Barremian–Valanginian age (Appendix 5). Palynomorphs from surface spoil surrounding the waterbore 2 km west of Woodleigh 1 also contains the *B. limata* Zone (Backhouse, 2000), implying that the base of the Birdrong Sandstone in Woodleigh 1 is a similar facies and possibly age to that in Woodleigh 2 and 2A. Most of the unit was deposited in a high-energy, nearshore marine environment, but the basal part (*B. limata* Zone) appears to be non-marine (Appendix 5). In other wells in the region, such as Coburn 1, Mooka 1, and Yaringa East 1, the undifferentiated *B. limata* Zone is not represented, implying a somewhat restricted distribution for this facies.

### Woodleigh Formation

Woodleigh 2A penetrated 298 m of the Woodleigh Formation (223 – 521.3 m), which is the thickest section of the formation known to date. The unit is absent in Woodleigh 1 and was not reached in Woodleigh 2. Previously it was known only from waterbores in the vicinity of Woodleigh Station, and descriptions from drillers' records are not detailed. The type section (the interval 210–235 m in the Woodleigh no. 7 waterbore) lies 24 km east-southeast of Woodleigh 2A, but does not show the base of the formation. The lower contact with the unnamed paraconglomerate is placed at the base of the dark-red to brown, low-gamma sandstone bed at 513 – 521.3 m, which probably is a transgressive unit, although the contact is not sharp. Prior to drilling at the Woodleigh 2 and 2A site, the formation was known only from six waterbores on Woodleigh Station (Iasky et al., 2001) for which palynological confirmation is available for only no. 1 and no. 7 (~2.5 km east and 11.5 km southwest of Woodleigh 1 respectively; McWhae et al., 1956).

In Woodleigh 2A, the Woodleigh Formation consists of laminated siltstone and mudstone interbedded with fine-grained, silty sandstone (Fig. 10). Laminae are on a millimetre scale and typically consist of a carbonaceous basal layer grading up into an oxidized layer with an abrupt contact with the next couplet. Woody material is common but noticeably absent in the basal 20 m, in which sandstone predominates. Fining-up cycles, 2–5 m thick, are common and local slumps are present. The shale is pyritic in places. Thin (centimetre-scale) gypsum layers are present at 434 m. A single granite clast about 5 cm in diameter, with shock-metamorphic features, is present at 498 m.



AJM366

12.04.01

**Figure 10. Core photograph of Woodleigh Formation, Woodleigh 2A (386.1 – 391.9 m)**

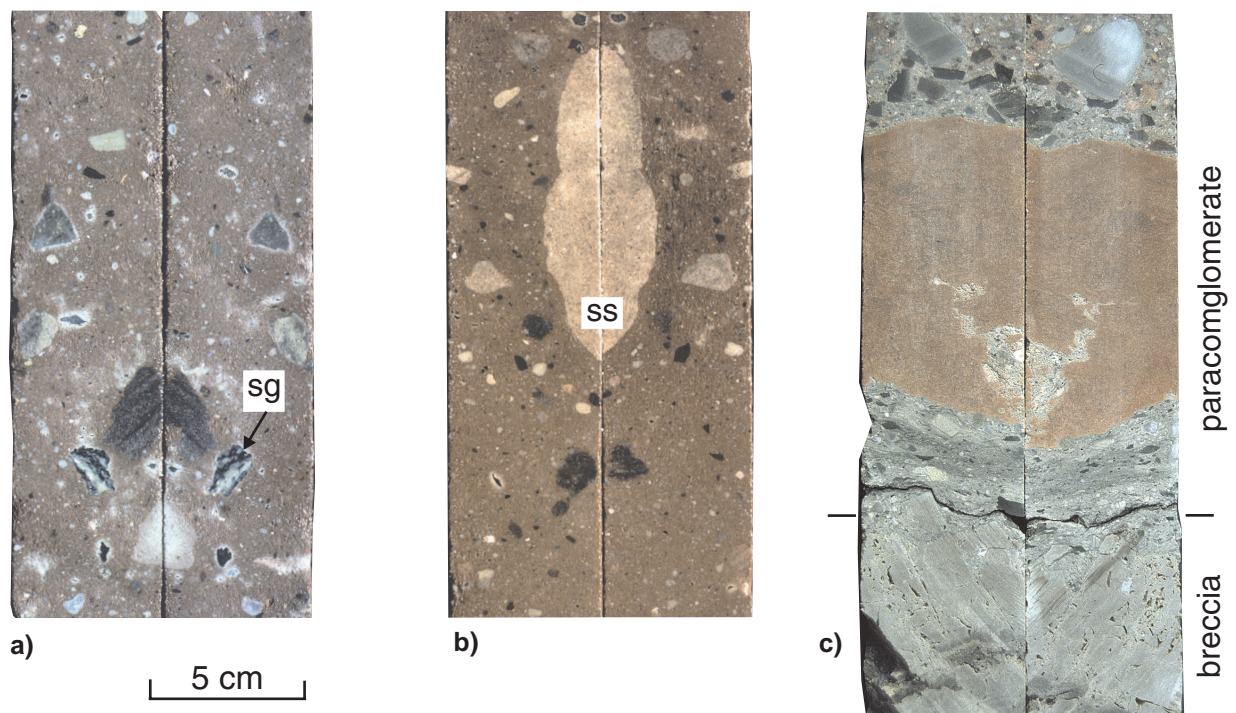
In Woodleigh 2A, the Woodleigh Formation contains Early Jurassic palynomorphs of the Bajocian–Toarcian *Callialasporites turbatus* spore-pollen zone (284 – 441.7 m) and possibly also from the *Corollina torosa* Zone (493 – 505.65 m). Below 474.3 m, the samples are dominated by palynomorphs reworked from the Sakmarian (Early Permian) *Pseudoreticulatispora confluens* Zone (Appendix 5). The prevalence of woody material, the lack of spiny acritarchs, marine fossils or bioturbation imply deposition in a relatively deep-water, anoxic lacustrine environment.

### Unnamed paraconglomerate

In Woodleigh 2A, an oxidized paraconglomerate, or matrix-supported sandy conglomerate, is present below the Woodleigh Formation between 521.3 and 587.2 m. The unnamed paraconglomerate consists of a relatively uniform, massive, red to pink, medium- to fine-grained sandstone supporting subangular to rounded clasts of sandstone. In thin section, nearly every quartz grain shows planar deformation features

(PDFs), even within sandstone clasts (Appendix 3). Rare clasts of granite with shock-metamorphic features, similar to those seen in the basement in Woodleigh 1 (Appendix 3), and shale are also present (Fig. 11). The only internal contacts evident within the unit are in the basal 1.5 m, which contains two 50 cm-thick beds composed predominantly of small dolomite clasts less than 2 cm across (Fig. 11c). The basal contact is abrupt on a dolomite breccia (Fig. 11c). The unit is left unnamed as it has not been intersected elsewhere in the region. Clasts are up to 15 cm across, but commonly are less than 7 cm. The larger clasts are mostly sandstone.

The only direct indication of age within this unit is from shale clasts that contain palynomorphs predominantly from the Sakmarian (Early Permian) *P. confluens* Zone, as well as rare Early Jurassic species (Appendix 5). The Early Jurassic palynomorphs, however, are rare and their presence may be due to contamination. Deposition by a gravity-flow process in a subaerial environment has most likely caused the oxidized appearance of the unit and the lack of internal stratification. The paucity and small size of the shocked granite clasts (rarely >4 cm) at a location so close to the centre of the structure indirectly supports an age much older than Jurassic for the impact, as it implies the paraconglomerate is a secondary deposit that considerably post-dates the formation and collapse of the central uplift. In some respects the unit resembles redeposited parts of the Lower Permian Lyons Group (Fig. 7) and its equivalent in the Perth Basin (Nangetty Formation), but there is no evidence of faceting or striation on any of the clasts. The preponderance of shocked quartz grains, however, indicates a provenance near the centre of the Woodleigh impact structure. In addition, shale clasts are derived from the upper part of the Lyons Group or, less likely, the laterally equivalent Holmwood Shale in the Perth Basin (Mory and Backhouse, 1997, fig. 3), thereby precluding such a correlation.



AJM354

13.02.01

**Figure 11.** Core (slabbed) photographs of unnamed paraconglomerate, Woodleigh 2A: a) 545.3 m; b) 580.3 m; c) contact between unnamed paraconglomerate and breccia at 587.2 m; shocked granite (sg) and sandstone (ss) clasts

## Unnamed breccia

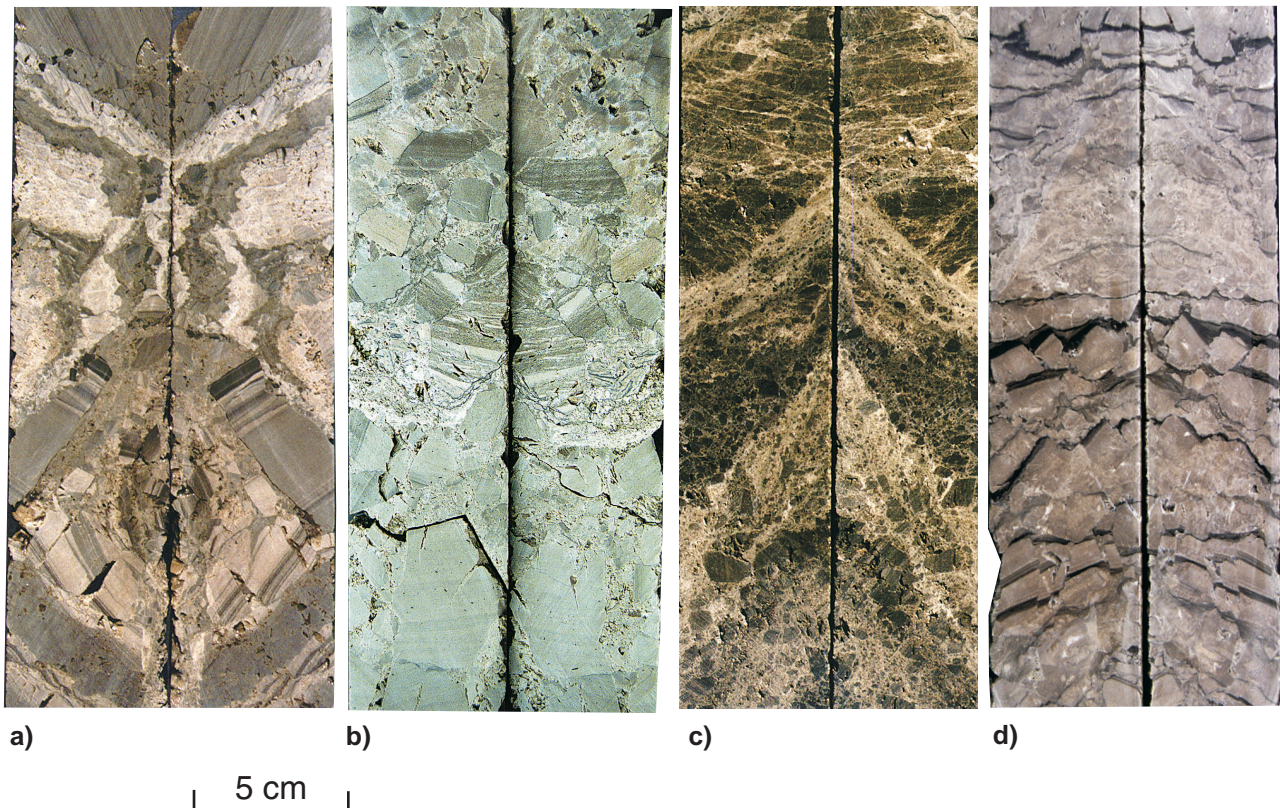
The interval 587.2 – 600.85 m consists of Upper Silurian dolomite clasts up to 1 m across, brecciated zones up to 75 cm thick, and thin siltstone beds (Fig. 12). The unit is identified as a breccia on the basis of high dips in the core (26–41°) in contrast to dips of less than 20° in the underlying unit (Table 1). The age of the clasts is based on an early Ludlow (Gorstian) conodont fauna (Appendix 6).

The excellent preservation of both dolomite and anhydrite textures appears to indicate dissolution of evaporites during a few million years of sedimentation, slumps, or partial collapse of the platform carbonates during evaporite diagenesis and dolomitization (El-Tabakh, M., 1999, written comm.). The alternating bands of crackle and mosaic textures within the unnamed breccia are derived probably from the dissolution of soluble salts, most likely halite. It also seems to contain some insoluble, dissolution residue layers and fractured intrasalt beds of dolomitic carbonates. If this unit is a salt-solution breccia, its thickness indicates there was once a much thicker evaporite section, perhaps hundreds of metres thick, which has since been removed. Some of the breccia clasts appear to be similar to the carbonate layers in the underlying Dirk Hartog Group, implying an evaporite basin that became progressively more saline (Warren, J. K., University of Brunei, 2000, written comm.). In the context of the Woodleigh impact structure, the breccia represents either a syndepositional facies of the Coburn Formation, an impact-related breccia on the floor of the crater, or a subsequent deposit that formed on an eroded slope of the crater. The lack of impact-shocked material in the breccia or obvious impact-related fracturing in the underlying formation, and the small thickness of the breccia imply that it is not directly related to the impact. It is also feasible that the breccia has been formed by a combination of the processes listed above. The breccia at 591.2 m (Fig. 12c), for example, has numerous fractures, and is more akin to a fault breccia than the remainder of the unit.

**Table 1. Bedding dips in Woodleigh 2A**

<i>Depth (m)</i>	<i>Apparent dips</i>	<i>Unit</i>
270–509	0–2°	Woodleigh Formation
592.1	26°	Unnamed breccia
594.9	35°	Unnamed breccia
595.6	43°	Unnamed breccia
596.8	37°	Unnamed breccia
597.2	41°	Unnamed breccia
597.8	40°	Unnamed breccia
598.1	38°	Unnamed breccia
600.0	36°	Unnamed breccia
601.0	13°	Coburn Formation
605.7	17°	Coburn Formation
606.0	16°	Coburn Formation
608.7	19°	Coburn Formation
609.2	16°	Coburn Formation
610.6	18°	Coburn Formation
611.3	17°	Coburn Formation
614.0	16°	Coburn Formation
615.5	17°	Coburn Formation
615.5	17°	Coburn Formation
615.8	18°	Coburn Formation
617.5	16°	Coburn Formation





AJM355

13.02.01

**Figure 12.** Core (slabbed) photographs of unnamed breccia, Woodleigh 2A: a) 588.0 m, dolomite breccia with large, laminated dolomite clasts; b) 589.9 m, dolomite breccia with minor vuggy porosity; c) 591.2 m, fractured dolomite breccia; d) 592.4 m, ?large clast of pre-impact brecciated, interbedded dolomite and mudstone

## Dirk Hartog Group

Hocking (1985) included the succession, now referred to as the Dirk Hartog Group, within the Kalbarri Group along with the Tumblagooda Sandstone, Kopke Sandstone, and the Sweeney Mia Formation. The Dirk Hartog Group of Hocking (1985) included the section later assigned to the Faure Formation by Gorter et al. (1994), who defined the underlying Dirk Hartog Group as consisting of (in ascending order) the Ajana Formation, Yaringa Evaporite, and Hamelin Formation. Formations within the group were revised by Mory et al. (1998), on the basis of new conodont data, as the Ajana Formation (with the basal Marron Member), Yaringa Formation, and the Coburn Formation (as Hamelin has a prior usage in the region). In Woodleigh 2A, only the Coburn Formation is represented.

### Coburn Formation

The Coburn Formation, intersected from 600.85 to 618.3 m (TD), consists of interbedded dolomite and gypsum with minor shale (Fig. 13). The lithofacies within the Coburn Formation appears to belong to a classic dolomitic–evaporite saltern association, where the dominant precipitates were alternating  $\text{CaSO}_4$  and carbonate (now dolomite) layers laid down within a widespread, shallow to ephemeral brineway (Warren, J. K., University of Brunei, 2000, written comm.). There is no indication of impact-related deformation.



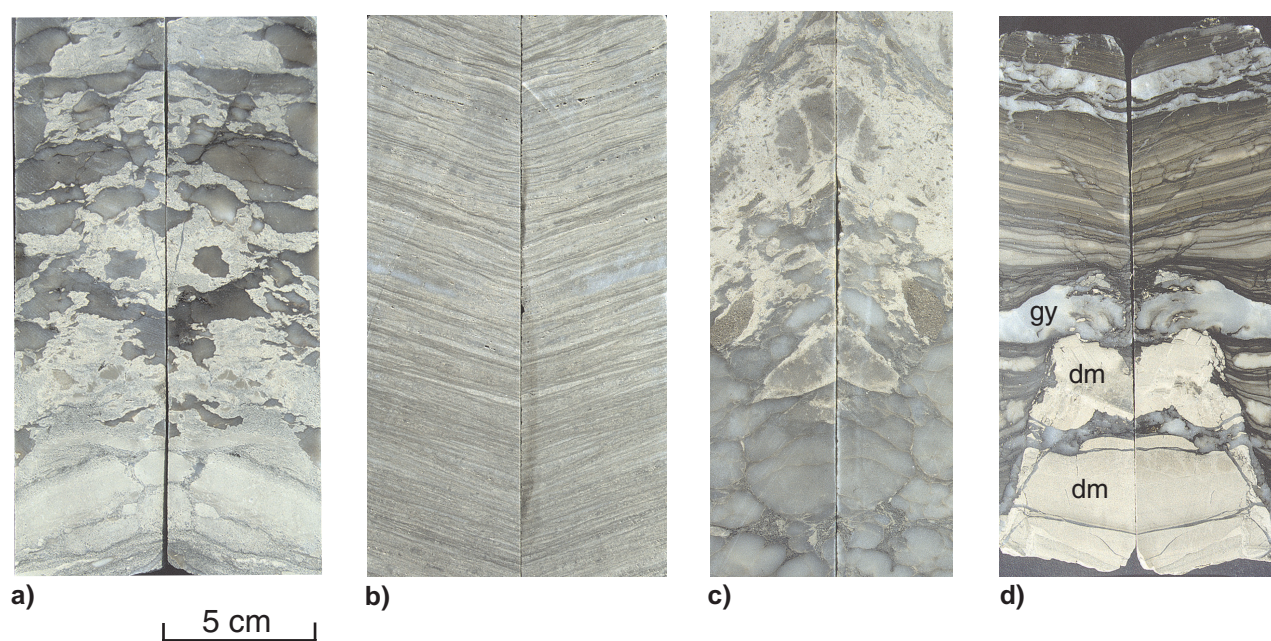


**Figure 13.** Core (slabbed) photographs of Coburn Formation, Woodleigh 2A: a) 606.9 m, pockets of anhydrite (?gypsum) in recrystallized dolomite; b) 609.2 m, laminated dolomite; c) 613.5 m, gypsum showing 'chicken-wire' fabric grading up into remobilized gypsum; d) 618.3 m, laminated dolomitic mudstone with minor deformation due to growth of interbedded gypsum (gy) overlying fractured, massive dolomite (dm)

Analysis of the limited conodont fauna (three species) suggests the interval 591.8 – 615.9 m may be confidently assigned to Fauna 4 of Mory et al. (1998), considered to be of early Ludlow (Gorstian) age (Late Silurian; Appendix 6). The only palynomorph identified to species level, *Tetrahedraletes medinensis*, has a known range of Late Ordovician to Early Devonian, but seems to be most commonly recorded from the Late Ordovician to Early Silurian (Appendix 5).

## Granitoid basement

Granitoid rocks are present in Woodleigh 1 from 171 to 333.1 m (TD). The only other basement rocks are exposed within the basin as inliers in the Merlinleigh Sub-basin to the northeast of the Woodleigh impact structure (Fig. 2), or lie at shallow depths at the northern end of the Wandagee Ridge (Hocking et al., 1987), and show no signs of impact. In the core from Woodleigh 1, the granitoid rocks (190.5 m to TD) are all variably brecciated, impact-shocked, and altered (see Appendices 3 and 4 for details of shock metamorphism), and commonly have mylonitic or cataclastic fabrics. For this reason, it is difficult to establish the precise nature of the precursor rocks, but some information can be obtained from the petrographic examination of thin sections and geochemical data, integrated with detailed core logging (Appendices 3 and 4). The essential minerals that are commonly present in various proportions in the Woodleigh granitoid rocks are quartz, microcline, orthoclase, anorthoclase, plagioclase, and biotite. Accessory phases such as muscovite, sericite, chlorite, titanite, epidote, garnet, and corundum are probably of post-impact origin and may be linked to hydrothermal processes and thermal metamorphism. The presence of garnet (andradite) in shocked granitoids is also documented from the central uplift of the Shoemaker Impact Structure (Pirajno and Glikson, in prep.). The Woodleigh granitoids contain S-type pseudotachylite veins and, in places, thin fractures containing sulfides (mostly pyrite).

The granitoid rocks of the Woodleigh central uplift intersected in Woodleigh 1 include: 1) biotite-rich granitic gneiss; 2) coarse-grained, megacrystic potassic granite; 3) leucocratic granite; 4) fine-grained, leucocratic biotite granite; and 5) mafic or intermediate granitoid (?enclaves). Foliated biotite–quartz rock with contorted leucocratic bands and large feldspar crystals (?porphyroblasts) was probably originally a granitic gneiss. It has a cataclastic to brecciated texture, and geochemical data suggest that it has a monzogranite composition (Appendix 3). The coarse-grained megacrystic granite has orthoclase and microcline phenocrysts in an inequigranular aggregate of quartz–feldspar–biotite, and was derived probably from a porphyritic syenogranite. The leucocratic granite is characterized by irregular, yellow-brown-coloured patches, and contains shocked and partly fused quartz and feldspar, as well as patches of bright-pink K-feldspar. The yellow-brown colouration is partly due to iron oxides and partly to the presence of abundant fluid inclusions (Appendix 3). The precursor of this granitoid type is unknown. Fine- to medium-grained leucocratic granite and biotite granite are massive to weakly foliated and largely consist of quartz, plagioclase, K-feldspar, and biotite. They were derived possibly from an aplitic granite.

At the thin-section scale, other lithologies containing biotite (?biotite schist), anthophyllite, actinolite, and plagioclase may have been either mafic enclaves or fragments of mafic units that were mixed with the host granitoids by the impact.

In attempting to obtain the age of the impact from the granitoid basement in Woodleigh 1, Neoproterozoic ages of 835–571 Ma have been obtained using a variety of techniques (Table 2). These ages, however, are unlikely to represent the age of the precursor rocks, but instead possibly dated Neoproterozoic heating events within the Pinjara Orogen (Myers, 1990; Libby et al., 1999). The few shocked PDFs in zircons separated from the granitoid in Woodleigh 1 (GSWA 149142; 198.35 – 198.5 m) yielded radiation-damaged grains and a scatter of Precambrian ages not considered meaningful (Armstrong, R., Australian National University, 1999, written comm.). Apatite fission-track analysis yielded Late Jurassic ages that post-date the impact (Appendix 7) and appear to be related to the breakup of Australia from Greater India. Similar Late Jurassic – Early Cretaceous ages were also obtained from some of the Ar–Ar analyses (Appendix 8) and K–Ar dating of clay minerals (Appendix 9).

**Table 2. Ages obtained from granitoid basement in Woodleigh 1**

<i>Method</i>	<i>Sample depth (m)</i>	<i>Age (Ma)</i>	<i>Error (Ma)</i>	<i>Reference</i>
Rb–Sr (biotite)	237	835	?	R. Armstrong, ANU, 1999, pers. comm.
Ar–Ar (biotite)	198.35 – 198.5	664–828	±9–22	Appendix 8
K–Ar (whole rock)	194.85	801	±17	Appendix 9
K–Ar (biotite–illite)	194.85	570.6	±12	Appendix 9

**NOTES:** Phanerozoic ages and analyses with large errors have been ignored

ANU: Australian National University

## Petroleum geology

### Source potential

Although the Cretaceous succession is immature, the one sample analysed from the Birdrong Sandstone (Woodleigh 2) is organic rich (2.84% total organic carbon; TOC), but has a low potential yield ( $S_1 + S_2$ ) of 1.34 mg/g rock (Appendix 10). By comparison, the Jurassic Woodleigh Formation has excellent source-rock potential with up to 7.7% TOC in shale beds and 44% TOC in associated woody material. Hydrocarbon-generating potential in the formation is up to 38 mg/g rock. The Rock-Eval parameters indicate that the kerogen from the Woodleigh Formation is oil- and gas-prone type II (Appendix 10). Pyrolysis-gas chromatography (PGC), which provides information on likely hydrocarbon products from source rocks on increasing maturation, confirms that the sample from 333.05 m is a good quality, gas-prone source. However, woody material in the sample from 441.7 m is of a gas-generating type. The liquid extract from 333.05 m was high (1317 ppm), and gas chromatography and mass spectrometry (GC-MS) confirms good generation potential for liquid hydrocarbons (Appendix 10).

Two of the three organic-rich samples from Silurian clasts within the unnamed breccia analysed by Rock-Eval pyrolysis are fair to good in organic richness (up to 2.24% TOC) and generating potential ( $S_1 + S_2$  up to 8.45 mg/g rock). The GC-MS data for extracted saturates confirm the good oil- and gas-prone kerogen in the Coburn Formation (Appendix 10).

### Maturation

Cretaceous and Jurassic mudstone beds are immature for oil generation as they exhibit vitrinite reflectance ranges of 0.24 – 0.45% (Appendix 10). Palynomorphs from the Cretaceous and Jurassic section also display low maturity (Appendix 5).

Two samples from the Coburn Formation yielded macerals with mean reflectance values of 0.50 and 0.52% (lamalginite and telalginite), indicating these samples are marginally mature for oil generation.  $T_{max}$  values from Rock-Eval analyses from this unit lie in the range 431–436°C, which is consistent with the reflectance data (Appendix 10).

Palynomorphs from the Coburn Formation have a thermal alteration index (TAI) of about 2+ with local grains up to 3-, indicating that this section is within the oil window (Appendix 5).

The conodont alteration index (CAI) of specimens recovered from the Coburn Formation is 1, which suggests that the Upper Silurian was not heated above 80°C and the maturity was equivalent to less than 0.80% Ro (Appendix 6).

An apatite fission-track analysis (AFTA) from the Woodleigh Formation indicates at least one cooling event within the Jurassic to Early Cretaceous. Three possible scenarios are outlined, but only two covering the Middle Jurassic to Early Cretaceous are consistent with previously recognized palaeothermal events — an early Jurassic event is less likely (Appendix 10).

Burial and maturation modelling of Woodleigh 2A suggests that the Woodleigh Formation reached its present level of maturity in the Jurassic. In addition, approximately 500–700 m has been eroded from the top of the Jurassic and 300–400 m has been eroded from the top of the Cretaceous, probably in the Late Jurassic – earliest Cretaceous and early Cainozoic respectively (Appendix 10).

## Reservoir characteristics

The Cretaceous Birdrong Sandstone is an excellent regional aquifer and has excellent reservoir potential. The extremely friable nature of the sands in Woodleigh 1, 2, and 2A, however, meant that it could not be easily cored so that porosity and permeability could not be measured.

The core samples of the Woodleigh Formation have porosities up to 24.7% (average 18.7%) and permeabilities up to 71.7 mD (average 15.4 mD). In the unnamed breccia, core porosity ranges up to 22.5% (average 19.7%) with permeability reaching a maximum of 15.4 mD (average 4.5 mD). A single sample from the unnamed breccia had a porosity of 24.6% and a permeability of 0.197 mD. In the Coburn Formation, the two measured porosities are 8.0 and 13.9%, with corresponding permeabilities of 0.241 and 7.94 mD (Appendix 11). In Woodleigh 1, the granitoid rocks have porosities (probably fracture) of 2–8%, averaging 5.6% (Appendix 11).

## Seals

Several potential seals were penetrated in Woodleigh 1, 2, and 2A. These include gypsum and tight dolostone beds in the Coburn Formation, and mudstone units in the Cretaceous and Lower Jurassic section. Overall, however, potential sealing sections in these wells appear to be thin at these locations. The shaley part of the Muderong Shale could be possibly a sealing unit, but is less than 10 m thick in the Woodleigh wells. The Woodleigh Formation in Woodleigh 2A has too high a proportion of thin sandstone beds to be an effective seal.

## Shows

No fluorescence was observed in the cores or cuttings. The only occurrence of petroleum is from a thin section at 284 m (Woodleigh Formation), in which possible bitumen is described in Appendix 10.

## Mineral potential

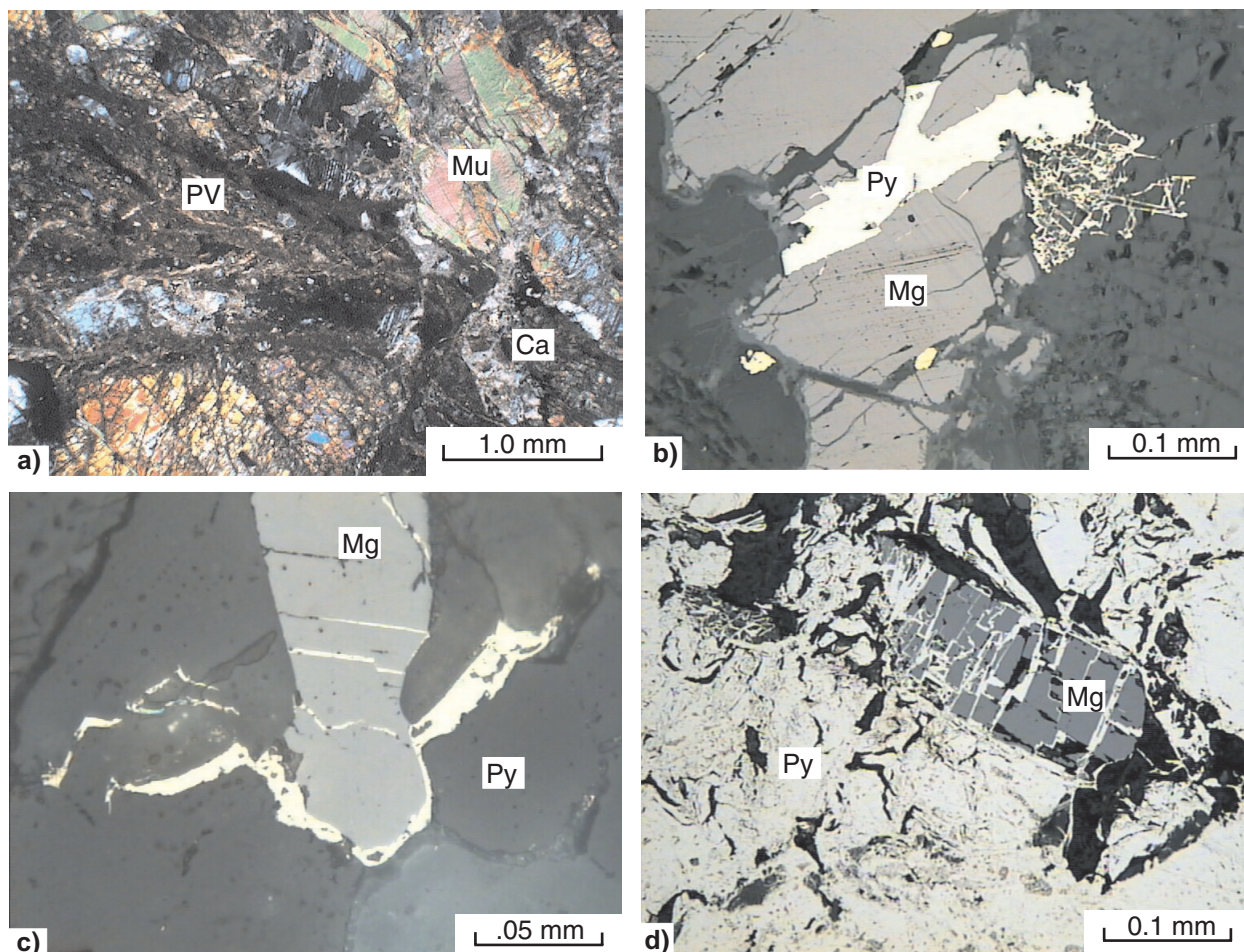
Although meteorite impacts are transient and high-energy events, the consequences in terms of ore formation or modification of existing mineralization can be considerable. There is already a substantial body of evidence to suggest that economically important mineral deposits owe their existence, directly or indirectly, to asteroid impact events. A key paper dealing with the economic potential of impact structures is Grieve and Masaitis (1994), who considered three types of mineral deposits that are associated with impact structures: 1) those that existed before the impacting event, but were subsequently modified during and after the impact; 2) those that formed as a direct consequence of the impact; and 3) post-impact hydrothermal activity and flow of fluids (including hydrocarbons) into fractures and faults caused by the impact, which may result in the formation of hydrothermal metalliferous deposits.

Large impacts induce considerable fracturing, thus enhancing the permeability of the target rocks. This could enhance or promote hydrothermal circulation within and around the structure, caused by cooling of impact melt sheets or transformation of kinetic to heat energy to the rocks beneath the melt sheet, or by both processes, or by related magmatic activity; for example, Sudbury (Grieve and Masaitis, 1994). Examples of hydrothermal ores that can be related to impacts are numerous, and



include Pb, Zn, Ag, and Ba at Siljan in Sweden, Pb–Zn associated with the Kardla Crater in Estonia (Puura et al., 2000), and Cu, Zn, Pb, and Au at Vermilion in the Sudbury structure (Grieve and Masaitis, 1994; Pirajno, 2001).

The extensively fractured and brecciated granitoid rocks cored in Woodleigh 1 commonly exhibit evidence of post-impact hydrothermal alteration and sulfide mineralization. This is shown by the presence of mineral phases such as albite, quartz, muscovite, chlorite, and calcite, which overprint the primary or impact-modified mineralogy and infill microfractures, or both (Fig. 14a; Appendix 3). In addition, the presence of abundant fluid inclusions (liquid and liquid + gas) within impact-related microstructures (e.g. PDFs; Appendix 3) implies that substantial volumes of fluids circulated through the impact-modified target rocks. A study of the fluid inclusions is beyond the scope of this Record, but should give some insight to the nature of the hydrothermal cell set up by the impact. Sulfides that have been recognized by reflected-



AJM360

16.02.01

**Figure 14.** Photomicrographs showing post-impact minerals: a) GSWA 132522, photomicrograph showing a pseudotachylite veinlet (PV) displaced by a late microfracture and overprinted by calcite (Ca); there are large muscovite (Mu) crystals in the brecciated groundmass material. Calcite and muscovite are post-impact minerals because they overprint shocked minerals and are not deformed or fractured. Crossed polars; b) GSWA 132522, reflected-light photomicrograph showing magnetite (Mg) cut by pyrite (Py); fine pyrite filling a network of microfractures and chalcopryrite blebs (yellow); c) GSWA 175208, reflected-light photomicrograph showing magnetite crystal (Mg) and pyrite (Py) filling small fractures; d) GSWA 175208, reflected-light photomicrograph showing massive pyrite (Py) associated with a fractured a magnetite crystal (Mg)

light optical microscopy include pyrite, marcasite, and chalcopyrite. Typically, these sulfides fill microfractures in the silicate matrix and in pre-existing ore minerals, such as ilmenite. Examples are shown in Figures 14b–d.

Hydrothermal alteration is especially common in samples that are extensively fractured with or without pseudotachylite veinlets (Fig. 14a). Textural relationships gleaned from petrographic work (see Appendix 3) suggest that the alteration paragenetic sequence is: quartz + albite → muscovite or sericite ± epidote → silica flooding → calcite.

At present, the economic mineral potential of the Woodleigh impact structure cannot be quantified. However, it is conceivable that hydrothermal convection cells were activated by a heat source provided by either the melt sheet or the underlying rocks, where kinetic energy is dissipated into heat — as within the shocked granitoids of the central uplift. It is also possible that some hydrothermal cells may have vented at the surface as hot springs. If this assumption is correct, zones of silicification should be present in the crater-basin infill and along fractures or faults associated with the original crater.

## Contribution to geological knowledge

The presence of PDFs, pseudotachylite veins, and breccia within the continuously cored, granitoid basement section in Woodleigh 1 at the centre of the multi-ring Woodleigh impact structure provide indisputable evidence of its impact origin.

Regionally, a pre-Early Jurassic age for the impact is defined by palynomorphs in the Woodleigh Formation, which overlies the structure, and a post-Early Devonian age is suggested by the regional extent of the Lower Devonian Faure Formation, Kopke Sandstone, and Sweeney Mia Formation, which appear to be the youngest units to be deformed by the structure (Iasky et al. 2001). The post-Early Permian (Sakmarian) age suggested by Mory et al. (2000a) was based on palynomorphs recovered from shale clasts in the unnamed paraconglomerate. However, that lower age limit conflicts with the Late Devonian – Early Carboniferous K–Ar ages from the granitoid in Woodleigh 1, and assumes the section intersected in Woodleigh 2A filled the crater immediately after the impact.

K–Ar isotopic ages of  $364 \pm 8$  to  $321 \pm 8$  Ma have been determined from the illite-rich, coarse-grained fraction of the central granitoid penetrated in Woodleigh 1 (Appendix 9). In addition, three analyses of illite and smectite from the matrix of the basal paraconglomerate (which contains PDF-bearing granite clasts) in Woodleigh 2A yielded similar ages — that is, ranging from near the Frasnian–Fammenian boundary (Late Devonian) to near the end of the Visean (Early Carboniferous). If the K–Ar ages from the granitoid in Woodleigh 1 reflect hydrothermal activity in the wake of the impact, they constrain the age of the impact to the Late Devonian. Superficially, this age appears likely as illite commonly forms in a temperature range between 200 and 300°C, and transforms to mica (muscovite) at temperatures higher than 300°C. To our knowledge, there are no other regional tectonic events in the Gascoyne Platform that have generated temperatures above 130°C (Ghori, 1999, figs 28, 29, and appendix 9), that is, there is no evidence for younger heating that could affect illite K–Ar systematics in the Woodleigh wells.

An analysis of palaeomagnetic inclinations from biotite–hornblende granitoid samples in Woodleigh 1 indicate mid-Carboniferous to possible Early Triassic age when plotted against the known polar wandering curve for Australia (Appendix 12). This



appears to be inconsistent with the K–Ar dating of illite and smectite from the granitoid, which have yielded a Late Devonian to Early Carboniferous age. The expected inclination for these earlier times is much shallower than for the later Palaeozoic ( $\sim\pm 30^\circ$ ), as compared to the observed  $+70^\circ$ , so as they stand, the two methods appear to be irreconcilable. If the K–Ar dates are indeed closer to the true age than the palaeomagnetic age, then either the assumption that the magnetic remanence was reset upon impact, or that the granitoid has not been grossly tilted since then, is incorrect. Ghorri (1999) notes that AFTA, vitrinite reflectance measurements, and basin modelling indicate that the levels of maximum burial, palaeotemperatures, and maturation attained across the Carnarvon Basin vary greatly, but the timing for the maximum rate of petroleum expulsion across the basin peaked during the Late Palaeozoic. It is possible that the remanence observed here could have arisen at this time. Unfortunately, the stability of K–Ar and Rb–Sr isotopic systematics in biotites and of U–Pb isotopic systematics in zircon, coupled with post-Lower Jurassic resetting of the Ar–Ar and K–Ar ages of feldspar and pseudotachylite, appear to preclude a precise isotopic age determination (Armstrong, R., Australian National University, 1999, written comm.; Appendices 8 and 9), and thus appear to be unable to resolve this dilemma.

Woodleigh 2A is the only cored section of the lacustrine Jurassic Woodleigh Formation (223 – 521.3 m), and thereby provides the most detailed palynological, stratigraphic, sedimentological, geochemical, and rock physics information for this lacustrine unit, which may be a crater-fill section. It is uncertain whether or not the underlying paraconglomerate (521.3 – 587.2 m) and breccia (587.2 – 600.85 m) units should be considered as separate entities below the Woodleigh Formation or basal members of that formation. Neither unit has been dated or is formally named, but the presence of shale clasts containing Early Permian palynomorphs near the base of the paraconglomerate provides a maximum age for that unit. If the paraconglomerate is Jurassic, then the paucity of shocked granitoid clasts within it implies that an earliest Jurassic age for the impact is unlikely. If the Late Devonian age interpreted from the K–Ar dates is correct, then the Jurassic section is a secondary fill, post-dating an erosional event that removed any earlier crater fill. Such an interpretation is indirectly supported by the relatively thick sections of the basal Cretaceous unit (Birdrong Sandstone) in the Woodleigh wells compared to the wells to the east, implying that in the central part of the structure, a depression persisted into the Early Cretaceous.

In Woodleigh 1, the Lower Cretaceous Winning Group lies directly on granitic basement, whereas within Woodleigh 2A it overlies almost 300 m of Jurassic and 66 m of possibly older strata (unnamed paraconglomerate) above a relatively undeformed Silurian section. The lack of Jurassic strata in Woodleigh 1 suggests that the central uplift of the Woodleigh impact structure was either elevated for a considerable period, or that it was reactivated prior to deposition of the Cretaceous. Burial and maturation modelling for Woodleigh 2A indicate about 500–700 m has been eroded from the top of the Jurassic, probably in the Late Jurassic – earliest Cretaceous, implying that the crater fill was once at least 900 m thick. The effect of the impact upon the regional maturity of the underlying strata appears negligible, as also noticed from studies of other structures (Gorter et al., 1996), probably because the effects of impacts are extremely local with high temperatures dissipating rapidly from the centre of the impact.

In Woodleigh 2A, the Woodleigh Formation is immature, thereby downgrading the source-rock potential of this carbonaceous unit. Burial and maturation modelling of Woodleigh 2A suggest that the underlying Silurian section became marginally mature in the Jurassic. Although the difference in maturity between the Silurian and Jurassic

in this well indicates little erosion at this level, there is little difference in the maturity of the Silurian between Woodleigh 2A (inferred to be about 0.5% Ro) and Yaringa 1 (0.50 – 0.64 % Ro). Therefore, erosion of the top of the Silurian in the order of 700 m can be implied in Woodleigh 2A (the thickness of the Devonian in Yaringa 1).

In Woodleigh 2A, the best reservoir properties are present in the unnamed paraconglomerate and the basal sandstone beds within the Woodleigh Formation.

Although impacts may induce considerable fracturing, thereby enhancing the permeability of the target rocks, as well as inducing structures that may form oil and gas traps, at present there are insufficient geophysical data to properly evaluate such plays within the Woodleigh impact structure. In addition, although the interpreted Devonian age of the structure suggests a favourable timing for the Woodleigh impact structure to entrap hydrocarbons, this age needs to be confirmed independently, before analogies can be made readily with productive impact structures such as Ames (450 Ma, 14 km diameter in Oklahoma, USA; Donofrio, 1998), and the 55 km-diameter Tookoonooka structure in Queensland (Gorter, 1998).

The lack of deformation in the Upper Silurian Coburn Formation (apart from gentle dips of 13–19°; Fig. 13) in Woodleigh 2A indicates that it was drilled outside of the central part of the Woodleigh impact structure. In Vredefort (?300 km in diameter), Chicxulub (170 km), Acraman (?90 km), and Gosses Bluff (24 km), for example, the outer aureoles (well over 50% of the whole of these impact structures) are flat to virtually undeformed (Therriault et al., 1993; Williams et al., 1996; Morgan and Warner, 1999; Iasky et al., 2001). In these instances, the size of the structure is defined by the outer ring faults and their geophysical expressions. If the Woodleigh impact structure has been fairly deeply eroded, that is to below the level of obvious impact deformation, then it is unlikely that drillholes could help define the size of the structure, apart from penetrating crater fill close to the outer ring faults. At present none of the wells or drillholes within the structure as proposed by Mory et al. (2000a,b) that have samples available from below the Cretaceous, are closer than 15 km to the outer margin and appear to intersect mid-Devonian or older strata (Iasky et al., 2001, fig. 8, appendix 1). In addition, it is possible that the Silurian section in Woodleigh 2A is part of a megabreccia, such that the short section of core cut may not be enough to differentiate between a megabreccia or solid bedrock.

## Acknowledgements

We thank Mick Clausen of Woodleigh Station for his generous assistance during the drilling, and Rob Hough at the Western Australian Museum for reviewing the petrology and mineral geochemistry (Appendix 3).

## References

- BACKHOUSE, J., 2000, Palynology of samples from the Woodleigh area: Western Australia Geological Survey, Palaeontology Report, 2000/2 (unpublished).
- DONOFRIO, R. R., 1998, North American impact structures hold giant field potential: *Oil & Gas Journal*, v. 96 (19), p. 69–83.
- FEWSTER, M. E., 1991, Carnarvon Basin Project results of exploration and recommendations for further work for Carpentaria Exploration Company: Western Australia Geological Survey, Statutory mineral exploration report, Item 11083 A58930 (unpublished).
- GHORI, K. A. R., 1999, Silurian–Devonian petroleum source-rock potential and thermal history, Carnarvon Basin, Western Australia: Western Australia Geological Survey, Report 72, 88p.
- GORTER, J. D., 1998, The petroleum potential of Australian Phanerozoic impact structures: *APPEA Journal*, v. 38, p. 159–187.
- GORTER, J. D., KORSCH, R. J., and NICOLL, R. S., 1996, Thermal history of the Gosses Bluff impact structure, central Australia, from conodont colour-alteration indices: implications for hydrocarbon prospectivity and erosional history: *AGSO Journal of Australian Geology and Geophysics*, Thematic Issue: Australian impact structures, v. 16, no. 4, p. 553–560.
- GORTER, J. D., NICOLL, R. S., and FOSTER, C. B., 1994, Lower Palaeozoic facies in the Carnarvon Basin, Western Australia: stratigraphy and hydrocarbon prospectivity, *in* *The Sedimentary Basins of Western Australia edited by P. G. PURCELL and R. R. PURCELL: Petroleum Exploration Society of Australia; Sedimentary Basins of Western Australia Symposium*, Perth, W.A., 1994, Proceedings, p. 373–396.
- GRIEVE, R. A. F., and MASAITIS, V. L., 1994, The economic potential of terrestrial impact craters: *International Geology Review*, v. 36, p. 105–151.
- HOCKING, R. M., 1985, Revised stratigraphic nomenclature in the Carnarvon Basin, W.A.: Western Australia Geological Survey, Record 1985/5, 22p.
- HOCKING, R. M., MOORS, H. T., and van de GRAAFF, W. J. E., 1987, Geology of the Carnarvon Basin, Western Australia: Western Australia Geological Survey, Bulletin 133, 289p.
- HOCKING, R. M., MORY, A. J., and WILLIAMS, I. R., 1994, An atlas of Neoproterozoic and Phanerozoic basins of Western Australia, *in* *The Sedimentary Basins of Western Australia edited by P. G. PURCELL and R. R. PURCELL: Petroleum Exploration Society of Australia; Sedimentary Basins of Western Australia Symposium*, Perth, W.A., 1994, Proceedings, p. 21–43.
- IASKY, R. P., and MORY, A. J., 1999, Geology and petroleum potential of the Gascoyne Platform, Southern Carnarvon Basin, Western Australia: Western Australia Geological Survey, Report 69, 46p.
- IASKY, R. P., MORY, A. J., and BLUNDELL, K. B., 2001, The geophysical interpretation of the Woodleigh impact structure, Southern Carnarvon Basin, Western Australia: Western Australia Geological Survey, Report 79, 41p.
- IASKY, R. P., MORY, A. J., and SHEVCHENKO, S., 1998, The structural evolution of the Gascoyne Platform, Southern Carnarvon Basin, W.A., *in* *The Sedimentary Basins of Western Australia 2 edited by P. G. PURCELL and R. R. PURCELL: Petroleum Exploration Society of Australia; Sedimentary Basins of Western Australia Symposium*, Perth, W.A., 1998, Proceedings, p. 589–598.
- LAYTON AND ASSOCIATES, 1981, Well completion report EP169: Woodleigh 1981/2 south Carnarvon Basin, W.A.: Western Australia Geological Survey, Statutory petroleum exploration report, S2075 A1 (unpublished).
- LIBBY, W. G., DE LAETER, J. R., and ARMSTRONG, R. A., 1999, Proterozoic biotite Rb–Sr dates in the northwestern part of the Yilgarn Craton, Western Australia: *Australian Journal of Earth Sciences*, v. 46, p. 851–860.
- McWHAE, J. R. H., PLAYFORD, P. E., LINDNER, A. W., GLENISTER, B. F., and BALME, B. E., 1956, The stratigraphy of Western Australia: *Geological Society of Australia, Journal*, v. 4, pt 2, 161p.
- MORGAN, J., and WARNER, M., 1999, Morphology of the Chicxulub impact: peak-ring crater or multi-ring basin?, *in* *Large meteorite impacts and planetary evolution 2 edited by B. O. DRESSLER and V. L. SHARPTON: Geoscience Canada, Special Paper 339*, p. 281–290.
- MORY, A. J., and BACKHOUSE, J., 1997, Permian stratigraphy and palynology of the Carnarvon Basin: Western Australia Geological Survey, Report 51, 41p.
- MORY, A. J., IASKY, R. P., GLIKSON, A. Y., and PIRAJNO, F., 2000a, Woodleigh, Carnarvon Basin, Western Australia: a new 120 km-diameter impact structure: *Earth and Planetary Science Letters*, v. 177, p. 119–128.
- MORY, A. J., IASKY, R. P., GLIKSON, A. Y., and PIRAJNO, F., 2000b, Response to ‘Critical comment on A. J. Mory et al., 2000, Woodleigh, Carnarvon Basin, Western Australia: a new 120 km diameter impact structure’, by W. U. Reimold and C. Koeberl: *Earth and Planetary Science Letters*, v. 184 (1), p. 359–365.
- MORY, A. J., NICOLL, R. S., and GORTER, J. D., 1998, Lower Palaeozoic correlations and maturity, Carnarvon Basin, W.A., *in* *Sedimentary Basins of Western Australia 2 edited by P. G. PURCELL and R. R. PURCELL: Petroleum Exploration Society of Australia; Sedimentary Basins of Western Australia Symposium*, Perth, W.A., 1998, Proceedings, p. 599–611.

- MORY, A. J., and YASIN, A. R., (compilers), 1998, GSWA Mooka 1 well completion report: Western Australia Geological Survey, Record 1998/6, 49p.
- MORY, A. J., and YASIN, A. R., (compilers), 1999, GSWA Barrabiddy 1 and 1A well completion report: Western Australia Geological Survey, Record 1999/3, 84p.
- MYERS, J. S., 1990, Pinjara Orogen, *in* Geology and Mineral Resources of Western Australia: Geological Western Australia Survey, Memoir 3, p. 265–274.
- PIRAJNO, F., 2001, Ore deposits and mantle plumes: Dordrecht, Kluwer Academic Publishers, 509p.
- PIRAJNO, F., and GLIKSON, A. Y., in prep., The Shoemaker Impact Structure, Western Australia: Western Australia Geological Survey, Report.
- PUURA, V., KÄRKI, A., KIRS, J., KIRSIMÄE, K., KLEESMENT, A., KONSA, M., NIIN, M., PLADO, J., SUUROJA, K., and SUUROJA, S., 2000, Impact-induced replacement of plagioclase by K-feldspar in granitoids and amphibolites at the Kärdla Crater, Estonia, *in* Impacts and the early Earth *edited by* I. GILMOUR and C. KOEBERL: Berlin, Springer-Verlag, p. 417–445.
- THERIAULT, A. M., REID, A. M., and REIMOLD, W. U., 1993, Original size of the Vredefort structure, South Africa: Lunar Planetary Science XXIV, p. 1419–1420.
- WILLIAMS, G. E., SCHMIDT, P. W., and BOYD, D. M., 1996, Magnetic signature and morphology of the Acraman impact structure, South Australia: AGSO Journal of Australian Geology and Geophysics, Thematic Issue: Australian impact structures, v. 16, no. 4, p. 431–442.
- YASIN, A. R., and MORY, A. J., (compilers), 1999a, Coburn 1 well completion report: Western Australia Geological Survey, Record 1999/5, 99p.
- YASIN, A. R., and MORY, A. J., (compilers), 1999b, Yaringa East 1 well completion report: Western Australia Geological Survey, Record 1999/7, 53p.

## Appendix 1

# Operations report

by J. Coker

### Introduction

Woodleigh 1 is a vertical corehole located using gravity data, in an area of poor seismic control, at the centre of a circular gravity anomaly (the Woodleigh impact structure) near the southeastern margin of the Gascoyne Platform, Southern Carnarvon Basin. The well was drilled by re-entering Woodleigh 1981/2, and coring from 190.5 to 333.1 m (total depth; TD). It lies about 164 km south-southeast of Carnarvon and 8 km west of the Woodleigh Homestead, at latitude 26°03'19"S, longitude 114°39'56"E, and an elevation of 108 m Australian Height Datum (AHD). The operational objective was to continuously core the supposed granite interpreted by Layton and Associates (1981) below the Mesozoic section to explain the nature of the circular gravity feature.

Woodleigh 2 and 2A are vertical stratigraphic holes located 14 km west of Woodleigh 1, on the western flank of the central uplift within the Woodleigh impact structure on the Gascoyne Platform, Southern Carnarvon Basin. The wells were drilled to 198 and 618.3 m respectively on Carbla Station about 164 km southeast of Carnarvon, and 20 km west of Woodleigh Homestead, at latitude 26°03'28"S, longitude 114°31'34"E, and an elevation of 67 m AHD. The operational objectives were to core the Woodleigh Formation and to investigate its lower contact. Woodleigh 2 and 2A were drilled next to a Carpentaria Exploration Pty Ltd drillhole, which contains the furthest occurrence of the Woodleigh Formation, confirmed by palynology, from the centre of the structure.

The drilling contractor, Mt Magnet Drilling, drilled Woodleigh 1 from 9 to 15 March 1999, Woodleigh 2 from 16 to 20 March 1999, and Woodleigh 2A from 21 to 27 March 1999 using a Hydco SD1000 rig mounted on a 8 4 Man diesel prime mover. Both Woodleigh 1 and 2A were geophysically logged by Geophysical Logging Technologies on 27 March 1999. A summary of the stratigraphy, logs run, casing used, and cores cut for the three wells is given in the well index sheets (Appendix 13).

### Wells histories

Woodleigh 1981/2, originally drilled by Leighton and Associates in 1981, was re-entered at 0900 hours on 9 March 1999 with the initial intention of using this hole as a waterbore. However, this proved difficult due to expanding clay in the Gearle Siltstone and running sand below 90 m; the hole was reamed out and casing advanced to the bottom, and continuous coring was commenced using a HQ (96 mm OD) bit. Although problems were encountered with unconsolidated sands from 92 to 171 m (Birdrong Sandstone), the hole was eventually cased off to a depth of 190.5 m at 1800 hours on 14 March, after which NQ coring commenced. Core recovery was generally good. Woodleigh 1 was terminated at 333.1 m on the 15 March 1999 at 1530 hours, and the HQ casing was retrieved with some difficulty. The hole was left open as a potential waterbore, and geophysically logged by Geophysical Logging Technologies late in the afternoon of 27 March 1999, while the drillers attempted to remove the casing from Woodleigh 2A.

Woodleigh 2 was spudded at 0600 hours on 16 March 1999 with a 6.25 inch (15.88 cm) bit and was drilled and cased to 6 m. Drilling continued to 193 m with a NQ string, but casing could not be advanced beyond 156 m due to lost circulation and running sands. Just 2.3 m of core was recovered from 193 to 198 m. The length of time the hole had been open meant continuing problems and it was decided to relocate 25 m to the east.

Woodleigh 2A was spudded at 0900 hours on 21 March 1999 with a 6.25 inch (15.88 cm) bit, which was changed to a 5.13 inch (13 cm) roller bit at 6 m. PVC casing was seated at 6 m (140 mm outer diameter — OD) and 30 m (100 mm OD). Drilling continued to 270 m with a HQ claw bit (96 mm OD) bit and the HQ casing was run in, but the hole caved in at 150 m. The casing was again run in, but this time with an advancer and was reamed down and seated at 270 m. Continuous NQ coring was started at 270 m in the upper part of the Jurassic Woodleigh Formation to TD at 618.3 m, with core recovery commonly poorer than in Woodleigh 1. Hole deviation surveys confirm that Woodleigh 2A was near vertical (Table 1.1), but only three were made because of the instability of the hole. Woodleigh 2A was terminated at 618.3 m, geophysically logged, and completed in the morning of 27 March 1999.

## **Operations**

### **Water supply**

Water proved difficult to obtain for Woodleigh 1. The original hole (Woodleigh 1981/2) could not be equipped due to swelling clays and running sand. Additionally, it was not possible to install a submersible pump in the nearest station bore (no. 2, 5 km east) and pipe the water due to the small diameter of its internal casing. It was then decided to commence coring from the base of Woodleigh 1981/2 and to cart water from nearby station bores to the location. At Woodleigh 2 and 2A, a large subartesian supply was obtained from the Birdrong Sandstone in the Carpentaria Exploration Pty Ltd hole drilled in 1992.

### **Drilling fluids**

A polymer mud (Aqua-Pac) was used for drilling Woodleigh 1, 2, and 2A. Proportions of the Aqua-Pac and water in mud were changed according to the drilling and formation conditions. Once hole conditions stabilized (below 198 m in Woodleigh 1 and below 415 m in Woodleigh 2A), coring proceeded without additives.

### **Drilling operations**

The drilling operations were carried out in two 12-hour shifts commencing at 0600 and 1800 hours. One driller and an offsider worked per shift. During maintenance and rig moves, the entire crew worked days.

Woodleigh 1 was drilled by continuous wireline coring from 190.5 to 333.1 m. Woodleigh 2 was drilled by a roller bit to 192 m and then by wireline coring to 198 m, after which the well became too unstable to continue. Initially, Woodleigh 2A was drilled with a roller bit to 270 m, and then by continuous wireline coring to 618.3 m.

A steel tank was used for mixing mud. Two interconnected mud pits were used for storing and recycling the returning mud from the annulus of the hole.

Drilling operations are outlined in chronological order in Figure 1.1 and Table 1.1.

### **Sample collection and handling**

Although Woodleigh 1 was drilled by re-entering Woodleigh 1981/2, 3 m-interval samples were collected while reaming from 170 to 190 m prior to wireline coring. Cuttings samples for Woodleigh 2 and 2A were collected to 192 and 270 m respectively, during drilling from the returning mud at the wellhead using a bucket, and amalgamated to make a 3 m composite sample. Unwashed cuttings (0.2 – 0.3 kg) were collected in cloth bags and dried.

Core length was measured using a steel tape and the percentage recovery was calculated for each run (Tables 1.2 and 1.3).

A 1:100 graphic sedimentological core log was recorded for Woodleigh 2A at the well site and has been placed in statutory petroleum exploration report S20566 in GSWA's library.



**Table 1.1. Chronological summary of drilling operations**

<i>Date</i>	<i>Start</i>	<i>Finish</i>	<i>Activity</i>
9 March 1999	0600	0900	Set up rig over Woodleigh 1981/2 with intention of developing as a waterbore
	0900	1200	Ream with R/C to 63 m to clean bore
	1200	1600	Pull rods and run in 100 mm casing. Casing stuck at 46 m
	1600	1800	Wash casing, slow progress
10 March 1999	0600	0900	Work PVC casing down to 56 m. Run polypipe down casing
	0900	1200	Attempting to develop bore while working PVC casing. Hydraulic pump fails and is sent to Perth for repairs
11 March 1999	0600	1800	Clean tanks, work on rig. New pump arrives late at night
12 March 1999	0600	1200	Fit new pump and test
	1200	1500	Continue attempt to develop Woodleigh 1981/2 as a waterbore
	1500	1800	Fault in pump, testing by engineer, new seal kit sent up from Perth
13 March. 1999	0600	0900	Repair and refit seals to hydraulic pump
	0900	1100	Run in HQ casing to 90 m. Hole caved in. Ream with HQ to 100.8 m
	1100	1500	Run in NQ mud rotary and wash collapsed sand from hole
	1500	1600	Drill HQ mud rotary and case with HQ to 116 m
	1600	1930	Wait on water. Attempt to fit submersible in station waterbore 5 km to east fails as internal diameter is too small
14 March 1999	0600	1200	Run HQ mud rotary down existing hole. Large amounts of sand
	1200	1300	Case off HQ to 190.5 m (just past TD of Woodleigh 1981/2 — 189 m)
	1300	1800	Continue NQ mud rotary to 151.4 m. Ream and wash sand and clay to bottom of hole
	1800	2400	Begin NQ wireline coring at 190.5 m
15 March 1999	0000	1530	TD at 333.1 m
	1530	1800	Pull NQ string
16 March 1999	0700	0900	Pull stuck HQ casing from Woodleigh 1
	0900	1200	<b>Move to Woodleigh 2</b>
	1200	1800	Set up over mineral exploration hole (for water) and ream to 84 m. Pull out of hole and run 100 mm casing
	1800	2400	Place submersible pump down hole and test. Pump shut down, run new pump and test
17 March 1999	0600	0630	Spud Woodleigh 2. Drill and case 6 m pre-collar
	0630	2130	Drill to 193 m with NQ mud rotary
	2130	2400	Case NQ to 163 m
18 March 1999	0000	0600	Case NQ to 193 m, unsuccessful due to unconsolidated formation, pull NQ casing
	0600	1800	Condition hole and wait on NQ casing to arrive from Perth
	1800	2400	Run and ream HQ to 156 m, lost circulation
19 March 1999	0000	0600	Regain circulation, ream to 156 m
	0600	1330	Ream HQ with claw bit from 156 to 192 m. Drill with HQ claw from 180 to 228 m
	1330	1800	Ream from 150 to 186 m, as stuck in unconsolidated formation. Rods stuck
	1800	2400	Ream HQ casing to 120 m
20 March 1999	0000	0400	NQ wireline core to 198 m. Run HQ casing to 198 m.
	0400	0600	Hole caved in. Cable fails trying to retrieve casing
	0600	1200	Repair cable
	1200	1930	Retrieve HQ casing from Woodleigh 2
21 March 1999	0600	0730	Continue to retrieve HQ casing from Woodleigh 2, move rig 25 m east
	0730	0900	<b>Commence Woodleigh 2A</b> , drill pre-collar to 6 m. Run 140 mm PVC pipe
	0900	1030	Drill to 30 m. Run 100 mm PVC pipe
	1030	2030	Drill with HQ claw to 132 m, flush and clean hole
22 March 1999	0600	1000	Drill HQ mud rotary to 270 m
	1000	1830	Condition hole, run in casing, hole caved in at 150 m. Ream hole
23 March 1999	0600	1230	Run in HQ string with casing advancer. Ream from 150 to 270 m
	1230	2400	NQ wireline core from 270 to 340 m
24 March 1999	0000	1100	Core to 367.5 m
	1100	1230	Change bit
	1230	1600	Core to 398 m
	1600	1800	Change bit
	1800	2400	Wash from 260 to 398 m, condition hole
25 March 1999	0000	0600	Pull rods out to seat tubes
	0600	1100	Core to 427 m
	1100	1300	Change bit
	1300	2400	Core to 490 m
26 March 1999	0000	2400	Core to 605 m
27 March 1999	0000	0300	Core to 618.3 m (TD)
	0300	0600	Flush hole
	0600	1130	Log inside drill string to 612 m
	1130	1345	Remove string
	1345	1445	Run dummy, stuck at ~400 m
	1445	2400	Attempt to pull out HQ casing, cut casing at 240 and 210 m
28 March 1999	0000	0800	Attempt to pull out HQ casing, cut casing at 180 m
	0800	1000	Twist off NQ casing at 130 m, pull casing, rig down

Table 1.2. Core recovery from Woodleigh 1

<i>Interval</i>		<i>Metres drilled</i>	<i>Metres recovered</i>	<i>Recovery rate (%)</i>	
<i>From (m)</i>	<i>To (m)</i>				
190.5	191.1	0.6	0.6	100.0	
191.1	192.4	1.3	1.3	100.0	
192.4	195.3	2.9	2.8	96.6	
195.3	201.1	5.8	4.7	81.0	
201.1	207.3	6.2	5.4	87.1	
207.3	210.1	2.8	4.0	142.9	
210.1	213.6	3.5	3.3	94.3	
213.6	216.2	2.6	2.6	100.0	
216.2	218.8	2.6	2.6	100.0	
218.8	222.3	3.5	3.5	100.0	
222.3	226.2	3.9	3.8	97.4	
226.2	227.3	1.1	1.1	100.0	
227.3	230.8	3.5	3.1	88.6	
230.8	237.2	6.4	6.2	96.9	
237.2	243.3	6.1	6.1	100.0	
243.3	249.3	6.0	6.0	100.0	
249.3	255.3	6.0	6.0	100.0	
255.3	261.3	6.0	6.0	100.0	
261.3	267.3	6.0	6.0	100.0	
267.3	273.3	6.0	6.0	100.0	
273.3	279.3	6.0	6.0	100.0	
279.3	282.3	3.0	2.8	93.3	
282.3	286.6	4.3	4.3	100.0	
286.6	291.3	4.7	4.7	100.0	
291.3	297.3	6.0	6.0	100.0	
297.3	303.3	6.0	6.0	100.0	
303.3	307.5	4.2	4.2	100.0	
307.5	311.8	4.3	4.3	100.0	
311.8	318.3	6.5	6.5	100.0	
318.3	321.2	2.9	2.9	100.0	
321.2	327.1	5.9	5.9	100.0	
327.1	329.3	2.2	2.2	100.0	
329.3	333.1	3.8	3.8	100.0	

Table 1.3. Core recovery from Woodleigh 2 and 2A

<i>Interval</i>		<i>Metres drilled</i>	<i>Metres recovered</i>	<i>Recovery rate (%)</i>	<i>Remarks</i>
<i>From (m)</i>	<i>To (m)</i>				
193.0	198.0	5.0	2.3	46.0	Woodleigh 2
270.0	271.9	1.9	1.4	73.7	Woodleigh 2A
271.9	276.3	4.4	4.2	95.5	
276.3	282.1	5.8	5.2	89.7	
282.1	286.2	4.1	3.5	85.4	
286.2	291.3	5.1	5.1	100.0	
291.3	297.3	6.0	5.9	98.3	
297.3	303.3	6.0	6.0	100.0	
303.3	309.3	6.0	6.0	100.0	
309.3	311.8	2.5	2.5	100.0	
311.8	317.3	5.5	6.4	116.4	
317.3	321.3	4.0	3.5	87.5	
321.3	325.5	4.2	4.2	100.0	
325.5	327.4	1.9	1.9	100.0	
327.4	329.5	2.1	2.1	100.0	
329.5	333.3	3.8	3.5	92.1	
333.3	338.8	5.5	5.2	94.5	
338.8	340.0	1.2	1.1	91.7	

Table 1.3. (continued)

<i>Interval</i>		<i>Metres drilled</i>	<i>Metres recovered</i>	<i>Recovery rate (%)</i>	<i>Remarks</i>
<i>From (m)</i>	<i>To (m)</i>				
340.0	342.6	2.6	2.5	96.2	
342.6	346.0	3.4	3.2	94.1	
346.0	349.8	3.8	3.4	89.5	
349.8	354.3	4.5	3.5	77.8	
354.3	358.2	3.9	2.5	64.1	
358.2	361.2	3.0	2.0	66.7	
361.2	366.3	5.1	5.0	98.0	
366.3	367.5	1.2	0.8	66.7	
367.5	372.2	4.7	3.7	78.7	
372.2	373.9	1.7	1.2	70.6	
373.9	377.6	3.7	2.5	67.6	
377.6	380.8	3.2	2.7	84.4	
380.8	381.9	1.1	0.7	63.6	
381.9	387.3	5.4	5.4	100.0	
387.3	391.3	4.0	3.3	82.5	
391.3	393.3	2.0	2.0	100.0	
393.3	398.0	4.7	4.7	100.0	
398.0	399.5	1.5	1.4	93.3	
399.5	402.3	2.8	2.1	75.0	
402.3	403.5	1.2	1.1	91.7	
403.5	408.3	4.8	4.0	83.3	
408.3	413.3	5.0	6.3	126.0	
413.3	417.3	4.0	3.0	75.0	
417.3	420.3	3.0	2.1	70.0	
420.3	422.1	1.8	1.3	72.2	
422.1	426.3	4.2	4.0	95.2	
426.3	432.5	6.2	4.6	74.2	
432.5	435.6	3.1	2.3	74.2	
435.6	438.3	2.7	2.3	85.2	
438.3	443.8	5.5	5.4	98.2	
443.8	447.3	3.5	3.4	97.1	
447.3	453.3	6.0	5.6	93.3	
453.3	459.9	6.6	6.2	93.9	
459.9	465.3	5.4	5.1	94.4	
465.3	469.3	4.0	4.0	100.0	
469.3	474.3	5.0	5.1	102.0	
474.3	480.3	6.0	6.0	100.0	
480.3	486.3	6.0	6.0	100.0	
486.3	489.4	3.1	3.1	100.0	
489.4	495.3	5.9	5.9	100.0	
495.3	501.3	6.0	6.0	100.0	
501.3	507.3	6.0	3.9	65.0	
507.3	513.3	6.0	2.6	43.3	
513.3	516.9	3.6	2.4	66.7	
516.9	522.3	5.4	2.2	40.7	
522.3	528.3	6.0	6.0	100.0	
528.3	534.3	6.0	5.1	85.0	
534.3	539.6	5.3	5.3	100.0	
539.6	543.3	3.7	3.6	97.3	
543.3	547.4	4.1	4.1	100.0	
547.4	552.3	4.9	4.9	100.0	
552.3	558.3	6.0	5.8	96.7	
558.3	564.3	6.0	5.3	88.3	
564.3	567.5	3.2	3.2	100.0	
567.5	573.3	5.8	5.7	98.3	
573.3	578.2	4.9	4.6	93.9	
578.2	582.3	4.1	4.1	100.0	
582.3	588.2	5.9	5.8	98.3	
588.2	594.3	6.1	6.1	100.0	
594.3	596.5	2.2	2.2	100.0	
596.5	597.6	1.1	1.1	100.0	
597.6	600.2	2.6	2.6	100.0	
600.2	604.1	3.9	3.9	100.0	
604.1	608.2	4.1	4.1	100.0	
608.2	612.3	4.1	4.1	100.0	
612.3	618.3	6.0	6.0	100.0	

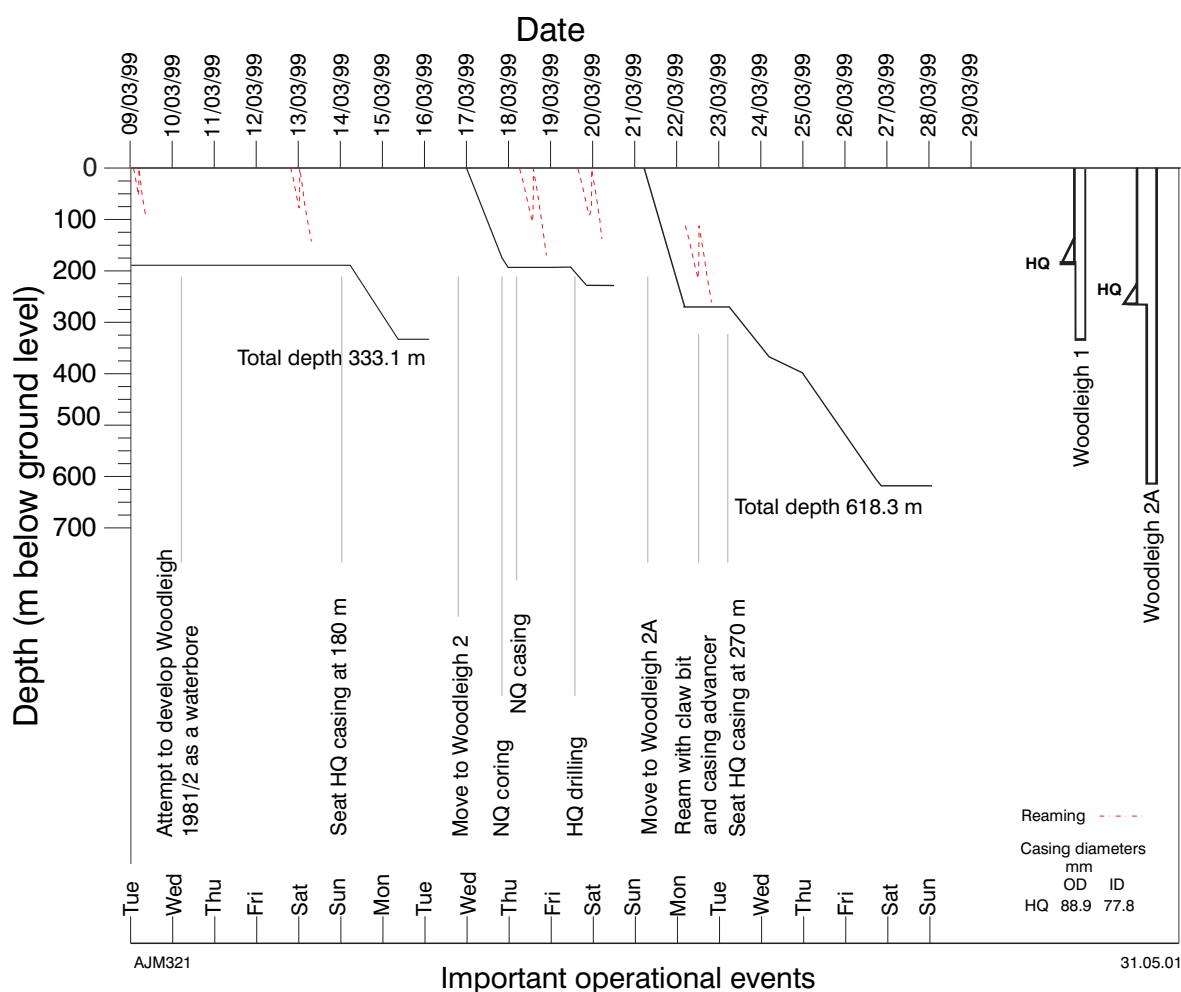


Figure 1.1. Time versus depth curve for Woodleigh 1 and 2A

## Casing

The casing strings used in Woodleigh 1, 2, and 2A are shown in Tables 1.4 and 1.5, and are depicted graphically in Figures 1.1 and 1.2 respectively, which also indicate the time and order in which they were installed. The casing was only seated temporarily so that it could be removed before abandonment. The strings were not cemented because hydrocarbons were not expected in these wells.

## Orientation surveys

Due to the instability of the holes, Eastman Camera surveys were run at irregular depths in Woodleigh 2A (Table 1.6) to measure the orientation of the hole. The azimuth plot at the top does not show the depths of individual points and is meant to show only the general direction of deviation. The hole consistently deviated to the north, although within only one degree from the true vertical, consistent with near-horizontal bedding at the site.

## Geophysical logging

The logs recorded by Geophysical Logging Technologies are shown in Tables 1.7 and 1.8. Logging of Woodleigh 1 was left until Woodleigh 2A was completed, but the hole had collapsed below 92 m. Woodleigh 2A could be safely entered only within the drill string to 612.6 m, so that the gamma and density tools could be used. Once the drill string was removed the hole

**Table 1.4. Casing strings used in Woodleigh 1**

<i>Casing</i>	<i>Outer diameter (mm)</i>	<i>Inner diameter (mm)</i>	<i>Depth interval (m)</i>
PVC	100.0	99.5	0–54
HQ	88.9	77.8	0 – 190.5

**Table 1.5. Casing strings used in Woodleigh 2A**

<i>Casing</i>	<i>Outer diameter (mm)</i>	<i>Inner diameter (mm)</i>	<i>Depth interval (m)</i>
PVC	140.0	139.5	0–6
PVC	100.0	99.5	0–30
HQ	88.9	77.8	0–270

**Table 1.6. Eastman camera  
directional-survey results  
for Woodleigh 2A**

<i>Depth (m)</i>	<i>Dip (degrees)</i>	<i>Azimuth (degrees)</i>
291.3	88	228
344.9	88	41
618	88	43

**Table 1.7. Geophysical logging of  
Woodleigh 1**

<i>Logs</i>	<i>Intervals logged (m)</i>
Gamma	92–0
Temperature	92–0
Calliper	92–0

**Table 1.8. Geophysical logging of  
Woodleigh 2A (through  
drillstring)**

<i>Logs</i>	<i>Intervals logged (m)</i>
Density	618.6 – 0
Gamma	618.6 – 0
Temperature	618.6 – 0
Calliper	618.6 – 0



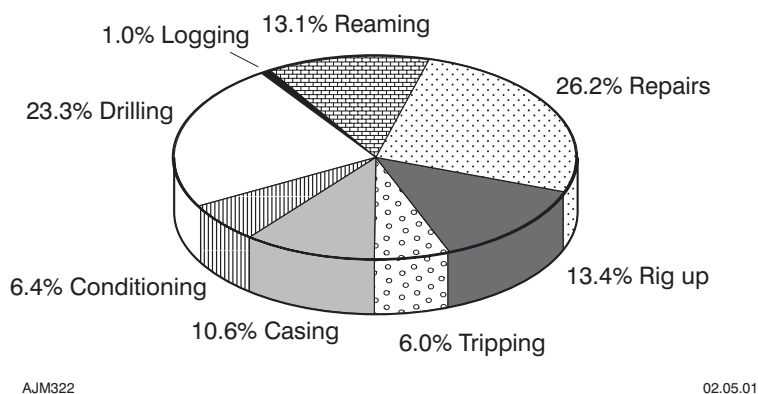


**Figure 1.2. Breakdown of operation time for Woodleigh 1**

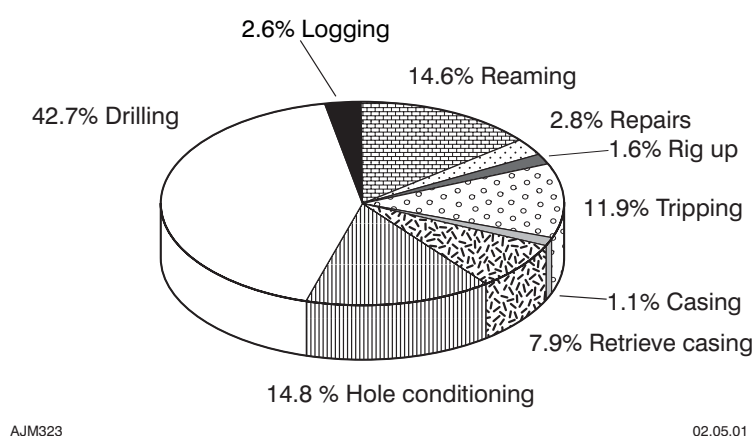


**Figure 1.3. Breakdown of operation time for Woodleigh 2 and 2A**

collapsed below 400 m. As the hole was cased to 270 m, an attempt was made to remove at least part, but after 6 m was extracted the casing became stuck and no further logging was considered feasible. After logging of Woodleigh 2A, 130 m of HQ casing was retrieved leaving HQ casing between 140 and 264 m. It was not possible to re-enter Woodleigh 2.

## Operation-time analysis

The relative duration of the operational activities for Woodleigh 1 is shown in Figure 1.2 and for Woodleigh 2 and 2A in Figure 1.3.

## Well completion

Woodleigh 1 and 2A were completed on 15 March 1999 and 27 March 1999 respectively, with all free casing and drill strings pulled out. Woodleigh 1 was left open for possible use as a waterbore. At Woodleigh 2 and 2A, a 10 cm-diameter PVC pipe was left at the top of the hole with a capped steel pipe cemented over it. The well names and total depths are recorded at the sites.

## Reference

LAYTON AND ASSOCIATES, 1981, Well completion report EP169: Woodleigh 1981/2 south Carnarvon Basin, W.A.: Western Australia Geological Survey, Statutory petroleum exploration report, S2075 A1 (unpublished).

## Appendix 2

### Impact terminology

by F. Pirajno

#### Introduction

Given that the terminology associated with impact structures has evolved dramatically in the last decade, the interested reader is referred to Melosh (1989) and French (1998) for comprehensive texts on impacts as a geological process. Other useful publications include Grieve (1990, 1994, 1997), Glikson (1993, 1996), Grieve et al. (1996), Koeberl and Anderson (1996), and Grady et al. (1998).

Impacts on planetary surfaces by celestial objects (such as asteroids or comets, collectively referred to as meteoroids or bolides) form craters, whose morphology are directly dependent on the size (diameter) of the impactor. The term 'hypervelocity impact crater' refers to the 'structure formed by a projectile that is large enough and coherent enough to penetrate the Earth's atmosphere with little or no deceleration, and to strike the ground at virtually its original cosmic velocity ( $>11$  km/s)' (French, 1998, p. 17). Three main types of crater morphologies are recognized: simple, complex, and multi-ringed. A fourth type, characterized by elliptical crater structures, is the product of impact angles of less than  $5^\circ$  from the horizontal, but these comprise less than 1% of known structures (Bottke et al., 2000). Simple impact craters are 'bowl-shaped' depressions, less than a few kilometres in diameter with a circular outline and uplifted rim, and are formed by impactors commonly less than 100 m in diameter. Well-known examples are the Meteor or Barringer Crater (1.2 km diameter) in Arizona (Shoemaker, 1963) and the Wolfe Creek (0.9 km diameter) crater in Western Australia (Guppy and Matheson, 1949; Albritton, 1989). It is important to note that the simple crater morphology is also dependent on the size, and hence, gravity of the target planetoid. Thus, a bolide comparable in size to that responsible for a simple crater on the Moon may produce a complex crater in the higher gravity of the Earth. Complex craters are formed by larger bolides (kilometre size) and are characterized by a central uplift and a flat floor surrounded by terraced rims; examples of complex craters can be observed on the Moon, such as Theophilus (diameter = 100 km). On Earth, an example of a complex structure is the Ries Crater in Germany. Multi-ring structures are the largest craters (few hundred kilometres) and have two or more rims inside an outer rim. On Earth, the only structures that claim to be in this category are Chicxulub (Gulf of Mexico; Morgan et al., 1997), Manicouagan (Quebec, Canada; Grieve and Head, 1983), Vredefort (southern Africa; Reimold and Gibson, 1996), Morokweng (southern Africa; Corner et al., 1997), and Woodleigh (Mory et al., 2000a,b).

#### Shatter cones

Shatter cones, diaplectic glass, pseudotachylite veins, and planar microstructures are produced by high-shock events and considered diagnostic of hypervelocity impacts.

Shatter cones are cone-shaped fractures in the shocked rocks, ranging in length from a few centimetres to several metres (Melosh, 1989). The striations and fractures that characterize shatter cones typically point toward the apex of the cone, and are considered diagnostic of meteorite impacts in non-sedimentary rocks, mainly because these are rheologically weaker than igneous or metamorphic rocks (French, 1998). None have been found in the Woodleigh impact structure.

## Diaplectic glass

Diaplectic glass is said of minerals ‘in which the crystal structure has been affected by the passage of a shock wave’ (Jackson, 1997) and is converted to an amorphous glass phase. Such glass is optically isotropic, preserves the original texture of the affected crystal, and forms at higher shock pressures (35–45 GPa) than planar microstructures (French, 1998). Diaplectic plagioclase glass is called maskelynite, of which good examples are observed in the shocked granitoid of the Woodleigh impact structure. Recent work (Chen and El Goresy, 2000) suggests that maskelynite may not always be diaplectic glass, but a dense, quenched melt. Pseudotachylite is typically found in low-porosity rocks (e.g. granite, gneiss) and is a ‘glassy or very fine grained fault rock ... that forms by local melting of the rock along a brittle fault plane, due to heat generated by rapid frictional sliding’ (Passchier and Trouw, 1996, p. 99–102). Pseudotachylite forms irregular veins and dyke-like bodies containing large and small, angular to resorbed fragments in an aphanitic, dark and glassy groundmass. Whereas tectonically formed pseudotachylites are mostly composed of breakdown products of wallrocks, impact-related pseudotachylite can show extensive resorption features attributed to shock fusion. The two types were defined by Spray (1998) as E-type and S-type pseudotachylites respectively. More than one type of pseudotachylite may be present in impact structures: the S-type associated with shock fusion and the E-type, consequent on friction-induced comminution, accompanied by a small amount of fusion (Spray, 1998).

## Planar microstructures

Planar microstructures are found commonly in silicate minerals (e.g. quartz, feldspar) within the target rocks. In quartz, planar microstructures are of two types: planar microfractures and planar deformation features (French, 1998). The former are multiple planar ‘cracks’ or ‘cleavages’ that develop at the lowest pressure of shock waves (5–8 GPa), with the cracks or cleavages being spaced about 5–20 µm apart. Planar fractures are not diagnostic of meteorite impacts (French, 1998). Planar deformation features (PDFs) are microstructures that form multiple sets of very narrow planar features and, therefore, are not cleavages or fractures. The spacing between individual planar features is roughly less than 2–10 µm (French, 1998), and their presence is considered as one of the most important diagnostic criteria for the recognition of impact structures (Stöffler and Langehorst, 1994). PDFs form at pressures in excess of 7 GPa (commonly around 20–30 GPa; French, 1998). However, strictly speaking, the presence of PDFs alone is not sufficient to argue that they are the product of hypervelocity impacts. Because PDFs in impactites form along crystallographic planes in the crystal lattice, it is desirable to measure the orientation of PDFs in individual grains and statistically establish their frequency along specific planes to confirm the impact origin of such rocks (Stöffler and Langehorst, 1994). Such a study, however, is beyond the scope of this Record.

## References

- ALBRITTON, C. C., 1989, Catastrophic episodes in Earth history: London, Chapman and Hall, 221p.
- BOTTKE, W. F., LOVE, S. G., and TYTELL, D., 2000, Interpreting the elliptical crater populations on Mars, Venus and the Moon: *Icarus*, v. 145, p. 108–121.
- CHEN, M., and EL GORESY, A., 2000, The nature of maskelynite in shocked meteorites: not diaplectic glass but a glass quenched from shock-induced dense melt at high pressures: *Earth and Planetary Science Letters*, v. 179, p. 489–502.
- CORNER, B., REIMOLD, W. U., BRANDT, D., and KOELBERL, C., 1997, Morokweng impact structure, Northwest Province, South Africa: geophysical imaging and shock petrographic studies: *Earth and Planetary Science Letters*, v. 146, p. 351–364.
- FRENCH, B. M., 1998, Traces of catastrophe – a handbook of shock-metamorphic effects in terrestrial meteorite impact structures: LPI Contribution No. 954, Lunar and Planetary Science Institute, Houston, 120p.
- GLIKSON, A. Y., 1993, Asteroids and early Precambrian crustal evolution: *Earth Science Reviews*, v. 35, p. 285–319.
- GLIKSON, A. Y., (compiler), 1996, A compendium of Australian impact structures, possible impact structures, and ejecta occurrences: *AGSO Journal of Australian Geology and Geophysics*, Thematic Issue: Australian impact structures, v. 16, no. 4, p. 371–625.

- GRADY, M. M., HUTCHISON, R., McCALL, G. J. H., and ROTHERY, D. A., (editors), 1998, Meteorites: flux with time and impact effects: Geological Society of London, Special Publication, no. 140, 278p.
- GRIEVE, R. A. F., 1990, Impact cratering on the Earth: *Scientific American*, v. 262, p. 44–51.
- GRIEVE, R. A. F., 1994, Impact: a natural hazard in planetary evolution: *Episodes*, v. 17, p. 9–17.
- GRIEVE, R. A. F., 1997, Extraterrestrial impact events: the record in the rocks and the stratigraphic column: *Palaeogeography, Palaeoclimatology, Palaeoecology*, v. 132, p. 5–23.
- GRIEVE, R. A. F., and HEAD, J. W., 1983, The Manicouagan impact structure: an analysis of its original dimension and form: *Journal of Geophysical Research*, v. 88, p. A807–A818.
- GRIEVE, R. A. F., LAGENHORST, F., and STÖFFLER, D., 1996, Shock metamorphism of quartz in nature and experiment: II. Significance in geoscience: *Meteoritics and Planetary Science*, v. 31, p. 6–35.
- GUPPY, D. J., and MATHESON, R. S., 1949, Wolfe Creek meteorite crater: Australia BMR, Geology and Geophysics, Report no. 1949/13, Geological Series no. 8, 5p.
- JACKSON, J. A., 1997, Glossary of Geology, fourth edition: Alexandria, Virginia, American Geological Institute, 769p.
- KOEBERL, C., and ANDERSON, R. R., 1996, The Manson impact structure, Iowa: anatomy of an impact crater: Geological Society of America, Special Paper 302, 468p.
- MELOSH, H. J., 1989, Impact cratering — A geological process: Oxford Monographs on Geology and Geophysics, no. 11, 245p.
- MORGAN, J., WARNER, M., THE CHICXULUB WORKING GROUP, BRITTAN, J., BUFFLER, R., CAMARGO, A., CHRISTESON, G., DENTON, P., HILDEBRAND, A., HOBBS, R., MACINTYRE, H., MACKENZIE, G., MAGUIRE, P., MARIN, L., NAKAMURA, Y., PILKINGTON, M., SHARPTON, V., SNYDER, D., SUAREZ, G., and TREJO, A., 1997, Size and morphology of the Chicxulub impact crater: *Nature*, v. 390 (6659), p. 472–476.
- MORY, A. J., IASKY, R. P., GLIKSON, A. Y., and PIRAJNO, F., 2000a, Woodleigh, Carnarvon Basin, Western Australia: a new 120 km-diameter impact structure: *Earth and Planetary Science Letters*, v. 177 (1–2), p. 119–128.
- MORY, A. J., IASKY, R. P., GLIKSON, A. Y., and PIRAJNO, F., 2000b, Response to ‘Critical comment on A. J. Mory et al., 2000, Woodleigh, Carnarvon Basin, Western Australia: a new 120 km-diameter impact structure’, by W. U. Reimold and C. Koeberl: *Earth and Planetary Science Letters*, v. 184 (1), p. 359–365.
- PASSCHIER, C. W., and TROUW, R. A. J., 1996, *Microtectonics*: Berlin, Springer-Verlag, 298p.
- REIMOLD, W. U., and GIBSON, R. L., 1996, Geology and evolution of the Vredefort impact structure: *South African Journal of African Earth Sciences*, v. 23, p. 125–162.
- SHOEMAKER, E. M., 1963, Impact mechanics at Meteor Crater, Arizona, in *The Solar System*, vol. 4 edited by B. MIDDLEHURST and G. P. KUIPER: Chicago University Press, p. 301–336.
- SPRAY, J. G., 1998, Localised shock- and friction-induced melting in response to hypervelocity impact, in *Meteorites: flux with time and impact effects* edited by M. M. GRADY, R. HUTCHISON, G. J. H. McCALL, and D. A. ROTHERY: Geological Society of London, Special Publication, no. 140, p. 195–204.
- STÖFFLER, D., and LANGEHORST, F., 1994, Shock metamorphism of quartz in nature and experiment: I. Basic observation and theory: *Meteoritics*, v. 29, p. 155–181.

## Appendix 3

### Petrology

by F. Pirajno

#### Introduction

Twenty-six core samples from Woodleigh 1 were collected from depths ranging from 191 to 310 m. These core samples include variably fractured and brecciated, biotite-rich gneissic granite, weakly foliated, fine-grained biotite granite, and a leucocratic granitoid. At present, it is not possible to decide whether the gneissic fabric of the granitoid rocks is due to tectonic or impact shock effects. Penetrative pseudotachylite–microbreccia veinlets are present in some of the samples. In addition, 21 samples were collected from the core of Woodleigh 2A.

In this Appendix, the petrography of 21 samples from Woodleigh 1 and nine from Woodleigh 2A is briefly discussed in the order in which they were penetrated. The position of the samples studied from Woodleigh 1 is shown in Figure 3.1. Samples from the same core in Woodleigh 1 were also analysed for major and trace elements at the Genalysis laboratory in Perth (this Appendix) and at the Research School of Earth Sciences, Australian National University (Appendix 5). Details of analytical methods and results are provided in Tables 4.1 and 4.2. In addition, four biotite granite gneiss samples were investigated by scanning electron microscopy (SEM) coupled with energy dispersive spectrometry (EDS), using the Jeol-6400 system at the Research School of Biological Science, Australian National University (Glikson et al., in prep.). Results of EDS analyses are discussed in Appendix 5. Utilizing the available petrographic and geochemical data, the principal shock and geochemical characteristics of impact-shocked materials are briefly treated in the last section of this Appendix.

#### Woodleigh 1 petrography

##### Depth 191.6 – 191.7 m. GSWA 149139

*Field name:* cataclastic/brecciated granite gneiss

*Main minerals:* quartz, plagioclase, microcline, biotite

*Accessories:* chlorite

*Description:* Interlocking assemblage consisting of shocked quartz and feldspar (plagioclase and microcline), with interstitial brown biotite. Biotite streaks and lenses form a tight fold. Feldspars appear locally to be partly melted (glass) and have developed PDFs at low angle to growth twins; they generally have a ‘blotchy’ appearance and are clouded by fine dustings of dark- to light-brown fluid inclusions. Microcline forms bent and fractured crystals. Quartz forms irregularly shaped grains (4–5 mm long) that are highly strained, extensively fractured, deformed, brecciated, and have glass (melt) patches, and most with sets of PDFs (Fig. 3.2a). Microfractures are common and form networks. Some contain unidentified tiny crystals (?corundum). Quartz grains locally show cataclastic breakages, commonly along margins; others are filled with fibrous quartz (indicating extension). Biotite forms streaks or bands; kinked and bent crystals, fractured in places; and in margins altered to chlorite. Small ?apatite, ?corundum, and a high relief mineral are fractured and perhaps partly melted. Also, there is a high relief isotropic mineral, anhedral and with a purplish tinge (not fluorite), associated with the glassy material.



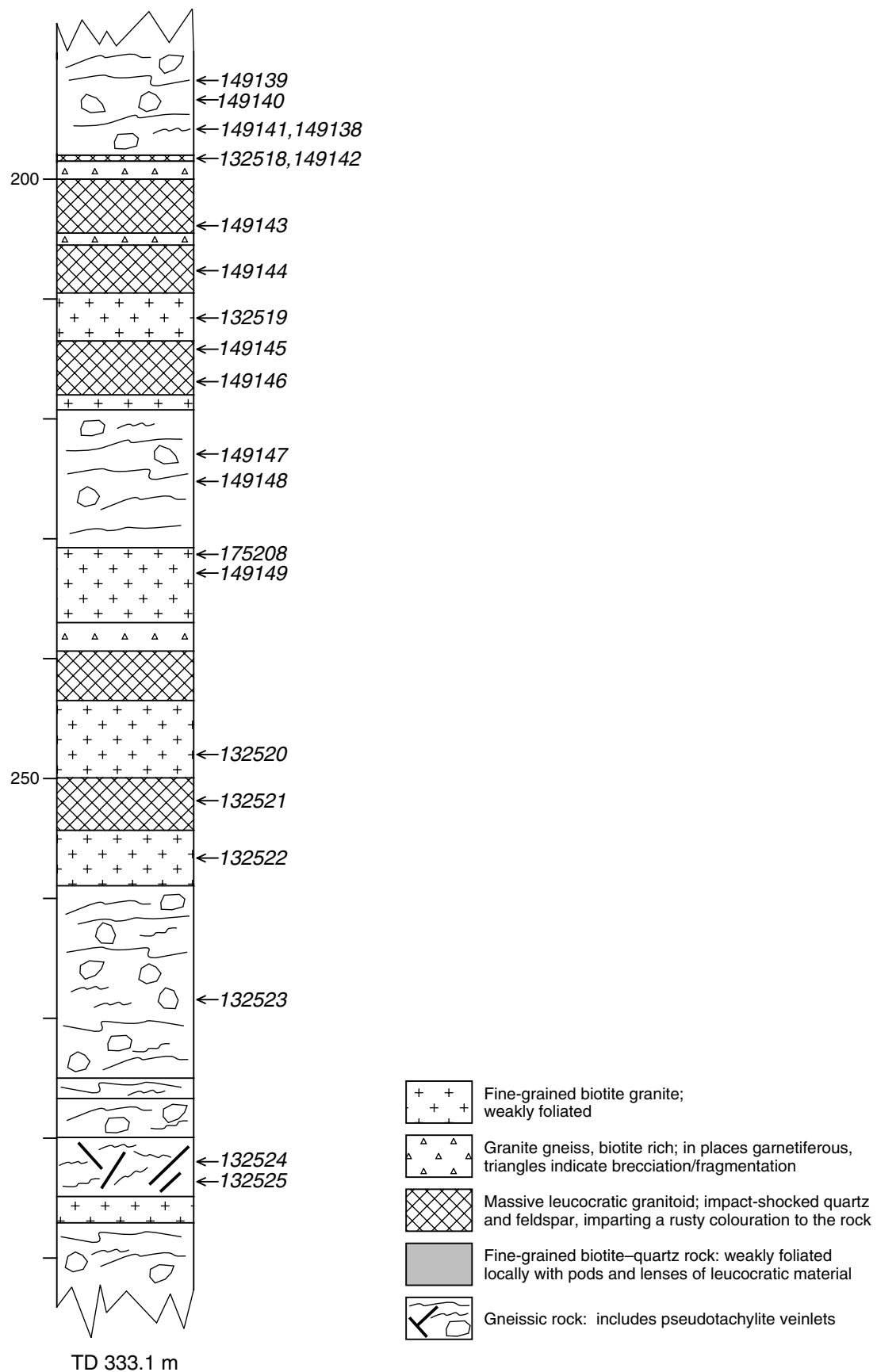
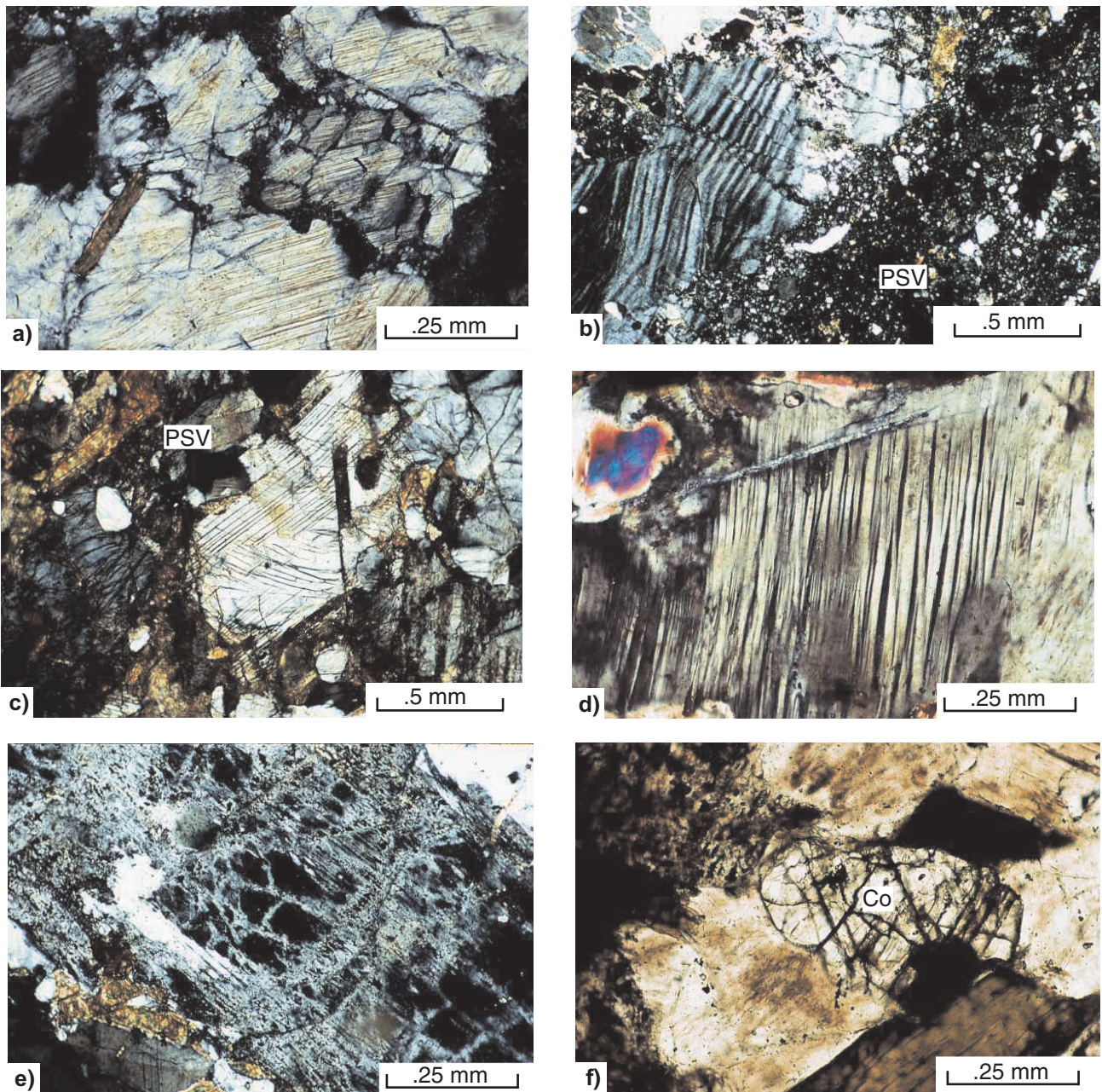


Figure 3.1. Log of granitoid basement in Woodleigh 1 showing position of samples



AJM357

13.02.01

**Figure 3.2.** Photomicrographs showing impact-related features in Woodleigh 1: a) GSWA 149139 (191.6 – 191.7 m), partly ?fused (dark material, glass, and diaplectic glass) quartz crystal with multiple sets of PDFs; cross polars; b) GSWA 149140 (193.7 – 193.8 m), S-type pseudotachylite vein (PSV) and plagioclase with deformed twin lamellae, possibly shock-induced; cross polars; c) GSWA 149141 (195.5 – 195.6 m), curved microfractures in plagioclase crystal, surrounded by PSV and resorbed crystals; cross polars; d) GSWA 149138 (195.6 – 195.8 m), deformed twin lamellae in plagioclase, possibly shock-induced; cross polars; e) GSWA 149138, reticulate texture of diaplectic plagioclase; cross polars; f) GSWA 149138, photomicrograph showing anhedral corundum crystal (Co); cross polars

### **Depth 193.7 – 193.8 m. GSWA 149140**

*Field name:* cataclastic/brecciated, coarse-grained granite gneiss, with pink K-feldspar-rich bands

*Main minerals:* quartz, microcline

*Accessories:* biotite, calcite, muscovite

*Description:* A quartz–microcline assemblage with accessory interstitial biotite. Feldspar is fractured, locally isotropic, blotchy, and has numerous fluid inclusions, which impart a strong turbidity to the crystals. Calcite blebs and granophyric (myrmekitic) intergrowths developed at margins of crystals or in cores. In one place, granophyric material formed at the margin of a microcline cut by pseudotachylite. Quartz is extensively fractured and contains multiple sets of PDFs. Isotropic glass, partially devitrified and recrystallized to a feldspar or granophyre, and with relicts of biotite, platelets of ‘polygonized’ quartz, some white mica, are all overprinted by late calcite. In one place, tiny ‘pits’ or spherules of unidentified material (average 9–10 µm, up to 37 µm) are embedded in shocked quartz. There is good evidence of grain boundary migration with the development of newly formed anhedral phases (commonly quartz) in the adjacent host crystal. There is a pseudotachylite veinlet (Fig. 3.2b) with abundant overprinting calcite. Muscovite fills microfractures and is associated with a late calcite.

### **Depth 195.5 – 195.6 m. GSWA 149141**

*Field name:* fine-grained, weakly foliated biotite granite

*Main minerals:* quartz, plagioclase, biotite

*Accessories:* calcite, muscovite, titanite

*Description:* Medium- to fine-grained rock; biotite defines a weak planar fabric. There is no K-feldspar in this rock. Bent, fractured plagioclase (oligoclase), commonly with deformation twin lamellae and PDFs; some plagioclase crystals have curved fractures (Fig. 3.2c), others have one set of twins. Reticulate diaplectic glass is locally developed in quartz crystals. Quartz crystals all have PDFs, either single or multiple sets. Quartz and feldspar are characterized by irregular, rounded resorbed edges infilled with glass material. Lobate grain boundaries and nucleation of a small, round quartz crystal in adjacent host is the result of grain boundary migration phenomena. Biotite is locally kinked or fractured, but otherwise appears undisturbed and redistributed to fill in cracks or microfractures in the rest of the rock. Calcite is either interstitial or overprints plagioclase; very minor muscovite is present predominantly in areas of partly fused or resorbed quartz.

### **Depth 195.6 – 195.8 m. GSWA 149138**

*Field name:* brecciated biotite granite and leucocratic granite with rust-brown patches

*Main minerals:* quartz, microcline, plagioclase, biotite

*Accessories:* muscovite, corundum, calcite

*Description:* Weak foliation defined by biotite; there is fragmentation, fracturing, and bending of crystals. Twinning lamellae in feldspar crystals are either shock-induced or deformed twins (Fig. 3.2d); common partly melted feldspars healed by newly formed quartz. Diaplectic glass is present in plagioclase (glass material produced by shock waves; Figs 3.2d and e). There are zones of opaque dustings (possibly apatite or corundum), which under high power (×50) appear as colourless, minute crystal fragments, from 27 to 7 µm across (average 14 µm); these may be tiny corundum crystals. Optically identified, isolated corundum crystals (0.5 mm across) are present (Fig. 3.2f). Biotite is fractured and kinked. Quartz and feldspar grains are shattered, deformed, and exhibit PDFs. Minor muscovite is present.



## Depth 198.0 – 198.5 m. GSWA 132518

*Field name:* pink, brecciated K-feldspar–biotite granite

*Main minerals:* quartz, K-feldspar, plagioclase, biotite

*Accessories:* muscovite, zircon, corundum, calcite, opaque minerals

*Description:* Quartz and feldspar form large plates (centimetre size) that are surrounded by a finer grained, granular aggregate of quartz–feldspar–biotite. Crystals of quartz, showing multiple sets of PDFs, K-feldspar, and plagioclase are intensely fractured; the plagioclase shows irregular ?K-feldspar domains that obliterate the albite twins, suggesting replacement. Fractures form networks and are filled with zeolite crystals, cryptocrystalline silica, and calcite, and post-date the PDFs (Fig. 3.3a). Most PDFs are decorated with trails of fluid inclusions. Biotite is also fractured or kinked. Zircon crystals display one set of PDFs (Fig. 3.3b). A corundum crystal is unaffected by shock metamorphism and may be a product of post-impact alteration. Submicroscopic grains of iron oxides are included in the fractured quartz and feldspar grains.

## Depth 198.35 – 198.5 m. GSWA 149142

*Field name:* cataclastic/brecciated granite gneiss (biotite-rich zones chaotically interlayered with leucosome)

*Main minerals:* quartz, feldspar, biotite

*Accessories:* calcite, opaque minerals

*Description:* In this section there are two zones: leucocratic and melanocratic. The two zones are separated by a late calcite veinlet. The leucocratic zone consists of a coarse-grained, granular mosaic of quartz and feldspar with interstitial, green biotite and microfracture-filling calcite. Quartz exhibits multiple sets of PDFs, whereas the feldspar has deformation twins; well-developed, reticulate diaplectic glass texture affects both quartz and feldspar (Fig. 3.3c). The melanocratic zone contains biotite, which defines a foliation, with abundant anhedral quartz grains and minor feldspar, with isotropic patches (glass). Biotite has green–brown pleochroism. This part of the section is possibly a quartz–biotite schist (?xenolith or enclave in granite). A veinlet of opaque material (possibly pyrite, reflected light work is necessary to confirm this) crosscuts the quartz–biotite schist. The quartz has sets of PDFs. Most biotite appears fresh and undeformed; however, a few crystals do show kinking and fracturing.

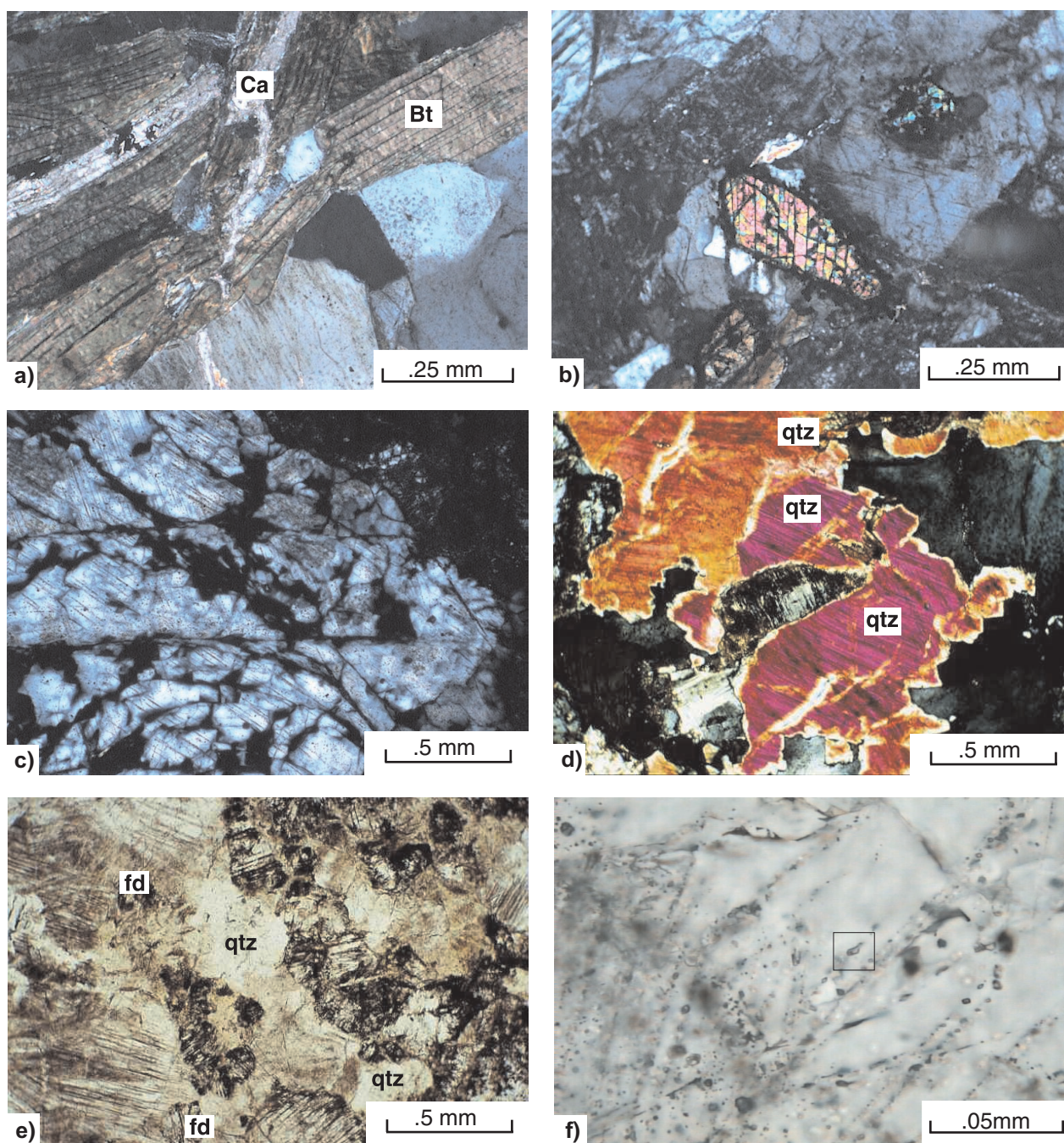
## Depth 203.85 – 203.9 m. GSWA 149143

*Field name:* leucocratic granite with rust-brown patches

*Main minerals:* quartz, K-feldspar, microcline, plagioclase

*Accessories:* calcite, muscovite, biotite

*Description:* An irregular, granoblastic-like aggregate formed by an assemblage consisting of large K-feldspar (orthoclase, locally poikilitic), microcline, and plagioclase plates is embedded and in places surrounded by anhedral, round quartz grains, all with PDFs. Feldspars are blotchy (brown to dark brown), turbid, and have shock-induced deformation lamellae. Orthoclase displays rotation and dislocation twins. There are local granophyric intergrowths. Muscovite forms sheaves of crystals at grain boundaries and replaces edges of feldspar or quartz crystals; muscovite also forms bunches of crystals associated with shocked quartz–feldspar assemblage. Biotite is minor and interstitial. Calcite forms veinlets or as interstitial material.



AJM358

13.02.01

**Figure 3.3.** Photomicrographs showing impact-related features in Woodleigh 1: a) GSWA 132518 (198.0 – 198.5 m), calcite (Ca) replacing biotite (Bt), probably the result of post-impact hydrothermal alteration; cross polars; b) GSWA 132518, zircon crystal with one set of possible PDFs, note surrounding PDFs in quartz and patches of diaplectic glass; cross polars; c) GSWA 149142 (198.35 – 198.5 m), good example of diaplectic glass in quartz (dark isotropic areas are glass); cross polars; d) GSWA 149144 (208.0 – 208.1 m), shocked quartz crystals (qtz) with multiple sets of PDFs; cross polars; e) GSWA 149144, shocked dark-brown feldspars (fd) and quartz (qtz) with PDFs. The brown colouration is due to the presence of abundant fluid inclusions and iron oxides, which impart a rusty appearance to the rock (see also Figs 3.4 and 3.5); cross polars; f) GSWA 149144, PDFs in quartz, decorated with fluid inclusions, boxed area shows a two-phase inclusion (L+V); cross polars



## Depth 208.0 – 208.1 m. GSWA 149144

*Field name:* fine-grained leucocratic granite

*Main minerals:* quartz, plagioclase, K-feldspar

*Accessories:* biotite, chlorite, calcite, corundum

*Description:* This sample has an irregular to chaotic aggregate of quartz, K-feldspar, and plagioclase crystals with abundant PDFs (Fig. 3.3d). Plagioclase and K-feldspar have a blotchy and brown cloudy appearance, due to iron oxide dustings and, in places, abundant fluid inclusions (Fig. 3.3e). Reticulate diaplectic glass textures are present in some quartz crystals. PDFs in quartz are decorated with fluid inclusions, mostly one-phase (liquid; L) and less commonly two-phase (liquid + gas; L + V) inclusions (Fig. 3.3f). Minor biotite and muscovite crystals display intense and chaotic fracturing, which are most probably shock features. Some muscovite is present at grain boundaries. Minor chlorite replaces biotite. Isolated, anhedral corundum crystals are present. There are late calcite overprints.

## Depth 211 m. GSWA 132519

*Field name:* fine-grained, greenish (sericitic) rock with patches or zones of leucocratic brown granite

*Main minerals:* sericite, anthophyllite, feldspar, quartz, epidote I

*Accessories:* titanite, calcite, apatite, epidote II

*Description:* Pervasively altered rock, mostly with sericite(–epidote; blue birefringence), is cut by later calcite veinlets. This alteration overprints shocked crystals. Sheaves of anthophyllite crystals (Fig. 3.4a), locally with single sets of planar microfractures, are associated with titanite crystals. Plagioclase and quartz are visible in small areas unaffected by the sericitic alteration. Epidote I occurs as fractured crystals. Yellow-brown quartz veinlets and patches (possibly devitrified glass) are present. There are isolated, euhedral apatite crystals, some with planar microfractures. Interstitial patches of quartz–albite crystals may relate to post-impact Na metasomatism. Late silica flooding overprints sericitic alteration. The alteration paragenesis is: quartz + albite → sericite ± epidote → silica flooding → calcite.

## Depth 213.25 – 213.4 m. GSWA 149145

*Field name:* medium-grained, leucocratic biotite granite with brown feldspars

*Main minerals:* quartz, microcline, plagioclase, biotite

*Accessories:* sericite, calcite

*Description:* Irregular aggregates of quartz and feldspar occur with interstitial biotite; large feldspar plates, with microfractures, are filled with calcite or granular quartz. Quartz is dark brown to brown due to abundant fluid inclusions. Feldspars also have PDFs and are locally and partly melted. PDFs are seen in quartz and shock-induced or shock-deformed twin lamellae in feldspars. Very fine grained sericite aggregates (late alteration product) commonly replace shocked feldspars. Sericite is overprinted by calcite. Biotite is kinked, but otherwise fresh. Crosscutting veinlets of pseudotachylite and calcite (mosaic of polygonal grains) are present; there are numerous calcite blebs.

## Depth 217.65 – 217.75 m. GSWA 149146

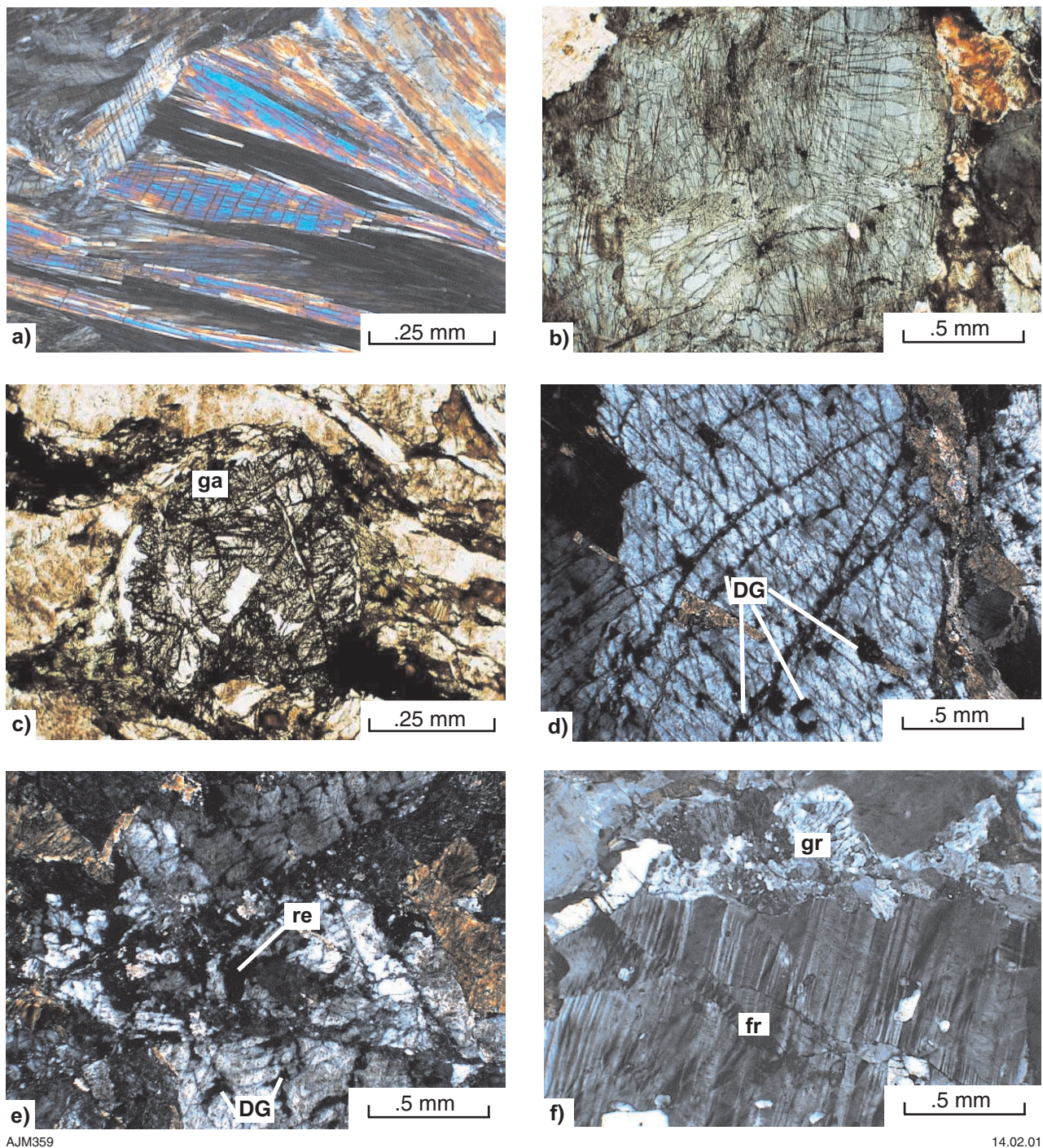
*Field name:* leucocratic biotite granite with rust-brown patches

*Main minerals:* microcline, plagioclase, quartz, biotite

*Accessories:* muscovite, corundum, chlorite

*Description:* The sample has a mylonitic to cataclastic texture with quartz ribbons interlayered with feldspars and biotite aggregates. Shocked quartz has PDFs and there are diaplectic feldspar





AJM359

14.02.01

**Figure 3.4.** Photomicrographs showing impact-related features in Woodleigh 1: a) GSWA 132519 (211 m), anthophyllite crystals displaying single sets of PDFs; cross polars; b) GSWA 149146 (217.65 – 217.75 m), photomicrograph showing shattered feldspar crystal with multiple sets of intersecting PDFs; cross polars; c) GSWA 149147 (222.35 – 222.5 m), garnet crystal (ga) in sheared, fragmented feldspars with melt veinlets (isotropic glass); cross polars; d) GSWA 149148 (224.9 – 225.0 m), diaplectic glass (DG), forming a reticulate texture in shocked feldspar; e) GSWA 149148, diaplectic glass (DG) grading into patches of resorbed material (re); f) GSWA 132521 (252.7 m), microfracture (fr) displacing shock lamellae in feldspar; interstitial patches of granophyric material (gr, quartz-feldspar crystallizing from a minimum melt; this could be a feature of the original granite — myrmekite); cross polars

(maskelynite), melt patches, and pseudotachylite veinlets. Partly fused feldspars are associated with an aggregate of round, droplet-like quartz–feldspars (equivalent of granophyre). Feldspars are also peppered with sericite flakes; locally sheaves of prehnite are present. Feldspar has a brown colouration; quartz is locally darker brown. This brown colouration appears to be due to the abundance of fluid inclusions, many of which decorate PDFs. Three types of fractures are present, from oldest to youngest (Fig. 3.4b): 1) PDFs, single or multiple sets; 2) multidirectional, stockwork-like or curved microfractures, locally filled with quartz; and 3) network-like microfractures, commonly infilled with late calcite. Fractures (1) and (2) are decorated with fluid inclusions. Muscovite is associated with biotite (?alteration). There are small, isolated corundum crystals and minor chlorite.

### **Depth 222.35 – 222.5 m. GSWA 149147**

*Field name:* cataclastic/brecciated biotite granite with leucocratic bands

*Main minerals:* feldspar, quartz, biotite, muscovite

*Accessories:* garnet, chlorite

*Description:* The sample is coarse grained, fractured, and sheared (almost a breccia); muscovite(–chlorite) form as irregular aggregates or along shear lines and microfractures (?hydrothermal). Quartz shows PDFs at a very fine scale; PDFs are almost obliterated or difficult to see because of crowding of numerous fluid inclusions, which impart a brown- or red-brown-coloured turbidity to the shocked quartz. Quartz also displays partial resorption. Both quartz and feldspar crystals show resorption features that typically result in a reticulate texture (with extinct patches being glass material), similar to that seen in high temperature rheo-ignimbrites as described in Pirajno (1990). Isolated garnet crystals (Fig. 3.4c) appear to be late post-tectonic and probably post-impact, locally overprinting opaque veinlets and silicate crystals. At least one corundum crystal (post-tectonic) is present.

### **Depth 224.9 – 225.0 m. GSWA 149148**

*Field name:* cataclastic/brecciated granite gneiss

*Main minerals:* plagioclase, K-feldspar, quartz, biotite

*Accessories:* calcite, muscovite, zircon

*Description:* The sample has a cataclastic-like texture with feldspar and quartz crystals wrapped around by biotite, with a crosscutting ?pseudotachylite veinlet. Shocked quartz has PDFs, commonly decorated with fluid inclusions; shocked feldspar shows the characteristic reticulate texture (Figs 3.4d and e) due to resorption or the presence of diaplectic glass or both, as described above for GSWA 149147. Biotite is fresh, but locally displays parallel fractures that may be either PDFs or a combination of kinking and cleavage. There is melting of plagioclase preferentially along one set of twin lamellae. Zircon forms as inclusions in biotite. Muscovite replaces biotite and feldspar has altered to fine sericite. Late calcite veinlets are present.

### **Depth 231.3 m. GSWA 175208**

*Field name:* grey, fine-grained mafic granitoid

*Main minerals:* hornblende, quartz, feldspar, biotite

*Accessories:* calcite, muscovite, magnetite, pyrite

*Description:* A granular assemblage of hornblende – brown biotite – feldspar, with lesser quartz, is cut by calcite veinlets. Disseminated magnetite blebs have ilmenite exsolution lamellae. The quartz, and to a lesser extent biotite, have PDFs; quartz commonly displays two sets of PDFs. Hornblende is turbid, extensively fractured, and locally has lost its green pleochroism. Microfractures in the hornblende form parallel sets resembling PDFs. Pyrite is present as



ehedral crystals associated with late calcite and as irregular blebs or infill of microfractures in magnetite crystals. Biotite is locally kinked and contains round zircon crystals, and is locally replaced by muscovite. Calcite and muscovite are post-impact minerals because they are not deformed or fractured.

### **Depth 232.9 – 233.05 m. GSWA 149149**

*Field name:* fine-grained biotite ?schist with bands of cataclastic granite gneiss

*Main minerals:* quartz, biotite, plagioclase, ?actinolite

*Accessories:* garnet, opaque minerals, zircon as inclusions in biotite, calcite

*Description:* The sample contains quartz–biotite–plagioclase mylonitic granitic gneiss, with fractured and displaced quartz grains and ribbons, separating biotite laminae. Biotite is commonly associated with opaque rods. There are shocked quartz grains (PDFs). Relicts of rounded feldspar (clast-like) have been replaced and altered to an assemblage of quartz, sericite, and ?prehnite. One part of the section contains common elongate and ‘damaged’ crystals, which probably represent actinolite, are greenish in colour with a high birefringence, medium relief, and an extinction angle ( $Z^{\circ}C$ ) of  $15^{\circ}$ . Euhedral garnet crystals possibly overprint the quartz–feldspar–biotite assemblage. Late, crosscutting calcite veinlets are present.

### **Depth 247.7 m. GSWA 132520**

*Field name:* fine-grained, leucocratic biotite granite

*Main minerals:* quartz, feldspar (plagioclase and K-feldspar), brown biotite

*Accessories:* epidote, sericite, calcite, chlorite, zircon

*Description:* The sample contains an assemblage of quartz, turbid plagioclase, K-feldspar, and biotite. Most quartz crystals, and less commonly feldspar, display single or multiple sets of PDFs. The PDFs in quartz are decorated with fluid inclusions. Patches of sericitic alteration are present. There is minor chlorite as alteration product of biotite. Epidote is present as interstitial grains. Zones of partly ?fused quartz–feldspar have been devitrified or recrystallized to a yellow-brown silica.

### **Depth 252.7 m. GSWA 132521**

*Field name:* leucocratic granite with rust-brown patches

*Main minerals:* quartz, microcline, biotite

*Accessories:* sericite, muscovite

*Description:* An interlocking, coarse-grained assemblage of quartz, microcline, and ?anorthoclase with interstitial accessory biotite(–muscovite) shows a mylonitic texture. Both quartz and microcline have single and multiple sets of PDFs (nearly all decorated with fluid inclusions, imparting a turbid appearance), and subgrain domains and deformation twins. Deformation twin lamellae also affect quartz crystals and appear to post-date the PDFs. These deformation twins may be due to post-impact stresses. These lamellae are in turn cut and displaced by later microfractures. There are dustings of sericite in the feldspars. Microfractures in feldspar crystals are healed by silica. Myrmekitic-like intergrowths replace quartz with PDFs and forms interstitial patches between quartz and microcline crystals (Fig. 3.4f). Partly ?fused and recrystallized material shows a typical mottled or blotchy appearance and has reticulate diaplectic glass (maskelynite).

## Depth 256.6 m. GSWA 132522

*Field name:* fine-grained amphibolite

*Main minerals:* quartz, plagioclase, green hornblende, biotite

*Accessories:* ilmenite, muscovite, calcite, chlorite

*Description:* The sample contains an assemblage of quartz–plagioclase–hornblende–biotite with a distinct planar fabric. All three minerals show shock metamorphic effects, such as kinking, microfracturing, and PDFs. Pre-impact veinlets cut through the rock and contain quartz or quartz–plagioclase with lesser biotite. The veinlet minerals are fractured, have PDFs, and the veinlet is displaced. Fractures are commonly filled with late calcite. Pseudotachylite veinlets are also present and displaced by later microshears. The biotite in the veinlets is altered to a pale-green chlorite (Fe–Mg chlorite with purple birefringence). About 5% vol. disseminated ilmenite blebs and elongate bodies are fractured and replaced along margins by rutile. Fractures in the ilmenite are locally filled with marcasite or pyrite. Scattered, minor chalcopyrite forms specks and as fracture infill. PDFs in shocked quartz are commonly decorated with abundant fluid inclusions, some of which are two phase (L + V) and about 5 µm across.

## Depth 269.2 m. GSWA 132523

*Field name:* granitic gneiss intermingled with bands of rust-brown granite

*Main minerals:* quartz, K-feldspar, microcline, biotite

*Accessories:* muscovite, illite, zircon

*Description:* The sample contains a coarse-grained quartz–feldspar–biotite assemblage that is extensively fractured and cut by numerous pseudotachylite and microbreccia veinlets. These minerals show varying degrees of shock-induced metamorphism in the form of isotropization (diaplectic glass), PDFs, and twin deformation lamellae. Typically, both shocked quartz and feldspar display a yellow-brown (rusty) colour in plane polarized light, probably due to a combination of finely disseminated iron oxides that have been expelled from the crystal lattice as a result of structural deformation, and the development of fluid inclusions. Muscovite is present as an alteration product and can be seen to replace biotite and to occur as neoformed sheaves that cut across shocked quartz (Fig. 3.5a). Fractured and rounded zircon crystals are associated with opaque minerals and locally with planar microstructures.

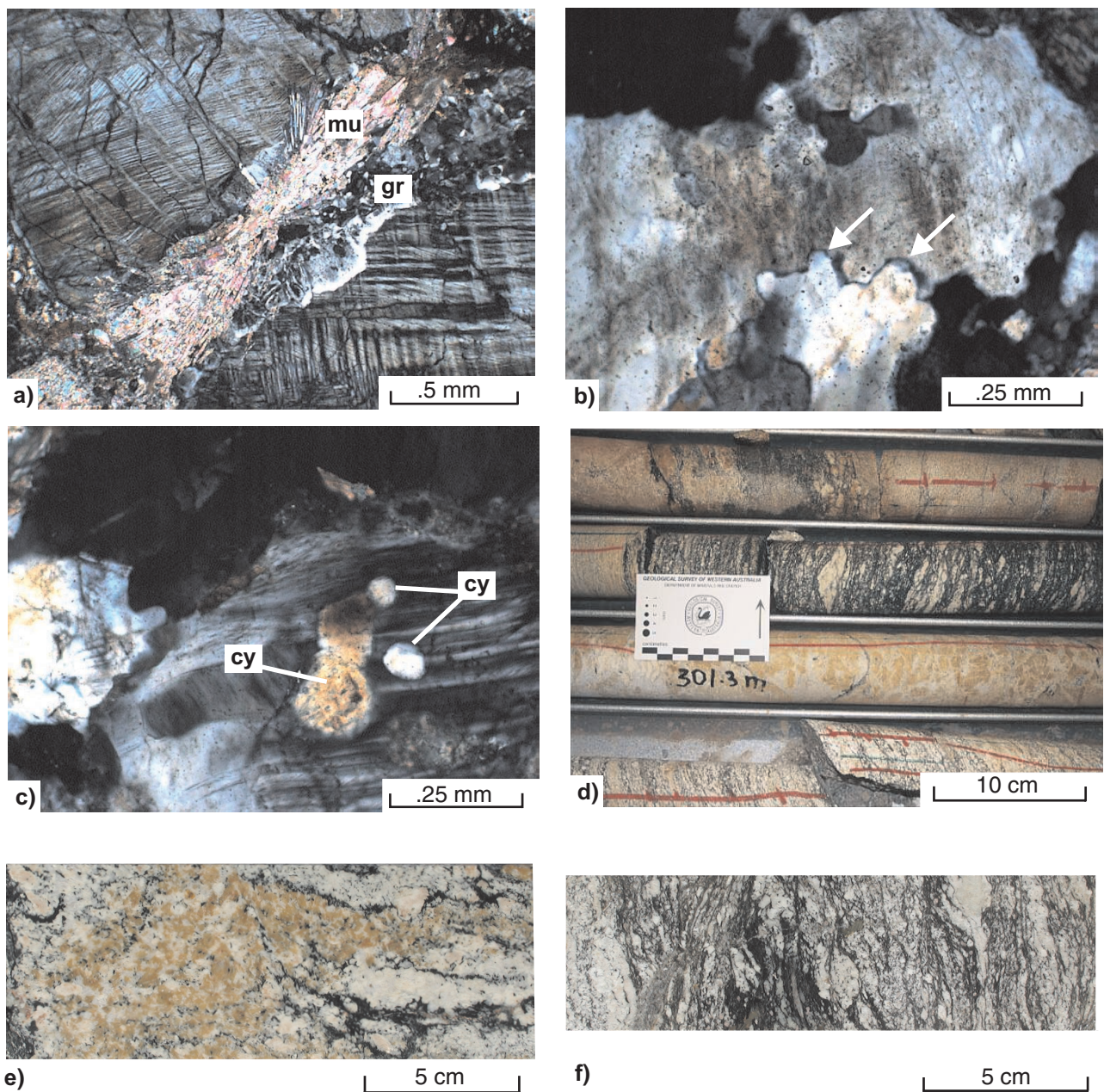
## Depth 282 m. GSWA 132524

*Field name:* brecciated granitoid with pseudotachylite veinlets

*Main minerals:* quartz, feldspar, biotite

*Accessories:* muscovite, sericite, chlorite, corundum, kaolinite

*Description:* This section consists of three parts: 1) a deformed quartz–feldspar–biotite granitoid assemblage; 2) biotite(–corundum), and 3) very fine grained, almost unresolvable, vein material. In the first part, quartz and feldspar crystals are deformed, elongated, and have interstitial biotite defining a distinct planar fabric. Muscovite, chlorite, and sericite are present as post-impact alteration phases; muscovite and blue-birefringent chlorite (Fe–Mg rich) replaced biotite; sericite forms crosscutting veinlets and infills a network of microfractures. There are good examples of quartz and zircon with single and multiple sets of planar microfractures and PDFs. The second part is essentially monomineralic (all biotite), with a planar fabric and minor, scattered anhedral corundum crystals. Here the biotite is locally replaced by muscovite. The third part is probably a pseudotachylite veinlet, and may be brown devitrified glass (melt) with numerous, very fine, unidentified crystallites and a few spherule-like structures, now replaced by kaolinite.



AJM361

16.02.01

**Figure 3.5.** Photomicrographs and photographs of core specimens (4.5 cm in diameter, top is to left) showing impact-related features in Woodleigh 1: a) GSWA 132523 (269.2 m), sheaves of muscovite (mu) overprint granophyric material (gr) at the boundary between quartz (with PDFs) and microcline. This muscovite was possibly formed during stages of post-impact hydrothermal activity; cross polars; b) GSWA 149144 (208.0 – 208.1 m), lobate crystal boundaries (arrows), probably the result of grain boundary migration (GBM), a process that leads to the bulging of a less dislocated crystal into another with a higher dislocation density. The bulging can lead to the nucleation of new crystals (commonly with a round shape) inside the host, as shown in c. The GBM is a process that results from intense deformation and is commonly observed in tectonically deformed and metamorphosed rocks; cross polars; c) GSWA 149143, lobate grain boundaries (left side) and nucleation of new crystals (cy) inside the host affected by higher dislocation density; cross polars; d) core (near 301 m) of shocked granitoid rock with yellow-brown (rusty) patches and strongly brecciated, biotite-rich gneissic granite, see also e; e) core specimen (192 m) of yellow-brown shocked granitoid with fragments of fine-grained leucocratic granite, rimmed by ?secondary biotite; f) core specimen (237.3 m) of fragmented and sheared biotite gneiss



## Depth 283 m. GSWA 132525

*Field name:* cataclastic/mylonitic rust-brown granite with biotite-rich streaks

*Main minerals:* quartz, feldspar, biotite

*Accessories:* muscovite, Fe–Mg-rich chlorite, zircon

*Description:* Coarse-grained microcline–quartz ribbons are bordered by biotite streaks forming a gneissic or ?cataclastic texture. There is one large microcline plate (about 3 cm long). There are bands of granulated quartz–biotite–muscovite, and muscovite and Fe–Mg-rich chlorite (purple interference colours) replace biotite. Myrmekitic intergrowths are common at grain boundaries. Shocked quartz has multiple sets of PDFs and there are shattered or diaplectic feldspar crystals (maskelynite). Localized reticulate diaplectic glass textures are seen. Interstitial quartz–albite or myrmekite-like intergrowths are found along crystal margins. Shocked zircons show single sets of possible PDFs. Lobate crystal boundaries indicative of grain boundary migration are associated with partly ?fused crystals.

## Geochemistry

A total of 18 core samples from Woodleigh 1 were analysed for major (11 samples) and trace (7 samples) elements. Laser inductively coupled plasma mass spectrometry (ICPMS) and X-ray fluorescence (XRF) analyses of shocked and pseudotachylite-injected granitoid samples were performed at the Genalysis laboratories in Perth. An additional seven analyses were carried out at the Research School of Earth Sciences, Australian National University (Appendix 4, Table 4.3). The analyses have not been combined because they were performed at different laboratories with different analytical standards. At this stage, analyses of meteoritic elements, such as platinum group elements (PGE), were not utilized due to inadequate detection levels. Results and details of analytical techniques are provided in Tables 3.1 and 3.2. EDS analyses carried out on selected samples are discussed in detail in Appendix 4 and summarized below.

Major and trace element analyses were used in order to detect changes in the chemistry of the target rocks in the central-uplift granitoids cored by Woodleigh 1. Because there are no available chemical analyses on unaltered, central-uplift granitic rocks in the region, the data from this study were normalized against the average granite (AG) of Levinson (1974). Results indicate that while the lithophile and chalcophile trace metals (Pb, Sn, Wo, Mo, Bi, Ag, Sb, Zn, Cu, Au) vary by factors in the range of 0.1 to 10.0 times relative to AG (Levinson, 1974; Best, 1982), the siderophile trace metals are strongly enriched, including V (6–20 times that of AG), Cr (up to 30 times AG), Co (10–50 times AG), and Ni (<10–120 times AG; Fig. 3.6). Major elements show moderate to strong K<sub>2</sub>O enrichment accompanied by SiO<sub>2</sub>, Na<sub>2</sub>O, TiO<sub>2</sub>, MgO, MnO, and P<sub>2</sub>O<sub>5</sub> depletions relative to AG (Fig. 3.7).

Semiquantitative and quantitative spot analyses by EDS of S-type pseudotachylite veins and blebs indicate significant enrichment in refractory elements relative to scanned whole-rock compositions of the Woodleigh shocked granitoid (Glikson et al., in prep.; see also Table 4.6). MgO is enriched by factors up to four, and can be as high as about 3% in pseudotachylite and diaplectic glasses. CaO is enriched by factors of up to three to levels less than 4% wt, and Al<sub>2</sub>O<sub>3</sub> is enriched by factors of up to two, reaching levels of less than 30% wt. Relative to whole rock compositions, SiO<sub>2</sub> is commonly depleted by 10–20%. Na<sub>2</sub>O and K<sub>2</sub>O are variably to strongly depleted. Diaplectic glass blebs within feldspars can be strongly enriched in MgO and FeO. The loss of Si, Na, K, and in some instances Fe, relative to Al, Mg, and Ca — possibly due to selective volatilization — provides a potential explanation for the source of K and Na in connection with extensive alkali metasomatism (fenitization) observed in the central granitoid uplifts of some impact structures; for example, the Shoemaker Impact Structure, Western Australia (Pirajno and Glikson, in prep.). The loss of alkalis in impactites has been recorded at other impact structures, where it is considered that the alkaline metals were mostly lost from the feldspars by shock metamorphism (Puura et al., 2000).

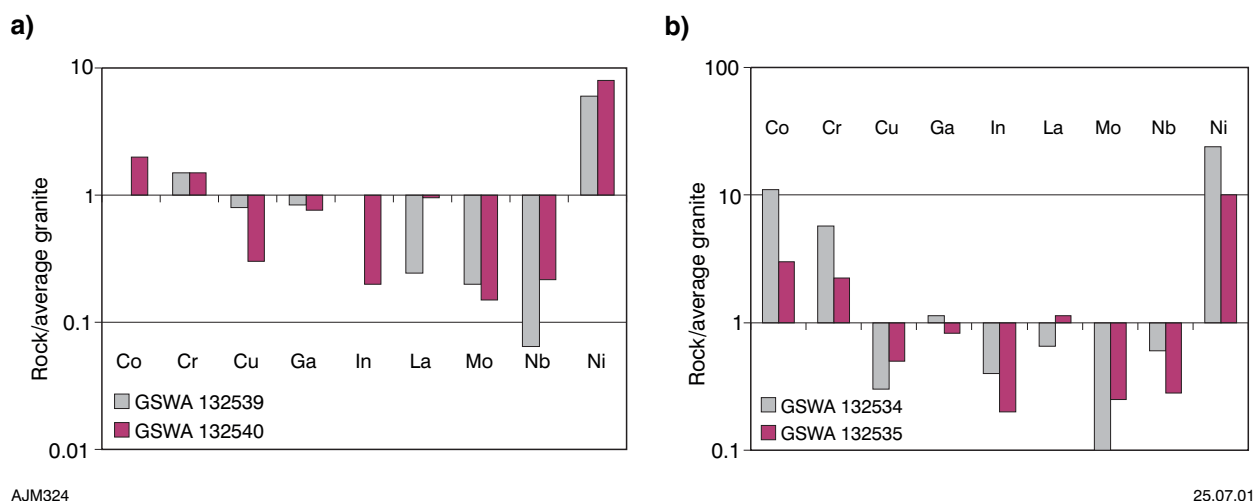


**Figure 3.6.** Bar diagram of selected trace elements, showing enrichment and depletion relative to average granite (Levinson, 1974): a) GSWA 132539 and 132540; b) GSWA 132534 and 132535. Note enrichment in Ni, Co, and Cr (meteoritic elements). Sample depths: GSWA 132534 — 192.5 m, GSWA 132535 — 210 m, GSWA 132539 — 300 m, GSWA 132540 — 315 m

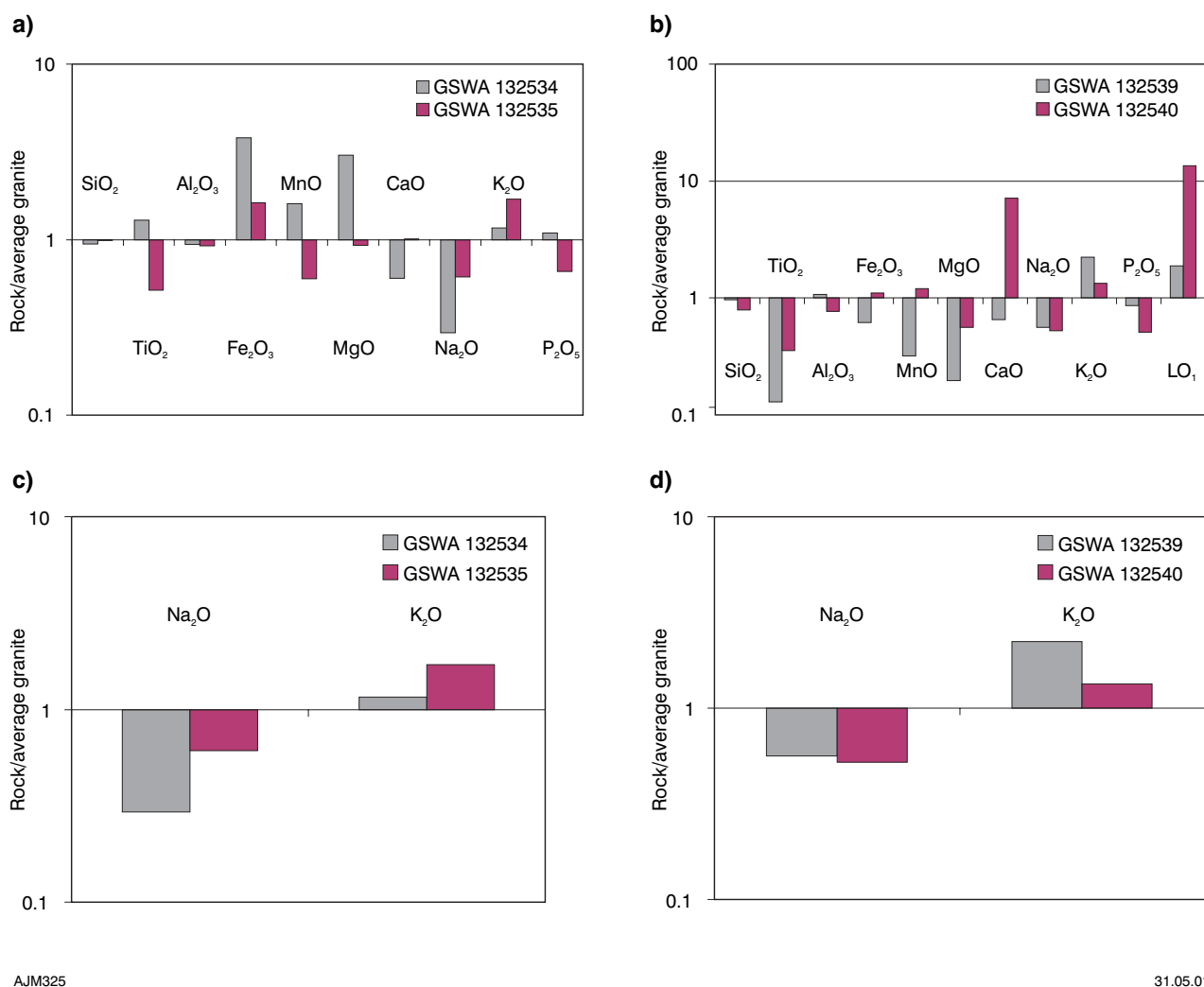


**Figure 3.7.** Bar diagrams of selected major oxides, showing enrichment and depletion relative to an average granite (Levinson, 1974): a) GSWA 132534 and 132535; b) GSWA 132539 and 132540; c) GSWA 132534 and 132535; d) GSWA 132539 and 132540. Note enrichment in K<sub>2</sub>O and depletion in Na<sub>2</sub>O. Sample depths as for Figure 3.6

Table 3.1. Whole-rock major and trace element analyses of core samples from Woodleigh 1

Sample no. Rock type	132527B Biotite-rich gneiss	132529B Biotite-rich gneiss	132531B Granite gneiss	132534 Leucocratic (shocked) granite	132535 Leucocratic (shocked) granite	132536 Aplitic biotite granite	132537 Leucocratic (shocked) granite	132538 Brecciated gneissic granite	132539 Leucocratic (shocked) granite	132540 Leucocratic (shocked) granite	149142 Mixed leucosome/ gneiss	Method
Depth (m)	196.6	219.5	264.3	192.5	210	247	260.4	225	300	315	198.35	
SiO <sub>2</sub>	46.0	43.2	69.0	67.2	70.6	69.6	73.3	65.7	69.0	56.1	71.6	/CALC
TiO <sub>2</sub>	2.67	2.04	0.63	0.40	0.16	0.35	0.14	0.57	0.04	0.11	0.12	/CALC
Al <sub>2</sub> O <sub>3</sub>	12.84	12.92	13.07	13.45	13.18	15.55	13.36	11.36	15.39	11.02	11.75	/CALC
Fe <sub>2</sub> O <sub>3</sub>	16.67	14.97	6.52	4.59	1.96	2.87	1.57	4.73	0.75	1.33	1.75	/CALC
MnO	0.245	0.363	0.168	0.08	0.03	0.029	0.019	0.08	0.016	0.06	0.03	/CALC
MgO	6.28	7.66	1.94	2.15	0.66	1.15	0.64	3.41	0.14	0.40	1.17	/CALC
CaO	6.7827	7.1499	1.2459	1.1106	1.8592	3.2582	2.1084	3.2905	1.2023	13.1661	2.755	/CALC
Na <sub>2</sub> O	1.2099	0.6052	1.672	1.0854	2.2554	3.9203	3.2248	1.6086	2.0701	1.9258	1.5378	/CALC
K <sub>2</sub> O	1.51	2.05	3.18	4.73	6.94	1.54	3.50	2.20	9.07	5.43	1.46	/CALC
P <sub>2</sub> O <sub>5</sub>	0.2776	0.1679	0.0372	0.1311	0.0789	0.1062	0.0474	0.0324	0.1036	0.0612	0.0128	/CALC
LOI	3.69	6.3	1.89	3.62	1.9	1.46	1.65	5.12	1.45	10.45	5.41	/CALC
<b>Total</b>	<b>97.9302</b>	<b>97.063</b>	<b>99.1851</b>	<b>98.4671</b>	<b>99.5935</b>	<b>99.8047</b>	<b>99.5406</b>	<b>98.0215</b>	<b>99.216</b>	<b>99.9931</b>	<b>97.5656</b>	
<b>Parts per million</b>												
Ag	0.1	0.1	—	—	—	—	—	—	0.4	0.2	—	AMS
As	2	1	2	—	1	1	—	8	1	—	1	AMS
Au	—	—	8	—	—	—	—	—	7	—	—	NIS/MS
Ba	146.4	101.2	349.5	515.0	735.9	278.6	478.5	292.3	439.4	482.1	151.9	AMS
Bi	0.18	0.33	0.07	0.06	0.05	0.01	0.05	0.10	0.06	0.04	0.03	AMS
Cd	0.1	0.4	—	—	—	—	—	—	—	0.1	—	AMS
Ce	26.74	17.31	92.91	33.90	55.83	45.19	66.28	65.06	11.74	44.39	24.08	AMS
Co	43	44	17	11	3	6	3	26	—	2	4	AOES
Cr	102	122	79	23	9	11	5	56	6	6	7	AOES
Cu	108	81	40	3	5	5	5	30	8	3	7	AMS
Ga	24.0	29.4	21.7	20.5	14.9	21.0	15.7	20.2	15.1	13.7	13.7	AMS
In	0.12	0.26	0.06	0.04	0.02	0.03	—	0.07	—	0.02	—	AMS
La	8.87	7.30	46.11	16.36	28.26	23.92	33.64	32.38	6.12	23.95	11.65	AMS
Mo	0.6	0.6	0.8	0.2	0.5	0.4	0.5	1.4	0.4	0.3	0.7	AMS
Nb	15.22	12.81	13.92	12.06	5.64	2.84	4.24	10.21	1.29	4.32	1.90	AMS
Ni	59	66	38	12	5	5	5	40	3	4	7	AOES
Pb	7	6	33	38	72	11	46	73	106	97	16	AMS
Pd	—	—	—	—	—	—	—	—	—	—	—	NIS/MS
Pt	—	—	—	—	—	—	—	—	—	—	—	NIS/MS
Rb	76.75	149.33	204.29	197.69	206.27	56.65	133.45	99.11	267.15	196.12	52.16	AMS
S	0.09	0.24	0.10	0.03	0.11	0.05	0.02	0.07	0.04	0.12	0.05	DOES
Sb	0.07	0.08	0.23	0.08	0.19	0.13	0.11	0.09	0.12	0.09	0.31	AMS

Table 3.1. (continued)

Sample no. Rock type	132527B Biotite-rich gneiss	132529B Biotite-rich gneiss	132531B Granite gneiss	132534 Leucocratic (shocked) granite	132535 Leucocratic (shocked) granite	132536 Aplitic biotite granite	132537 Leucocratic (shocked) granite	132538 Brecciated gneissic granite	132539 Leucocratic (shocked) granite	132540 Leucocratic (shocked) granite	149142 Mixed leucosome/ gneiss	Method
Depth (m)	196.6	219.5	264.3	192.5	210	247	260.4	225	300	315	198.35	
Se	—	—	—	—	—	—	—	—	—	—	—	AMS
Sn	3.4	18.6	1.7	2.5	1.6	1.7	1.1	1.7	1.6	2.1	—	AMS
Sr	120.44	88.35	94.24	85.51	132.06	243.17	187.22	75.01	132.21	131.73	123.53	AMS
Ta	1.48	1.43	1.39	2.13	0.53	0.33	0.48	0.91	0.32	0.54	0.51	AMS
Te	—	—	—	—	—	—	—	—	—	—	—	AMS
Th	1.98	0.20	25.16	10.67	18.54	10.31	25.04	16.54	2.78	9.14	8.71	AMS
U	0.83	3.50	3.59	2.01	3.37	0.47	4.55	4.48	1.98	4.74	4.68	AMS
V	397	435	95	75	14	30	15	89	2	12	18	AMS
Y	35.45	29.01	18.70	13.04	6.49	2.29	6.92	8.12	5.19	14.19	6.06	AOES
Zn	150	185	89	66	22	58	36	41	11	94	14	AOES
Cs	2.709	5.538	5.134	5.670	1.396	1.022	5.404	1.011	1.302	1.936	1.113	AMS
Fe	11.66	10.47	4.56	3.21	1.37	2.01	1.10	3.31	0.53	0.93	1.22	DOES
Hf	1.22	1.67	1.44	1.84	2.21	1.46	1.97	2.03	1.03	0.99	1.18	AMS
Ir	—	—	—	—	—	—	—	—	—	—	—	AMS
Nd	19.39	11.80	36.45	13.26	20.26	15.69	24.05	25.02	4.73	17.38	9.74	AOES
Os	—	—	—	—	—	—	—	—	—	—	—	NIS/MS
Pr	3.987	2.408	10.033	3.601	5.832	4.422	6.824	6.896	1.255	4.758	2.610	AMS
Rh	—	2	—	—	—	1	—	1	2	—	—	NIS/MS
Ru	—	—	—	—	—	—	—	—	—	—	—	NIS/MS
Tl	0.33	0.69	1.03	0.82	0.80	0.27	0.44	0.31	1.01	0.79	0.19	AMS

NOTES: All major- and trace-element analyses were carried out by Genalysis Laboratory Services, Perth

— Below detection limit  
AMS: Multi-acid attack and inductively plasma mass spectrometry  
AOES: Multi-acid attack and inductively plasma optical (atomic) emission spectrometry  
/CALC: Results determined by calculation using reported data from above methods  
DOES: Digestion by oxidative alkaline fusion, Na peroxide, and HCl; inductively plasma optical (atomic) emission spectrometry  
NIS/MS: Nickel sulfide digestion and inductively plasma mass spectrometry

Table 3.2. Whole-rock trace element analyses of core samples from Woodleigh 1

Sample no. Rock type	132527 Biotite-rich gneiss	132528 Rusty shocked granite	132529 Biotite-rich gneiss	132530 Fine-grained biotite granite	132531 Granite gneiss	132532 Rust-coloured shocked granite	132533 Rust-coloured shocked granite	Method
Depth (m)	196.6	205.8	219.5	235.8	264.3	264.3	327.2	
Parts per million								
Ag	0.2	0.1	0.1	0.1	0.2	0.1	0.1	A/MS
As	9	1	3	1	2	1	1	A/MS
Au	5	5	5	5	5	5	5	NIS/MS
Ba	150	560	108	265	380	460	640	A/MS
Bi	0.33	0.04	0.3	0.02	0.07	0.02	0.1	A/MS
Co	45	0.9	48	6.2	17.5	1.2	1.6	A/OES
Cr	116	2	125	6	102	2	32	A/OES
Cu	58	1	52	2	30	1	5	A/MS
Mo	1.1	0.4	0.4	0.2	1	0.3	0.4	A/MS
Ni	56	2	66	2	35	3	4	A/OES
Pb	12	62	6	12	26	66	100	A/MS
Pd	2	2	2	2	2	2	2	NIS/MS
Pt	2	2	2	2	2	2	2	NIS/MS
Sb	0.15	0.05	0.05	0.05	0.05	0.05	0.05	A/MS
Sn	4.3	1	19.5	0.6	2	1	3.3	A/MS
V	390	6	410	30	98	4	8	A/MS
W	0.4	0.2	1.2	0.1	0.7	0.2	0.7	A/MS
Zn	145	16	170	56	84	15	25	A/OES
Ir	2	2	2	2	2	2	2	A/MS
Os	2	2	2	2	2	2	2	NIS/MS
Rh	1	1	1	1	1	1	1	NIS/MS
Ru	2	2	2	2	2	2	2	NIS/MS

NOTES: All trace-element analyses were carried out by Genalysis Laboratory Services, Perth

A/MS: Multi-acid attack and inductively plasma mass spectrometry

A/OES: Multi-acid attack and inductively plasma optical (atomic) emission spectrometry

NIS/MS: Nickel sulfide digestion and inductively plasma mass spectrometry



## Woodleigh 2A petrography

### Depth 499.5 m. GSWA 169324

*Field name:* granite clast

*Main minerals:* unidentified clay, kaolinite, illite, sericite

*Accessories:* opaque minerals

*Description:* The sample consists of an assemblage of unidentified clay, light-brown kaolinite, illite, and sericite in a brecciated texture; clasts of clay minerals are cemented by illite and sericite. A weak pleochroism of the sericite indicates that it may be a replacement of biotite. Dustings of opaque minerals could be organic material. This material is a highly weathered product of an unknown protolith (?granite).

### Depth 545.3 m. GSWA 169325

*Field name:* paraconglomerate

*Main minerals:* quartz, feldspar (plagioclase and microcline), biotite, muscovite

*Accessories:* sericite, glass, chlorite, garnet

*Description:* Round to angular lithic fragments are embedded in a finely brecciated, pseudotachylite-like matrix (Fig. 3.8a). One fragment is 2–3 cm across and consists of an assemblage of grain-supported, subrounded to angular quartz and subordinate feldspar (plagioclase and microcline) grains, from 1 mm to less than 0.1 mm across, with interstitial sericite and muscovite. All quartz grains show undulose extinction and many have PDFs. Patches of isotropic material are also present, and are most probably glass (?S-type pseudotachylite; Fig. 3.8b). One lithic fragment, about 1.5 cm across, consists of shocked quartz, biotite, and muscovite, all with sets of microfractures or PDFs or both. In addition, quartz crystals exhibit domains of curved microfractures enclosing PDFs; the sinuous or curved microfractures are decorated with fluid inclusions, whereas the sets of PDFs have no or few fluid inclusions (as seen with the available magnification; Figs 3.8c, d, and e). A weakly foliated fabric is defined by the elongation of the mineral grains and surrounding micas. One clast is possibly derived from gneissic granite (Fig. 3.8f). The pseudotachylite-like material is a microbreccia that consists of angular shocked (PDFs) quartz grains in a comminuted dark matrix, locally containing isotropic material (glass).

### Depth 548.6 m. GSWA 169326

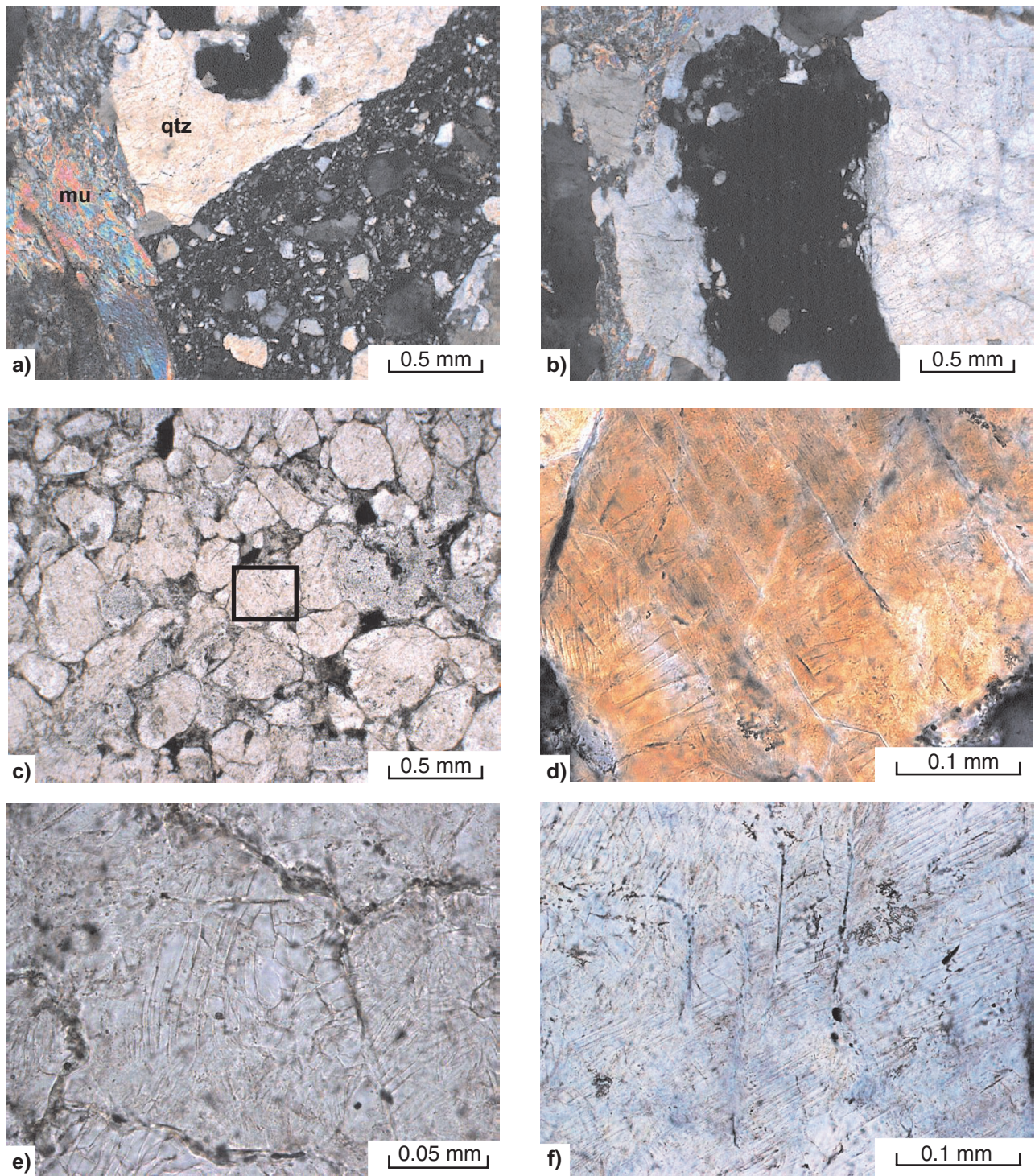
*Field name:* granite clast in paraconglomerate

*Main minerals:* quartz, microcline, biotite, muscovite, carbonate

*Accessories:* sericite, garnet, opaque minerals (?sulfides)

*Description:* The granitic clast is associated with smaller carbonate clasts and finely brecciated material (Fig. 3.9a). The clast consists of intensely shocked, rust-coloured quartz (Fig. 3.9b), with multiple sets of PDFs and subsequent subgrain development, which displace the PDF sets; partially resorbed and amorphized microcline (maskelynite); chaotically disposed, abundant red-brown biotite; and muscovite crystals. The microcline is also traversed by elongate muscovite crystals (?filling microfractures). Interstitial fine sericite is present and isolated garnet crystals (Fig. 3.9b) have fractures infilled by sericite. Carbonate clasts are partially resorbed and intermingled with the granitic material. Other lithic fragments include sandstone enclosed in microbreccia material (Fig 3.9c). One volcanoclastic lithic fragment is recognizable by its glass shard (see also GSWA 169331). These clasts are in contact with finely comminuted material containing subrounded to angular quartz grains (microbreccia), all showing abundant non-oriented, subgrain development and faint traces of PDFs. Subgrain development results from intense dislocation of the crystal lattice. The microbreccia consists of angular quartz fragments, all showing strain and shocked features, set in a finely comminuted matrix, with mostly unresolvable dark material (?glass).



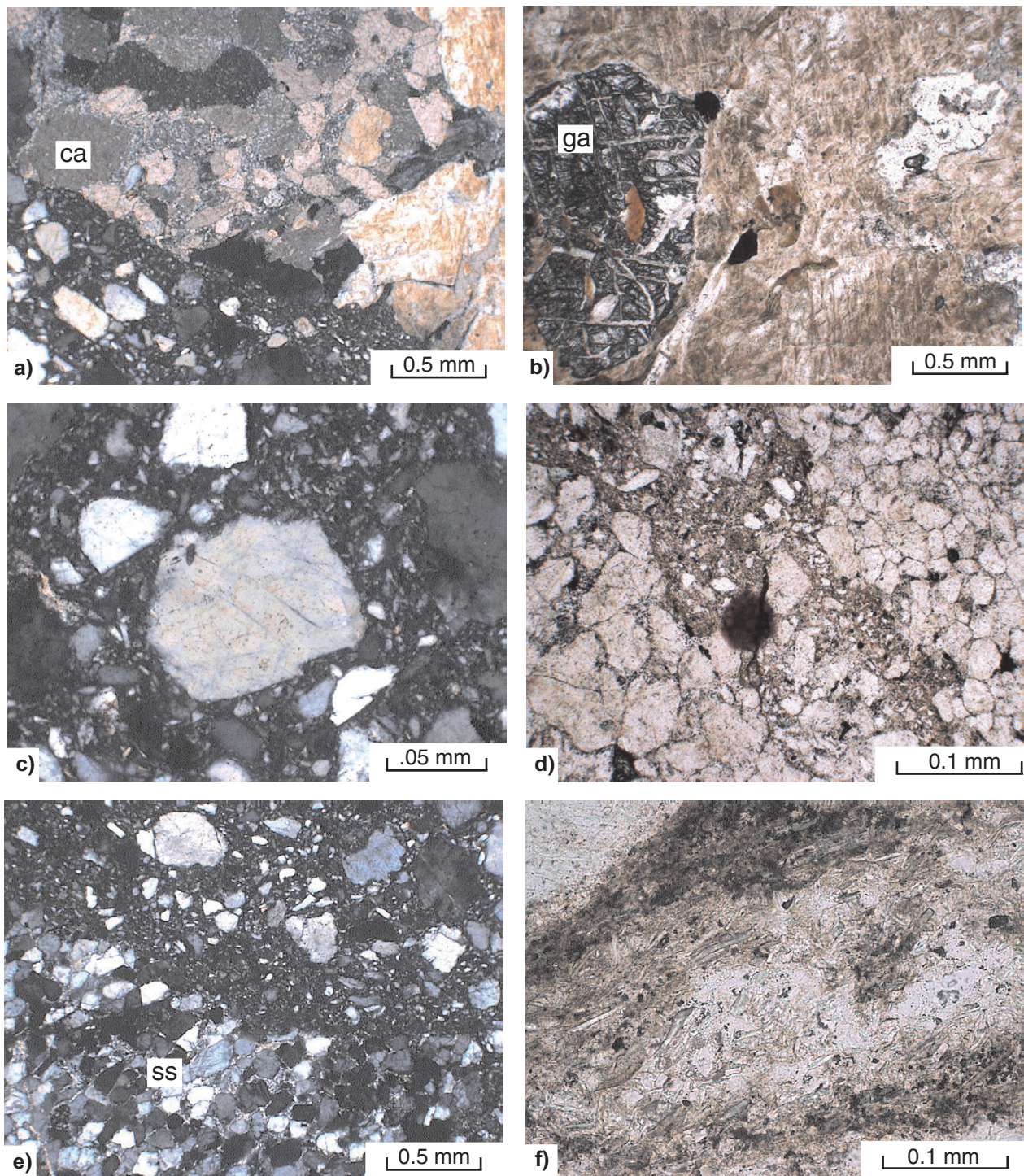


FMP598

21.03.01

**Figure 3.8.** Photomicrographs of core specimens from Woodleigh 2A paraconglomerate showing: a) GSWA 169325 (545.3 m), shocked quartz (qtz) and muscovite (mu), part of a granite lithic fragment in microbreccia containing shocked angular quartz grains in an aphanitic matrix; cross polars; b) GSWA 169325, shocked quartz crystal showing PDFs and cut by a patch of isotropic glass, note partially resorbed edges and relict fragments in the glass material; cross polars; c) GSWA 169325, grain-supported sandstone lithic fragment, quartz grain indicated by square is shown in d); d) this quartz exhibits multiple sets of PDFs and crosscutting microfractures; plane-polarized light; e) GSWA 169325, shocked quartz grain in sandstone showing PDFs and curved microfractures, plane-polarized light; f) GSWA 169325, well-defined sets of PDFs and crosscutting microfractures in quartz crystal from granite clast; plane-polarized light





FMP599

21.03.01

**Figure 3.9.** Photomicrographs of core specimens from Woodleigh 2A paraconglomerate showing: a) GSWA 169326 (548.6 m), carbonate lithic fragment (ca) in contact with shocked quartz crystals from a granitic fragment, carbonate grains are partly resorbed and recemented; cross polars; b) GSWA 169326, rust-coloured, shocked quartz crystals and garnet (ga) in granite fragment; plane-polarized light; c) GSWA 169326, detail of microbreccia with shocked quartz grain and dark, aphanitic matrix; cross polars; d) GSWA 169327 (553.0 m) two sandstone clasts with different grain size separated by breccia material, probably generated by friction (note spalled off fragments); plane-polarized light; e) GSWA 169329 (575.2 m), sandstone lithic fragment (ss) composed of shocked quartz grains with minor interstitial sericite, embedded in microbreccia that contains angular and shocked quartz set in a ?glassy aphanitic matrix; cross polars; f) GSWA 169331 (585.1 m), volcaniclastic lithic fragment with chloritized glass shards; plane-polarized light



**Depth 553.0 m. GSWA 169327**

*Field name:* paraconglomerate

*Main minerals:* quartz

*Accessories:* feldspar, illite, Fe oxides

*Description:* Portions of two subrounded lithic fragments, greater than 2 cm across, are enclosed in finely brecciated material. The two fragments are in contact with one another, and this contact is marked by microbreccia, with pieces of said fragments spalled off (Fig. 3.9d). The two lithics are grain-supported sandstone of different grain size; one consists of quartz grains, from 0.25 to 1 mm across, the other has grains from less than 0.1 to 0.5 mm. All are strained (undulose extinction) and exhibit straight or curved microfractures and PDFs; fine illite and trains of iron oxides are interstitial and mark the grain boundaries. Some grains show a reticulate texture and partial amorphization, similar to maskelynite. The microbreccia that surrounds the lithic fragments consists of angular quartz grains in a finely comminuted matrix composed of quartz and dark, unresolvable material (?glass).

**Depth 554.9 m. GSWA 169328**

*Field name:* granite clast in paraconglomerate

*Main minerals:* quartz, sericite

*Accessories:* iron oxides, feldspar, muscovite

*Description:* Grain-supported sandstone with quartz and subordinate feldspar grains ranging in size from 0.2 to 1 mm across. In addition to strong undulose extinction, all grains exhibit features of shock metamorphism (microfractures, PDFs); sericite, iron oxides, and minor muscovite constitute interstitial material between the component clastic grains. As in previous cases, this sandstone is in contact with microbreccia (?pseudotachylite). The microbreccia contains angular fragments of quartz, minor biotite, and carbonate. As observed in previous Woodleigh 2A samples, PDFs have few or no fluid inclusions, which is in contrast with the PDFs from Woodleigh 1 samples, all of which contain abundant fluid inclusions.

**Depth 575.2 m. GSWA 168329**

*Field name:* granite clast in paraconglomerate

*Main minerals:* quartz, sericite

*Accessories:* iron oxides, tourmaline

*Description:* Fine-grained sandstone, composed of rounded quartz grains from 0.1 to 0.25 mm across, with interstitial sericite is associated with blebs of iron oxides (Fig 3.9e). Rare tourmaline forms rounded grains (0.1 mm) and small euhedral crystals; the rounded grains show microfractures. Most quartz grains display PDFs, but not as well defined as in the above samples; there are, however, abundant microfractures, commonly decorated with numerous fluid inclusions. The sandstone is in contact with microbreccia (?pseudotachylite), which in addition to angular quartz grains, also contains some shocked zircons.

**Depth 580.2 m. GSWA 169330**

*Field name:* paraconglomerate

*Main minerals:* quartz

*Accessories:* microcline, sericite, iron oxides

*Description:* Lithic fragments, from 0.2, 0.5, less than 1, to greater than 3 cm, are embedded in microbreccia material. The greater than 3 cm lithic fragment is a grain-supported sandstone with no interstitial material, and rounded to subrounded quartz grains that range in size from 0.2 to 2 mm across. Minor microcline is also present. All quartz grains have strong undulose

extinction and show abundant, curved microfractures and less commonly sets of PDFs. The 1 cm lithic fragment is a finer grained sandstone (0.1 – 1 mm) with minor interstitial material (sericite – iron oxides); quartz shows strong undulose extinction and microfractures, but PDFs are rare or poorly displayed. Two 0.5 cm-size fragments are of a ferruginous, fine-grained sandstone; here, quartz grains are angular to rounded and range in size from 0.1 to 0.25 mm across, and there is abundant interstitial iron oxide, possibly hematite. The microbreccia surrounding the clasts contains a fragment of altered and foliated greywacke (angular quartz grains in a foliated matrix of phyllosilicate minerals), sandstone fragments, a polycrystalline quartz grain (2 mm across), and angular to subangular quartz grains, all embedded in a fine comminuted matrix composed of quartz and unresolvable, dark material (possibly devitrified glass). Quartz grains all show strong undulose extinction and microfractures; PDFs are present in several grains.

### **Depth 585.1 m. GSWA 169331**

*Field name:* paraconglomerate

*Main minerals:* quartz

*Accessories:* microcline, sericite, iron oxides

*Description:* There is one lithic fragment that is more than 2 cm across, and two other lithic fragments (4 and 2 mm) that are embedded in microbreccia material. The larger fragment has quartz grains ranging in size from 0.5 to 1.5 mm across; the quartz grains are in contact with one another, and have no interstitial material. Locally, the quartz grains have serrated or granulated boundaries, or both. Multiple sets of subparallel microfractures delimit small polygonal domains that enclose PDFs. The microbreccia consists of angular and subangular quartz with microfractures and PDFs, fragments of sandstone, microcline crystals, an oxidized (ferruginous) fragment of greywacke, some carbonate, and two 1 mm-long fragments of chloritized volcanoclastic rock (glass shards), all set in a finely comminuted quartzose matrix (Fig 3.9f).

### **Depth 586.9 m. GSWA 169332**

*Field name:* dolomitic breccia

*Main minerals:* quartz, carbonate

*Accessories:* chlorite, mica, microcline, iron oxides

*Description:* Heterolithic microbreccia, containing fragments of micritic carbonate, sandstone, ferruginous sandstone, chloritized volcanoclastic, angular to subangular quartz grains, and subordinate microcline, is embedded in a very fine carbonate matrix. Here, the crystals do not exhibit shock metamorphic features, such as PDFs, although most quartz grains have strong undulose extinction and curved or subparallel sets of microfractures. This rock appears to be more like a lithic sedimentary breccia, or possibly a reworked, lithic breccia ejecta.

## **Shock metamorphic features in Woodleigh 1 and 2A**

Features induced by shock metamorphism in samples of Woodleigh 1 and 2A include planar microstructures (PDFs and planar microfractures) in quartz, micas, zircon, and feldspar, E- and S-type pseudotachylite veinlets (formed by the interaction of the initial shock wave with the target rock), and reticulate diaplectic glass in feldspar (maskelynite). In addition, shocked granitoid (Woodleigh 1) is commonly characterized by a patchy pink or reddish-brown colour. This feature is probably due partly to the presence of iron oxides, possibly derived from the alteration of ferromagnesian silicate minerals, and partly to the presence of abundant fluid inclusions. It is not clear whether this pink-brown granitoid is affected by post-impact shear stress and alteration or impact-related shock. PDFs in Woodleigh 1 are decorated with abundant fluid inclusions (mostly monophase, but two-phase inclusions are also present), suggesting circulation of large volumes of fluids, perhaps associated with post-impact hydrothermal



activity. By contrast, the PDFs in Woodleigh 2A quartz grains appear free of fluid inclusions; sets of PDFs are enclosed in small structural domains delimited by sets of curved or subparallel microfractures. All quartz grains commonly display varying degrees of undulose extinction, recrystallization, and subgrain boundaries. In addition, grain boundaries are irregular or lobate or both, a feature that is characteristic of high-grade metamorphic conditions (Fig. 3.5b). Another feature that is commonly observed in thin sections from Woodleigh 1 is the nucleation of round, new crystals from the lobate grain boundaries towards the interior of the host crystal, resulting in enhanced lobate boundaries and inclusions of neoformed crystals in the host (Fig. 3.5c). This is a phenomenon known as 'grain boundary migration recrystallization' (Passchier and Trouw, 1996). Grain boundary migration is not diagnostic of impact shock metamorphism, because it occurs as a result of strong deformation of crystalline rocks. In the present case, however, it is likely that grain boundary migration took place as a result of impact-related pressure and deformation.

Multiple sets of PDFs are present in Woodleigh 1 quartz grains (e.g. Fig. 3.2a), K-feldspar, anorthoclase, plagioclase, and possibly zircon (e.g. Fig. 3.3b). The pervasive shock-thermal alteration has produced distinctly reconstituted, leucocratic, medium-grained granitoid rocks with rust-coloured patches (Figs 3.5d and e). Woodleigh 1 rocks display irregular reticulate or polygonal patterns of diaplectic K-feldspars, anorthoclase, and plagioclase (Fig. 3.4d). Diaplectic minerals are disordered or amorphous mineral phases produced by shock waves, but without melting (Jackson, 1997). Biotite displays kink bands, edge resorption, and concordant to transgressive S-type pseudotachylite veins; locally PDFs are also present. Some biotite (fresh and undeformed) may be the product of post-impact K metasomatism. Laser Raman spectroscopy observations confirm the existence of pristine glass containing relict, nanometre-scale feldspar and quartz grains, but only a small fraction of hydrous alteration phases (Glikson et al., in prep.). Some of the pseudotachylite veinlets show devitrification features characterized by nucleation of quartz and K-feldspar (commonly microcline) with a spherulitic appearance or granophyric texture. Isolated corundum crystals locally replace feldspar, suggesting reconcentration of alumina as a refractory element. Accessory phases in the shocked granitoid include zircon, monazite, and apatite, whereas post-impact hydrothermal alteration effects include calcite veinlets, pyrite growth in pseudotachylite veins and microfractures, epidote, and fine sericite aggregates replacing shocked feldspar grains.

Both in Woodleigh 1 and 2A, altered zones in shocked quartz and feldspars take on a reddish-brown colour due to oxidation of iron and the presence of numerous fluid inclusions. Woodleigh 1 shows features of melt devitrification (e.g. GSWA 149146), which involves nucleation of quartz and K-feldspar (generally microcline) and results in a spherulitic or granophyric texture (Lofgren, 1971). The spherulitic texture is more common and generally consists of blebs, or roundish bodies of quartz and feldspar.

The examined core samples from Woodleigh 2A are all paraconglomerate consisting of lithic fragments of various sandstone types, granite, carbonate, and volcanoclastic rocks, embedded in microbreccia predominantly characterized by angular fragments of quartz, subordinate carbonate, and feldspar in a fine comminute quartzose and isotropic matrix (?devitrified glass). It is unclear whether or not the unnamed paraconglomerate is a primary crater-fill lithic breccia or a secondary gravity-flow deposit much younger than the impact.

## References

- BEST, M. G., 1982, *Igneous and metamorphic petrology*: New York, W. H. Freeman and Co., 630p.
- GLIKSON, A. Y., MERNAGH, T. P., PIRAJNO, F., MORY, A. J., and IASKY, R. P., in prep., Woodleigh multi-ring impact basin, Western Australia: geochemical meteoritic signatures and differential volatilisation and condensation: Meteoritics.
- JACKSON, J. A., (editor), 1997, *Glossary of Geology*, fourth edition: Alexandria, Virginia, American Geological Institute, 769p.
- LEVINSON, A. A., 1974, *Introduction to exploration geochemistry*: Calgary, Applied Publishing, 614p.
- LOFGREN, G., 1971, Experimentally produced devitrification textures in natural rhyolitic glass: Geological Society of America, Bulletin, v. 82, p. 111–124.
- PASSCHIER, C. W., and TROUW, R. A. J., 1996, *Microtectonics*: Berlin, Springer-Verlag, 298p.

- PIRAJNO, F., 1990, Geology, geochemistry and mineralisation of the Erongo Volcanic Complex, Namibia: South African Journal of Geology, v. 93, p. 485–504.
- PIRAJNO, F., and GLIKSON, A. Y., in prep., The Shoemaker Impact Structure, Western Australia: Western Australia Geological Survey, Report.
- PUURA, V., KÄRKI, A., KIRS, J., KIRSIMÄE, K., KLEESMENT, A., KONSA, M., NIIN, M., PLADO, J., SUUROJA, K., and SUUROJA, S., 2000, Impact-induced replacement of plagioclase by K-feldspar in granitoids and amphibolites at the Kärda Crater, Estonia, *in* Impacts and the early Earth *edited by* I. GILMOUR and C. KOEBERL: Berlin, Springer-Verlag, p. 417–445.

## Appendix 4

# Electron microscopy and energy dispersive spectrometry probe investigation

by A. Y. Glikson

(Research School of Earth Sciences, Australian National University)

## Introduction

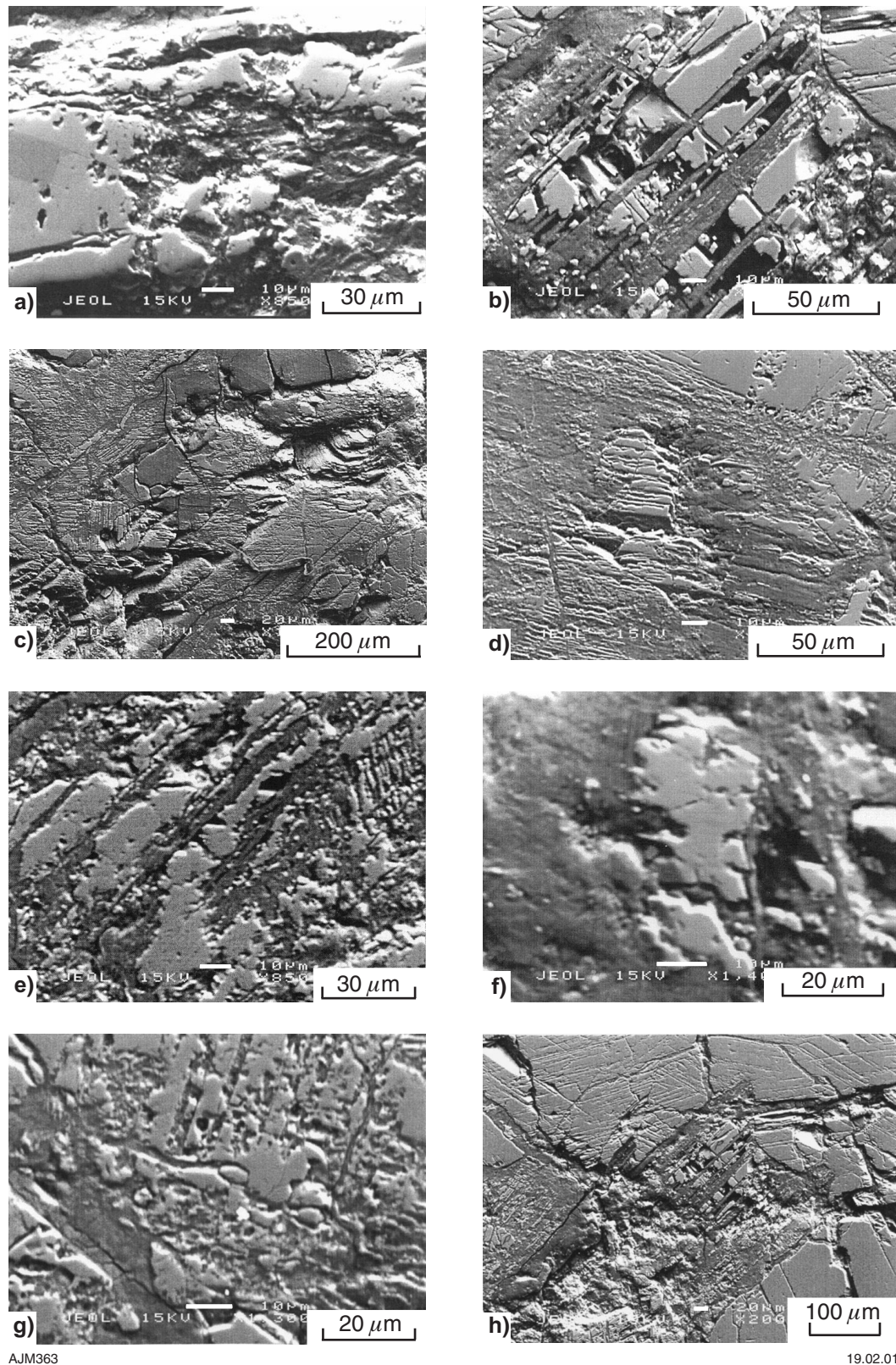
Scanning electron microscopy (SEM), energy dispersive electron probe spectrometry (EDS), Laser Raman spectroscopy, laser inductively coupled plasma mass spectrometry (ICPMS), and whole-rock major and trace X-ray fluorescence (XRF) and ICPMS analyses were performed on seven samples of shocked granitoids from Woodleigh 1. This Appendix documents the principal textural features observed by SEM. The specification of geochemical and electron probe analytical methodology, and its accuracy and precision are also discussed. The chemical composition of mineral phases, pseudotachylite veins, and whole rock are given in Tables 4.1 – 4.7. Laser Raman work and laser ICPMS results, broader interpretations of the data, and their implications to the origin of the Woodleigh impact structure are presented elsewhere (Glikson et al., in prep.).

## Electron microscopy

The shocked granitoids are penetratively injected by microbreccia–metaglass veins (pseudotachylite) and their petrography described in Appendix 3. Shocked feldspars contain abundant micron-scale, amorphous material along planar deformation features (PDFs), as well as internal micron-scale areas (Figs 4.1 and 4.2). Where abundant amorphous material is present, a honeycomb-like textured, crystalline–amorphous pattern (referred to as reticulate texture in Appendix 3) is evident within the feldspars, representing an unusual form of partial diaplectic crystal to glass transformation. The shocked granitoids display extreme compositional variability due to shock-metamorphic differentiation between feldspar-rich and quartz-rich components on a micron to millimetre scale. In the samples studied, mineral assemblages are dominated by biotite–anorthoclase–K-feldspar–quartz(–monazite–zircon–pyrite–calcite).

Core samples from Woodleigh 1 used for this study are from 191.6 to 191.7 m (GSWA 149139), 193.7 to 193.8 m (149140), 198.35 to 198.5 m (149142), and 203.85 to 203.9 m (149146). All four samples consist of heavily shock-modified and veined, biotite-bearing K-feldspar–anorthoclase–quartz granitoid injected by subparallel systems of amorphous, microbrecciated ‘pseudotachylite’ veins, which locally constitute up to 20% of the material. Both K-feldspar and anorthoclase are dominated by diaplectic glass, which occupies former cleavage and PDF planes, resulting in reticulate honeycomb-like patterns and features showing embayed corrosion and rounded spots. K-feldspar grains commonly display embayed resorption, whereas anorthoclase grains more commonly retain somewhat rectangular, intracrystalline cleavage surfaces. On the basis of their penetrative and corrosive relations with individual mineral grains and the occurrence of glass, the pseudotachylites, with which this study is concerned, are clearly S-type (S-PT; Spray, 1998). These veinlets are sharply injected into shocked PDF quartz grains, which show relatively little corrosion but grade into, and show diffuse relations with, the heavily resorbed, partly amorphized feldspar grains (Figs 4.1 and 4.2). The S-PT veins range in thickness from a few centimetres down to sub-micron scale in quartz and biotite. Grains affected in this way show relatively minor marginal corrosion or absorption or both. Such grains contain abundant angular to partly resorbed fragments of quartz and feldspar set in amorphous material, identified in part as glass by Laser Raman analyses (Glikson et al., in prep.). Biotite flakes show marginal absorption or corrosion features or both,





AJM363

19.02.01

**Figure 4.1.** SEM images of desegregated feldspar grains displaying extensive development of diaplectic glass along PDF planes and as irregular patches and spots, and injected by pseudotachylite veins: a) K-feldspar grain fraying out into K-feldspar-glass matrix; b) anorthoclase injected by amorphous glass – microbreccia along former PDF planes; c) extensive desegregation of K-feldspar along several PDF planes; d) relict blebs of K-feldspar within diaplectic glass grading into pseudotachylite veins; e) extensive development of pseudotachylite microbreccia along PDF planes in K-feldspar; f) relict-embayed K-feldspar in amorphous pseudotachylite; g) blebs of relict feldspar showing development of glass along PDFs grading into pseudotachylite; h) pseudotachylite containing diaplectic anorthoclase forming a vein between PDF-bearing quartz grains



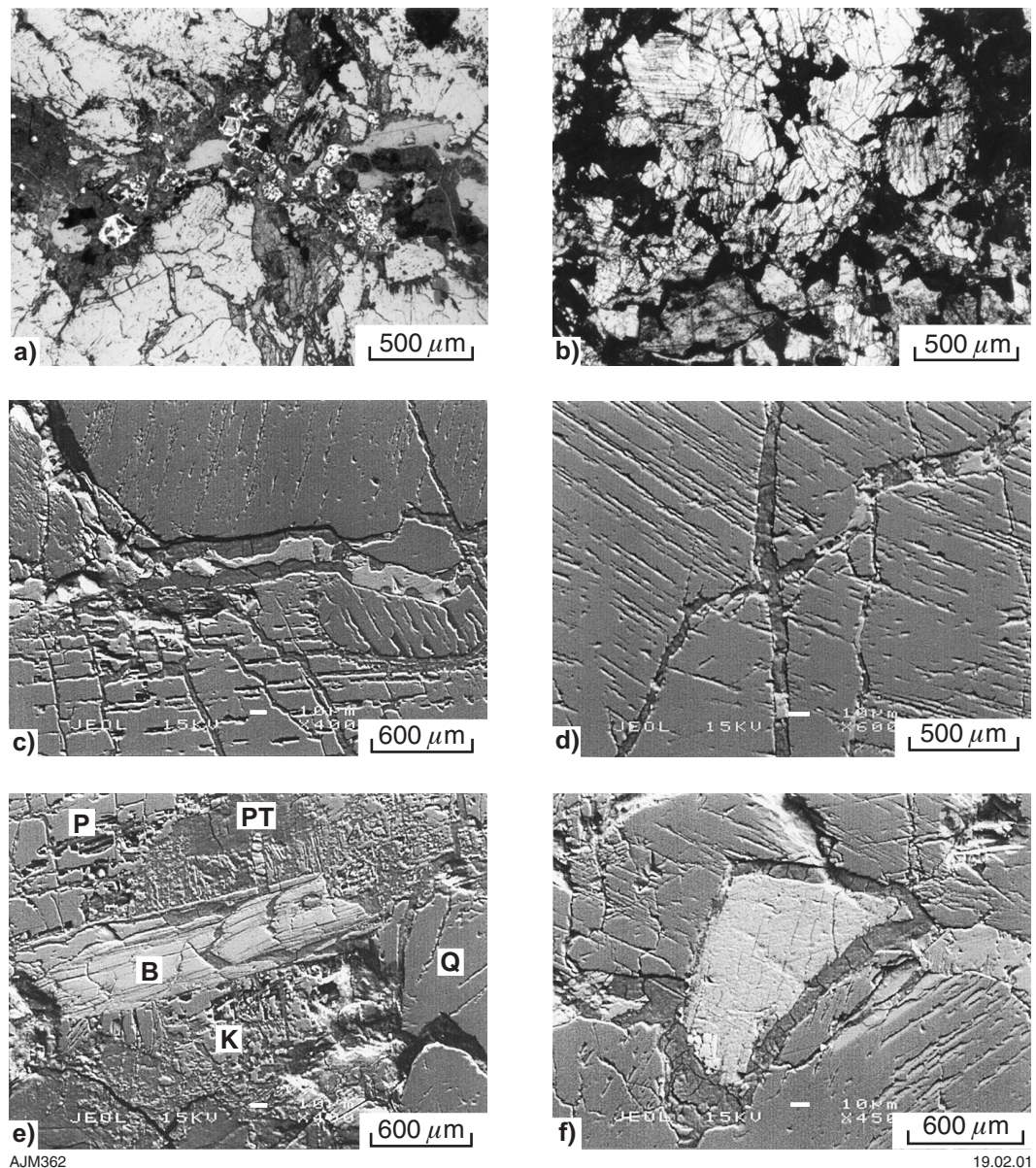


**Figure 4.2.** Optical microphotographs and SEM images of pseudotachylite veins injected into quartz and biotite grains: a) optical microphotograph of pseudotachylite vein injected into an aggregate of quartz and containing late pyrite crystals; b) optical microphotograph of an aggregate of PDF-bearing quartz; c) pseudotachylite vein partly replaced by carbonate, injected between PDF-bearing quartz grains; d) pseudotachylite veins injected into PDF-bearing quartz; e) flake of biotite (B) injected by pseudotachylite and surrounded by partly diaplectic K-feldspar (K) and plagioclase (P), containing amorphous microbreccia (PT). Quartz (Q) grains are least affected by solid-state fusion, confined to narrow PDF zones; f) a flake of biotite surrounded by pseudotachylite veins within an aggregate of PDF-bearing quartz grains

and are typically enveloped by S-PT veins, which also inject the biotite both across and along cleavage planes (Figs 4.1 and 4.2). Minor apatite, monazite, and shocked zircon are associated with biotite and feldspar. The S-PT veins are locally replaced by post-deformation calcite veinlets and euhedral pyrite. Hydrous alteration phases are uncommon in these samples, although in other parts of the drill core, white micas and other hydrous mineral phases are common (see Appendix 3).



## Analytical methods

Drill core samples of shocked, biotite-bearing granitoids were selected by optical microscopy for Laser Raman spectroscopy, whole-rock geochemistry, and SEM coupled with EDS analysis. Seven silicate and trace element XRF analyses were performed (analyst: Ulrich Senff, Geology Department, Australian National University), using PW1200 and PW1400 (for Sc, V, Cr, Co, Th, U) following in part methods by Norrish and Hutton (1969), Norrish and Chappell (1977), and Chappell (1991). Precision and detection limits are presented in Table 4.1. For major element determination ( $\text{SiO}_2$ ,  $\text{TiO}_2$ ,  $\text{Al}_2\text{O}_3$ ,  $\text{Fe}_2\text{O}_3$ ,  $\text{MnO}$ ,  $\text{MgO}$ ,  $\text{CaO}$ ,  $\text{Na}_2\text{O}$ ,  $\text{K}_2\text{O}$ ,  $\text{P}_2\text{O}_5$ ,  $\text{SO}_3$ ) samples were prepared as glass discs, with the exception that the flux used consisted of 12 parts lithium tetraborate to 22 parts lithium metaborate. The glass discs were prepared by the quench press method, which produces thin glass discs that are critically thick up to Cu–Ka radiation for the present flux. These glass discs were measured on a PW1400 wavelength dispersive XRF spectrometer. Calibration for major elements was carried out by measuring glass discs made from high purity compounds. The resulting calibrations were checked against certified reference materials. Major element concentrations are also determined on the pressed powder samples. These suffer from the usual disadvantages associated with the determination of light elements in pressed powders, that is, effects due to variation in particle size distribution and mineralogy. However, the concentrations are of sufficient quality for matrix correction of the trace constituents.

Most trace elements were determined on pressed powder samples using a SPECTRO X-Lab energy dispersive XRF spectrometer. This spectrometer uses secondary targets to modify the primary tube radiation for sample excitation. The targets  $\text{Al}_2\text{O}_3$  and  $\text{B}_4\text{C}$  are used to produce polarized radiation, thereby lowering the background levels and, therefore, detection limits. Elements analysed using the  $\text{B}_4\text{C}$  target are Fe to Nb, Hf to W, Hg to Bi, and Th. Elements analysed with the  $\text{Al}_2\text{O}_3$  target are Mo, Ag to La, Ce to Nd, and U. A secondary Co target is used to excite K to Mn for analysis. This target only produces Co lines, which are efficient in exciting these elements. Use of this target also results in minimal background since no continuum radiation is produced. Elements Na–S are determined using a graphite target. This target reflects the Rh–L lines that are optimal in exciting this group of elements with again minimal background.

Calibration of the spectral instrument was performed using about 130 certified reference materials prepared in duplicate and pure compounds crushed in quartz. Powders were also measured on a PW1400 wavelength dispersive XRF spectrometer for Sc, V, Cr, and Co. The analytical lines for these light trace elements are more difficult to correct for overlap effects in the energy dispersive system and are better determined with a wavelength dispersive spectrometer. The wavelength dispersive spectrometer can also more efficiently excite these elements, using a Cr tube for Sc, a W tube for V and Cr, and a Au tube for Co. Calibration of this spectrometer is performed using pure compounds crushed in acid-washed quartz.

An additional six samples were analysed for selected trace elements by Genalysis Laboratory Services Pty Ltd, Perth, Western Australia (Appendix 3).

Energy dispersive spectrometric analyses were conducted on a Jeol 6400 at the Research School of Biological Studies, Australian National University (analyst: A. Y. Glikson). The study included reconnaissance X-ray mapping at centimetre scale involving semiquantitative EDS scanning of element concentrations larger than about 0.5% (Brink, 1993). In this method, X-ray counts are read at 15 keV accelerating voltage, with spectra collection time of 80 secs (~120 secs real time) at about 8000 cps. Semiquantitative whole-rock analysis was performed by scanning analyses over areas ranging from  $40 \times 50 \mu\text{m}$  to  $140 \times 200 \mu\text{m}$ . Spot analyses were carried with a ~1  $\mu\text{m}$ -size beam. Accuracy and precision were monitored using reference standards by Astimex Scientific Limited MINM25-53 (Serial Number 95-050). Table 4.2 presents estimates of accuracy (mean departure of replicate analyses from the recommended value, RV) and of precision (standard deviation of replicate analyses, SD), based on analyses of standard olivine, diopside, almandine garnet, albite, and barite.

**Table 4.1. Detection limits and precision of oxides determined on wavelength dispersive XRF using a glass-disc of standard composition**

	<i>Method</i>	<i>Detection limit</i>	<i>Average composition</i>	<i>Precision/error</i>
<b>Percentage</b>				
SiO <sub>2</sub>	PW1200	0.02	71.039	0.3
Al <sub>2</sub> O <sub>3</sub>	PW1200	0.02	14.250	0.15
TiO <sub>2</sub>	PW1200	0.003	0.312	0.005
Fe <sub>2</sub> O <sub>3</sub>	PW1200	0.002	2.507	0.02
MnO	PW1200	0.002	0.034	0.002
MgO	PW1200	0.006	0.933	0.04
CaO	PW1200	0.006	2.173	0.02
Na <sub>2</sub> O	PW1200	0.012	3.982	0.05
K <sub>2</sub> O	PW1200	0.002	3.836	0.02
P <sub>2</sub> O <sub>5</sub>	PW1200	0.003	0.131	0.005
SO <sub>3</sub>	PW1200	0.003	0.005	0.003
<b>Parts per million</b>				
Sc	PW1400	1.0	—	—
V	PW1400	2.0	—	—
Cr	PW1400	2.0	—	—
Co	PW1400	2.0	—	—
Ni	PW1200	1.0	—	—
Cu	PW1200	1.0	—	—
Zn	PW1200	1.0	—	—
Ga	PW1200	0.7	—	—
Ge	PW1200	0.7	—	—
As	PW1200	0.6	—	—
Se	PW1200	0.6	—	—
Br	PW1200	0.6	—	—
Rb	PW1200	0.5	—	—
Sr	PW1200	0.5	—	—
Y	PW1200	0.8	—	—
Zr	PW1200	0.8	—	—
Nb	PW1200	0.9	—	—
Mo	PW1200	1.0	—	—
Ag	PW1200	0.4	—	—
Cd	PW1200	0.3	—	—
In	PW1200	0.5	—	—
Sn	PW1200	0.6	—	—
Sb	PW1200	0.8	—	—
Te	PW1200	1.0	—	—
I	PW1200	2.0	—	—
Cs	PW1200	2.0	—	—
Ba	PW1200	2.0	—	—
La	PW1400	5.0	—	—
Ce	PW1200	3.0	—	—
Pr	PW1200	2.0	—	—
Nd	PW1200	2.5	—	—
Hf	PW1200	3.0	—	—
Ta	PW1200	4.0	—	—
W	PW1200	3.0	—	—
Tl	PW1200	0.7	—	—
Pb	PW1200	1.0	—	—
Bi	PW1200	1.0	—	—
Th	PW1400	1.0	—	—
U	PW1400	1.0	—	—

**NOTES:** PW1200: Energy dispersive spectrometer  
PW1400: Wavelength dispersive spectrometer

Table 4.2. Precision and accuracy of repeated measurements of standard minerals on the Jeol 6400 SEM/EDS

	Olivine		Precision		Accuracy		Diopside		Precision		Accuracy		Almandine		Precision		Accuracy		Albite		Precision		Accuracy		Barite		Precision		Accuracy	
	standard	RV	(n = 5)	%OAP	(n = 5)	%OAP	standard	RV	(n = 5)	%OAP	(n = 5)	%OAP	standard	RV	(n = 5)	%OAP	(n = 5)	%OAP	standard	RV	(n = 5)	%OAP	(n = 5)	%OAP	standard	RV	(n = 4)	%OAP	(n = 4)	%OAP
SiO <sub>2</sub>	41.85		±0.15		±2.0		55.37		±0.27		±0.40		39.19		±0.44		±1.47		68.52		±0.22		±0.90		-		-		-	
TiO <sub>2</sub>	-		-		-		0.08		-		-		-		-		-		-		-		-		-		-		-	
FeO (total)	6.51		±0.24		±13		0.05		-		-		23.27		±0.12		±1.96		-		-		-		-		-		-	
MnO	0.12		-		-		0.05		-		-		0.59		±0.11		±0.34		-		-		-		-		-		-	
MgO	51.75		±0.42		±1.4		18.62		±0.23		±0.20		10.7		±0.11		±2.5		-		-		-		-		-		-	
NiO	0.20		±0.15		-		-		-		-		-		-		-		-		-		-		-		-		-	
CaO	-		-		-		25.73		±0.20		±0.69		4.2		±0.05		±2.95		0.13		±0.03		±73		-		-		-	
Al <sub>2</sub> O <sub>3</sub>	-		-		-		-		-		-		22.05		±0.16		±0.33		19.54		±0.19		±0.60		-		-		-	
Na <sub>2</sub> O	-		-		-		-		-		-		-		-		-		-		-		±1.10		-		-		-	
K <sub>2</sub> O	-		-		-		-		-		-		-		-		-		0.22		-		-		-		-		-	
BaO	-		-		-		-		-		-		-		-		-		-		-		-		-		-		-	
SO <sub>3</sub>	-		-		-		-		-		-		-		-		-		-		-		-		65.7		±0.48		±0.2	
<b>Total</b>	<b>100.43</b>						<b>99.90</b>						<b>100.0</b>						<b>100.00</b>						<b>33.31</b>		<b>±0.24</b>		<b>±1.8</b>	

NOTES: Precision: standard deviation of X readings on the Jeol 6400

Accuracy: departure of the mean of X readings on the Jeol 6400 from the recommended value (RV) of the mineral standard in percentage of the amount present (%OAP)

n: number of analyses

## Results

The mean composition of the granitoids, based on seven XRF analyses and numerous EDS scanning analyses, approximates monzogranite (Tables 4.3 and 4.5), but is commonly enriched relative to low-Ca granites in Mg, Fe, Ca, Ni, Co, and Cr (Tables 4.4 and 4.5). Energy dispersive spectrometry and laser ICPMS studies indicate enrichment of the S-PT veins and amorphous intra-feldspar diaplectic spots in refractory Al and Mg and depletion in the volatile Si and K relative to bulk rock compositions.

Major element analytical data for seven shock-metamorphosed granitoids (Table 4.3) display a marked compositional heterogeneity (normative Qz ~19–74%; Or ~4–47%; Ab ~4–24%; An ~2–14%), reflecting shock-induced partial fusion of feldspars and consequent partial migration and injection of Al-rich melt and microbreccia as S-PT veins. Whole-rock compositions also show marked variations in MgO (0.65 – 3.75%), Fe<sub>2</sub>O<sub>3</sub> (1.35 – 12.93%), and CaO (0.54 – 2.93%). The high to very high combined volatiles (~2–11%) are attributable to the high water contents of the incorporated S-PT veins. An estimate of the original overall composition of the shocked granitoids is complicated by the high standard deviations shown by the analyses (Table 4.5). Excluding the relatively more-anomalous compositions of GSWA 149139 (Fe<sub>2</sub>O<sub>3</sub> = 12.93%; MgO = 3.75%) and 132521 (>10% volatiles; Table 4.3) results in lower standard deviations (Table 4.5). However, standard deviations for ferromagnesian elements (FeO, MgO, CaO, TiO<sub>2</sub>) and K<sub>2</sub>O are still about or over 50% of the mean composition (Table 4.5), casting doubt on confident estimates of mean original composition of the shocked granitoids. With these uncertainties in mind, the mean normative composition B (Qz ~40%; Ab ~16%; An ~8%; Or ~20%) and the K<sub>2</sub>O:Na<sub>2</sub>O:CaO ratio (~0.5:0.25:0.25) broadly correspond to monzogranite composition, according to the International Union of Geological Sciences (IUGS) classification (Le Bas and Streckeisen, 1991). Abundances of SiO<sub>2</sub> and Al<sub>2</sub>O<sub>3</sub> are similar to low-Ca granites (Turekian and Wedepohl, 1961). However, CaO, MgO, and Fe<sub>2</sub>O<sub>3</sub> abundances are intermediate between those of low-Ca and high-Ca granitoids (Table 4.5). Potassium and sodium have low abundances in the shocked granitoids compared to low-Ca granites (Tables 4.3 and 4.5). Chalcophile trace elements (V, Cu, Zn) display a wide dispersion above and below the fields of low-Ca and high-Ca granites (Figs 4.3 and 4.4), whereas ferromagnesian trace element (Ni, Co, Cr) levels are high by factors of up to 2 relative to high-Ca granites (Tables 4.3, 4.4, and 4.5).

Energy dispersive spectrometry analyses of pseudotachylite veins and diaplectic, intra-feldspar amorphous zones and spots indicate combined volatile contents in the range of 5–15% (Table 4.6). In comparing whole-rock major element compositions with point and scanning analyses of S-PT veins and diaplectic amorphous material (DG) fractions, consistent chemical enrichment/depletion trends are observed (Figs 4.3 and 4.4). The more refractory major elements (Al, Mg, and in many instances Ca) are mostly enriched in the S-PT and DG relative to whole-rock compositions (Figs 4.3 and 4.4; Table 4.7). By contrast, SiO<sub>2</sub>, K<sub>2</sub>O, and in some instances Na<sub>2</sub>O, are commonly depleted in S-PT and DG relative to whole rock compositions, that is SiO<sub>2</sub> by a factor of about 0.8 and K<sub>2</sub>O by factors as low as 0.5. Variable relations pertain to Fe, which is depleted in S-PT veins in quartz and feldspar and less depleted in S-PT veins within biotite, suggesting some breakdown of the latter phase. Diaplectic amorphous zones within K-feldspars are enriched in K relative to whole-rock compositions. Surprisingly high levels of Mg occur in these glasses (Tables 4.6 and 4.7; Figs 4.3 and 4.4). This enrichment can be traced from Mg-free, fresh K-feldspar points, to hydrated K-feldspar points (<1.2% MgO), to amorphous points (<4.0% MgO; Table 4.6). Whereas SiO<sub>2</sub> and Al<sub>2</sub>O<sub>3</sub> levels in the hydrated feldspar spots are similar to the host feldspar, K<sub>2</sub>O is somewhat decreased and MgO and FeO markedly enriched.

Contributions to S-PT and DG from the breakdown of host phases are indicated by enrichment of FeO in veins in biotite and K<sub>2</sub>O in spots within K-feldspars. The DG zones and spots within K-feldspar are consistent with their host phases with respect to SiO<sub>2</sub> and Al<sub>2</sub>O<sub>3</sub>, strongly enriched in MgO, FeO, and CaO, and strongly depleted in K<sub>2</sub>O and Na<sub>2</sub>O. The DG zones and spots within anorthoclase are consistent with their host phases with respect to SiO<sub>2</sub> and K<sub>2</sub>O. In addition, the DG is strongly enriched in MgO and FeO and depleted in Na<sub>2</sub>O and CaO. The petrogenetic implications of these observations are discussed in Glikson et al. (in prep.).

**Table 4.3. XRF major and minor element analyses of seven shocked granitoid samples from the basement uplift intersected by Woodleigh 1A**

Sample no.	132521	132526	149138	149139	149140	149141	149150
<b>Silicate analysis</b>							
	<b>Percentage</b>						
SiO <sub>2</sub>	62.26	85.87	72.79	55.01	72.79	69.43	66.03
TiO <sub>2</sub>	0.558	0.138	0.111	1.54	0.123	0.311	0.587
Al <sub>2</sub> O <sub>3</sub>	12.76	5.42	13.33	15.04	13.04	14.75	14.40
Fe <sub>2</sub> O <sub>3</sub> (total)	5.34	1.86	1.35	12.93	1.57	2.70	5.85
MnO	0.154	0.028	0.025	0.172	0.035	0.035	0.126
MgO	2.67	0.65	0.67	3.75	0.91	1.27	1.95
CaO	2.70	1.93	0.539	2.33	1.58	2.93	2.27
Na <sub>2</sub> O	0.43	0.91	1.46	2.06	2.26	2.88	1.87
K <sub>2</sub> O	2.06	0.716	7.87	3.63	4.25	1.56	2.86
P <sub>2</sub> O <sub>5</sub>	0.024	0.323	0.091	0.259	0.045	0.067	0.045
S	0.118	0.027	0.010	0.826	0.010	0.011	0.130
Volatiles	~11	~2	~2	~2	~3	~4	~4
<b>Total (dry)</b>	<b>89.07</b>	<b>97.86</b>	<b>98.25</b>	<b>97.55</b>	<b>96.61</b>	<b>95.95</b>	<b>96.12</b>
<b>CIPW Norm</b>							
	<b>Percentage</b>						
Quartz	42.54	73.64	32.28	19.28	38.76	38.73	37.01
Corundum	4.97	0.41	1.65	4.11	1.96	3.16	4.21
Orthoclase	12.17	4.23	46.51	21.45	25.11	9.22	16.9
Albite	3.64	7.7	12.35	17.43	19.12	24.37	15.82
Anorthite	13.24	7.46	2.08	9.87	7.54	14.1	10.97
Hypersthene	6.65	1.62	1.67	9.34	2.27	3.16	4.11
Enstatite	6.65	1.62	1.67	9.34	2.27	3.16	4.11
Haematite	5.34	1.86	1.35	12.93	1.57	2.7	5.85
Ilmenite	0.32	0.06	0.05	0.37	0.07	0.07	0.27
Rutile	0.39	0.11	0.08	1.35	0.08	0.27	0.45
Apatite	0.06	0.77	0.22	0.61	0.11	0.16	0.11
<b>Petrochemical indices</b>							
Diff. index	58.35	85.57	91.14	58.17	83	72.31	69.74
Colour index	12.7	3.64	3.15	23.98	3.99	6.21	10.67
Pl = Ab+An	16.88	15.16	14.43	27.3	26.67	38.47	26.79
100An/(Ab+An)	78.44	49.22	14.41	36.15	28.29	36.65	40.94
100An/(An+Ab)	78.44	49.22	14.41	36.15	28.29	36.65	40.94
Ab = Ab+1.85Ne	3.64	7.7	12.35	17.43	19.12	24.37	15.82
Q = Q+0.3En+.23Fs	44.53	74.13	32.78	22.08	39.44	39.67	38.24
Ol = Ol+.7En+.8Fs	4.66	1.13	1.17	6.55	1.59	2.22	2.88
Ne = Ne+.54Ab	1.97	4.17	6.7	9.45	10.36	13.21	8.58
Q = Q+.46Ab	46.19	77.65	38.44	30.06	48.2	50.83	45.49
<b>Trace elements</b>							
	<b>Parts per million</b>						
Sc	18	7	4	47	5	4	18
V	126	22	14	248	19	34	91
Cr	19	24	8	75	6	10	74
Co	18	6	6	40	4	8	18
Ni	17	9	5	43	4	6	29
Cu	4	36	3	193	6	2	12
Zn	52	35	23	132	22	31	78
Ga	21	8	11	25	15	18	19
Ge	1.0	0.9	0.9	2.1	1.4	0.6	1.5
As	-0.3	-0.2	-0.4	-0.4	-0.3	-0.3	-0.5
Se	-0.2	-0.1	-0.1	0.5	-0.1	0.1	-0.2
Br	3	2	4	6	8	3	8
Rb	93	64	179	190	90	73	163
Sr	102	70	96	108	99	207	129
Y	22	15	13	30	10	6	23
Zr	57	21	62	166	43	117	162
Nb	11	5	5	14	6	4	13
Mo	-0.3	-0.2	-0.2	0.5	-0.2	-0.2	0.3
Ag	-0.1	0.1	0.3	0.3	0.2	0.1	-0.1
Cd	0.3	-0.1	0.2	-0.1	0.2	-0.1	-0.1
In	-0.1	-0.1	-0.1	-0.1	-0.1	-0.1	-0.1
Sn	1.3	1.4	1.4	1.4	1.3	0.9	1.3
Sb	0.2	0.2	0.2	-0.1	0.1	0.1	-0.1
Te	-0.2	-0.2	-0.2	-0.2	-0.2	-0.2	-0.2



Table 4.3. (continued)

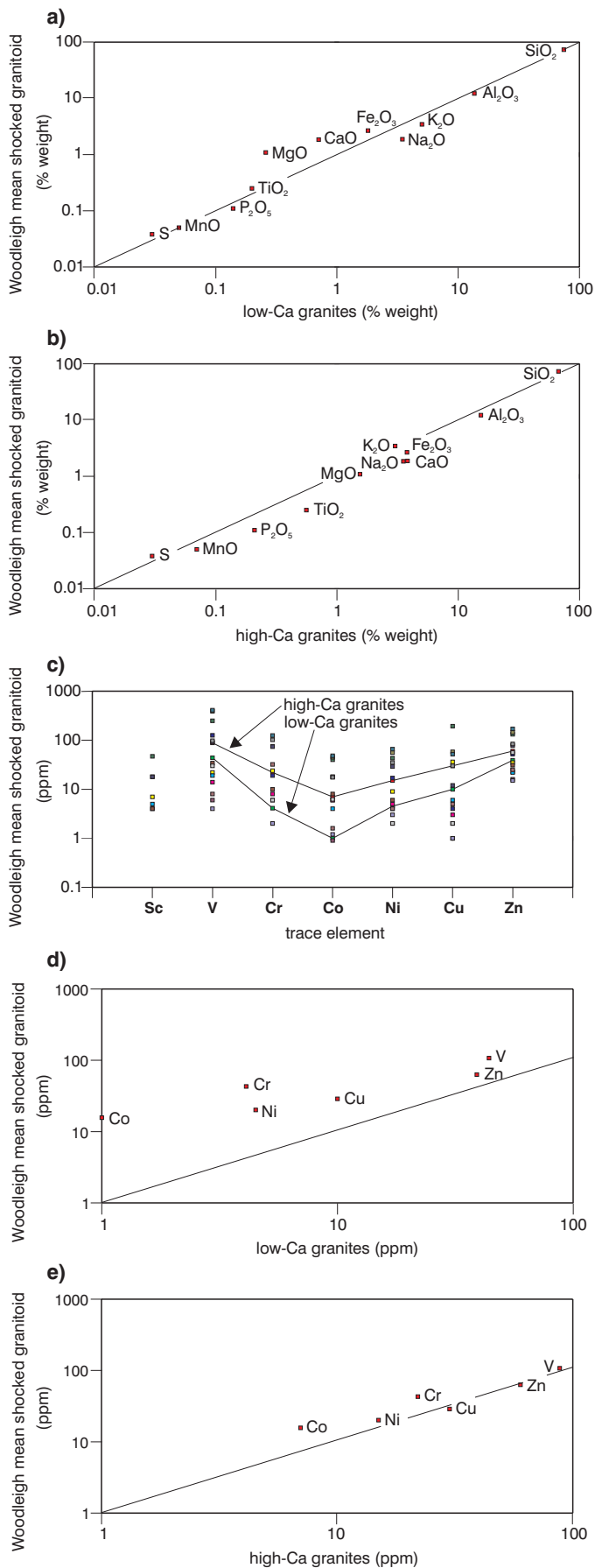
Sample no.	132521	132526	149138	149139	149140	149141	149150
I	-0.3	-0.3	-0.4	-0.4	-0.4	-0.3	-0.4
Cs	1.3	1.3	0.9	7.6	1.0	-0.5	0.6
Ba	165	58	881	264	410	213	588
La	7	9	12	18	9	7	33
Ce	18	20	28	45	23	20	73
Pr	-2	2	-2	-2	-2	-2	-2
Nd	5	9	6	15	6	5	15
Hf	2	0	2	7	1	3	7
Ta	5	-2	1	-6	1	-1	2
W	1	-1	2	-2	2	2	2
Tl	-0.4	-0.3	-0.4	-0.6	-0.3	-0.4	0.4
Pb	21	13	57	17	32	20	45
Bi	-0.3	-0.2	-0.3	0.3	-0.2	-0.2	-0.3
Th	9	3	11	5	8	8	15
U	17	3	2	2	1	1	3

NOTES: Ab: Albite  
An: Anorthoclase  
En: Enstatite  
Fs: Feldspar

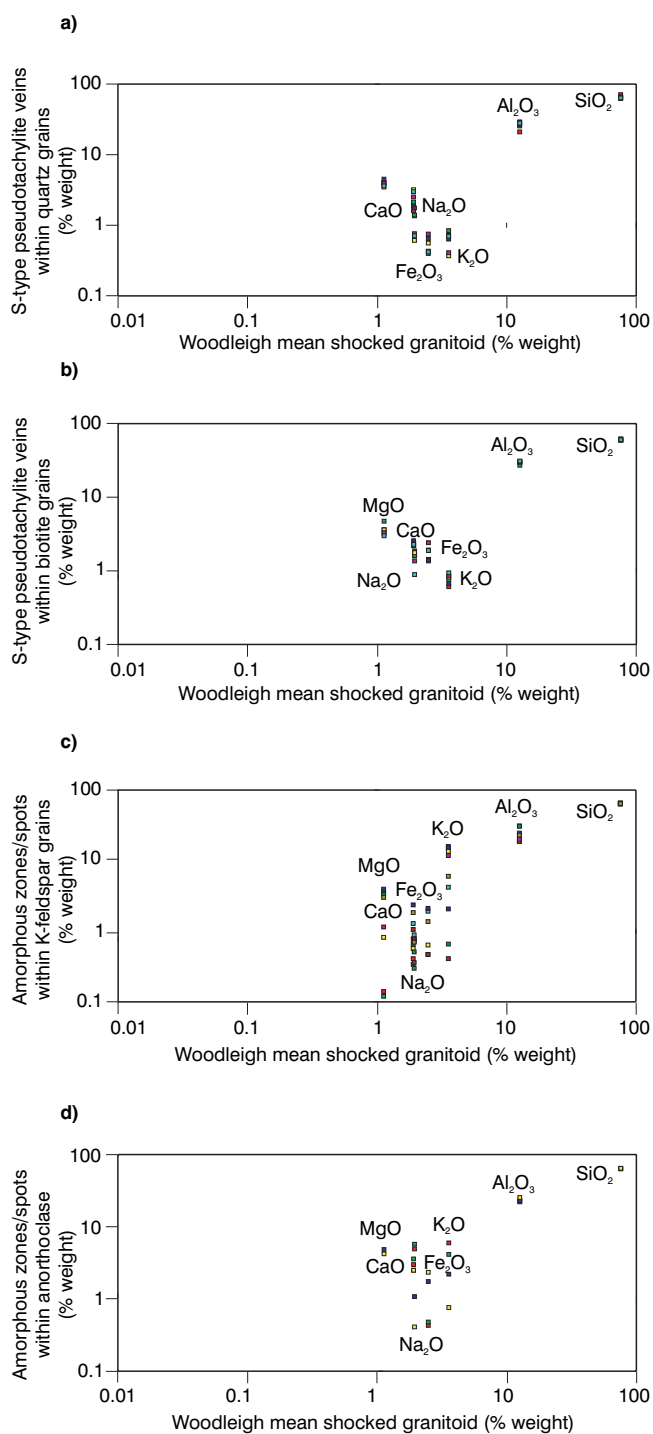
Ne: Nepheline  
Ol: Oligoclase  
Pl: Plagioclase  
Q: Quartz

Table 4.4. Trace metal data for seven samples of pseudotachylite-injected, shocked gneiss compared with average high-Ca and low-Ca granite of Turekian and Wedepohl (1961)

Sample no.	132527	132528	132529	132530	132531	132532	132533	high-Ca granite	low-Ca granite
Parts per million									
Ag	0.2	0.1	0.1	0.1	0.2	0.1	0.1	0.051	0.037
As	9	1	3	1	2	1	1	—	—
Au	5	5	5	5	5	5	5	0.004	0.004
Ba	150	560	108	265	380	460	640	420	840
Bi	0.33	0.04	0.3	0.02	0.07	0.02	0.1	—	—
Co	45	0.9	48	6.2	17.5	1.2	1.6	7	1
Cr	116	2	125	6	102	2	32	22	4.1
Cu	58	1	52	2	30	1	5	30	10
Mo	1.1	0.4	0.4	0.2	1	0.3	0.4	1	1.3
Ni	56	2	66	2	35	3	4	15	4.5
Pb	12	62	6	12	26	66	100	15	19
Pd	2	2	2	2	2	2	2	—	—
Pt	2	2	2	2	2	2	2	—	—
Sb	0.15	0.05	0.05	0.05	0.05	0.05	0.05	0.2	0.2
Sn	4.3	1	19.5	0.6	2	1	3.3	1.5	3.0
V	390	6	410	30	98	4	8	88	44
Wo	0.4	0.2	1.2	0.1	0.7	0.2	0.7	1.3	2.2
Zn	145	16	170	56	84	15	25	60	39
Ru	2	2	2	2	2	2	2	—	—
Rh	1	1	1	1	1	1	1	—	—
Os	2	2	2	2	2	2	2	—	—
Ir	2	2	2	2	2	2	2	—	—



**Figure 4.3. Comparisons between major elements and ferromagnesian trace-element composition of Woodleigh mean shocked granitoid (WMSG) and the composition of average low-Ca and high-Ca granites (Turekian and Wedepohl, 1961): a) major elements of WMSG vs low-Ca granites; b) major elements of WMSG vs high-Ca granites; c) trace metal compositional range of WMSG compared with low-Ca granites (lower curve) and high-Ca granites (higher curve); d) trace metals of WMSG vs low-Ca granites; e) trace metals of WMSG vs high-Ca granites**



AJM331

01.05.01

**Figure 4.4. Comparisons between Woodleigh shocked granitoid (mean of five XRF analyses) and EDS analyses of S-type pseudotachylite veins (S-PT) for sample 149142 (data from Table 4.7) within; a) quartz grains; and b) biotite grains; and amorphous diaplectic glass zones and spots within; c) K-feldspar; and d) anorthoclase**

**Table 4.5. Mean composition of shocked granitoid of the Woodleigh basement uplift (based on data reported in Tables 4.3 and 4.4) compared with average low-Ca and average high-Ca granite compositions (Turekian and Wedepohl, 1961)**

	<i>A</i>	<i>B</i>	<i>low-Ca</i> <i>granites</i>	<i>high-Ca</i> <i>granites</i>
<b>Silicate analysis</b>			<b>Percentage</b>	
SiO <sub>2</sub>	69.17 ± 16.5	73.38 ± 7.5	74.25	67.19
TiO <sub>2</sub>	0.48 ± 0.5	0.25 ± 0.2	0.20	0.56
Al <sub>2</sub> O <sub>3</sub>	12.68 ± 3.3	12.19 ± 3.8	13.6	15.4
FeO (total)	4.06 ± 3.7	2.40 ± 1.62	1.81	3.79
MnO	0.08 ± 0.06	0.05 ± 0.04	0.05	0.07
MgO	1.69 ± 1.17	1.09 ± 0.54	0.26	1.55
CaO	2.04 ± 0.8	1.85 ± 0.88	0.71	3.54
Na <sub>2</sub> O	1.69 ± 0.8	1.88 ± 0.75	3.47	3.82
K <sub>2</sub> O	3.28 ± 2.3	3.45 ± 2.8	5.04	3.02
P <sub>2</sub> O <sub>5</sub>	0.12 ± 0.11	0.11 ± 0.12	0.14	0.21
S	0.16 ± 0.29	0.038 ± 0.05	0.03	0.03
<b>Trace elements</b>			<b>Parts per million</b>	
Sc (7 analyses)	14.7 ± 15.5	—	—	—
V (14 analyses)	107.1 ± 140.9	—	44	88
Cr (14 analyses)	42.9 ± 45.5	—	4.1	22
Co (14 analyses)	15.7 ± 16.7	—	1	7
Ni (14 analyses)	20.1 ± 21.9	—	4.5	15
Cu (14 analyses)	28.9 ± 51.1	—	10	30
Zn (14 analyses)	63.1 ± 51.7	—	39	60
<b>Mean CIPW norm</b>			<b>Percentage</b>	
Quartz	40.3	44.1	—	—
Corundum	2.9	2.3	—	—
Orthoclase	19.4	20.4	—	—
Albite	14.3	15.9	—	—
Anorthite	9.3	8.4	—	—
Hypersthene	4.1	2.6	—	—
Enstatite	4.1	2.5	—	—
Haematite	4.5	2.6	—	—
Ilmenite	0.17	0.1	—	—
Rutile	0.4	0.2	—	—
Apatite	0.29	0.27	—	—

**NOTES:** A: mean and standard deviation of seven silicate analyses  
B: mean and standard deviation of five less-altered analyses; excluding two anomalous samples from A



Table 4.6. EDS analyses of shocked granitoid GSWA 149142 (198.35 – 198.5 m)

	SiO <sub>2</sub>	TiO <sub>2</sub>	Al <sub>2</sub> O <sub>3</sub>	FeO	MnO	MgO	CaO	Na <sub>2</sub> O	K <sub>2</sub> O	Total	Volatiles
<b>1. EDS scanning area analyses (normalized to 100%)</b>											
A	80.05	–	12.68	1.50	–	1.41	2.10	0.68	1.59	–	–
B	77.62	–	14.35	1.30	0.33	1.50	2.19	1.14	1.57	–	–
C	77.43	0.29	15.25	0.95	–	1.48	2.03	0.90	1.67	–	–
D	81.83	–	11.43	0.64	–	1.07	2.13	1.41	1.48	–	–
Mean	79.23	–	13.42	1.10	–	1.36	2.11	1.03	1.57	–	–
<b>2. EDS spot analyses of pseudotachylite veins cutting through quartz (oxides normalized to 100%)</b>											
A	70.98	–	21.04	0.43	–	3.89	1.61	1.36	0.72	100	10.72
B	65.64	–	25.55	0.40	–	4.02	2.13	1.40	0.84	100	11.34
C	64.23	–	26.43	0.65	–	4.50	1.87	1.76	0.64	100	5.27
D	62.65	–	29.12	0.56	–	3.49	3.19	0.61	0.37	100	14.15
E	62.87	–	28.76	0.75	–	3.94	2.52	0.76	0.41	100	20.55
F	63.51	–	28.03	0.42	–	3.62	3.0	0.71	0.70	100	21.30
<b>3. EDS spot analyses of pseudotachylite/microbreccia veins (PTV) cutting through biotite (oxides normalized to 100%)</b>											
A	60.33	–	30.30	1.36	–	3.62	2.19	1.60	0.61	100	4.01
B	62.11	–	27.15	1.43	–	4.74	2.20	1.61	0.76	100	15.53
C	60.20	–	30.15	1.40	–	3.16	2.56	1.86	0.67	100	9.87
D	59.51	–	30.17	1.92	–	3.61	2.20	1.77	0.82	100	3.89
E	59.55	–	30.13	2.42	–	3.29	2.38	1.36	0.86	100	17.61
F	60.23	–	30.95	1.89	–	3.0	2.28	0.89	0.94	100	17.4
<b>4. EDS spot analysis of a single grain of K-feldspar, hydrated K-feldspar, contained glass spot, and glass spots from other K-feldspar grains (normalized to 100%)</b>											
K-feldspar Pt A	64.95	–	19.13	–	–	0.14	0.41	0.77	14.60	100	0.91
K-feldspar Pt B	65.00	–	18.72	–	–	0.12	–	0.30	15.86	100	1.46
K-feldspar Pt C	65.28	–	18.64	–	–	0	0.34	–	15.40	100	0.59
Hydrated K-feldspar Pt D	64.63	–	18.98	0.64	–	0.82	0.57	0.78	13.58	100	12.27
Hydrated K-feldspar Pt E	65.10	–	19.94	0.47	–	1.15	0.78	0.76	11.79	100	11.09
Glass spot Pt F	65.23	–	22.86	1.92	–	3.61	1.29	0.89	4.21	100	27.51
Glass spot in other K-feldspar grains	63.15	–	31.00	0.47	–	3.56	1.06	0.36	0.41	100	26.83
Glass spot in other K-feldspar grains	64.05	–	30.84	–	–	3.29	0.66	0.51	0.66	100	26.5
Glass spot in other K-feldspar grains	64.18	–	24.62	2.11	–	3.94	2.36	0.71	2.07	100	14.78
Glass spot in other K-feldspar grains	64.09	–	23.01	1.37	–	3.01	1.84	0.70	5.99	100	12.43
<b>5. EDS spot analyses of a single grain of anorthoclase with hydrated contained glass spots (normalized to 100%)</b>											
Anorthoclase spot A	63.41	–	22.08	0.43	–	–	3.0	4.92	5.97	100	4.89
Anorthoclase spot B	63.58	–	22.48	0.48	–	–	3.59	5.74	4.14	100	4.81
Glass spot 1	64.43	–	23.20	1.75	–	4.85	2.50	1.08	2.20	100	12.64
Glass spot 2	64.34	–	25.43	2.34	–	4.22	2.50	0.41	0.76	100	15.30

**Table 4.7. Comparisons between mean whole-rock compositions analysed by XRF (five analyses, based on Table 4.1), S-type pseudotachylite veins cutting through quartz and biotite, and diaplectic glasses in feldspars in shocked granitoid in GSWA 149142**

	<i>mean of 5 XRF whole-rock analyses</i>	<i>1 Mean of 6 S-PT (qz)</i>	<i>2 Mean S-PT (bi)</i>	<i>3 Mean DG (kf)</i>	<i>4 Mean DG (an)</i>
SiO <sub>2</sub>	73.38	65.00	60.3	64.6	63.9
Al <sub>2</sub> O <sub>3</sub>	12.19	26.5	29.8	22.8	23.3
FeO	2.40	0.5	1.73	1.16	1.25
MgO	1.09	3.9	3.57	1.96	4.53
CaO	1.85	2.4	2.30	1.03	2.9
Na <sub>2</sub> O	1.88	1.1	1.51	0.64	3.03
K <sub>2</sub> O	3.45	0.61	0.77	8.45	3.26

**NOTES:** 1: mean S-PT veins within qz      an: anorthoclase      DG: diaplectic glasses in feldspars  
2: mean S-PT veins within biotite      bi: biotite      S-PT: S-type pseudotachylite veins  
3: mean DG spots in K-feldspar      kf: K-feldspar  
4: mean DG spots in anorthoclase      qz: quartz

## Summary

SEM and EDS studies, Laser Raman spectroscopy, laser ICPMS, and whole-rock major and trace XRF and ICPMS studies were conducted on shocked granitoid samples from the central uplift of the Woodleigh impact structure. The shocked granitoids display extreme compositional variability due to shock-metamorphic differentiation of feldspar-rich and quartz-rich components. Their mean composition approximates monzogranite, but is enriched relative to low-Ca granites in Mg, Fe, Ca, Ni, Co, and Cr. The shocked granitoids are penetratively injected and criss-crossed by microbreccia-glass veins, and may be classified in terms of shock-metamorphosed granitoid basement, injected by S-PT veins (defined after Spray, 1998), or alternatively represent subcrater granitoid megabreccia injected by impact melt. Shocked feldspars contain abundant micron-scale, amorphous material along PDFs, as well as distinct rounded inclusions. Where abundant amorphous material is present, a honeycomb-like textured, crystalline–amorphous pattern ensues within the feldspars, representing an uncommon form of partial diaplectic transformation. EDS and laser ICPMS studies indicate enrichment of the S-PT and amorphous, intra-feldspar spots in refractory Al and Mg, and depletion in the volatile Si and K relative to bulk rock compositions. Laser ICPMS traverses indicate strong enrichment of ferromagnesian elements (Mg, Ni, Co, Cr) in the S-PT veins. The origin and mode of transport of these enriched zones imply possible derivation of ferromagnesian trace-element-enriched melt and vapour phases from the exploding projectile and their injection into, and condensation throughout, much of the shocked granitoid, including condensation in texturally isolated, micron-scale spots within feldspars. More details and implications from the data presented in this Appendix are provided by Glikson et al. (in prep.).

## References

- BRINK, F. J., 1993, A review of X-ray mapping: La Trobe University, Bendigo, report (unpublished), 18p.
- CHAPPELL, B. W., 1991, Trace element analysis of rocks by X-ray spectrometry, *in* *Advances in X-ray analysis*, 34 edited by C. S. BARRETT: New York, Plenum Press, p. 263–290.
- GLIKSON, A. Y., PIRAJNO, F., MORY, A. J., IASKY, R. P., EGGINS, S., and MERNAGH, T. P., in prep., Shock metamorphism and possible meteoritic element enrichment in granitoid basement uplift, Woodleigh impact structure, Carnarvon Basin, Western Australia.
- LE BAS, M. J., and STRECKEISEN, A. L., 1991, The IUGS systematics of igneous rocks: *Journal of the Geological Society*, London, v. 148, p. 825–833.

- NORRISH, K., and HUTTON, J. T., 1969, An accurate X-ray spectrographic method for the analysis of a wide range of geological samples: *Geochimica et Cosmochimica Acta*, v. 33, p. 431–453.
- NORRISH, K., and CHAPPELL, B. W., 1977, X-ray fluorescence spectrometry, *in* *Physical methods in determinative mineralogy*, 2nd edition *edited by* J. ZUSSMAN: London, Academic Press, p. 201–272.
- SPRAY, J. G., 1998. Localised shock- and friction-induced melting in response to hypervelocity impact: Geological Society of London, Special Publication, no. 140, p. 195–204.
- TUREKIAN, K. K., and WEDEPOHL, K. H., 1961, Distribution of the elements in some units of the Earth's crust: Geological Society of America, Bulletin, no. 72, p. 175–185.

## Appendix 5

### Palynology

by J. Backhouse  
(Backhouse Biostrat Pty Ltd)

#### Introduction

Palynological results from Woodleigh 1, 2, and 2A are based on the samples listed in Table 5.1. The three samples from Woodleigh 1, four cuttings samples and three core samples from Woodleigh 2, and 11 cuttings samples from Woodleigh 2A are Cretaceous in age. Pre-Cretaceous strata are only evident in the deepest well, Woodleigh 2A, in which 17 samples are dated as Jurassic and five samples are dated as pre-Devonian, probably Late Silurian. Three samples are barren and one clast from the Jurassic section contains material that is probably pre-Devonian in age. Estimates of organic yield are based on the amount of residue produced after acid digestion. Counts of palynomorphs were not done for cuttings samples as the proportion of caved palynomorphs can never be determined with certainty. Counts of 300 specimens were made on high yielding samples and counts of 200 or less were made on low yielding samples. A palynological summary of all samples is provided in Table 5.2. The distribution of dinoflagellate cysts (dinocysts) in cuttings samples is detailed in Figure 5.1, in which taxa are arranged in alphabetical order. The distribution of taxa in core samples in Woodleigh 2A is set out in Figure 5.2, and the distribution of reworked taxa in the cored interval of Woodleigh 2A is shown in Table 5.3.

The major zonal subdivision used in the Cretaceous and Jurassic is based on Helby et al. (1987). The informal Cretaceous subzones are based on unpublished work by B. S. Ingram, N. Hooker, and R. Morgan.

#### Palynological observations and comments: Woodleigh 2 and 2A

##### 87–90 to 111–114 m, ?*Canninginopsis denticulata* dinoflagellate zone

These cuttings samples yielded moderately rich and generally diverse assemblages. Assignment to the *Canninginopsis denticulata* Zone is qualified by the presence of *Dingodinium cerviculum* Cookson and Eisenack 1958 in the highest sample, and *Endoceratium ludbrookiae* (Cookson and Eisenack 1958) in the 102–105 m sample. *D. cerviculum* does not range above the *Muderongia tetracantha* Zone, and the presence of a single specimen in this sample may be either down-hole or laboratory contamination. The presence of *E. ludbrookiae* is evidence for the presence of the *E. ludbrookiae* Zone somewhere higher in the well, or possibly in the upper part of this interval. The overall composition of assemblages in all three samples is consistent with the *C. denticulata* Zone, thereby indicating an Albian age.

##### 120–123 to 129–132 m, *Diconodinium davidii* dinoflagellate zone

*Diconodinium davidii* Morgan 1975 is present in the higher sample and *Muderongia tetracantha* (Gocht 1957) is present in both assemblages, indicating that the *D. davidii* Zone has been penetrated at, or above, 120–123 m. There is no evidence in either sample of the *M. australis* Zone, and therefore, both samples are assumed to be within the *D. davidii* Zone. The presence of the dinocysts *Carpodinium granulatum* Cookson and Eisenack 1962b and *Fibradinium variculum* Stover and Helby 1987d support this zone assignment. The two assemblages contain



Table 5.1. Description of palynological samples from Woodleigh 1, 2, and 2A

Well	Depth (m)	Sample type	Organic yield (cc/gm)	Lithology
1	144–150	Cuttings <sup>(a)</sup>	0.002	Sandstone, silty
1	150–156	Cuttings <sup>(a)</sup>	0.045	Claystone chips
1	156–160	Cuttings <sup>(a)</sup>	0.057	Sandstone, silty
2A	87–90	Cuttings	0.010	Claystone, white with dark chips
2A	102–105	Cuttings	0.169	Claystone, dark grey, carbonaceous
2A	111–114	Cuttings	0.075	Claystone, medium grey
2A	120–123	Cuttings	0.036	Claystone, medium grey
2A	129–132	Cuttings	–	Claystone, medium grey
2A	135–138	Cuttings	0.059	Sandstone, medium grey
2	144–147	Cuttings	0.053	Claystone, medium grey
2A	144–147	Cuttings	0.085	Claystone, medium grey, sandy
2	153–156	Cuttings	0.030	Claystone, medium grey, sandy
2A	153–156	Cuttings	0.019	Sandstone, light grey, clayey
2	165–168	Cuttings	0.023	Sandstone, light grey, clayey
2A	165–168	Cuttings	0.008	Sandstone, light grey, clayey
2	177–180	Cuttings	0.018	Sandstone, light grey, clayey
2A	177–180	Cuttings	0.017	Sandstone, light grey, clayey
2	193.2	Core	–	Siltstone, carbonaceous
2	196.0	Core	0.078	Siltstone, carbonaceous
2	197.6	Core	–	Siltstone, carbonaceous
2A	284.0	Core	0.067	Siltstone with carbonaceous laminae
2A	333.05	Core	0.113	Siltstone with carbonaceous laminae
2A	361.0	Core	0.096	Siltstone with carbonaceous laminae
2A	391.9	Core	0.036	Claystone with carbonaceous laminae
2A	441.7	Core	0.167	Siltstone and claystone, laminated
2A	474.3	Core	0.045	Claystone, light grey
2A	482.15	Core	0.019	Siltstone, light grey
2A	493.2	Core	0.003	Siltstone, pale grey to white
2A	502.2	Core	0.019	Claystone, light grey
2A	505.15	Core	0.004	Siltstone, light grey, laminated
2A	541.65	Core	0.008	Siltstone pebble, medium grey,
2A	586.4	Core	0.002	Siltstone chips, grey
2A	586.95	Core	0.022	Siltstone pebble, grey
2A	590.35	Core	0.076	Siltstone, medium grey
2A	590.6	Core	0.148	Siltstone, medium grey
2A	592.4	Core	0.148	Siltstone, laminated, grey
2A	596.3	Core	0.115	Siltstone, laminated, grey
2A	600.3	Core	0.009	Siltstone, medium grey, dolomitic
2A	604.05	Core	0.026	Dolomite, light grey, laminated
2A	608.9	Core	0.020	Dolomite, light grey, laminated

NOTE: (a) cuttings sample collected while reaming

numerous palynomorphs that are probably caved from the overlying *C. denticulata* Zone. The environment of deposition appears to be marine, and the high dinocyst component suggests it is shelfal. The interval is dated as late Aptian.

### 135–138 to 177–180 m, *Muderongia australis* dinoflagellate zone

Most samples from this interval yielded rich and diverse assemblages that contain some *M. australis* Zone species and common, caved, Albian dinocysts. All six samples from Woodleigh 2A and the highest and lowest samples from Woodleigh 2 contain the index species *Muderongia australis* Helby 1987. The absence of *Muderongia mcwhaei* Cookson and Eisenack 1958 from all samples, even as caved specimens, is evidence for the absence of the *Odontochitina operculata* Zone in this well. Variation within the *M. australis* Zone has allowed it to be subdivided. The five highest samples in Woodleigh 2A (135–138 to 165–168 m), and the three highest samples in Woodleigh 2, are all assigned to the informal upper *M. australis* subzone because they appear to be above the range of *Scriniadinium attadalense* (Cookson and Eisenack 1958), which is present in the samples below. The assemblage from 165–168 m

Well														Species
1	2		2A		2A	2A								
Depth (m)														
156-160	150-156	144-150	177-180	165-168	153-156	150-153	144-147	135-138	129-132	120-123	111-114	102-105	87-90	
X									X					<i>Adnatosphaeridium tutulosum</i>
			X											<i>Aldorfia deflandrei</i>
	X													<i>Aprobolocysta alata</i>
	X	X	X	X	X	X	X			X	X	X		<i>Aptea polymorpha</i>
										X	X	X	X	<i>Apteodinium granulatum</i>
				X										<i>Avellodinium lepidum</i>
														<i>Batiacasphaera asperata</i>
	X	X								X	X	X	X	<i>Batiacasphaera</i> spp.
														<i>Batiacasphaera subtilis</i>
	X				X					X				<i>Batioladinium micropodium</i>
	X				X	X		X	X	X		X	X	<i>Canningia colliveri</i>
						X					X			<i>Canninginopsis denticulata</i>
	X													<i>Canninginopsis intermedia</i>
										X	X	X		<i>Carpodinium granulatum</i>
				X	X			X						<i>Cassiculosphaeridia magna</i>
	X			X	X			X	X	X	X			<i>Cassiculosphaeridia reticulata</i>
														<i>Chlamdophorella nyei</i>
									X				X	<i>Chlamydophorella urna</i>
														<i>Circulodinium attadalicum</i>
	X	X	X	X				X	X	X	X	X	X	<i>Circulodinium distinctum</i>
X	X		X	X					X	X	X	X		<i>Cleistosphaeridium ancoriferum</i>
														<i>Coronifera oceanica</i>
	X									X	X	X	X	<i>Craspedodinium indistinctum</i>
	X	X		X							X	X		<i>Cribroperidinium apione</i>
X	X	X	X	X	X	X	X	X	X	X	X	X		<i>Cribroperidinium edwardsii</i>
X	X	X	X	X	X	X	X	X	X	X	X	X		<i>Cribroperidinium muderongense</i>
														<i>Cyclonephelium attadalicum</i>
	X												X	<i>Cyclonephelium clathromarginatum</i>
														<i>Cyclonephelium compactum</i>
														<i>Cymatiosphaera</i> sp.
X										X				<i>Diconodinium davidii</i>
														<i>Diconodinium glabrum</i>
													X	<i>Diconodinium multispinum</i>
X	X		X					X	X			X		<i>Diconodinium pusillum</i>
X	X		X	X	X	X	X	X	X	X		X	X	<i>Diconodinium</i> spp.
													X	<i>Dingodinium cerviculum</i>
												X		<i>Dinopterygium tuberculatum</i>
	X									X				<i>Discorsia nanna</i>
X	X			X				X	X	X	X	X	X	<i>Endoceratium ludbrookiae</i>
		X												<i>Endoceratium turneri</i>
					X	X	X				X	X	X	<i>Epitricysta vincensis</i>
					X	X	X		X	X		X	X	<i>Exochosphaeridium</i> spp.
														<i>Fibradinium variculum</i>
X					X	X	X		X	X	X	X		<i>Florentinia</i> spp.
	X			X	X	X	X	X		X	X	X		<i>Fromea amphora</i>
														<i>Fromea monilifera</i>
	X		X								X			<i>Gonyaulacysta cassidata</i>
<i>M. australis</i>			<i>M. australis</i>		<i>M. australis</i>				<i>D. davidii</i>	<i>?C. denticulata</i>				
Zone														

**Figure 5.1. Distribution of dinocysts from Cretaceous cuttings samples in Woodleigh 1, 2, and 2A**

**Figure 5.1. (continued)**

[illegible]

**Figure 5.2.** Distribution of all palynomorphs in core samples from Woodleigh 2 and 2A.  
C — common; P — present



Depth (m)																				Species				
608.90	604.50	600.30	596.30	592.40	590.60	590.35	586.95	586.40	541.65	505.15	502.20	493.20	482.15	474.30	441.70	391.90	361.00	333.05	284.00				197.60	196.00
																	1 1 5 1 2 1 11 1 12 1 1 1 1 15 1 P P						Laevigatosporites belfordii Leptolepidites verrucatus Microcachyridites antarcticus Neoraistrickia equalis Neoraistrickia truncata Nevesisporites dailyi Osmundacidites dubius Podocarpidites ellipticus Reticuloidosporites arcus Retitriletes circolumenus Staplinisporites telatus Triletes tuberculiformis Lycopodiadites asperatus Saccate pollen indet. Leptolepidites pudens Retitriletes eminulus	
0	0	0	0	0	0	0	80	0	58	200	200	200	200	200	200	300	300	300	300	300	300	200		Total count
Barren interval	?Late Silurian						?C. torosa						C. turbatus/ C. torosa		C. turbatus				B. limbata					
Zone																								

Figure 5.2. (continued)

Table 5.2. Palynological summary of samples from Woodleigh 1, 2, and 2A

Well	Depth (m)	Yield	Thermal maturity	Environment	Zone	Estimated age
1	144–150	Low	1+	Marine	<i>M. australis</i>	Barremian
1	150–156	Moderate	1+	Marine	<i>M. australis</i>	Barremian
1	156–160	Moderate	1+	Marine	<i>M. australis</i>	Barremian
2A	87–90	Moderate	1+	Marine	? <i>C. denticulata</i>	Albian
2A	102–105	Moderate	1+	Marine	? <i>C. denticulata</i>	Albian
2A	111–114	High	1+	Marine	? <i>C. denticulata</i>	Albian
2A	120–123	High	1+	Marine	<i>D. davidii</i>	late Aptian
2A	129–132	Moderate	1+	Marine	? <i>D. davidii</i>	late Aptian
2A	135–138	High	1+	Marine	<i>M. australis</i> (upper)	early Aptian – Barremian
2	144–147	Moderate	1+	Marine	<i>M. australis</i> (upper)	early Aptian – Barremian
2A	144–147	High	1+	Marine	<i>M. australis</i> (upper)	early Aptian – Barremian
2A	150–153	High	1+	Marine	<i>M. australis</i> (upper)	early Aptian – Barremian
2	153–156	Moderate	1+	Marine	<i>M. australis</i> (upper)	early Aptian – Barremian
2A	153–156	High	1+	Marine	<i>M. australis</i> (upper)	early Aptian – Barremian
2	165–168	Moderate	1+	Marine	<i>M. australis</i> (upper)	early Aptian – Barremian
2A	165–168	Low	1+	Marine	<i>M. australis</i> (upper)	early Aptian – Barremian
2	177–180	Moderate	1+	Marine	<i>M. australis</i> (middle)	early Aptian – Barremian
2A	177–180	High	1+	Marine	<i>M. australis</i> (middle)	early Aptian – Barremian
2	193.2	Very low	1+	Non-marine	<i>B. limbata</i>	Barremian–Valanginian
2	196	Low	1+	Non-marine	<i>B. limbata</i>	Barremian–Valanginian
2	197.6	High	1+	Non-marine	<i>B. limbata</i>	Barremian–Valanginian
2A	284	High	1+	Non-marine	<i>C. turbatus</i>	Bajocian–Toarcian
2A	333.05	High	1+	Non-marine	<i>C. turbatus</i>	Bajocian–Toarcian
2A	361	High	1+	Non-marine	<i>C. turbatus</i>	Bajocian–Toarcian
2A	391.9	High	1+	Non-marine	<i>C. turbatus</i>	Bajocian–Toarcian
2A	441.7	High	1+	Non-marine	<i>C. turbatus</i>	Bajocian–Toarcian
2A	474.3	Low	1+	Non-marine	<i>C. turbatus/C. torosa</i>	Aalenian–Hettangian
2A	482.15	Moderate	1+	Non-marine	<i>C. turbatus/C. torosa</i>	Aalenian–Hettangian
2A	493.2	Low	1+	Non-marine	? <i>C. torosa</i>	?Pliensbachian–Hettangian
2A	502.2	Low	1+	Non-marine	? <i>C. torosa</i>	?Pliensbachian–Hettangian
2A	505.15	Low	1+	Non-marine	? <i>C. torosa</i>	?Pliensbachian–Hettangian
2A	541.65	Low	1+	Non-marine	? <i>C. torosa</i>	?Pliensbachian–Hettangian
2A	586.4	Very low	3	Non-marine	Indeterminate	Indeterminate
2A	586.95	Very low	1+	Non-marine	? <i>C. torosa</i>	?Pliensbachian–Hettangian
2A	590.35	Very low	2/2+	Marine	?	?Ordovician to Early Silurian
2A	590.6	Barren	–	–	Indeterminate	Indeterminate
2A	592.4	Very low	2/2+	Marine	?	?Ordovician to Early Silurian
2A	596.3	Low	2/2+	Marine	?	?Ordovician to Early Silurian
2A	600.3	Low	2/2+	Marine	?	?Ordovician to Early Silurian
2A	604.05	Barren	–	–	Indeterminate	Indeterminate
2A	608.9	Very low	–	–	Indeterminate	Indeterminate

in Woodleigh 2A is rather unusual because it has a low yield of dinocysts, but contains common *Pterospermella aureolata* (Cookson and Eisenack 1958) and some large *Cymatiosphaera* sp. These are probable algal cysts, and they are not common in more diverse marine assemblages. This assemblage may represent a nearshore or modified marine environment, or even a lacustrine environment within the upper *M. australis* subzone, although it is noted that *P. aureolata* is present in several higher samples and seems to be a consistent component of the *M. australis* Zone in this location.

The lowest samples, 177–180 m in both wells, contain several specimens of both *Ovoidinium cinctum* (Cookson and Eisenack 1958) and *S. attadalense*. The last appearance datum (LAD) of *S. attadalense* is a marker for the top, or near top, of the middle *M. australis* informal subzone. The first appearance datum (FAD) of *O. cinctum* is the marker for the base of the upper *M. australis* informal subzone and the *O. cinctum* Acme zone of Helby et al. (1987). Therefore, the ranges of these two species are considered not to overlap. However, the ranges of these two dinocysts overlapped in GSWA Mooka 1 (Backhouse, 1998), indicating a likely correlation between these samples and the 80.45 and 86 m samples in that well. These

Table 5.3. Distribution of all reworked palynomorphs in core samples from Woodleigh 2A

Depth (m)										Palynomorph	Probable original age
586.95	586.40	541.65	505.15	502.20	493.20	482.15	474.30	441.70	391.90		
24			4	13	14	9	18	1		<i>Plicatipollenites</i> spp.	Permian
5		5	6		4	5	2			<i>Punctatisporites gretensis</i>	Permian
2			1	1						<i>Verrucosiporites andersonii</i>	Permian
2			1	12	8	9				<i>Alisporites</i> (large)	Permian
4		4	20	40	14	18	47			<i>Alisporites</i> (small)	Permian
5		1	4	1	1	3	3			<i>Protohaploxypinus amplus</i>	Permian
5		21	40	27	44	28	36			<i>Cycadopites cymbatus</i>	Permian
2			2	1	1					<i>Brevitriletes cornutus</i>	Permian
4		3	7	4	3	9	9			<i>Striatites</i> indet.	Permian
1			1	6		5	1			<i>Indotriletes splendens</i>	Permian
1			1	2	1	5	3		1	<i>Jayantispores pseudozonatus</i>	Permian
1		1	5	10	10	18	7			<i>Densosporites rotundidentatus</i>	Permian
3		1	3		2		2			<i>Caheniasaccites elephas</i>	Permian
1		1	1	3	2		1			<i>Protohaploxypinus limpidus</i>	Permian
2		1	5	5	8	15	7			<i>Pseudoreticulatispora confluens</i>	Permian
2			1			1	2			<i>Pteruchipollenites gracilis</i>	Permian
2		4	4	1	2	2				<i>Punctatisporites</i> spp.	Permian–Carboniferous
3				1	1	2	6			<i>Potonieisporites novicus</i>	Permian
2		11	43	31	57	43	17	1		<i>Microbaculispora tentula</i>	Permian
1			4	12	4	6				<i>Leiotriletes directus</i>	Permian
1				1	1					<i>Geminospora lemurata</i>	late Devonian
		2	3		2		1			<i>Emphanisporites rotatus</i>	Devonian
		1					1			<i>Marsupipollenites triradiatus</i>	Permian
		1								<i>Retusotriletes nigrifellus</i>	Permian
			1		1					Devonian spore indet.	Devonian
			1	5	2	3				<i>Gondisporites wilsonii</i>	Permian
			4	1	1	1	2			<i>Leiotriletes virkii</i>	Permian
			1	2		1	5			<i>Limitisporites rectus</i>	Permian
			1	4	1	3				<i>Marsupipollenites striatus</i>	Permian
			1							<i>Rattiganispora minor</i>	Permian
			?							<i>Spelaetriletes ybertii</i>	Late Carboniferous
			1	7	1	1	1			<i>Striatoabietes multistriatus</i>	Permian
			3	P			1			<i>Tetraporina tetragona</i>	Permian
				1						<i>Corisaccites alutas</i>	Permian
				2						Devonian acritarchs	Devonian
				1	4	3				<i>Horriditriletes ramosus</i>	Permian
				1		1				<i>Horriditriletes tereteangulatus</i>	Permian
				P		1				<i>Interradispora</i> sp.	Permian
				1	3	1				<i>Jayantispores variabilis</i>	Permian
				1	1	1	1	1		<i>Potonieisporites balmei</i>	Permian
				1						<i>Pseudoreticulatispora pseudoreticulata</i>	Permian
				1						<i>Striatopodocarpites fusus</i>	Permian
					1					<i>Dibolisporites disfacies</i>	Permian–Carboniferous
					1	1	2			<i>Microbaculispora micronodosa</i>	Permian
							2			<i>Scheuringipollenites maximus</i>	Permian
							1			<i>Scheuringipollenites ovatus</i>	Permian
73	0	57	169	199	195	195	178	3	1	<b>Total count of reworked palynomorphs</b>	

records indicate a short but significant interval in this area where these species overlap. There is a small, but possibly significant, unsampled interval between the lowest sample and the next lowest sample (165–168 m). It is possible that the *O. cinctum* Acme occurs in this interval, and the specimens of *O. cinctum* present in the 177–180 m assemblages are caved.

All 10 samples from this interval are dated as early Aptian to Barremian and appear to represent shallow, shelfal marine conditions, or restricted conditions in the case of the 165–168 m sample in Woodleigh 2A.

### **193.2 to 197.6 m, *Balmeiopsis limbata* spore-pollen zone**

These three samples from Woodleigh 2 are all devoid of marine forms, and seem to represent a non-marine interval of Early Cretaceous age. The lowest sample yielded a rich and diverse assemblage of spores and pollen, the 196 m assemblage is less diverse and the highest sample is nearly barren, but contains a few spores consistent with the underlying samples. The samples are dated by the presence of *Balmeiopsis limbata* (Balme 1956) and *Cicatricosisporites* sp. cf. *C. hughesii* Dettman 1963 in the 197.6 m sample, and the two highest samples are considered to be the same age on the basis of the broad similarity of the assemblages. The 196 and 197.6 m samples are dominated by small *Cyathidites* sp. The lower sample also contains abundant *Baculatisporites comaumensis* (Cookson 1953) and significant numbers of *Araucariacites australis* Cookson 1947, *Contignisporites cooksoniae* (Balme 1957), and *Reticuloidosporites arcus* (Balme 1957). The 196 m sample contains abundant small *Circulisporites* sp., an acritarch of presumed algal origin that is not usually common. These unusual assemblages point to a non-marine, lacustrine setting of Barremian to Valanginian age.

### **284 to 441.7 m, *Callialasporites turbatus* spore-pollen zone**

The five samples in this interval gave high yields of palynomorphs dominated by *Araucariacites australis*, *Callialasporites turbatus* (Balme 1957), *Corollina torosa* (Reissinger 1950), and a membranous form of *Corollina* (*Corollina* sp., which lacks a striate equatorial band and commonly bears small granules). Other spores and pollen species are relatively infrequent, and in particular, *Callialasporites dampieri* (Balme 1957) and *C. segmentatus* (Balme 1957) are present, but rare. The interval is placed in the *C. turbatus* spore-pollen zone. The absence of *Exesipollenites tumulus* Balme 1957, which is commonly present in the lower *C. turbatus* Zone, suggests these samples are from the upper part of the zone, or that the local palaeovegetation did not include the particular plant that produced this pollen type. Permian reworking is evident in the two lowest samples, but is a minor component of the assemblages compared to the massive reworking evident in the samples below. The age of this interval is estimated to be Bajocian to Toarcian.

### **474.3 to 482.15 m, ?*Callialasporites turbatus*/*Corollina torosa* spore-pollen zone**

The Jurassic spore-pollen content of these two samples resembles that in the overlying interval in including *Corollina* and *Callialasporites turbatus*. Diversity is lower, *Corollina* spp. and *C. turbatus* are far fewer, and the abundance of reworked forms is significantly higher. Indeed reworked palynomorphs dominate the assemblages, as they do in the interval below. Because Jurassic spores and pollen are so few, it is not certain where these assemblages should be placed biostratigraphically. The interval may be correlated with the upper part of the *C. torosa* Zone, which contains *C. turbatus*. However, the assemblages may also represent an impoverished *C. turbatus* Zone palynoflora. The age of the assemblages is somewhere in the range Aalenian to Hettangian. The environment of deposition is uncertain. Evidently it was non-marine, and allowed an influx of sediment derived largely from the Permian.

### **493.2 to 586.95 m, ?*Corollina torosa* spore-pollen zone**

Of the six samples in this interval, five have low or very low yields of Jurassic palynomorphs with large numbers of mainly Early Permian reworked forms, and one sample (586.4 m) also gave a very low yield of much older material. This last sample appears to be from a clast of much older rock, probably of pre-Devonian age. The presence of *C. torosa* and *Corollina* sp. without *C. turbatus* or *C. dampieri* is commonly indicative of the *C. torosa* Zone. However, these samples are rather unusual because *Corollina* is rare, and the majority of palynomorphs appear to be reworked from the Permian and Devonian. Therefore, the assignment to the *C. torosa* Zone, which is dated as Pliensbachian to Hettangian (Early Jurassic), is provisional.



### 590.35 to 600.3 m, ?Late Silurian

The only palynomorphs recorded through this interval are *Tetrahedraletes medinensis* Strother and Traverse 1979, leiospheres of various sizes, an unidentified acritarch (*Lophosphaeridium* sp.), and scolecodonts. A possible Late Silurian age is proposed based on the similarity of the palynology in this interval to that in GSWA Mooka 1 (122 km to the north) between 339.1 and 407.75 m, which is dated by conodonts as Late Silurian (Ludfordian; Nicholl, 1998). The only palynomorph identified to species level, *T. medinensis*, has a known range of Late Ordovician to Early Devonian, but seems to be most commonly recorded from the Late Ordovician to Early Silurian. The abundance of scolecodonts through this section, and the occurrence of acritarchs and leiospheres attest to a marine environment of deposition.

### 604.5 to 608.9 m, Indeterminate

Neither of these samples yielded unequivocal palynomorphs. The higher sample contained virtually no organic material, and the lower sample yielded unstructured sheets of possible organic origin, and one small granular body that could possibly be interpreted as an acritarch. No age is suggested.

### Reworked palynomorph assemblages

The outstanding feature of the Jurassic interval in Woodleigh 2A is the extraordinary proportion of reworked palynomorphs from 391.9 to 586.95 m, but particularly from 474.3 m down (Fig. 5.2, Table 5.3). A few are Devonian, possibly Early or Middle Devonian, and one Carboniferous spore is tentatively identified, but the great majority of palynomorphs counted as reworked originate in the Permian. However, Late Permian forms do not seem to be represented in any sample. In all samples that contain reworked forms, the greatest number of Permian species are ones commonly represented in the *Pseudoreticulatispora confluens* Zone, or a very short stratigraphic level above or below it (Foster and Waterhouse, 1988; Backhouse, 1991). Evidence for slightly higher Permian zones (*Pseudoreticulatispora pseudoreticulata* and *Striatopodocarpites fusus* Zones) is seen only in the 502.2 m and possibly the 474.3 m sample. Jurassic pollen, notably forms of *Corollina*, are present in low numbers in all but one sample, and display a somewhat lower spore-colour maturation level than the Permian forms. The presence of Jurassic pollen is evidence that the Permian and Devonian palynomorphs are reworked.

## Palynological observations: Cretaceous intervals in Woodleigh 1

### 144–150 to 156–160 m, *Muderongia australis* Zone

*M. australis* is present in the highest sample, and *O. cinctum* is present in the middle sample. *S. attadalense* is not seen in this well, so the middle subzone of the *M. australis* Zone was probably not reached. The interval is placed in the upper subzone of Barremian to earliest Aptian age.

### Maturity

The Cretaceous intervals in all wells show low thermal maturity, with a thermal alteration index (TAI) of about 1+. Maturity is higher in the Palaeozoic samples from 590.35 to 600.3 m, with most grains showing a TAI of approximately 2 to 2+, just above or just within the hydrocarbon generation window, although maturity is difficult to judge in these samples, which contain few identifiable palynomorphs. The most mature organic material, approximately TAI 3, is in a clast from 586.4 m.

## References

- BACKHOUSE, J., 1991, Permian palynostratigraphy of the Collie Basin, Western Australia: Review of Palaeobotany and Palynology, v. 67, p. 237–314.
- BACKHOUSE, J., 1998, Appendix 2 — Palynology, in GSWA Mooka 1 well completion report, Gascoyne Platform, Southern Carnarvon Basin, Western Australia *compiled by* A. J. MORY and A. R. YASIN: Western Australia Geological Survey, Record 1998/6, p. 28–32
- FOSTER, C. B., and WATERHOUSE, J. B., 1988, The *Granulites confluens* Oppel-zone and Early Permian marine faunas from the Grant Formation on the Barbwire Terrace, Canning Basin, Western Australia: Australian Journal of Earth Science, v. 35, p. 135–157.
- HELBY, R., MORGAN, R., and PARTRIDGE, A. D., 1987, A palynological zonation of the Australian Mesozoic, in Studies in Australian Mesozoic palynology *edited by* P. A. JELL: Association of Australasian Palaeontologists, Memoir 4, p. 1–94.
- NICOLL, R. S., 1998, Appendix 4 — Conodonts, in GSWA Mooka 1 well completion report, Gascoyne Platform, Southern Carnarvon Basin, Western Australia *compiled by* A. J. MORY and A. R. YASIN: Western Australia Geological Survey, Record 1998/6, p. 35–36.

## Appendix 6

### Conodonts

by R. S. Nicoll  
(Department of Geology, Australian National University)

#### Introduction

Six dolomite core samples over the interval 591.8 – 615.9 m were processed by Laola Pty Ltd using a buffered 10% solution of formic acid, as suggested by Jeppsson and Anehus (1995). The samples were approximately  $\frac{1}{3}$  cuts of the core and were not crushed. The residues were sieved and the fraction over 80  $\mu\text{m}$  was separated using heavy liquid with a density of 2.75 g/cc. The heavy residues were then examined using a binocular microscope for conodonts. A net weight of 9.36 kg was processed this way (Table 6.1). All six samples yielded sparse conodont faunas consisting of a total of 112 elements and 158 element fragments (Table 6.2), which have been placed in the GSWA petroleum relinquishment collection.

#### Identification and discussion

Conodonts from the six samples examined can be assigned to three species (Table 6.2): *Kockelella absidata*, *Ozarkodina* sp. M, and *Panderodus* sp. *Kockelella absidata*, which has been previously reported as a constituent of Fauna 4 in the Silurian of the Carnarvon Basin (Mory et al., 1998). Another specimen of *Ozarkodina* sp. M was found after re-examining samples from Mooka 1 (334.0 – 335.1 m), reported by Mory et al. (1998). The Mooka 1 specimen also occurs with both *K. absidata* and *Panderodus* sp. and was assigned to Fauna 4 by Mory et al. (1998). The Mooka 1 material had been previously identified as *Ozarkodina confluens* (Mory et al., 1998, appendix 1), but that identification is now considered to be in error.

A comparison of specimens of *Ozarkodina* sp. M with other species from the Carnarvon Basin suggests that this species was derived probably from *Ozarkodina broenlundi* Aldridge, of late Llandovery age. *O. broenlundi* was considered to be an element of Fauna 2 of Mory et al. (1998). This comparison also suggests that *O. sp. M* may have been the ancestor of a new species of *Ozarkodina* (*O. sp. nov Z*) recovered from the interval 580.0 – 581.4 m in Coburn 1 (Nicoll, 1999), which had been assigned to Fauna 5 of Mory et al. (1998).

Table 6.1. Samples processed for conodonts, Woodleigh 2A

Depth (m)	Lithology	Sample type	GSWA no.	Amount processed (kg)	Conodonts/ other fossils
591.8 – 592.8	Thinly bedded dolomite and dolomitic siltstone	Core	169335	1.17	Yes/scolecodonts, ostracods (internal molds), pellets
596.5 – 598.0	Thinly bedded dolomite and dolomitic siltstone	Core	169336	2.51	Yes/ostracods, pellets
605.2 – 606.15	Laminated dolomite	Core	169337	1.42	Yes/ostracods (internal molds), crinoid stem plate
608.4 – 609.65	Laminated dolomite	Core	169338	1.36	Yes
610.35 – 611.25	Laminated dolomite	Core	169339	1.22	Yes
614.3 – 615.9	Laminated dolomite	Core	169340	1.68	Yes

Table 6.2. Conodont fauna from Woodleigh 2A

Depth (m)	GSWA no.	Number of elements <sup>(a)</sup>	Species	Element types	Number of fragments	CAI
591.8 – 592.8	169335	1	indet.	indet. S (1), indet fragments (2)	2	1
596.5 – 598.0	169336	20	<i>Kockelella absidata</i> <i>Ozarkodina</i> sp. M <i>Panderodus</i> sp.	Pa (1), Sa (1), indet. S (9) Pa (2) (2)	46	1
605.2 – 606.15	169337	61	<i>Kockelella absidata</i> <i>Ozarkodina</i> sp. M <i>Panderodus</i> sp.	Pa (10), Pb (3), M (3), Sa (4), Sc (9), indet. S (11) Pa (6) (2)	65	1
608.4 – 609.65	169338	14	<i>Kockelella absidata</i> <i>Ozarkodina</i> sp. M	Pa (6), Pb (1), indet. S (1) Pa (2)	3	1
610.35 – 611.25	169339	2	<i>Ozarkodina</i> sp. M	Pa (1), indet. Sc element (1)	1	1
614.3 – 615.9	169340	14	<i>Kockelella absidata</i>	Pa (2), Sa (2), indet. S (9)	41	1

NOTES: (a) Not all elements in this category were well enough preserved for the element type or species to be identified

CAI: Conodont alteration index

Analysis of the limited conodont fauna suggests that the interval 591.8 – 615.9 m in Woodleigh 2A may be confidently assigned to Fauna 4 of Mory et al. (1998), considered to be of early Ludlow (Gorstian) age.

Species diversity of Fauna 4 in the Carnarvon Basin varies from 1 to 5 taxa (Mory et al., 1998). This diversity is partly dependent on the number of elements recovered from any single sample and the sample size (weight), but also may be related to other factors. These include the stratigraphic level of the sample within the formation and its position relative to the margin of the basin. Samples from the middle part of the unit appear to have higher diversity and Yaringa 1 and GSWA Mooka 1 wells, with 5 and 4 species respectively, may represent a deeper part of the basin.

More extensive sampling from several wells would be needed to confirm these preliminary observations.

The preservation of Silurian conodont elements recovered from this well (and all other wells sampled in the basin) is commonly relatively poor, with many broken elements and small fragments of elements. This fragmentation may, in part, be related to post-depositional compaction in the sediments and in part to the processing techniques, especially during sieving. There is no indication of abrasion of element surfaces indicative of reworking of elements.

All of the specimens from Woodleigh 2A have a conodont alteration index (CAI) of 1, indicating that the formation has not been heated above 80°C equivalent to a vitrinite reflectance value of less than 0.8% Ro (Epstein et al., 1977).

## References

- EPSTEIN, A. G., EPSTEIN, J. B., and HARRIS, L. D., 1977, Conodont colour alteration — An index to organic metamorphism: United States Geological Survey, Professional Paper 995, p. 1–27.
- JEPPSSON, L., and ANEHUS, R., 1995, A buffered formic acid technique for conodont extraction: *Journal of Paleontology*, v. 69, pt 4, p. 790–794.
- MORY, A. J., NICOLL, R. S., and GORTER, J. D., 1998, Lower Palaeozoic correlations and thermal maturity, Carnarvon Basin, W.A., in *The Sedimentary Basins of Western Australia 2* edited by P. G. PURCELL and R. R. PURCELL: Petroleum Exploration Society of Australia; Sedimentary Basins of Western Australia Symposium, Perth, W.A., 1998, Proceedings, p. 599–612.
- NICOLL, R. S., 1999, Appendix 5 — Conodonts, in *Coburn 1 well completion report, Gascoyne Platform, Southern Carnarvon Basin, Western Australia compiled by A. R. YASIN and A. J. MORY*: Western Australian Geological Survey, Record 1999/5, p. 64–67.



## Appendix 7

### Apatite fission-track analysis of basement samples

by

**B. P. Kohn, U. D. Weber, and A. Raza**  
(School of Earth Sciences, University of Melbourne)

#### Summary

Two granitoid samples from Woodleigh 1 yielded apparent Late Jurassic apatite fission-track ages, which post-date the impact:

190.9 – 192.9 m (GSWA 169333)	146 ± 7 Ma	Mean track length: 12.36 ± 0.23 µm
247.0 – 249.9 m (GSWA 169334)	150 ± 13 Ma	Mean track length: 12.15 ± 0.21 µm

#### Fission-track analysis

Apatite fission-track analysis (AFTA) uses the temperature sensitive nature of fission tracks in apatite to estimate maximum palaeotemperatures and the time of commencement of cooling from maximum palaeotemperatures. The method is based on the spontaneous fission of  $^{238}\text{U}$  in uranium-bearing minerals, such as apatite, producing narrow tubes of intense damage throughout geological time. New tracks have the same length when formed ( $\sim 16 \pm 1 \mu\text{m}$ ) and are produced continuously through time. If the mineral is subjected to a sufficiently high temperature for a long enough time, all existing fission tracks will fade (anneal) and eventually disappear, effectively resetting the fission-track clock. The process of annealing is the key to the investigation of thermal histories by fission-track studies. Useful summaries of fission-track dating and annealing are given by Wagner and Van den haute (1992) and Gallagher et al. (1998).

Experimental studies and borehole observations have revealed a wide temperature interval over which gradual annealing occurs. This led to the development of the concept of the annealing zone, in which fission tracks under geological conditions anneal increasingly between ambient surface temperatures and about 110°C. Annealing is more rapid at temperatures exceeding about 60°C. With greater annealing, the tracks become increasingly shorter. The longer the rock resides in the annealing zone, the greater the proportion of shortened tracks.

Because of the numerous possible time-temperature scenarios for a sample, it is clear that an AFTA age alone can be interpreted in a number of ways. However, when combined with fission-track length details, the data allow more rigorous constraints to be placed on the interpretation of an observed age. As the AFTA age and length data reflect a combination of the time over which tracks have been retained in apatite and the thermal history of the host material, integration of the two can differentiate uniquely between different types of thermal history below temperatures of about 110°C. Using the annealing algorithms of Laslett et al. (1987), models can be used to calculate the fission-track age and track-length distributions that would result from a given thermal history on a geological time scale. In this way, plausible thermal histories can be tested against actual fission-track data. Gallagher (1995) has automated this procedure to give a quasi-reversed modelling approach using a computer program, which combines a simulation of numerous possible thermal histories with statistical testing of the outcome against the observed fission-track measurements. The model uses a Monte Carlo approach and a genetic algorithm to provide rapid convergence to an acceptable fit to the observed apatite fission-track data.

## Analytical techniques

Two basement samples from Woodleigh 1 were crushed and ground, and apatites in the 63–250 µm size range were separated using standard magnetic and heavy liquid techniques. The fission-track methodology employed is described by Kohn et al. (1997). In brief, grains were mounted in epoxy resin, polished, and etched in 5N HNO<sub>3</sub> for 20 seconds at room temperature. Neutron irradiations were carried out in the X-7 position of the High Flux Australian Reactor at Lucas Heights, N.S.W. AFTA ages were determined by the external detector method using Brazil Ruby muscovite to record induced tracks. Muscovite detectors were etched for 30 minutes in 48% HF at room temperature to reveal induced tracks. Thermal neutron fluences were monitored by measuring the track density in muscovite attached to the Corning-5 standard glass (Bellemans et al., 1995). Track counting was performed under transmitted light on a Zeiss Axiotron microscope using a dry ×100 objective at a total magnification of ×1250. Ages were calculated using the zeta calibration method and errors are expressed at the one standard deviation level. Horizontal, confined, fossil fission-track lengths were measured in grains with polished surfaces approximately parallel to the crystallographic c-axis. Measurements were made using the same microscope magnification as for age measurements with a camera lucida and digitizing tablet attached to a computer. The number of confined tracks counted was the maximum possible observed in the entire mount prepared for each sample.

## Results

Sample details and AFTA data are presented in Table 7.1. Both samples yield apparent Late Jurassic – Early Cretaceous AFTA ages (which are concordant within the analytical uncertainties) and mean track lengths of 12.15 to 12.36 µm.

The apparent AFTA ages are only slightly older than the strata immediately overlying the basement rocks (i.e. Early Cretaceous) and the mean track lengths are of intermediate length. This indicates that the apatites have been annealed as a consequence of the post-impact thermal history of the sample site. Clearly, the AFTA ages do not directly date a discrete geological event, that is, they do not measure the age of the Woodleigh impact structure. Rather, they probably relate to sedimentary burial, but the magnitude of heating required to produce the observed annealing could not have been achieved by approximately 180 m of Mesozoic strata presently overlying the basement (Mory et al., 2000).

Preliminary thermal-history modelling suggests that the AFTA data are compatible with an episode of accelerated cooling during Middle Jurassic to Early Cretaceous time. This involved between approximately 30–60°C of cooling from palaeotemperatures of greater than about 90°C. The timing of this cooling is similar to that of uplift and erosion reported along the eastern margin of the Gascoyne Platform during the Early Cretaceous and related to the separation of Australia from Greater India (Mory et al., 2000). Hence, the observed AFTA age and mean track-length reduction in the basement apatites is probably related to annealing during deeper burial under a thicker Lower Jurassic section overlying the basement, which was subsequently removed. However, the possibility that annealing also occurred under an elevated palaeogeotherm cannot be excluded.

Table 7.1. Apatite fission-track data from basement in Woodleigh 1

Sample no.	Lithology	Depth (m)	No. of grains	Standard track density ( $10^6 \text{ cm}^{-2}$ )	Fossil track density ( $10^6 \text{ cm}^{-2}$ )	Induced track density ( $10^6 \text{ cm}^{-2}$ )	Uranium content (ppm)	Chi square probability (%)	Age dispersion (%)	Fission-track age (Ma) ( $\pm 1\sigma$ )	Mean track-length $\pm$ std error ( $\mu\text{m}$ )	Standard Deviation ( $\mu\text{m}$ )
169333	granite gneiss	190.9 – 192.9	17	1.570 (5287)	3.402 (847)	6.672 (1661)	53	97.2	0.00	146 $\pm$ 7 <sup>(a)</sup>	12.36 $\pm$ 0.23 (60)	1.76
169334	biotite granite	247.0 – 249.9	7	1.610 (5287)	2.212 (218)	4.332 (427)	34	19.7	0.98	150 $\pm$ 13 <sup>(a)</sup>	12.15 $\pm$ 0.21 (46)	1.40
169334	biotite granite	247.0 – 249.9	10	1.390 (46347)	1.211 (245)	2.176 (440)	20	10.0	20.11	147 $\pm$ 12 <sup>(b)</sup>	–	–

**NOTES:** Brackets show the number of tracks counted or measured

Standard and induced track densities measured on external mica detectors ( $g = 0.5$ ) and fossil track densities on internal mica surfaces

(a) Apatite ages determined by Ursula Weber, calculated using  $zeta = 369 \pm 8$  for dosimeter glass Corning-5

(b) Apatite ages determined by Asaf Raza, calculated using  $zeta = 384 \pm 5$  for dosimeter glass Corning-5

## References

- BELLEMANS, F., DE CORTE, F., and VAN DEN HAUTE, P., 1995, Composition of SRM and CN U-doped glasses: significance for their use as thermal neutron fluence monitors in fission track dating: *Radiation Measurements*, v. 24, p. 153–160.
- GALLAGHER, K., 1995, Evolving temperature histories from apatite fission track data: *Earth and Planetary Science Letters*, v. 136, p. 421–435.
- GALLAGHER, K., BROWN, R. W., and JOHNSON, C., 1998, Fission track analysis and its applications to geological problems: *Annual Review of Earth and Planetary Sciences*, v. 26, p. 519–572.
- KOHN, B. P., FEINSTEIN, S., FOSTER, D. A., STECKLER, M. S., and EYAL, M., 1997, Thermal history of the eastern Gulf of Suez: II Reconstruction from apatite fission track and  $^{40}\text{Ar}/^{39}\text{Ar}$  K-feldspar measurements: *Tectonophysics*, v. 283, p. 219–239.
- LASLETT, G. M., GREEN, P. F., DUDDY, I. R., and GLEADOW, A. J. W., 1987, Thermal annealing of fission tracks in apatite 2. A quantitative analysis: *Chemical Geology (Isotope Geoscience Section)*, v. 65, p. 1–13.
- MORY, A. J., IASKY, R. P., GLIKSON, A. Y., and PIRAJNO, F., 2000, Woodleigh, Carnarvon Basin, Western Australia: a new 120 km-diameter impact structure: *Earth and Planetary Science Letters*, v. 177, p. 119–128.
- WAGNER, G. A., and VAN DEN HAUTE, P., 1992, *Fission track dating*: Dordrecht, Kluwer Academic Publishers, 285p.



## Appendix 8

### UV laser Ar–Ar analysis

by S. P. Kelley

(Department of Earth Science, Open University, Milton Keynes, U.K.)

#### Analytical techniques

A shocked grainitoid sample from the 198.35 – 198.5 m interval in Woodleigh 1 was prepared by roughly polishing one side of a block and sticking to a glass slide. The upper side was then ground till the sample was about 150  $\mu\text{m}$  thick and washed ultrasonically in methanol to dissolve the Lakeside resin. The areas containing the grains to be analysed by UVLamp were broken from the rest of the slice. The rockchip was cleaned in an ultrasonic bath for 20 minutes in methanol and then deionized water, and individually packaged in aluminium foil. The rock chips were loaded together with biotite age standard GA1550 (Renne et al., 1998). The sample was irradiated at the McMaster reactor in Canada and standards yielded a J value for the sample of  $0.01172 \pm 0.000039$ .

Following irradiation, the sample was loaded (with the polished side uppermost) into the ultra-violet (UV) port of the UVLamp Ar dating system at the Open University (an ultraviolet laser probe  $^{40}\text{Ar}$ – $^{39}\text{Ar}$  extraction technique described in Kelley et al., 1994). The laser port was baked to 120°C overnight using a heat lamp to remove atmospheric contamination. A 10 Hz pulsed quadrupled Nd-YAG laser ( $\lambda = 266 \text{ nm}$ ), with a pulse length of 10 ns, a beam diameter of about 10  $\mu\text{m}$ , and delivering about 1 mJ per pulse, was rastered over  $50 \times 50 \mu\text{m}$  regions of the K-feldspar for approximately nine minutes. A Märzhäuser MAC 4000 computerized X-Y stage, attached to a customized Leica DM microscope, was used to control the laser and view the samples during analysis. Scanning-electron microscope and backscattered scanning-electron microscope montages were used to identify areas for Ar analysis. Analyses of the edges and crenulated areas of biotite grains were made by ablating about 200  $\mu\text{m}$  grooves approximately 10  $\mu\text{m}$  wide. Biotite cores, K-feldspar, and quartz were ablated using 50 and 100  $\mu\text{m}$  squares.

Gas released by ablation was getters to remove all active gases ( $\text{CO}_2$ ,  $\text{H}_2\text{O}$ ,  $\text{CH}_4$ , etc.). The remaining noble gases were equilibrated into a high sensitivity, MAP 215-50 noble gas mass spectrometer. The automated extraction and data acquisition system was computer controlled. Representative five minute, extraction system, blank measurements obtained during the experiments were  $^{40}\text{Ar} = 9 \times 10^{-12}$ ,  $^{39}\text{Ar} = 2 \times 10^{-14}$ ,  $^{38}\text{Ar} = 3 \times 10^{-14}$ ,  $^{37}\text{Ar} = 7 \times 10^{-13}$ , and  $^{36}\text{Ar} = 2 \times 10^{-13} \text{ cm}^3 \text{ STP}$ . Blanks were run before and after every analysis and these were used to correct the data for background counts. The Ar data were corrected for blanks, mass spectrometer discrimination, and nuclear-induced interferences ( $^{36/37}\text{Ca} = 0.000255$ ;  $^{39/37}\text{Ca} = 0.00076$ ;  $^{40/39}\text{K} = 0.0085$ ).

#### Results

Twenty-one analyses were performed (Table 8.1). Ten analyses of biotite yielded ages ranging from  $664 \pm 10$  to  $840 \pm 10 \text{ Ma}$ , a far larger range than would be expected from an unaltered grain in granite. Analyses of biotite cores unaffected by crenulation yielded the oldest ages, from  $759 \pm 14$  to  $840 \pm 10 \text{ Ma}$ , though this is still far higher than expected from analytical errors. Crenulated and grain boundary areas of the biotite grain and small biotite grains in quartz grains yielded ages from  $664 \pm 10$  to  $772 \pm 14 \text{ Ma}$ , indicating greater argon loss or later cooling. In particular, a traverse from the grain boundary of a relatively undeformed biotite yielded increasing ages from the boundary to 20  $\mu\text{m}$  into the grain (ages ranging from  $697 \pm 18$  to  $772 \pm 14 \text{ Ma}$ ).

Table 8.1. UV laser Ar-Ar analyses

Analysis	Description	$^{40}\text{Ar}/^{39}\text{Ar}$	$\pm$	$^{38}\text{Ar}/^{39}\text{Ar}$	$\pm$	$^{37}\text{Ar}/^{39}\text{Ar}$	$\pm$	$^{36}\text{Ar}/^{39}\text{Ar}$	$\pm$	$^{39}\text{Ar}$ ( $\text{cm}^{-3}\times 10^{-14}$ )	$^{40}\text{Ar}/^{39}\text{Ar}$	$\pm$	Age (Ma)
<b>Biotite analyses</b>													
1	biotite 1 core 50 $\mu\text{m}^2$ , 200 $\mu\text{m}$ from rim	47.34	0.76	0.0217	0.0033	0.0107	0.0095	0.0000	0.0047	192.7	47.34	1.58	796 $\pm$ 22
2	biotite 1 rim 50 $\mu\text{m}^2$ , 25 $\mu\text{m}$ from rim	53.03	0.28	0.0147	0.0024	0.0594	0.0097	0.0082	0.0024	189.4	53.03	0.76	840 $\pm$ 10
3	biotite 2 rim 50 $\mu\text{m}^2$ , 25 $\mu\text{m}$ from rim	44.61	0.61	0.0307	0.0039	0.0925	0.0100	0.0000	0.0027	166.4	44.61	1.01	759 $\pm$ 14
4	crenulated biotite region 1 100 $\mu\text{m}^2$	37.95	0.50	0.0133	0.0013	0.0356	0.0058	0.0000	0.0015	348.7	37.95	0.66	664 $\pm$ 10
5	crenulated biotite region 2 100 $\mu\text{m}^2$	42.87	0.15	0.0086	0.0005	0.0000	0.0000	0.0000	0.0020	457.2	42.87	0.60	734 $\pm$ 9
6	crenulated biotite region 3 100 $\mu\text{m}^2$	49.72	0.58	0.0162	0.0014	0.0800	0.0052	0.0000	0.0028	358.9	49.72	1.02	828 $\pm$ 14
7	12 small (<20 $\mu\text{m}$ diameter) biotite grains in melt	38.25	0.48	0.0182	0.0044	0.1260	0.0423	0.0000	0.0071	114.8	38.25	2.16	668 $\pm$ 32
<b>Biotite edge traverse</b>													
8	biotite 3 rim + melt 2 line raster	40.24	0.32	0.0094	0.0066	4.7165	0.0688	0.0000	0.0041	123.5	40.24	1.25	697 $\pm$ 18
9	biotite 3 rim line raster, 5 $\mu\text{m}$ from rim	41.41	0.28	0.0230	0.0030	0.9996	0.0107	0.0000	0.0008	272.7	41.41	0.38	714 $\pm$ 6
10	biotite 3 core-rim line raster, 20 $\mu\text{m}$ from rim	45.56	0.21	0.0094	0.0005	0.0614	0.0050	0.0000	0.0034	422.6	45.56	1.02	772 $\pm$ 14
<b>Melt analyses</b>													
11	melt 1 line raster, 230 x 50 $\mu\text{m}$ laser pit	51.13	3.01	0.8137	0.1224	69.0683	3.9433	0.0011	0.1136	4.0	51.13	33.65	847 $\pm$ 445
12	3 large melt sections in biotite	—	—	—	—	—	—	—	—	0.0	—	—	—
<b>Feldspar analyses</b>													
13	clear, orange K-feldspar 1 core 50 $\mu\text{m}^2$	7.00	0.08	0.0177	0.0049	0.0824	0.0184	0.0000	0.0035	131.1	7.00	1.03	142 $\pm$ 20
14	clear, orange K-feldspar 2 core 100 $\mu\text{m}^2$	7.71	0.05	0.0163	0.0030	0.0695	0.0159	0.0000	0.0024	270.8	7.71	0.70	156 $\pm$ 14
15	very clear orange K-feldspar 3 core 100 $\mu\text{m}^2$	6.44	0.09	0.0224	0.0020	0.0895	0.0087	0.0000	0.0055	259.3	6.44	1.64	131 $\pm$ 32
16	very clear orange K-feldspar 3 core 100 $\mu\text{m}^2$	6.59	0.06	0.0177	0.0055	0.0806	0.0123	0.0000	0.0019	262.1	6.59	0.57	134 $\pm$ 11
17	white, cloudy altered K-feldspar 1 core 100 $\mu\text{m}^2$	3.27	0.02	0.0111	0.0020	0.0309	0.0049	0.0000	0.0008	669.7	3.27	0.22	68 $\pm$ 5
18	yellow/white altered K-feldspar 2 core 100 $\mu\text{m}^2$	36.47	3.74	0.1764	0.0385	1.2898	0.7371	0.0007	0.1243	6.6	36.47	36.87	642 $\pm$ 546
19	yellow/white altered K-feldspar 2 core 100 $\mu\text{m}^2$	9.11	0.31	0.0237	0.0096	0.1858	0.0306	0.0000	0.0053	127.3	9.11	1.61	183 $\pm$ 31
20	white, cloudy altered feldspar 1 core 100 $\mu\text{m}^2$	113.54	22.37	0.0000	0.0000	1.9521	3.5121	0.0039	0.5504	1.2	113.54	162.69	1527 $\pm$ 1476
<b>Quartz analysis</b>													
21	clear quartz 100 $\mu\text{m}^2$	9.11	18.16	0.0000	0.0000	8.7842	1.3249	0.0032	0.3593	1.4	9.11	107.71	183 $\pm$ 2058

Two areas of melt veins within the biotite grains were analysed. The first (analysis 11, Table 8.1) yielded very small amounts of argon and an age with very large errors, but indistinguishable from the biotite age. The second analysis yielded no  $^{39}\text{Ar}$  above blank levels, indicating no detectable potassium in the melt. It seems likely that the laser beam extracted a very small sliver of adjacent biotite during the first melt analysis, since previous work has shown that heating of the adjacent grains is insignificant (Laser-probe  $^{40}\text{Ar}/^{39}\text{Ar}$  dating of coesite and stishovite-bearing pseudotachylites and the age of the Vredefort impact event; Spray et al., 1995). Therefore, it was not possible to measure the melt age directly and heating of the adjacent biotite grains only caused argon loss over distances of 20  $\mu\text{m}$  within the grains. The ages from biotite grain edges and small grains within quartz (analysis 7, Table 8.1) did not yield reproducible ages and thus, cannot be used to indicate a probable impact age for the Woodleigh impact structure. The small amount of argon loss could have been caused by a transient heat pulse, which may have had a high temperature, if of short duration. For example, a pulse of 500°C lasting one year would have caused an overall loss of 1.5% and 20  $\mu\text{m}$ -deep, argon-loss profiles. However, similar profiles can be generated by longer lasting, lower temperature heat pulses.

Although K-feldspar microstructure is likely to be more complex, in the absence of good age constraints, K-feldspar (analyses 13–17, 19) and plagioclase (analyses 18,19) were analysed from the same sample. K-feldspars yielded ages from  $68 \pm 5$  to  $183 \pm 31$  Ma, and plagioclase yielded ages from  $642 \pm 546$  to  $1527 \pm 1476$  Ma. Clearly there was too little potassium in the plagioclase to yield precise ages at the spatial resolution used, but the older apparent ages are still indicative of some gas and ages probably older than the K-feldspars. The K-feldspars clearly indicate later heating, probably during the Cretaceous; further work might illuminate the thermal history, though the shocked nature of the samples may prevent this type of analysis. If we make the assumption that the K-feldspar grains exhibit the type of microstructure seen in other granitic samples, the subgrain or domain size for diffusion would be 1–6  $\mu\text{m}$ . A heating event of 200°C lasting 10 Ma would be sufficient to cause the amount of argon loss seen in the K-feldspars, assuming they originally exhibited ages around 800 Ma. This later heating would have had no significant effect on the biotite ages and indeed could not have caused the argon loss from biotite, since they do not exhibit Cretaceous ages at the grain margins (cf. analysis 8, Table 8.1).

In summary, the UV laser Ar–Ar data do not add to the constraints on the age of the Woodleigh impact structure. However, they can be used to constrain the thermal history. The impact may have caused a transient heating pulse, but argon loss from biotite grains indicates that a square-shaped pulse at 500°C lasting a year would have been sufficient to yield the observed ages. The biotite grains provided no evidence for ages younger than  $664 \pm 10$  Ma. Plagioclase and quartz yielded no ages due to the low content of potassium, and the small size of samples analysed do not indicate any excess argon in the system. The K-feldspars yielded Cretaceous ages indicating later heating during burial with temperatures reaching perhaps 150–200°C.

## References

- KELLEY, S. P., ARNAUD, N. O., and TURNER, S. P., 1994, High spatial resolution  $^{40}\text{Ar}/^{39}\text{Ar}$  investigations using an ultra-violet laser probe extraction technique: *Geochimica et Cosmochimica Acta*, v. 58, p. 3519–3525.
- RENNE, P. R., SWISHER, C. C., DEINO, A. L., KARNER, D. B., OWENS, T. L., and DEPAOLO, D. J., 1998, Intercalibration of standards, absolute ages and uncertainties in  $^{40}\text{Ar}/^{39}\text{Ar}$  dating: *Chemical Geology*, v. 145 (1–2), p. 117–152.
- SPRAY, J. G., KELLEY, S. P., and REIMOLD, W. U., 1995, Laser probe argon- $^{40}\text{Ar}/^{39}\text{Ar}$  dating coesite- and stishovite-bearing pseudotachylites and the age of the Vredefort impact event: *Meteoritics*, v. 30, p. 335–343.

## Appendix 9

### K–Ar dating

by I. T. Uysal

(Isotope Geochemistry Laboratory, Department of Earth Sciences,  
University of Queensland)

#### Summary

Eighteen samples were analysed from Woodleigh 1 and 2A, and the geologically most plausible K–Ar ages are summarized in Table 9.1, that is, ages between Middle Devonian and Early Jurassic as indicated by the regional stratigraphy.

#### K–Ar dating method

The K–Ar dating method requires the measurement of the potassium element and argon isotopic composition. The argon isotopic composition is determined by isotope dilution using  $^{38}\text{Ar}$  as a tracer (Dalrymple and Lanphere, 1969). Mineral separates and whole rock chips are fused in a molybdenum crucible under vacuum, using a radiofrequency generator positioned around the crucible and enclosing vacuum line. The gases produced are purified by getters and analysed on a VG Gas Analysis 8-80 mass spectrometer operated in the static mode at 2 keV accelerating voltage.

Ages are calculated from data corrected for machine mass discrimination and system blanks using the decay constants of Steiger and Jager (1977). The  $\text{K}_2\text{O}$  content of the samples is determined by induction coupled plasma optical emission spectrophotometry (ICPOES). The quoted errors are at 1 standard deviation (SD) and include all uncertainties in the measurement of the isotope ratios and potassium contents, and are calculated using the method of Cox and Dalrymple (1967). Replicate analysis ( $n = 13$ ) of separate loads of the Australian National University standard biotite have yielded a mean K–Ar age of  $97.8 \pm 2.1$  Ma (cf.  $97.9 \pm 0.9$  Ma; McDougall and Roksandic, 1974).

**Table 9.1. Potassium–argon analyses**

<i>Sample</i>	<i>Size fraction analysed</i>	<i>Minimum K–Ar age (Ma)</i>	<i>Calculated error (1 <math>\sigma</math>)</i>
Woodleigh 1, 225 m	1–0.2 $\mu\text{m}$	363	$\pm 8$ Ma
Woodleigh 1, 222.3 m	1–0.2 $\mu\text{m}$	336	$\pm 8$ Ma
Woodleigh 2A, 551.9 m	0.3–2 $\mu\text{m}$	364	$\pm 8$ Ma
Woodleigh 2A, 551.9 m	<0.2 $\mu\text{m}$	339	$\pm 7$ Ma
Woodleigh 2A, 585.2 m	<0.3 $\mu\text{m}$	352	$\pm 8$ Ma
Woodleigh 2A, 586.9 m	<0.3 $\mu\text{m}$	342	$\pm 7$ Ma
Woodleigh 2A, 587 m-A	<0.2 $\mu\text{m}$	341	$\pm 7$ Ma
Woodleigh 2A, 587 m-B	<0.2 $\mu\text{m}$	321	$\pm 9$ Ma
GL-O International Standard (published value):	–	95.0	$\pm 1.7$ Ma
Value obtained after analysing Woodleigh 2A, 586.9 m	–	94.9	$\pm 1.2$ Ma

NOTE:  $\sigma$ : Standard deviation



## Sample preparation

The illite separation included X-ray diffraction (XRD) analysis of the illite separates as described in Uysal et al. (2001). The usual procedure for the  $K_2O$  determination is ICPOES analysis of a 50–100 mg split of each prepared sample. After the  $K_2O$  analysis, the Ar analysis is conducted on the remainder of the sample material. An international age standard is run periodically as a check on the Ar analysis. An age standard (GL-O; Odin et al., 1982) was analysed immediately after sample Woodleigh 2A, 586.9 m <0.3  $\mu m$ . The determined age was within analytical precision of the recommended age for the standard.

## Results

The results from the K–Ar dating are listed in Table 9.2.

## Discussion

K–Ar analysis of a whole rock biotite-rich sample (without any clay content; 194.85 m, Woodleigh 1) yielded an age of 801 Ma, whereas separates of the biotite yielded mixed ages because they are partly altered to clays. The results suggest that the formation of biotite is primary and it is not related to a hydrothermal process during the impact event. Such a hydrothermal process caused only the alteration of biotite to clays. By comparison, two illite samples from Woodleigh 1 are pure alteration products of the biotite and yielded ages of 363 and 336 Ma. These samples are without any biotite content and contain only smectite-rich, mixed-layered illite–smectite, but no discrete illite. Smectite-rich clays yielded ages between 182 and 110 Ma. Poor argon retentivity of smectite-rich illite–smectite minerals during younger thermal events is the cause of these younger and inconsistent ages. Therefore, the K–Ar data of the smectitic minerals reflect mixed ages, which are geologically meaningless.

## References

- COX, A., and DALRYMPLE, G. B., 1967, Statistical analysis of geomagnetic reversal data and the precision of potassium–argon dating: *Journal Geophysical Research*, v. 72, p. 2603–2614.
- DALRYMPLE, G. B., and LANPHERE, M. A., 1969, Potassium argon dating: San Francisco, W. H. Freeman.
- MCDUGALL, I., and ROKSANDIC, Z., 1974, Total fusion  $^{40}Ar/^{39}Ar$  ages using the HIFAR reactor: *Journal Geological Society Australia*, v. 21, p. 81–89.
- ODIN, G. S., and 35 collaborators, 1982, Interlaboratory standards for dating purposes, in *Numerical dating in stratigraphy* edited by G. S. ODIN: Chichester, John Wiley and Sons, p. 123–150.
- STEIGER, R. H., and JAGER, E., 1977, Subcommittee on geochronology — convention on the use of decay constants in geochronology and cosmochronology: *Earth and Planetary Science Letters*, v. 36, p. 359–362.
- UYSAL, I. T., GOLDING, S. D., and THIEDE, D. S., 2001, K–Ar and Rb–Sr dating of authigenic illite–smectite in Late Permian coal measures, Queensland, Australia: implication for thermal history: *Chemical Geology*, v. 171 (3–4), p. 195–211.

Table 9.2. Results from potassium-argon analyses

Sample	Wodeleigh 1 194.85 m	Wodeleigh 1 194.85 m, 4–2 $\mu$ m	Wodeleigh 1 194.85 m, 2–1 $\mu$ m	Wodeleigh 1 203.85 – 203.9 m	Wodeleigh 1 208.0 – 208.1, <0.2 $\mu$ m
Lab number	—	—	—	—	—
Date analysed	12 September 2000	15 September 2000	12 September 2000	1 September 2000	30 August 2000
Analyst	T. Uysal	T. Uysal	T. Uysal	T. Uysal	T. Uysal
Sample type	Whole rock (no clay)	Biotite-illite	Biotite-illite	Smectite-rich illite/smectite	Smectite-rich illite/smectite
Weight % K <sub>2</sub> O in sample	5.6	2.98	2.31	1.89	1.08
Sample weight in gms	0.0828	0.0272	0.0808	0.1156	0.1235
Spike <sup>40</sup> Ar/ <sup>38</sup> Ar	0.001680	0.001680	0.001680	0.001680	0.001680
Spike <sup>38</sup> Ar/ <sup>36</sup> Ar	5.36845 × 10 <sup>-5</sup>	5.36845 × 10 <sup>-5</sup>	5.36845 × 10 <sup>-5</sup>	5.36845 × 10 <sup>-5</sup>	5.36845 × 10 <sup>-5</sup>
Sample <sup>40</sup> Ar <sub>mixture</sub> / <sup>38</sup> Ar <sub>mixture</sub>	15.0338	1.8925	3.5455	2.4268	4.8994
Sample <sup>38</sup> Ar <sub>mixture</sub> / <sup>36</sup> Ar <sub>mixture</sub>	1071.8680	1712.8160	842.0800	201.6400	69.1050
Orifice <sup>40</sup> Ar/ <sup>38</sup> Ar correction %	2.5419	1.7852	2.2337	1.9636	2.3360
Orifice <sup>38</sup> Ar/ <sup>36</sup> Ar correction %	2.6263	1.8445	2.3079	2.0289	2.4136
Mass discrimination <sup>40</sup> Ar/ <sup>38</sup> Ar %	-2.4017	-2.4017	-2.4017	-2.4017	-2.4017
Mass discrimination <sup>38</sup> Ar/ <sup>36</sup> Ar %	-2.4017	-2.4017	-2.4017	-2.4017	-2.4017
Spike volume in cc or ml (STP)	1.01935 × 10 <sup>-6</sup>	1.01935 × 10 <sup>-6</sup>	1.01935 × 10 <sup>-6</sup>	1.01935 × 10 <sup>-6</sup>	1.01935 × 10 <sup>-6</sup>
<sup>40</sup> K (moles/gm)	1.38749 × 10 <sup>-7</sup>	7.358346 × 10 <sup>-8</sup>	5.72342 × 10 <sup>-8</sup>	4.68280 × 10 <sup>-8</sup>	2.67588 × 10 <sup>-8</sup>
Total correction <sup>40</sup> Ar/ <sup>38</sup> Ar %	0.1402	-0.6165	-0.168	-0.4381	-0.0657
Total correction <sup>38</sup> Ar/ <sup>36</sup> Ar %	0.2246	-0.5572	-0.0938	-0.3728	-0.0119
Corrected <sup>40</sup> Ar <sub>mixture</sub> / <sup>38</sup> Ar <sub>mixture</sub>	15.05485	1.88083	3.53954	2.41617	4.89618
Corrected <sup>38</sup> Ar <sub>mixture</sub> / <sup>36</sup> Ar <sub>mixture</sub>	1074.275416	1703.272189	841.290129	200.8882861	69.1132235
Final <sup>40</sup> Ar <sub>radiogenic</sub> / <sup>38</sup> Ar	14.79637	1.72169	3.20314	0.96019	0.63625
Final <sup>38</sup> Ar/ <sup>40</sup> Ar <sub>radiogenic</sub>	0.06758	0.58082	0.31219	1.04146	1.57172
<sup>40</sup> Ar <sub>radiogenic</sub> in moles/gm	8.12843 × 10 <sup>-9</sup>	2.87917 × 10 <sup>-9</sup>	1.80321 × 10 <sup>-9</sup>	3.77815 × 10 <sup>-10</sup>	2.34336 × 10 <sup>-10</sup>
<sup>40</sup> Ar <sub>radiogenic</sub> / <sup>40</sup> K	5.85835 × 10 <sup>-2</sup>	3.89949 × 10 <sup>-2</sup>	3.15058 × 10 <sup>-2</sup>	8.06815 × 10 <sup>-3</sup>	8.75735 × 10 <sup>-3</sup>
<sup>40</sup> Ar total in cc or ml	1.53462 × 10 <sup>-5</sup>	1.91723 × 10 <sup>-6</sup>	3.60803 × 10 <sup>-6</sup>	2.46292 × 10 <sup>-6</sup>	4.99092 × 10 <sup>-6</sup>
<sup>40</sup> Ar <sub>radiogenic</sub> %	98.2831	91.5387	90.4959	39.7401	12.9947
<sup>36</sup> Ar total in cc or ml	9.48872 × 10 <sup>-10</sup>	5.98466 × 10 <sup>-10</sup>	1.21165 × 10 <sup>-9</sup>	5.07421 × 10 <sup>-9</sup>	1.4749 × 10 <sup>-8</sup>
<sup>36</sup> Ar total (moles/gm)	15.1137 × 10 <sup>-13</sup>	9.81812 × 10 <sup>-13</sup>	6.69151 × 10 <sup>-13</sup>	1.9587 × 10 <sup>-12</sup>	5.32909 × 10 <sup>-12</sup>
Age (Ma)	801 ± 17	571 ± 12	474 ± 10	134 ± 4	145 ± 12

Table 9.2. (continued)

Sample	Woodleigh 1 213.25 – 213.4 m, 2 – 0.2 $\mu$ m	Woodleigh 1 213.25 – 213.4 m, <0.2 $\mu$ m	Woodleigh 1 222.3 – 222.5 m	Woodleigh 1 222.3 – 222.5 m
Lab number	–	–	–	–
Date analysed	15 August 2000	14 August 2000	27 July 2000	26 October 2000
Analyst	T. Uysal	T. Uysal	T. Uysal	T. Uysal
Sample type	Smectite-rich illite/smectite	Smectite-rich illite/smectite	Illite and mixed layered illite/smectite	Illite
				Illite-smectite
Weight % K <sub>2</sub> O in sample	2.04	1.26	2.22	2.28
Sample weight in gms	0.108	0.1152	0.0866	0.0326
Spike $^{40}\text{Ar}/^{38}\text{Ar}$	0.001680	0.001680	0.001680	0.001680
Spike $^{38}\text{Ar}/^{36}\text{Ar}$	$5.36845 \times 10^{-5}$	$5.36845 \times 10^{-5}$	$5.36845 \times 10^{-5}$	$5.36845 \times 10^{-5}$
Sample $^{40}\text{Ar}_{\text{mixture}}/^{38}\text{Ar}_{\text{mixture}}$	1.5588	1.4447	2.8485	1.5744
Sample $^{38}\text{Ar}_{\text{mixture}}/^{36}\text{Ar}_{\text{mixture}}$	838.4916	354.2786	488.2480	1163.9505
Orifice $^{40}\text{Ar}/^{38}\text{Ar}$ correction %	1.5289	1.3899	2.0667	1.6165
Orifice $^{38}\text{Ar}/^{36}\text{Ar}$ correction %	1.5798	1.4362	2.1353	1.6703
Mass discrimination $^{40}\text{Ar}/^{38}\text{Ar}$ %	-2.4017	-2.4017	-2.4017	-2.4017
Mass discrimination $^{38}\text{Ar}/^{36}\text{Ar}$ %	-2.4017	-2.4017	-2.4017	-2.4017
Spike volume in cc or ml (STP)	$1.01935 \times 10^{-6}$	$1.01935 \times 10^{-6}$	$1.01935 \times 10^{-6}$	$1.01935 \times 10^{-6}$
$^{40}\text{K}$ (moles/gm)	$5.05445 \times 10^{-8}$	$3.12186 \times 10^{-8}$	$5.50043 \times 10^{-8}$	$5.64909 \times 10^{-8}$
Total correction $^{40}\text{Ar}/^{38}\text{Ar}$ %	-0.8728	-1.0118	-0.335	-0.7852
Total correction $^{38}\text{Ar}/^{36}\text{Ar}$ %	-0.8219	-0.9655	-0.2664	-0.7314
Corrected $^{40}\text{Ar}_{\text{mixture}}/^{38}\text{Ar}_{\text{mixture}}$	1.54515	1.43008	2.83891	1.56208
Corrected $^{38}\text{Ar}_{\text{mixture}}/^{36}\text{Ar}_{\text{mixture}}$	831.6000376	350.8580401	486.9473073	1155.437366
Final $^{40}\text{Ar}_{\text{radiogenic}}/^{38}\text{Ar}$	1.20423	0.60231	2.24706	1.32070
Final $^{38}\text{Ar}/^{40}\text{Ar}_{\text{radiogenic}}$	0.83041	1.66026	0.44503	0.75717
$^{40}\text{Ar}_{\text{radiogenic}}$ in moles/gm	$5.07186 \times 10^{-10}$	$2.37822 \times 10^{-10}$	$1.18026 \times 10^{-9}$	$1.84276 \times 10^{-9}$
$^{40}\text{Ar}_{\text{radiogenic}}/^{40}\text{K}$	$1.00344 \times 10^{-2}$	$7.61794 \times 10^{-3}$	$2.14576 \times 10^{-2}$	$3.26205 \times 10^{-2}$
$^{40}\text{Ar}$ total in cc or ml	$1.57504 \times 10^{-6}$	$1.45775 \times 10^{-6}$	$2.89384 \times 10^{-6}$	$1.5923 \times 10^{-6}$
$^{40}\text{Ar}_{\text{radiogenic}}$ %	77.9363	42.1174	79.1521	84.5477
$^{36}\text{Ar}$ total in cc or ml	$1.22577 \times 10^{-9}$	$2.90531 \times 10^{-9}$	$2.09335 \times 10^{-9}$	$8.8222 \times 10^{-10}$
$^{36}\text{Ar}$ total (moles/gm)	$5.06458 \times 10^{-13}$	$1.12538 \times 10^{-12}$	$1.07865 \times 10^{-12}$	$1.20758 \times 10^{-12}$
Age (Ma)	$165 \pm 4$	$127 \pm 4$	$336 \pm 8$	$489 \pm 11$
				$110 \pm 5$

Table 9.2. (continued)

Sample	Woodleigh 1 222.3 – 222.5 m, 0.2 – 0.1 $\mu\text{m}$	Woodleigh 1 224.9 – 225.0 m	Woodleigh 2A 551.9 m, <0.2 $\mu\text{m}$	Woodleigh 2A 551.9 m, 0.3 – 2.0 $\mu\text{m}$
Lab number	–	–	–	QA 812
Date analysed	27 July 2000	1 August 2000	18 August 2000	1 March 2000
Analyst	T. Uysal	T. Uysal	T. Uysal	D. S. Thiede
Sample type	Smectite-rich illite/smectite	Illite and illite/smectite	Illite	Illite
Weight % $\text{K}_2\text{O}$ in sample	3.61	2.1	5.83	6.03
Sample weight in gms	0.1029	0.0952	0.08	0.0761
Spike $^{40}\text{Ar}/^{38}\text{Ar}$	0.001680	0.001680	0.001680	0.001680
Spike $^{38}\text{Ar}/^{36}\text{Ar}$	$5.36845 \times 10^{-5}$	$5.36845 \times 10^{-5}$	$5.36845 \times 10^{-5}$	$5.36845 \times 10^{-5}$
Sample $^{40}\text{Ar}_{\text{mixture}}/^{38}\text{Ar}_{\text{mixture}}$	2.7889	2.9696	6.8762	5.9666
Sample $^{38}\text{Ar}_{\text{mixture}}/^{36}\text{Ar}_{\text{mixture}}$	541.2173	679.5000	777.1429	1313.9500
Orifice $^{40}\text{Ar}/^{38}\text{Ar}$ correction %	2.0541	2.1352	2.4001	2.4052
Orifice $^{38}\text{Ar}/^{36}\text{Ar}$ correction %	2.1223	2.2062	2.4798	2.4851
Mass discrimination $^{40}\text{Ar}/^{38}\text{Ar}$ %	-2.4017	-2.4017	-2.4017	-2.4017
Mass discrimination $^{38}\text{Ar}/^{36}\text{Ar}$ %	-2.4017	-2.4017	-2.4017	-2.4017
Spike volume in cc or ml (STP)	$1.01935 \times 10^{-6}$	$1.01935 \times 10^{-6}$	$1.01935 \times 10^{-6}$	$1.03720 \times 10^{-6}$
$^{40}\text{K}$ (moles/gm)	$8.94439 \times 10^{-8}$	$5.20311 \times 10^{-8}$	$1.44448 \times 10^{-7}$	$1.49403 \times 10^{-7}$
Total correction $^{40}\text{Ar}/^{38}\text{Ar}$ %	-0.3476	-0.2665	-0.0016	0.0035
Total correction $^{38}\text{Ar}/^{36}\text{Ar}$ %	-0.2794	-0.1955	0.0781	0.0834
Corrected $^{40}\text{Ar}_{\text{mixture}}/^{38}\text{Ar}_{\text{mixture}}$	2.77921	2.96169	5.87611	5.9668
Corrected $^{38}\text{Ar}_{\text{mixture}}/^{36}\text{Ar}_{\text{mixture}}$	539.7051389	679.1715775	777.7497986	1315.045834
Final $^{40}\text{Ar}_{\text{radiogenic}}/^{38}\text{Ar}$	2.24659	2.54079	5.51160	5.75703
Final $^{38}\text{Ar}/^{40}\text{Ar}_{\text{radiogenic}}$	0.44512	0.39358	0.18144	0.17370
$^{40}\text{Ar}_{\text{radiogenic}}$ in moles/gm	$9.93095 \times 10^{-10}$	$1.21399 \times 10^{-9}$	$3.13378 \times 10^{-9}$	$3.50134 \times 10^{-9}$
$^{40}\text{Ar}_{\text{radiogenic}}/^{40}\text{K}$	$1.11030 \times 10^{-2}$	$2.33319 \times 10^{-2}$	$2.16949 \times 10^{-2}$	$2.34344 \times 10^{-2}$
$^{40}\text{Ar}$ total in cc or ml	$2.83298 \times 10^{-6}$	$3.01899 \times 10^{-6}$	$5.98981 \times 10^{-6}$	$6.18877 \times 10^{-6}$
$^{40}\text{Ar}_{\text{radiogenic}}$ %	80.8358	85.7887	93.7967	96.4843
$^{36}\text{Ar}$ total in cc or ml	$1.88872 \times 10^{-9}$	$1.50309 \times 10^{-9}$	$1.31064 \times 10^{-9}$	$7.88718 \times 10^{-9}$
$^{36}\text{Ar}$ total (moles/gm)	$8.19048 \times 10^{-13}$	$7.04539 \times 10^{-13}$	$7.31058 \times 10^{-13}$	$4.62482 \times 10^{-13}$
Age (Ma)	$182 \pm 4$	$363 \pm 8$	$339 \pm 7$	$364 \pm 8$

Table 9.2. (continued)

Sample	Woodleigh 2A 585.2m <0.3 $\mu$ m	Woodleigh 2A 586.9m <0.3 $\mu$ m	Woodleigh 2A 587.2 m	Woodleigh 2A 587.2 m
Lab number	QA 813	QA 814	—	—
Date analysed	2 March 2000	2 August 2000	2 August 2000	17 August 2000
Analyst	D. S. Thiede	D. S. Thiede	T. Uysal	T. Uysal
Sample type	Illite	Illite	Illite	Illite (weathered)
Weight % K <sub>2</sub> O in sample	4.5625	4.47	5.06	4.66
Sample weight in gms	0.0797	0.0783	0.0825	0.0505
Spike <sup>40</sup> Ar/ <sup>38</sup> Ar	0.001680	0.001680	0.001680	0.001680
Spike <sup>38</sup> Ar/ <sup>36</sup> Ar	5.36845 × 10 <sup>-5</sup>	5.36845 × 10 <sup>-5</sup>	5.36845 × 10 <sup>-5</sup>	5.36845 × 10 <sup>-5</sup>
Sample <sup>40</sup> Ar <sub>mixture</sub> / <sup>38</sup> Ar <sub>mixture</sub>	4.7549	4.4001	5.4397	3.9952
Sample <sup>38</sup> Ar <sub>mixture</sub> / <sup>36</sup> Ar <sub>mixture</sub>	796.3962	955.2195	598.1000	213.9056
Orifice <sup>40</sup> Ar/ <sup>38</sup> Ar correction %	2.2925	2.2770	2.3753	2.2705
Orifice <sup>38</sup> Ar/ <sup>36</sup> Ar correction %	2.3686	2.3526	2.4542	2.3459
Mass discrimination <sup>40</sup> Ar/ <sup>38</sup> Ar %	-2.4017	-2.4017	-2.4017	-2.4017
Mass discrimination <sup>38</sup> Ar/ <sup>36</sup> Ar %	-2.4017	-2.4017	-2.4017	-2.4017
Spike volume in cc or ml (STP)	1.03720 × 10 <sup>-6</sup>	1.03720 × 10 <sup>-6</sup>	1.01935 × 10 <sup>-6</sup>	1.01936 × 10 <sup>-6</sup>
<sup>40</sup> K (moles/gm)	1.13044 × 10 <sup>-7</sup>	1.10752 × 10 <sup>-7</sup>	1.25370 × 10 <sup>-7</sup>	1.15955 × 10 <sup>-7</sup>
Total correction <sup>40</sup> Ar/ <sup>38</sup> Ar %	-0.1092	-0.1247	-0.0264	-0.1312
Total correction <sup>38</sup> Ar/ <sup>36</sup> Ar %	-0.0331	-0.0491	0.0525	-0.0558
Corrected <sup>40</sup> Ar <sub>mixture</sub> / <sup>38</sup> Ar <sub>mixture</sub>	4.74971	4.39461	5.43826	3.98999
Corrected <sup>38</sup> Ar <sub>mixture</sub> / <sup>36</sup> Ar <sub>mixture</sub>	796.1325929	954.7504872	598.410025	213.7862107
Final <sup>40</sup> Ar <sub>radiogenic</sub> / <sup>38</sup> Ar	4.39369	4.10004	4.96011	2.62414
Final <sup>38</sup> Ar/ <sup>40</sup> Ar <sub>radiogenic</sub>	0.22760	0.24390	0.20161	0.38108
<sup>40</sup> Ar <sub>radiogenic</sub> in moles/gm	2.55148 × 10 <sup>-9</sup>	2.42352 × 10 <sup>-9</sup>	2.73476 × 10 <sup>-9</sup>	2.36362 × 10 <sup>-9</sup>
<sup>40</sup> Ar <sub>radiogenic</sub> / <sup>40</sup> K	2.25707 × 10 <sup>-2</sup>	2.18824 × 10 <sup>-2</sup>	2.18135 × 10 <sup>-2</sup>	2.03839 × 10 <sup>-2</sup>
<sup>40</sup> Ar total in cc or ml	4.9264 × 10 <sup>-6</sup>	4.55809 × 10 <sup>-6</sup>	5.54349 × 10 <sup>-6</sup>	4.06719 × 10 <sup>-6</sup>
<sup>40</sup> Ar <sub>radiogenic</sub> %	92.5044	93.2969	91.2077	65.7681
<sup>36</sup> Ar total in cc or ml	1.3028 × 10 <sup>-9</sup>	1.08636 × 10 <sup>-9</sup>	1.70342 × 10 <sup>-9</sup>	4.76808 × 10 <sup>-9</sup>
<sup>36</sup> Ar total (moles/gm)	7.29419 × 10 <sup>-13</sup>	6.19112 × 10 <sup>-13</sup>	9.21352 × 10 <sup>-13</sup>	4.21318 × 10 <sup>-12</sup>
Age (Ma)	352 ± 8	342 ± 7	341 ± 7	321 ± 8.6

NOTES: Constants used in analyses (15 digit precision used in calculation):

Decay constant  $\lambda_K$  [yr<sup>-1</sup>]: 4.962 × 10<sup>-10</sup> (Steiger and Jäger, 1977)  
 Decay constant  $\lambda_K + \lambda_K^*$  [yr<sup>-1</sup>]: 5.81 × 10<sup>-11</sup> (Steiger and Jäger, 1977)  
<sup>40</sup>K/K [mol/mol]: 1.167 × 10<sup>-4</sup>  
 grams K/grams K<sub>2</sub>O: 0.8301  
 grams K/mole K: 39.0983  
 Atmosphere <sup>40</sup>Ar/<sup>38</sup>Ar: 1581  
 Atmosphere <sup>36</sup>Ar/<sup>38</sup>Ar: 5.35



## Appendix 10

### Petroleum geochemistry

by K. A. R. Ghorl

#### Introduction

The hydrocarbon-generating potential and thermal maturity of the succession in Woodleigh 2 (TD 198 m) and 2A (TD 618.3 m) were evaluated from 13 core samples, one from Woodleigh 2 and 12 from Woodleigh 2A. Of these samples, one is from the Cretaceous Birdrong Sandstone in Woodleigh 2, and nine are from the Jurassic Woodleigh Formation and three are clasts of the Coburn Formation within the unnamed breccia in Woodleigh 2A. All likely source-rock lithologies (fine-grained intervals of light to dark grey) were sampled for source rock analyses and a sandstone bed was sampled from the Jurassic Woodleigh Formation for apatite fission-track analysis (AFTA). In addition to these samples, Graeme Beardsmore from the Earth Science Department of Monash University sampled 17 cores for thermal conductivity measurements. The petroleum source potential, type, and maturity of the section in Woodleigh 2 and 2A is summarized in Figure 10.1.

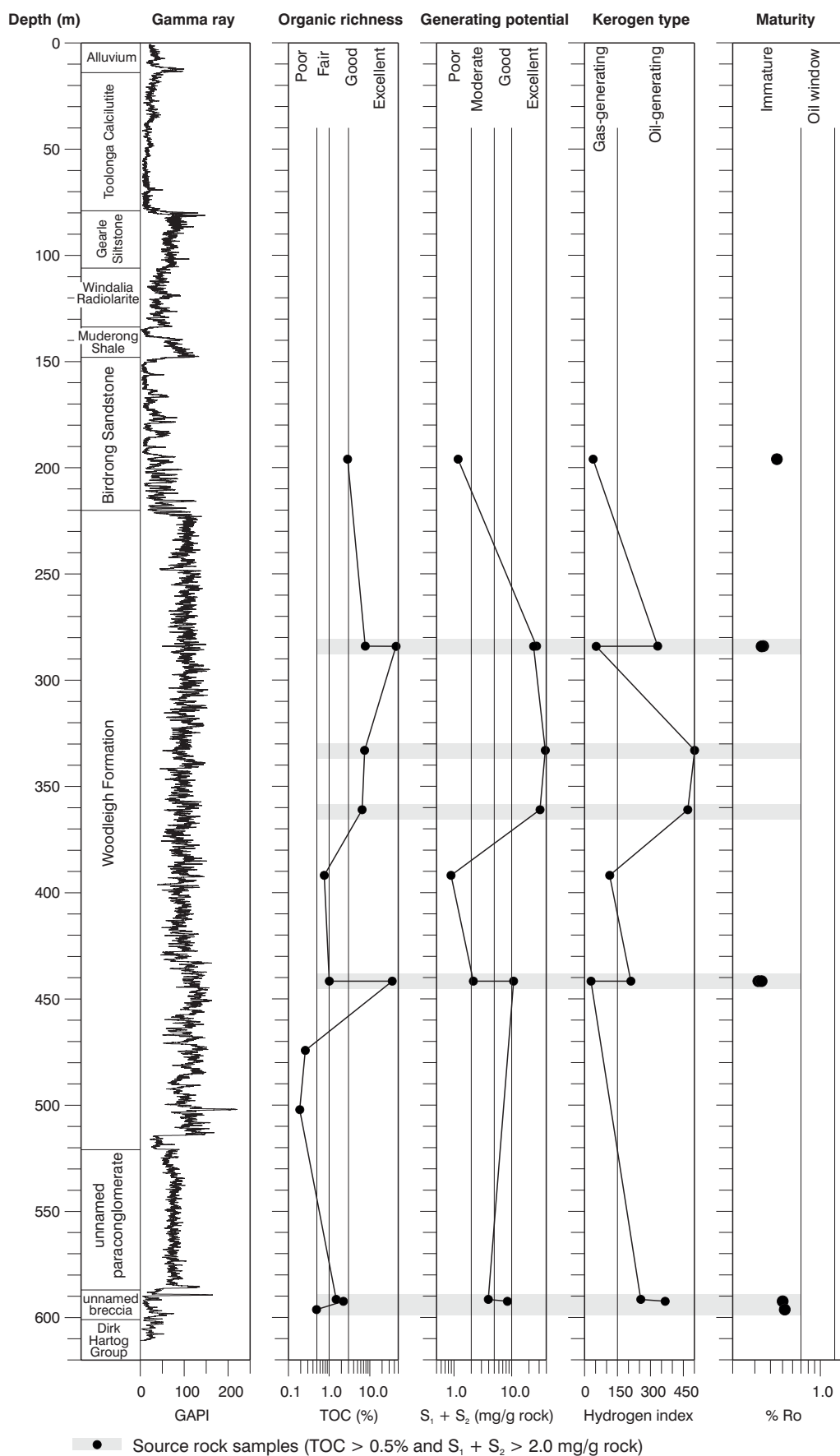
Total organic carbon (TOC) and Rock-Eval pyrolysis were undertaken to evaluate the organic richness and hydrocarbon-generating potential of the section, whereas organic petrology, the Rock-Eval parameter  $T_{max}$ , and AFTA indicate the level and timing of thermal maturity. The TOC and Rock-Eval pyrolysis analyses were carried out by Geotechnical Services Pty Ltd, organic petrology was done by Keiraville Konsultants Pty Ltd, and AFTA was by Geotrack International Pty Ltd. The number and type of geochemical analyses carried out is summarized in Table 10.1.

#### Source-rock potential

Hydrocarbon-generating potential in Woodleigh 2 and 2A is quantified from TOC content, a measure of organic richness, and potential yield ( $S_1 + S_2$ ) from Rock-Eval pyrolysis. Ten of the 13 samples screened by TOC analysis are organic rich (0.5% TOC) and were analysed by Rock-Eval pyrolysis to assess their hydrocarbon-generating potential (Table 10.2). The Rock-Eval pyrolysis shows that samples from the Woodleigh Formation have excellent hydrocarbon-generating potential, whereas samples from the Cretaceous and unnamed breccia have fair and good hydrocarbon-generating potential respectively. The Cretaceous sample from the Birdrong Sandstone is organic rich (2.84% TOC), but with comparatively low hydrocarbon-generating potential (1.34 mg/g rock  $S_1 + S_2$ ). Samples from the Jurassic Woodleigh Formation are excellent in organic richness, with shale beds ranging up to 7.7% TOC, but beds rich in woody material reach up to 44% TOC. Their hydrocarbon-generating potential ranges up to 38 mg/g rock  $S_1 + S_2$ . Two of the three organic-rich samples from Silurian clasts within the unnamed breccia analysed by Rock-Eval pyrolysis are fair to good in organic richness and generating potential (Table 10.2; Fig. 10.2). A photograph of the unnamed breccia, from which the Silurian clast was sampled, is shown in Figure 12d.

#### Source-rock type

Pyrolysis-gas chromatography (PGC) and extract analyses were used to supplement the Rock-Eval pyrolysis to determine the type of kerogen present. A plot of the Rock-Eval parameters and hydrogen index (HI) versus  $T_{max}$  indicate that the kerogen present in organic-rich shale samples from the Woodleigh Formation and the unnamed breccia is oil- and gas-generating type II (Fig. 10.3). By comparison, the kerogen in samples of woody material from the



AJM335

01.05.01

Figure 10.1. Petroleum source-rock potential, type, and maturity, Woodleigh 2 and 2A

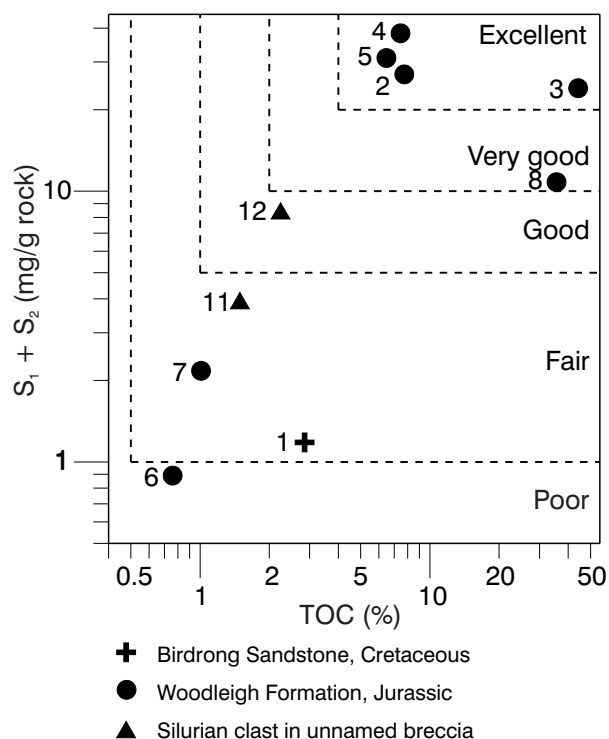
**Table 10.1. Geochemical analyses carried out on core samples from Woodleigh 2 and 2A**

<i>Analysis type</i>	<i>Samples</i>	<i>Purpose</i>	<i>Analyst</i>
Total organic carbon (TOC)	13	Source potential	Geotech
Rock-Eval pyrolysis	10	Source potential	Geotech
Pyrolysis gas chromatography	3	Source potential	Geotech
Gas chromatography mass spectrometry	3	Source potential	Geotech
Organic petrology	7	Source maturity	KK
Apatite fission-track analysis (AFTA)	1	Palaeotemperature	Geotrack
Thermal conductivity	17	Basin modelling	Monash University

**NOTES:** Geotech: Geotechnical Services Pty Ltd  
Geotrack: Geotrack International Pty Ltd  
KK: Keiraville Konsultants Pty Ltd

Woodleigh Formation, which have excellent organic richness and generating potential, and the organic-rich sample from the Birdrong Sandstone, which has low generating potential, are gas-generating type III.

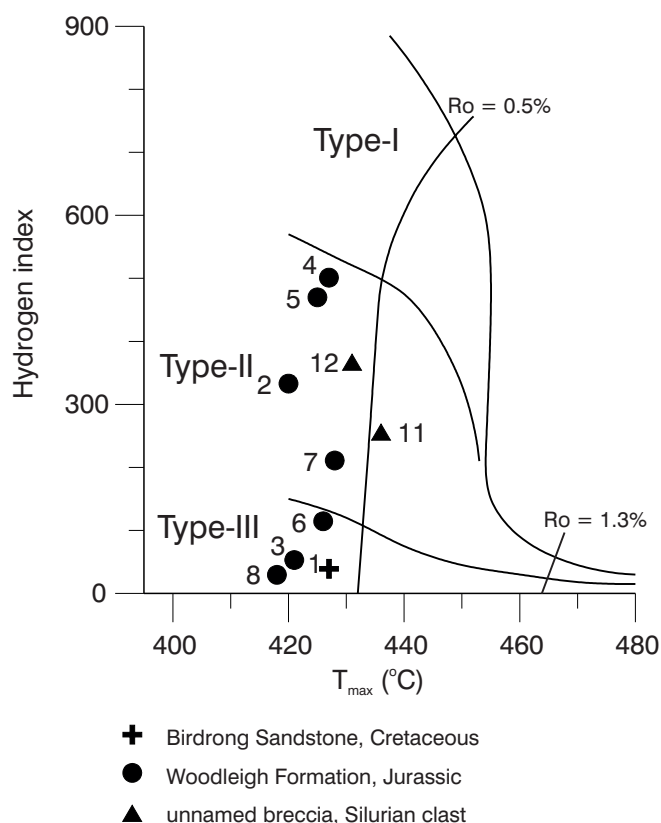
Two samples from the Woodleigh Formation and one from the unnamed breccia were analysed by PGC to confirm the quality of the kerogen, because it provides a more accurate guide than Rock-Eval pyrolysis to oil- versus gas-generating potential of kerogen. Tables 10.3 to 10.6 list basic analytical data, alkene and alkane components, aromatic and phenolic components, and selected parameters. The PGC plot confirms that woody material from the Woodleigh Formation is a gas-generating type (Fig. 10.4b).



AJM336

01.05.01

**Figure 10.2. Petroleum-generating potential, Woodleigh 2 and 2A. See Table 10.2 to relate sample number to sample depth**



AJM337

01.05.01

**Figure 10.3. Kerogen typing by Rock-Eval pyrolysis of organic-rich samples from Woodleigh 2 and 2A. See Table 10.2 to relate sample number to sample depth**

A plot of oil proneness ( $C_5$  to  $C_{31}$  alkanes + alkenes) versus the gas-oil generation index (GOGI;  $(C_1-C_5)/C_{6+}$ ), indicates that the kerogen in the sample from the Woodleigh Formation is predominantly oil generating, whereas the sample from the unnamed breccia is oil and gas generating (Fig. 10.5).

A sample from the Woodleigh Formation (333.1 m) was extracted and saturates were analysed by gas chromatography and mass spectrometry (GC-MS). Similarly, a sample of the Silurian clast within the unnamed breccia (592.4 m) was extracted, and the saturates as well as the branched and cyclic hydrocarbons were analysed by GC-MS. Tables 10.7 to 10.10 and 10.11 and 10.12 summarize extract, liquid chromatography, saturate GC-MS data, and GC-MS data of branched and cyclic saturated hydrocarbons. Figures 10.6a and 10.6b and 10.7a to 10.7d show the chromatograms of saturated hydrocarbons and the mass spectrograms of branched and cyclic saturated hydrocarbons respectively.

The liquid chromatography of samples from the Woodleigh Formation indicate good oil-generating potential (Fig. 10.8). The GC-MS data for extracted saturates (Fig. 10.9) and for branched and cyclic hydrocarbons (Fig. 10.10) are consistent with deposition in a highly reducing terrestrial environment. These analyses confirm the good oil-prone quality of kerogen in the Woodleigh Formation and oil- and gas-prone kerogen in the Coburn Formation.

**Table 10 2. TOC and Rock-Eval pyrolysis data of core samples from Woodleigh 2 and 2A**

Depth (m)	Sample type	No.	$T_{max}$ (°C)	$S_1$	$S_2$	$S_3$	$S_1 + S_2$	$S_2/S_3$	PI	TOC (%)	HI	OI
				(mg/g rock)								
196.0 <sup>(a)</sup>	core	1	427	0.06	1.12	1.34	1.18	0.84	0.05	2.85	39	47
284.0	core	2	420	1.23	25.77	1.73	27.00	14.90	0.05	7.74	333	22
284.1	core <sup>(b)</sup>	3	421	0.60	23.40	24.70	24.00	0.95	0.03	44.19	53	56
333.1	core	4	427	0.97	37.33	1.59	38.30	23.48	0.03	7.45	501	21
361.0	core	5	425	0.65	30.40	1.33	31.05	22.86	0.02	6.47	470	21
391.9	core	6	426	0.02	0.87	0.42	0.89	2.07	0.02	0.76	114	55
441.7	core	7	428	0.04	2.13	0.35	2.17	6.09	0.02	1.01	211	35
441.7	core <sup>(b)</sup>	8	418	0.32	10.48	14.87	10.80	0.70	0.03	35.58	29	42
474.3	core	9	—	—	—	—	—	—	—	0.26	—	—
502.2	core	10	—	—	—	—	—	—	—	0.19	—	—
591.5	core	11	436	0.12	3.82	0.68	3.94	5.62	0.03	1.49	256	46
592.4	core	12	431	0.23	8.22	0.83	8.45	9.90	0.03	2.24	367	37
596.3	core	13	—	—	—	—	—	—	—	0.49	—	—

**NOTES:** (a) sample from Woodleigh 2  
(b) woody material  
HI: hydrogen index  
OI: oxygen index  
PI: production index  
 $S_1$ : existing hydrocarbons (HC)

$S_2$ : pyrolytic yield (HC)  
 $S_3$ : organic carbon dioxide  
 $S_1 + S_2$ : potential yield  
TOC: total organic carbon  
 $T_{max}$ : temperature of maximum pyrolytic yield ( $S_2$ )

**Table 10.3. Basic analytical data from pyrolysis-gas chromatography of core samples from Woodleigh 2A**

Depth (m)	333.05	441.7a	592.4	Depth (m)	333.05	441.7a	592.4
Compound	Value	Value	Value	Compound	Value	Value	Value
C <sub>5</sub> n-alkene	4.510	0.000	2.682	C <sub>22</sub> n-alkene	0.522	0.000	0.201
C <sub>5</sub> n-alkane	4.510	0.000	2.682	C <sub>23</sub> n-alkane	0.417	0.000	0.116
C <sub>6</sub> n-alkene	1.769	0.000	1.447	C <sub>23</sub> n-alkene	0.534	0.000	0.174
C <sub>6</sub> n-alkane	1.108	0.000	0.973	C <sub>24</sub> n-alkane	0.407	0.000	0.125
C <sub>7</sub> n-alkene	1.476	0.000	1.296	C <sub>24</sub> n-alkene	0.383	0.000	0.160
C <sub>7</sub> n-alkane	1.241	0.000	1.098	C <sub>25</sub> n-alkane	0.302	0.000	0.085
C <sub>8</sub> n-alkene	1.334	0.000	1.036	C <sub>25</sub> n-alkene	0.379	0.000	0.143
C <sub>8</sub> n-alkane	0.928	0.000	0.811	C <sub>26</sub> n-alkane	0.195	0.000	0.062
C <sub>9</sub> n-alkene	1.046	0.000	0.751	C <sub>26</sub> n-alkene	0.262	0.000	0.121
C <sub>9</sub> n-alkane	0.773	0.000	0.610	C <sub>27</sub> n-alkane	0.160	0.000	0.052
C <sub>10</sub> n-alkene	1.066	0.000	0.722	C <sub>27</sub> n-alkene	0.249	0.000	0.098
C <sub>10</sub> n-alkane	1.096	0.000	0.659	C <sub>28</sub> n-alkane	0.115	0.000	0.033
C <sub>11</sub> n-alkene	1.106	0.000	0.661	C <sub>28</sub> n-alkene	0.168	0.000	0.069
C <sub>11</sub> n-alkane	0.782	0.000	0.547	C <sub>29</sub> n-alkane	0.056	0.000	0.025
C <sub>12</sub> n-alkene	1.038	0.000	0.573	C <sub>29</sub> n-alkene	0.149	0.000	0.049
C <sub>12</sub> n-alkane	0.658	0.000	0.413	C <sub>30</sub> n-alkane	0.000	0.000	0.014
C <sub>13</sub> n-alkene	0.877	0.000	0.445	C <sub>30</sub> n-alkene	0.076	0.000	0.041
C <sub>13</sub> n-alkane	0.807	0.000	0.445	C <sub>31</sub> n-alkane	0.000	0.000	0.000
C <sub>14</sub> n-alkene	0.959	0.000	0.597	C <sub>31</sub> n-alkene	0.054	0.000	0.027
C <sub>14</sub> n-alkane	0.845	0.000	0.429	C <sub>1</sub> -C <sub>4</sub>	23.929	50.294	32.047
C <sub>15</sub> n-alkene	0.941	0.000	0.474	C <sub>5</sub>	9.468	6.264	6.872
C <sub>15</sub> n-alkane	0.884	0.000	0.450	C <sub>6</sub> -C <sub>8</sub>	21.613	15.394	28.701
C <sub>16</sub> n-alkene	0.689	0.000	0.362	C <sub>9</sub> -C <sub>14</sub>	26.418	27.421	22.458
C <sub>16</sub> n-alkane	0.688	0.000	0.361	C <sub>15</sub> -C <sub>31</sub>	18.572	0.627	9.922
C <sub>17</sub> n-alkene	0.632	0.000	0.292	Benzene	1.279	1.293	0.945
C <sub>17</sub> n-alkane	0.706	0.000	0.354	Toluene	1.590	2.052	0.910
C <sub>18</sub> n-alkene	0.541	0.000	0.247	Ethylbenzene	0.372	0.226	0.236
C <sub>18</sub> n-alkane	0.536	0.000	0.292	m- + p-xylene	1.130	0.775	0.786
C <sub>19</sub> n-alkene	0.516	0.000	0.209	Styrene	0.368	0.121	0.292
C <sub>19</sub> n-alkane	0.571	0.000	0.253	o-xylene	0.511	0.246	0.310
C <sub>20</sub> n-alkene	0.490	0.000	0.171	Phenol	0.477	3.283	0.433
C <sub>20</sub> n-alkane	0.560	0.000	0.256	o-cresol	0.000	0.679	0.000
C <sub>21</sub> n-alkane	0.445	0.000	0.156	m- + p-cresol	0.000	2.356	0.000
C <sub>21</sub> n-alkane	0.600	0.000	0.212	C <sub>2</sub> phenol	0.422	0.273	0.306
C <sub>22</sub> n-alkane	0.442	0.000	0.131	C <sub>2</sub> phenol	0.000	0.395	0.000



Table 10.4. Alkene and alkane component from pyrolysis-gas chromatography of core samples from Woodleigh 2A

Depth (m)	Carbon number	Alkane + Alkene			Alkane			Alkene			Alkane/ Alkene
		A	B	C	A	B	C	A	B	C	
333.05	1	—	—	—	—	—	—	—	—	—	—
	2	—	—	—	—	—	—	—	—	—	—
	3	—	—	—	—	—	—	—	—	—	—
	4	—	—	—	—	—	—	—	—	—	—
	5	9.021	3.367	0.452	4.510	1.684	0.226	4.510	1.684	0.226	1.00
	6	2.877	1.074	0.144	1.108	0.414	0.056	1.769	0.660	0.089	0.63
	7	2.717	1.014	0.136	1.241	0.463	0.062	1.476	0.551	0.074	0.84
	8	2.262	0.844	0.113	0.928	0.346	0.046	1.334	0.498	0.067	0.70
	9	1.819	0.679	0.091	0.773	0.289	0.039	1.046	0.390	0.052	0.74
	10	2.162	0.807	0.108	1.096	0.409	0.055	1.066	0.398	0.053	1.03
	11	1.888	0.705	0.095	0.782	0.292	0.039	1.106	0.413	0.055	0.71
	12	1.696	0.633	0.085	0.658	0.246	0.033	1.038	0.387	0.052	0.63
	13	1.684	0.629	0.084	0.807	0.301	0.040	0.877	0.327	0.044	0.92
	14	1.804	0.673	0.090	0.845	0.315	0.042	0.959	0.358	0.048	0.88
	15	1.825	0.681	0.091	0.884	0.330	0.044	0.941	0.351	0.047	0.94
	16	1.377	0.514	0.069	0.688	0.257	0.034	0.689	0.257	0.035	1.00
	17	1.338	0.499	0.067	0.706	0.264	0.035	0.632	0.236	0.032	1.12
	18	1.077	0.402	0.054	0.536	0.200	0.027	0.541	0.202	0.027	0.99
	19	1.087	0.406	0.054	0.571	0.213	0.029	0.516	0.193	0.026	1.11
	20	1.050	0.392	0.053	0.560	0.209	0.028	0.490	0.183	0.025	1.14
	21	1.045	0.390	0.052	0.600	0.224	0.030	0.445	0.166	0.022	1.35
	22	0.964	0.360	0.048	0.522	0.195	0.026	0.442	0.165	0.022	1.18
	23	0.951	0.355	0.048	0.534	0.199	0.027	0.417	0.156	0.021	1.28
	24	0.790	0.295	0.040	0.383	0.143	0.019	0.407	0.152	0.020	0.94
	25	0.681	0.254	0.034	0.379	0.141	0.019	0.302	0.113	0.015	1.25
	26	0.457	0.171	0.023	0.262	0.098	0.013	0.195	0.073	0.010	1.34
	27	0.409	0.153	0.020	0.249	0.093	0.012	0.160	0.060	0.008	1.56
	28	0.283	0.106	0.014	0.168	0.063	0.008	0.115	0.043	0.006	1.46
	29	0.205	0.077	0.010	0.149	0.056	0.007	0.056	0.021	0.003	2.66
	30	0.076	0.028	0.004	0.076	0.028	0.004	0.000	0.000	0.000	—
	31	0.054	0.020	0.003	0.054	0.020	0.003	0.000	0.000	0.000	—
441.7a	1	—	—	—	—	—	—	—	—	—	—
	2	—	—	—	—	—	—	—	—	—	—
	3	—	—	—	—	—	—	—	—	—	—
	4	—	—	—	—	—	—	—	—	—	—
	5	0.000	0.000	0.000	0.000	0.000	0.000	0.000	0.000	0.000	—
	6	0.000	0.000	0.000	0.000	0.000	0.000	0.000	0.000	0.000	—
	7	0.000	0.000	0.000	0.000	0.000	0.000	0.000	0.000	0.000	—
	8	0.000	0.000	0.000	0.000	0.000	0.000	0.000	0.000	0.000	—
	9	0.000	0.000	0.000	0.000	0.000	0.000	0.000	0.000	0.000	—
	10	0.000	0.000	0.000	0.000	0.000	0.000	0.000	0.000	0.000	—
	11	0.000	0.000	0.000	0.000	0.000	0.000	0.000	0.000	0.000	—
	12	0.000	0.000	0.000	0.000	0.000	0.000	0.000	0.000	0.000	—
	13	0.000	0.000	0.000	0.000	0.000	0.000	0.000	0.000	0.000	—
	14	0.000	0.000	0.000	0.000	0.000	0.000	0.000	0.000	0.000	—
	15	0.000	0.000	0.000	0.000	0.000	0.000	0.000	0.000	0.000	—
	16	0.000	0.000	0.000	0.000	0.000	0.000	0.000	0.000	0.000	—
	17	0.000	0.000	0.000	0.000	0.000	0.000	0.000	0.000	0.000	—
	18	0.000	0.000	0.000	0.000	0.000	0.000	0.000	0.000	0.000	—
	19	0.000	0.000	0.000	0.000	0.000	0.000	0.000	0.000	0.000	—
	20	0.000	0.000	0.000	0.000	0.000	0.000	0.000	0.000	0.000	—
	21	0.000	0.000	0.000	0.000	0.000	0.000	0.000	0.000	0.000	—
	22	0.000	0.000	0.000	0.000	0.000	0.000	0.000	0.000	0.000	—
	23	0.000	0.000	0.000	0.000	0.000	0.000	0.000	0.000	0.000	—
	24	0.000	0.000	0.000	0.000	0.000	0.000	0.000	0.000	0.000	—
	25	0.000	0.000	0.000	0.000	0.000	0.000	0.000	0.000	0.000	—
	26	0.000	0.000	0.000	0.000	0.000	0.000	0.000	0.000	0.000	—
	27	0.000	0.000	0.000	0.000	0.000	0.000	0.000	0.000	0.000	—
	28	0.000	0.000	0.000	0.000	0.000	0.000	0.000	0.000	0.000	—
	29	0.000	0.000	0.000	0.000	0.000	0.000	0.000	0.000	0.000	—
	30	0.000	0.000	0.000	0.000	0.000	0.000	0.000	0.000	0.000	—
	31	0.000	0.000	0.000	0.000	0.000	0.000	0.000	0.000	0.000	—

Table 10.4. (continued)

Depth (m)	Carbon number	Alkane + Alkene			Alkane			Alkene			Alkane/ Alkene
		A	B	C	A	B	C	A	B	C	
592.4	1	—	—	—	—	—	—	—	—	—	—
	2	—	—	—	—	—	—	—	—	—	—
	3	—	—	—	—	—	—	—	—	—	—
	4	—	—	—	—	—	—	—	—	—	—
	5	5.364	0.441	0.197	2.682	0.220	0.098	2.682	0.220	0.098	1.00
	6	2.420	0.199	0.089	0.973	0.080	0.036	1.447	0.119	0.053	0.67
	7	2.394	0.197	0.088	1.098	0.090	0.040	1.296	0.107	0.048	0.85
	8	1.847	0.152	0.068	0.811	0.067	0.030	1.036	0.085	0.038	0.78
	9	1.361	0.112	0.050	0.610	0.050	0.022	0.751	0.062	0.028	0.81
	10	1.381	0.114	0.051	0.659	0.054	0.024	0.722	0.059	0.026	0.91
	11	1.208	0.099	0.044	0.547	0.045	0.020	0.661	0.054	0.024	0.83
	12	0.986	0.081	0.036	0.413	0.034	0.015	0.573	0.047	0.021	0.72
	13	0.890	0.073	0.033	0.445	0.037	0.016	0.445	0.037	0.016	1.00
	14	1.026	0.084	0.038	0.429	0.035	0.016	0.597	0.049	0.022	0.72
	15	0.924	0.076	0.034	0.450	0.037	0.017	0.474	0.039	0.017	0.95
	16	0.723	0.059	0.027	0.361	0.030	0.013	0.362	0.030	0.013	1.00
	17	0.646	0.053	0.024	0.354	0.029	0.013	0.292	0.024	0.011	1.21
	18	0.539	0.044	0.020	0.292	0.024	0.011	0.247	0.020	0.009	1.18
	19	0.462	0.038	0.017	0.253	0.021	0.009	0.209	0.017	0.008	1.21
	20	0.427	0.035	0.016	0.256	0.021	0.009	0.171	0.014	0.006	1.50
	21	0.368	0.030	0.014	0.212	0.017	0.008	0.156	0.013	0.006	1.36
	22	0.332	0.027	0.012	0.201	0.017	0.007	0.131	0.011	0.005	1.53
	23	0.290	0.024	0.011	0.174	0.014	0.006	0.116	0.010	0.004	1.50
	24	0.285	0.023	0.010	0.160	0.013	0.006	0.125	0.010	0.005	1.28
	25	0.228	0.019	0.008	0.143	0.012	0.005	0.085	0.007	0.003	1.68
	26	0.183	0.015	0.007	0.121	0.010	0.004	0.062	0.005	0.002	1.95
	27	0.150	0.012	0.006	0.098	0.008	0.004	0.052	0.004	0.002	1.88
	28	0.102	0.008	0.004	0.069	0.006	0.003	0.033	0.003	0.001	2.09
	29	0.074	0.006	0.003	0.049	0.004	0.002	0.025	0.002	0.001	1.96
	30	0.055	0.005	0.002	0.041	0.003	0.002	0.014	0.001	0.001	2.93
	31	0.027	0.002	0.001	0.027	0.002	0.001	0.000	0.000	0.000	—

NOTES: A: % of resolved compounds in S<sub>2</sub>  
 B: mg/g rock (Rock-Eval)  
 C: (mg/g rock)/TOC  
 S<sub>2</sub>: pyrolytic yield  
 TOC: total organic carbon

**Table 10.5. Aromatic and phenolic component from pyrolysis-gas chromatography of core samples from Woodleigh 2A**

Depth (m)	Type	Compound	Value		
			A	B	C
333.05	Aromatic	Benzene	1.279	0.477	0.064
		Toluene	1.590	0.594	0.080
		Ethylbenzene	0.372	0.139	0.019
		m- + p-xylene	1.130	0.422	0.057
		Styrene	0.368	0.137	0.018
	Phenolic	o-xylene	0.511	0.191	0.026
		Phenol	0.477	0.178	0.024
		o-cresol	0.000	0.000	0.000
		m- + p-cresol	0.000	0.000	0.000
		C <sub>2</sub> phenol	0.422	0.158	0.021
		C <sub>2</sub> phenol	0.000	0.000	0.000
441.7a	Aromatic	Benzene	1.293	0.136	0.004
		Toluene	2.052	0.215	0.006
		Ethylbenzene	0.226	0.024	0.001
		m- + p-xylene	0.775	0.081	0.002
		Styrene	0.121	0.013	0.000
	Phenolic	o-xylene	0.246	0.026	0.001
		Phenol	3.283	0.344	0.010
		o-cresol	0.679	0.071	0.002
		m- + p-cresol	2.356	0.247	0.007
		C <sub>2</sub> phenol	0.273	0.029	0.001
		C <sub>2</sub> phenol	0.395	0.041	0.001
592.4	Aromatic	Benzene	0.945	0.078	0.035
		Toluene	0.910	0.075	0.033
		Ethylbenzene	0.236	0.019	0.009
		m- + p-xylene	0.786	0.065	0.029
		Styrene	0.292	0.024	0.011
	Phenolic	o-xylene	0.310	0.025	0.011
		Phenol	0.433	0.036	0.016
		o-cresol	0.000	0.000	0.000
		m- + p-cresol	0.000	0.000	0.000
		C <sub>2</sub> phenol	0.306	0.025	0.011
		C <sub>2</sub> phenol	0.000	0.000	0.000

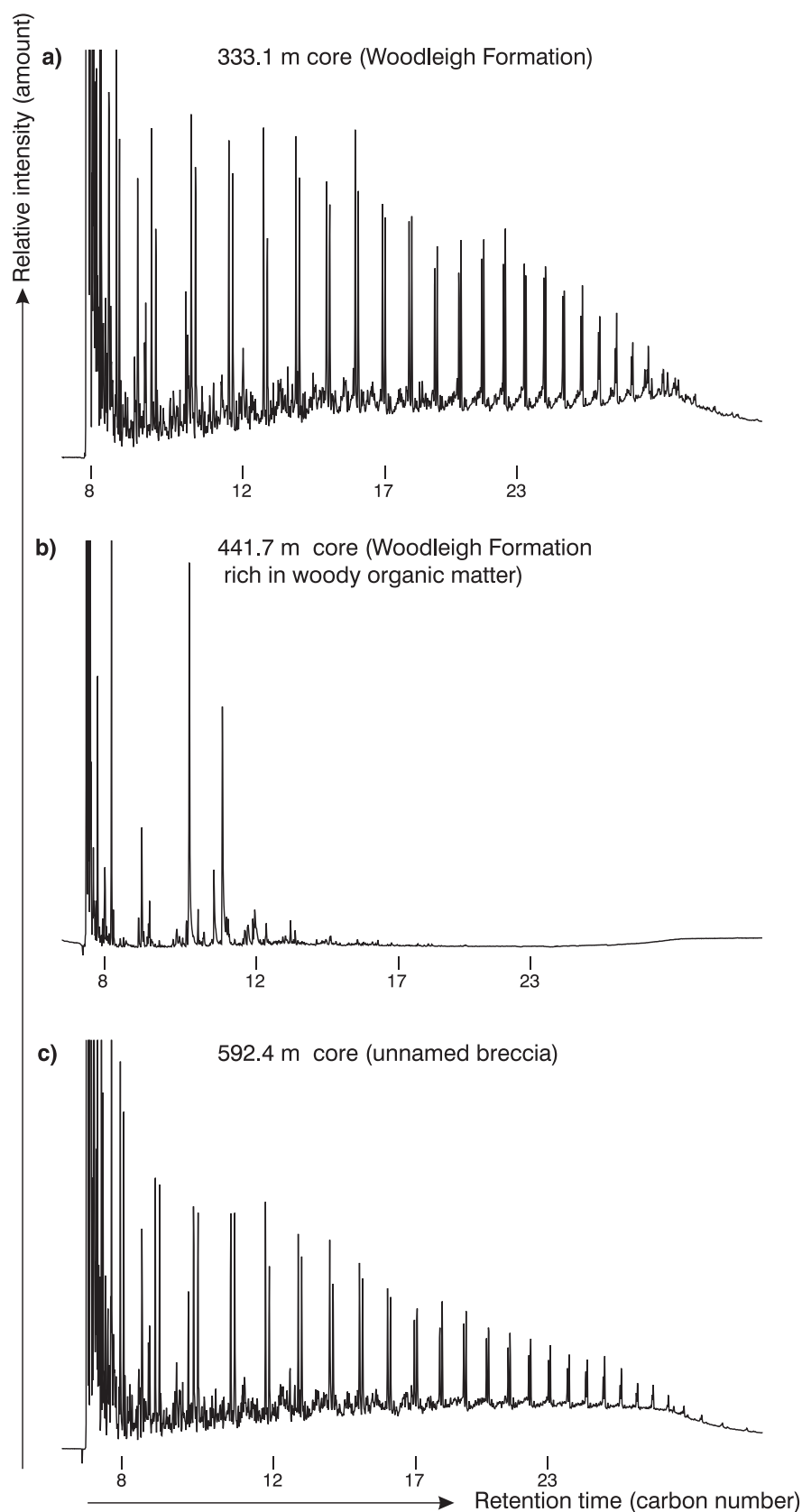
**NOTES:** A: % of resolved compounds in S<sub>2</sub>  
 B: mg/g rock (Rock-Eval)  
 C: (mg/g rock)/TOC  
 S<sub>2</sub>: pyrolytic yield  
 TOC: total organic carbon

Table 10.6. Selected parameters from pyrolysis-gas chromatography of core samples from Woodleigh 2A

Depth (m)	Parameter	Value			
		A	B	C	D
333.05	C <sub>1</sub> -C <sub>4</sub> abundance (all compounds)	23.93	8.93	1.20	—
	C <sub>5</sub> -C <sub>8</sub> abundance (all resolved compounds)	31.08	11.60	1.56	—
	C <sub>5</sub> -C <sub>8</sub> abundance (alkanes + alkenes)	16.88	6.30	0.85	—
	C <sub>9</sub> -C <sub>14</sub> abundance (all resolved compounds)	26.42	9.86	1.32	—
	C <sub>9</sub> -C <sub>14</sub> abundance (alkanes + alkenes)	11.05	4.13	0.55	—
	C <sub>15</sub> -C <sub>31</sub> abundance (all resolved compounds)	18.57	6.93	0.93	—
	C <sub>15</sub> -C <sub>31</sub> abundance (alkanes + alkenes)	13.67	5.10	0.68	—
	C <sub>9</sub> -C <sub>31</sub> abundance (all resolved compounds)	44.99	16.79	2.25	—
	C <sub>9</sub> -C <sub>31</sub> abundance (alkanes + alkenes)	24.72	9.23	1.24	—
	C <sub>5</sub> -C <sub>31</sub> abundance (all resolved compounds)	76.07	28.40	3.81	—
	C <sub>5</sub> -C <sub>31</sub> abundance (alkanes + alkenes)	41.60	15.53	2.08	—
	C <sub>5</sub> -C <sub>31</sub> alkane abundance	20.07	7.49	1.01	—
	C <sub>5</sub> -C <sub>31</sub> alkene abundance	21.53	8.04	1.08	—
	C <sub>5</sub> -C <sub>8</sub> alkane/alkene	—	—	—	0.86
	C <sub>9</sub> -C <sub>14</sub> alkane/alkene	—	—	—	0.81
	C <sub>15</sub> -C <sub>31</sub> alkane/alkene	—	—	—	1.15
	C <sub>5</sub> -C <sub>31</sub> alkane/alkene	—	—	—	0.93
	(C <sub>1</sub> -C <sub>5</sub> )/C <sub>6+</sub>	—	—	—	0.50
	R	—	—	—	0.85
441.7a	C <sub>1</sub> -C <sub>4</sub> abundance (all compounds)	50.29	5.27	0.15	—
	C <sub>5</sub> -C <sub>8</sub> abundance (all resolved compounds)	21.66	2.27	0.06	—
	C <sub>5</sub> -C <sub>8</sub> abundance (alkanes + alkenes)	0.00	0.00	0.00	—
	C <sub>9</sub> -C <sub>14</sub> abundance (all resolved compounds)	27.42	2.87	0.08	—
	C <sub>9</sub> -C <sub>14</sub> abundance (alkanes + alkenes)	0.00	0.00	0.00	—
	C <sub>15</sub> -C <sub>31</sub> abundance (all resolved compounds)	0.63	0.07	0.00	—
	C <sub>15</sub> -C <sub>31</sub> abundance (alkanes + alkenes)	0.00	0.00	0.00	—
	C <sub>9</sub> -C <sub>31</sub> abundance (all resolved compounds)	28.05	2.94	0.08	—
	C <sub>9</sub> -C <sub>31</sub> abundance (alkanes + alkenes)	0.00	0.00	0.00	—
	C <sub>5</sub> -C <sub>31</sub> abundance (all resolved compounds)	49.71	5.21	0.15	—
	C <sub>5</sub> -C <sub>31</sub> abundance (alkanes + alkenes)	0.00	0.00	0.00	—
	C <sub>5</sub> -C <sub>31</sub> alkane abundance	0.00	0.00	0.00	—
	C <sub>5</sub> -C <sub>31</sub> alkene abundance	0.00	0.00	0.00	—
	C <sub>5</sub> -C <sub>8</sub> alkane/alkene	—	—	—	—
	C <sub>9</sub> -C <sub>14</sub> alkane/alkene	—	—	—	—
	C <sub>15</sub> -C <sub>31</sub> alkane/alkene	—	—	—	—
	C <sub>5</sub> -C <sub>31</sub> alkane/alkene	—	—	—	—
	(C <sub>1</sub> -C <sub>5</sub> )/C <sub>6+</sub>	—	—	—	1.30
	R	—	—	—	—
592.4	C <sub>1</sub> -C <sub>4</sub> abundance (all compounds)	32.05	2.63	1.18	—
	C <sub>5</sub> -C <sub>8</sub> abundance (all resolved compounds)	35.57	2.92	1.31	—
	C <sub>5</sub> -C <sub>8</sub> abundance (alkanes + alkenes)	12.02	0.99	0.44	—
	C <sub>9</sub> -C <sub>14</sub> abundance (all resolved compounds)	22.46	1.85	0.82	—
	C <sub>9</sub> -C <sub>14</sub> abundance (alkanes + alkenes)	6.85	0.56	0.25	—
	C <sub>15</sub> -C <sub>31</sub> abundance (all resolved compounds)	9.92	0.82	0.36	—
	C <sub>15</sub> -C <sub>31</sub> abundance (alkanes + alkenes)	5.82	0.48	0.21	—
	C <sub>9</sub> -C <sub>31</sub> abundance (all resolved compounds)	32.38	2.66	1.19	—
	C <sub>9</sub> -C <sub>31</sub> abundance (alkanes + alkenes)	12.67	1.04	0.46	—
	C <sub>5</sub> -C <sub>31</sub> abundance (all resolved compounds)	67.95	5.59	2.49	—
	C <sub>5</sub> -C <sub>31</sub> abundance (alkanes + alkenes)	24.69	2.03	0.91	—
	C <sub>5</sub> -C <sub>31</sub> alkane abundance	11.93	0.98	0.44	—
	C <sub>5</sub> -C <sub>31</sub> alkene abundance	12.76	1.05	0.47	—
	C <sub>5</sub> -C <sub>8</sub> alkane/alkene	—	—	—	0.86
	C <sub>9</sub> -C <sub>14</sub> alkane/alkene	—	—	—	0.83
	C <sub>15</sub> -C <sub>31</sub> alkane/alkene	—	—	—	1.28
	C <sub>5</sub> -C <sub>31</sub> alkane/alkene	—	—	—	0.93
	(C <sub>1</sub> -C <sub>5</sub> )/C <sub>6+</sub>	—	—	—	0.64
	R	—	—	—	0.76

NOTES: A: % of resolved compounds in S<sub>2</sub>  
 B: mg/g rock (Rock-Eval)  
 C: (mg/g rock)/TOC  
 D: no units

R: m- + p-xylene/n-octene  
 S<sub>2</sub>: pyrolytic yield  
 TOC: total organic carbon

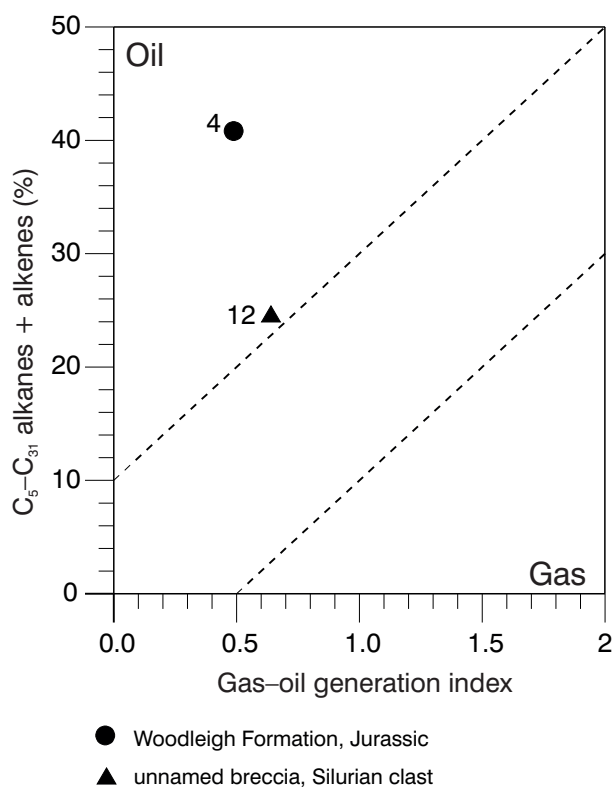


AJM338

01.05.01

**Figure 10.4.** Gas chromatograms from pyrolysis-gas chromatography of three organic-rich samples from Woodleigh 2 and 2A: a,b) Jurassic Woodleigh Formation; c) unnamed breccia





AJM339

30.05.01

**Figure 10.5. Kerogen typing by pyrolysis-gas chromatography of organic-rich samples from Woodleigh 2A. See Table 10.2 to relate sample number to sample depth**

**Table 10.7. Extract concentrations from extraction and liquid chromatography of core samples from Woodleigh 2A**

Depth (m)	Rock extracted (g)	Total extract (ppm)	Loss on column (ppm)	Hydrocarbons			Non-hydrocarbons		Total (ppm)
				Saturates (ppm)	Aromatics (ppm)	Total (ppm)	NSOs (ppm)	Asphaltene (ppm)	
333.1	6.9	1316.9	—	—	—	—	—	—	—
592.4	19.2	1056.2	114.5	156.1	260.1	416.2	525.5	—	525.5

**NOTES:** ppm: parts per million  
NSOs: nitrogen, sulfur, and oxygen compounds

**Table 10.8. Extract composition from extraction and liquid chromatography of core samples from Woodleigh 2A**

Depth (m)	Hydrocarbons			Nonhydrocarbons NSOs (%)	Saturates/ Aromatics (ratio)	Hydrocarbons/ Non-hydrocarbons (ratio)
	Saturates (%)	Aromatics (%)	Total (%)			
333.1	—	—	—	—	—	—
592.4	16.6	27.6	44.2	55.8	0.6	0.8

**NOTE:** NSOs: nitrogen, sulfur, and oxygen compounds

**Table 10.9.** Alkane composition from saturate gas chromatography and mass spectrometry of core samples from Woodleigh 2A

Depth (m)	Pristane/ phytane	Pristane/ n-C <sub>17</sub>	Phytane/ n-C <sub>18</sub>	CPI (1)	CPI (2)	(C <sub>21</sub> +C <sub>22</sub> )/ (C <sub>28</sub> +C <sub>29</sub> )
333.1	0.17	0.50	4.03	5.62	7.14	2.03
592.4	0.87	0.32	0.36	1.03	1.02	0.68

NOTES: CPI: carbon preference index

$$CPI(1) = \frac{(C_{23} + C_{25} + C_{27} + C_{29}) \text{ wt}\% + (C_{25} + C_{27} + C_{29} + C_{31}) \text{ wt}\%}{2 \times (C_{23} + C_{25} + C_{27} + C_{29}) \text{ wt}\%}$$

$$CPI(2) = \frac{(C_{21} + C_{23} + C_{25}) \text{ wt}\% + (C_{23} + C_{25} + C_{27}) \text{ wt}\%}{2 \times (C_{21} + C_{23} + C_{25}) \text{ wt}\%}$$

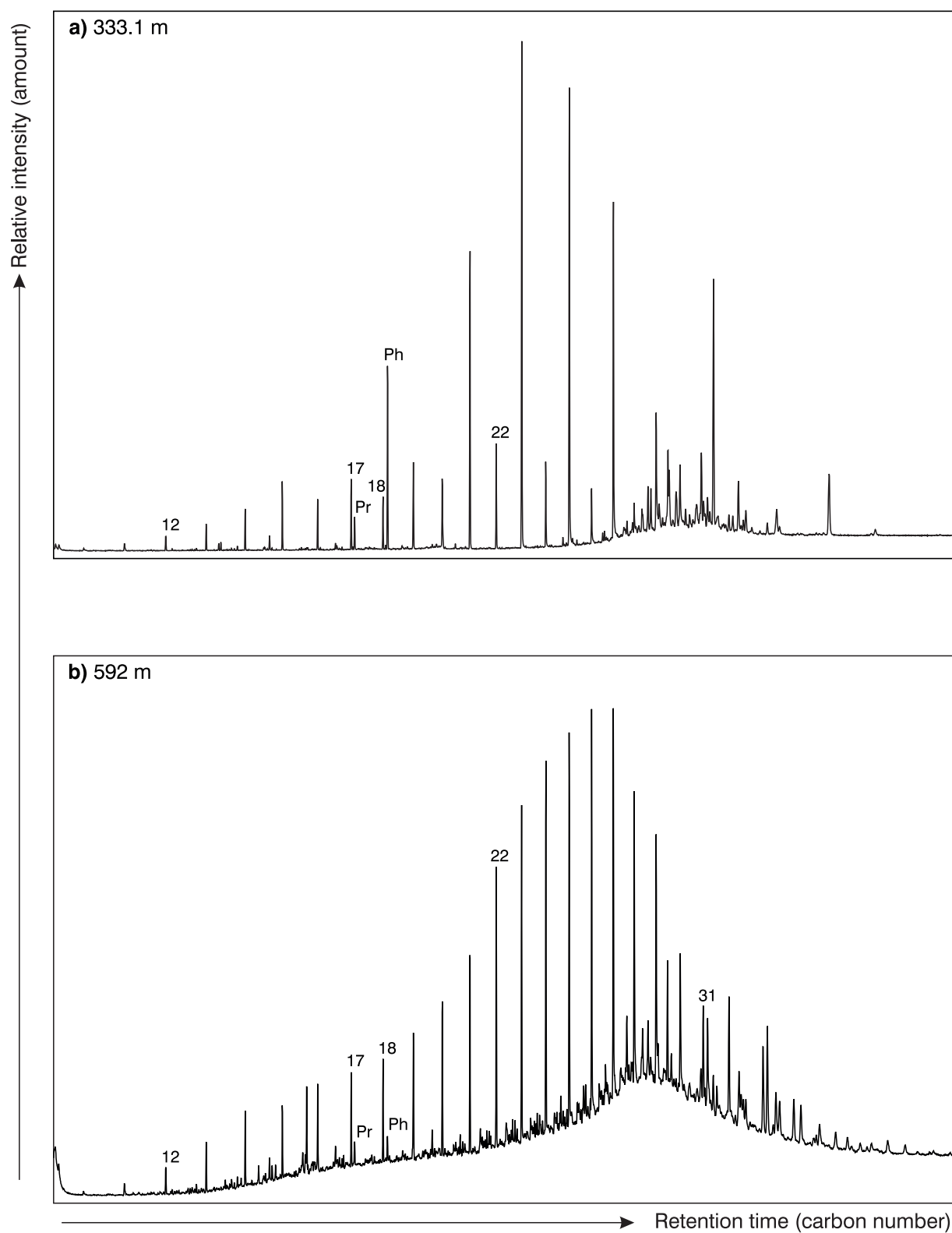
**Table 10.10.** Normal alkane distributions from saturate gas chromatography and mass spectrometry of core samples from Woodleigh 2A

Depth (m)	n-C <sub>12</sub>	n-C <sub>13</sub>	n-C <sub>14</sub>	n-C <sub>15</sub>	n-C <sub>16</sub>	n-C <sub>17</sub>	n-C <sub>18</sub>	n-C <sub>19</sub>	n-C <sub>20</sub>	n-C <sub>21</sub>	n-C <sub>22</sub>	n-C <sub>23</sub>	n-C <sub>24</sub>	n-C <sub>25</sub>	n-C <sub>26</sub>	n-C <sub>27</sub>	n-C <sub>28</sub>	n-C <sub>29</sub>	n-C <sub>30</sub>	n-C <sub>31</sub>
333.1	0.6	0.9	1.3	2.1	1.6	2.2	1.1	1.6	2.5	10.2	3.3	18.7	2.9	17.4	2.0	12.3	1.0	5.7	2.2	1.1
592.4	0.8	1.2	1.7	1.7	1.9	2.1	0.7	2.2	3.7	4.7	6.0	7.8	8.9	9.9	9.6	10.0	8.5	7.3	4.6	2.7

NOTE: n: normal

**Table 10.11. Basic analytical data of branched and cyclic saturated hydrocarbons from gas chromatography and mass spectrometry of core sample from 592.4 m in Woodleigh 2A**

<i>Compound</i>	<i>Ion</i>	<i>Value</i>	<i>Compound</i>	<i>Ion</i>	<i>Value</i>
Rearranged drimane (R1)	123	21951	C <sub>28</sub> S diasterane	259	12472
Eudesmane	123	0	C <sub>28</sub> R diasterane	259	10985
Rearranged drimane (R2)	123	13331	C <sub>29</sub> S diasterane	259	30027
Drimane	123	60245	C <sub>29</sub> R diasterane	259	21258
Homodrimane	123	360709	C <sub>27</sub> R isosterane	218	9634
C <sub>18</sub> 19-nor labdane	109	0	C <sub>27</sub> S isosterane	218	9074
C <sub>19</sub> 19-nor labdane	109	0	C <sub>28</sub> R isosterane	218	10466
C <sub>19</sub> 19-nor isopimarane	123	0	C <sub>28</sub> S isosterane	218	5943
Rimuane	123	0	C <sub>29</sub> R isosterane	218	23083
17-nor tetracyclane	123	0	C <sub>29</sub> S isosterane	218	22618
Beyerane	123	0	Ts	191	127734
Iso pimarane	123	0	Unknown U1	191	0
Phyllo cladane	123	0	Tm	191	542133
Kaurane	123	0	C <sub>27</sub> 17B(H)-tris norhopane	191	44317
C <sub>19</sub> tricyclic terpane	191	42883	C <sub>28</sub> 25,30-bis norhopane	191	0
C <sub>20</sub> tricyclic terpane	191	35093	C <sub>28</sub> 29,30-bis norhopane	191	0
C <sub>21</sub> tricyclic terpane	191	16031	C <sub>29</sub> diahopane	191	33617
C <sub>22</sub> tricyclic terpane	191	25735	C <sub>28</sub> 28,30-bis norhopane	191	0
C <sub>23</sub> tricyclic terpane	191	18246	C <sub>29</sub> 25-norhopane	191	0
C <sub>24</sub> tricyclic terpane	191	24089	C <sub>29</sub> Hopane	191	525922
C <sub>25</sub> tricyclic terpane R+S	191	8843	C <sub>29</sub> Ts	191	87594
C <sub>24</sub> tetracyclic terpane	191	88274	C <sub>30</sub> diahopane	191	66014
C <sub>26</sub> S tricyclic terpane	191	2077	C <sub>29</sub> moretane	191	139397
C <sub>26</sub> R tricyclic terpane	191	1962	Oleanane	191	0
C <sub>26</sub> tetracyclic terpane	191	62277	C <sub>30</sub> hopane	191	896298
C <sub>28</sub> S tricyclic terpane	191	0	C <sub>30</sub> 30-norhopane	191	0
C <sub>28</sub> R tricyclic terpane	191	0	C <sub>29</sub> BB hopane	191	50236
C <sub>29</sub> S tricyclic terpane	191	0	C <sub>30</sub> moretane	191	265109
C <sub>29</sub> R tricyclic terpane	191	0	Taraxastane	191	0
C <sub>21</sub> sterane (pregnane)	217	6117	C <sub>31</sub> S hopane	191	600823
C <sub>22</sub> sterane (homopregnane)	217	2148	C <sub>31</sub> R hopane	191	708686
C <sub>27</sub> S diasterane	217	28562	Gammacerane	191	0
C <sub>27</sub> R diasterane	217	14940	C <sub>30</sub> BB hopane	191	131220
C <sub>28</sub> S diasterane	217	13052	C <sub>31</sub> (S+R) moretane	191	234243
C <sub>28</sub> R diasterane	217	15363	C <sub>32</sub> S hopane	191	368543
C <sub>27</sub> S normal sterane	217	22026	C <sub>32</sub> R hopane	191	351904
C <sub>29</sub> S diasterane	217	53400	C <sub>32</sub> S moretane	191	45854
C <sub>27</sub> R isosterane	217	5658	C <sub>32</sub> R moretane	191	73015
C <sub>27</sub> S isosterane	217	9801	C <sub>31</sub> (S+R) BB hopane	191	0
C <sub>27</sub> R normal sterane	217	33630	C <sub>33</sub> S hopane	191	180922
C <sub>29</sub> R diasterane	217	34027	C <sub>33</sub> R hopane	191	158625
CD3-cholestane IS	234	28370	C <sub>32</sub> (S+R) BB hopane	191	0
C <sub>28</sub> S normal sterane	217	4468	C <sub>34</sub> S hopane	191	174200
C <sub>28</sub> R isosterane	217	0	C <sub>34</sub> R hopane	191	137015
C <sub>28</sub> S isosterane	217	0	C <sub>35</sub> S hopane	191	49663
C <sub>28</sub> R normal sterane	217	18987	C <sub>35</sub> R hopane	191	44602
C <sub>29</sub> S normal sterane	217	35268	bicadinane W	369	0
C <sub>29</sub> R isosterane	217	19030	bicadinane T	369	0
C <sub>29</sub> S isosterane	217	20419	bicadinane T1	369	0
C <sub>29</sub> R normal sterane	217	56842	bicadinane R	369	0
C <sub>30</sub> S normal sterane	217	0	C <sub>28</sub> 25,30-bisnorhopane	177	0
C <sub>30</sub> R isosterane	217	0	C <sub>29</sub> 25-norhopane	177	0
C <sub>30</sub> S isosterane	217	0	C <sub>29</sub> hopane	177	203731
C <sub>30</sub> R normal sterane	217	0	C <sub>31</sub> 2-Me hopane	205	30499
C <sub>30</sub> S 4a methylsterane	231	0	C <sub>32</sub> S 2-methylhopane	205	37780
C <sub>30</sub> R+S 4a BB methylsterane	231	0	C <sub>32</sub> R 2-methylhopane	205	50478
C <sub>30</sub> R 4a methylsterane + dino	231	0	C <sub>31</sub> S hopane	205	211836
C <sub>27</sub> S diasterane	259	16556	C <sub>31</sub> R hopane	205	260422
C <sub>27</sub> R diasterane	259	10569	C <sub>31</sub> 3-methylhopane	205	79273



AJM340

01.05.01

**Figure 10.6.** Gas chromatograms of core samples from Woodleigh 2A: a) Jurassic Woodleigh Formation; b) clasts of Silurian Coburn Formation from unnamed breccia

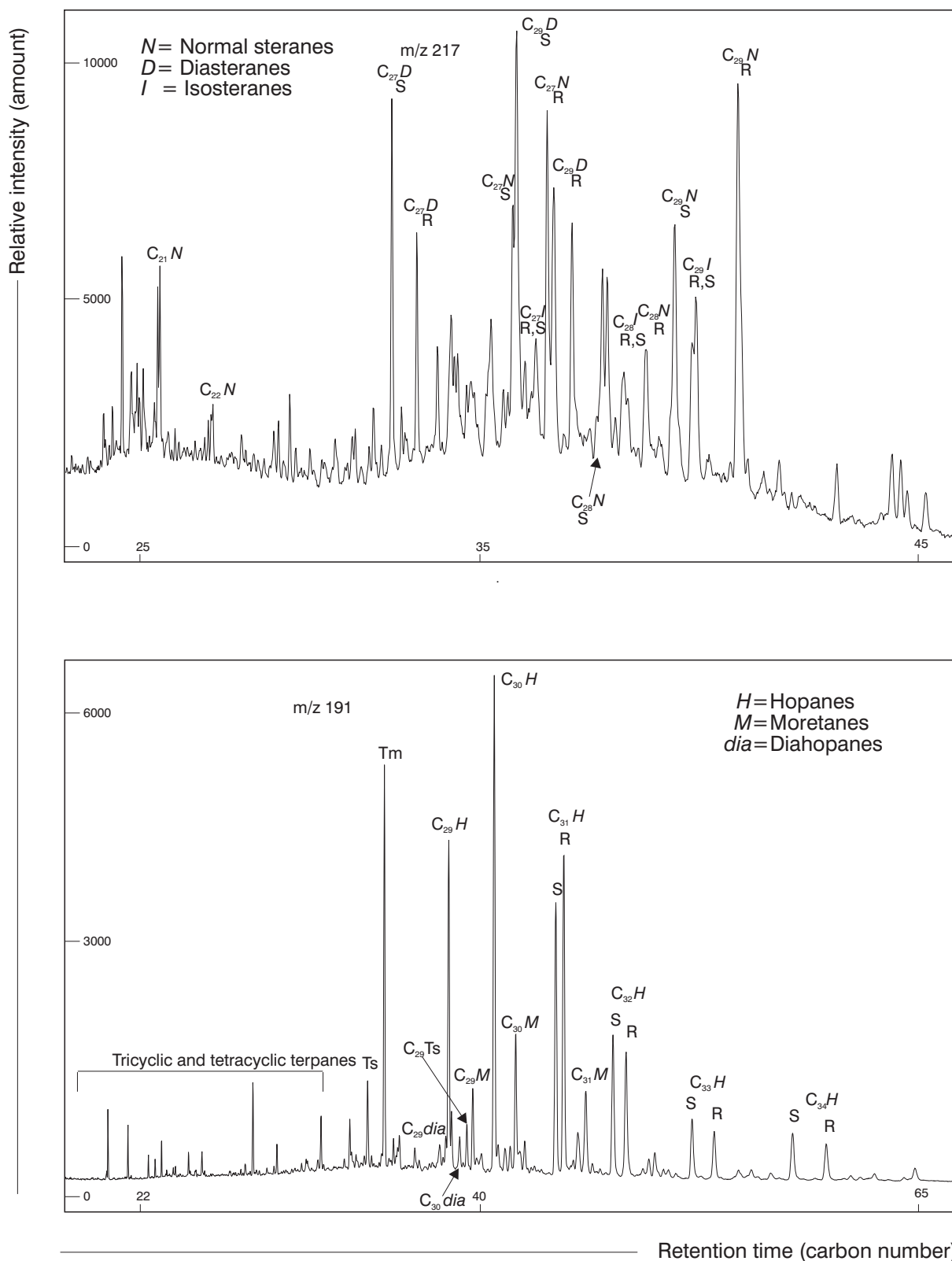
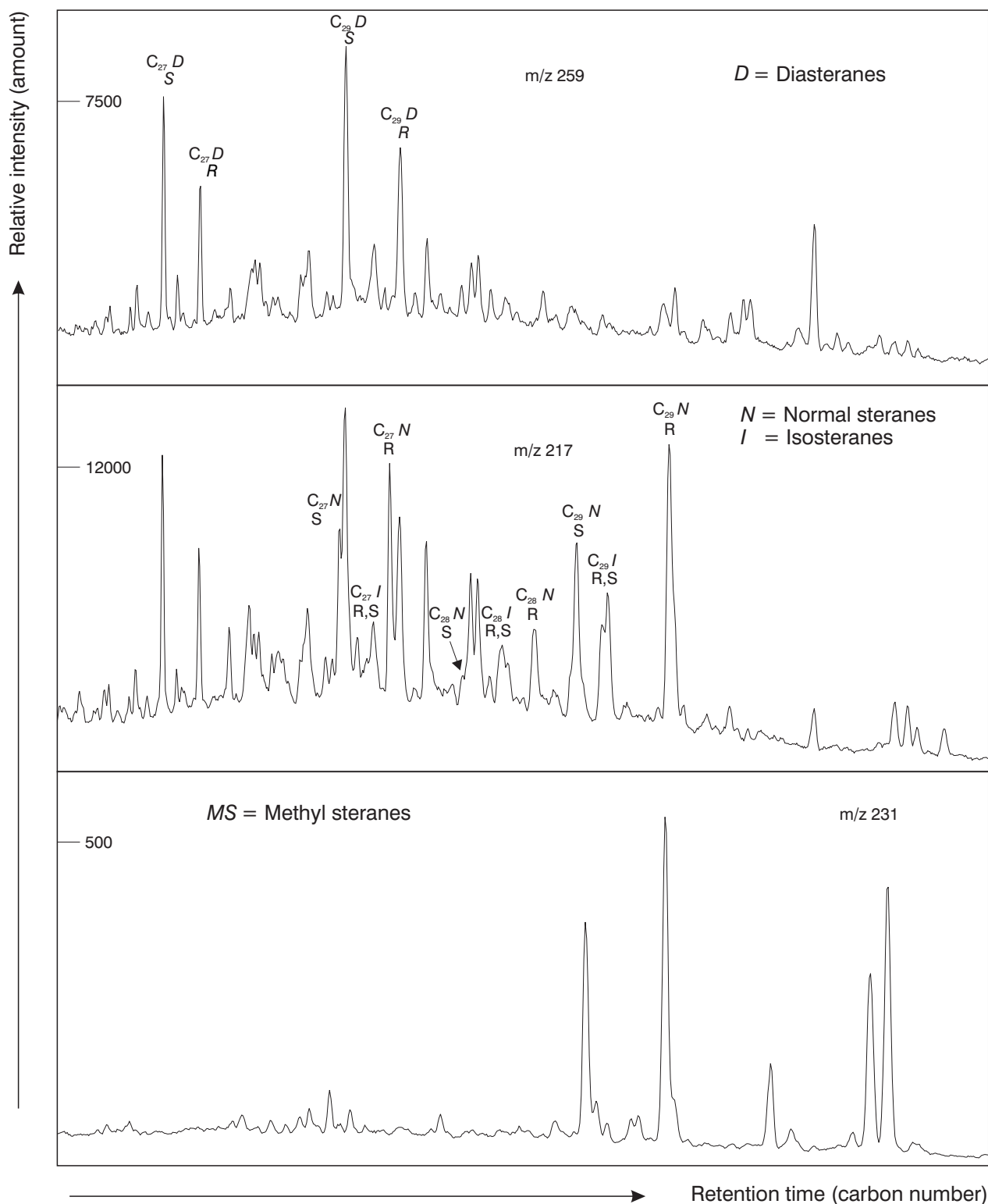


Figure 10.7a. Mass chromatograms of a core sample (592.4 m) from Woodleigh 2A: steranes and hopanes



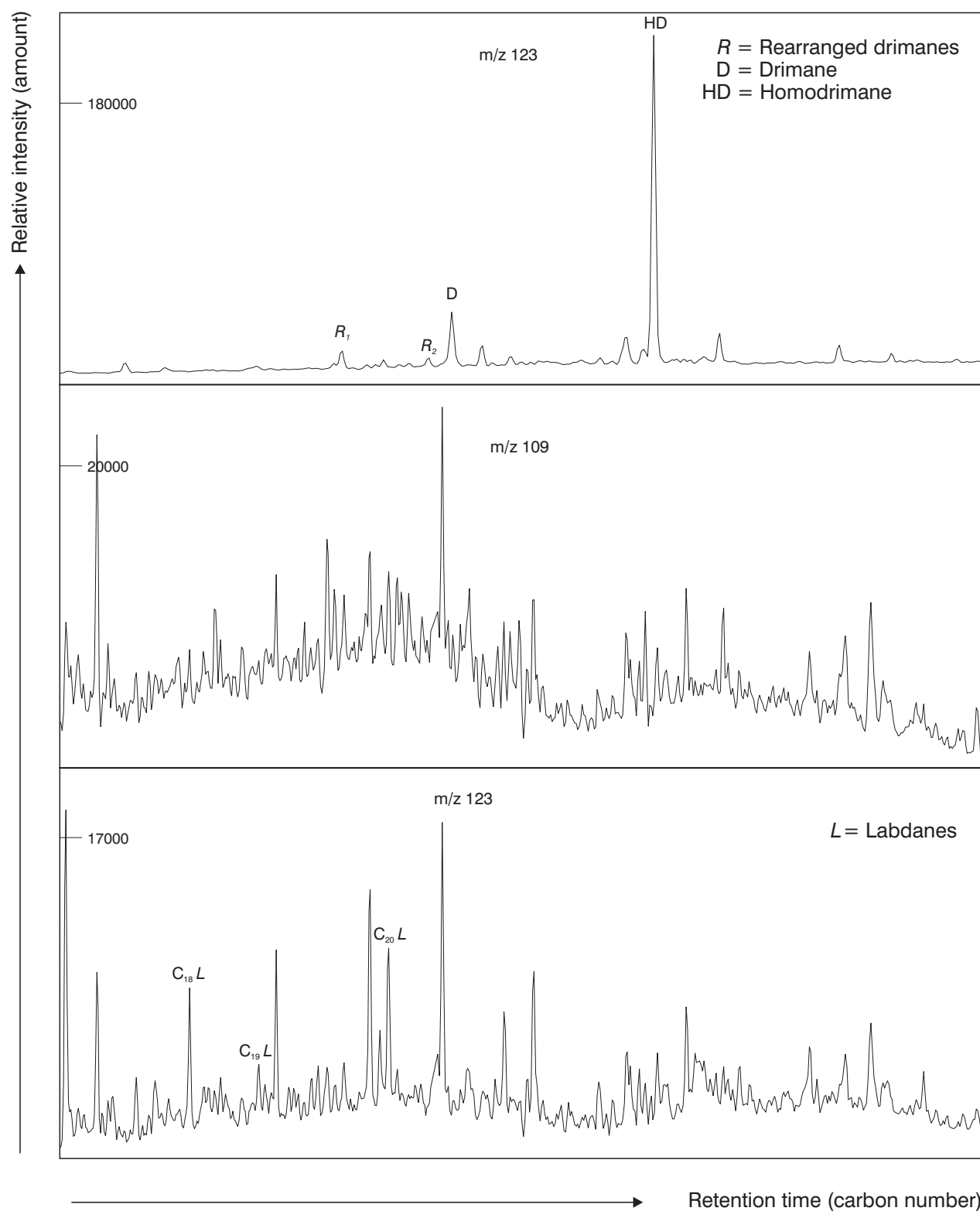




AJM343

25.07.01

Figure 10.7c. Mass chromatograms of a core sample (592.4 m) from Woodleigh 2A: m/z 259, 217, and 231 steranes



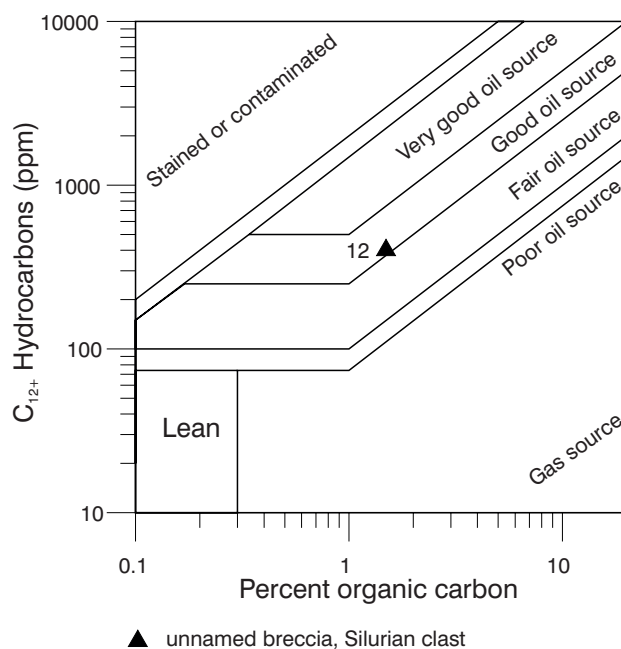
AJM344

25.07.01

**Figure 10.7d. Mass chromatograms of a core sample (592.4 m) from Woodleigh 2A: m/z 123 and 109**

**Table 10.12.** Selected parameters of branched and cyclic saturated hydrocarbons from gas chromatography and mass spectrometry of core sample from 592.4 m in Woodleigh 2A

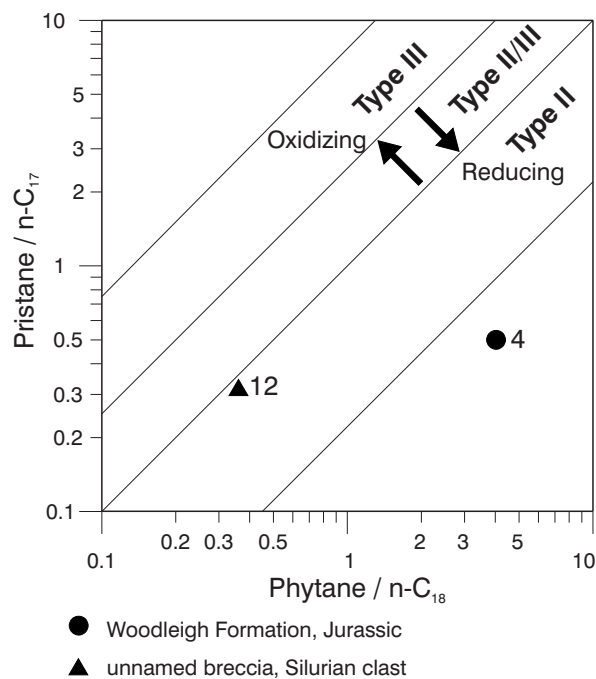
Parameters	Ion(s)	Value
1 — 18 <sub>a</sub> (H)-hopane/17 <sub>a</sub> (H)-hopane (Ts/Tm)	191	0.24
2 — C <sub>30</sub> hopane/C <sub>30</sub> moretane	191	3.38
3 — C <sub>31</sub> 22S hopane/C <sub>31</sub> 22R hopane	191	0.85
4 — C <sub>32</sub> 22S hopane/C <sub>32</sub> 22R hopane	191	1.05
5 — C <sub>29</sub> 20S sterane/C <sub>29</sub> 20R sterane	217	0.62
6 — C <sub>29</sub> steranes (20S / 20S+20R)	217	0.38
7 — C <sub>29</sub> steranes/C <sub>29</sub> steranes + C <sub>29</sub> steranes	217	0.30
8 — C <sub>27</sub> /C <sub>29</sub> diasteranes	259	0.53
9 — C <sub>27</sub> /C <sub>29</sub> steranes	217	0.59
10 — 18 <sub>a</sub> (H)-oleanane/C <sub>30</sub> hopane	191	—
11 — C <sub>29</sub> diasteranes/C <sub>29</sub> $\alpha\alpha\alpha$ steranes + C <sub>29</sub> $\alpha\beta\beta$ steranes	217	0.62
12 — C <sub>30</sub> (hopane + moretane)/C <sub>29</sub> (steranes + diasteranes)	191/217	5.44
13 — C <sub>15</sub> drimane/C <sub>16</sub> homodrimane	123	0.17
14 — Rearranged drimanes/normal drimanes	123	0.08



AJM345

31.05.01

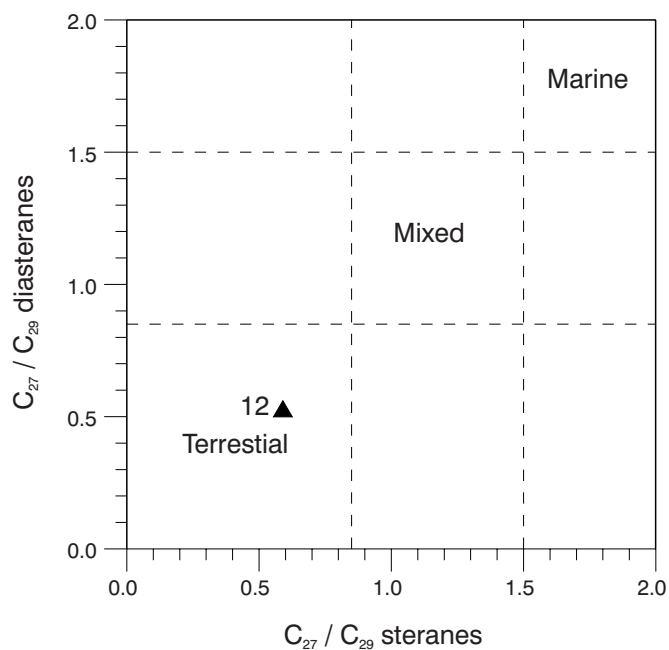
**Figure 10.8.** Source-rock rating as a function of C<sub>12+</sub> hydrocarbon yields versus organic richness for samples from Woodleigh 2A. See Table 10.2 to relate sample number to sample depth



AJM346

31.05.01

**Figure 10.9. Kerogen typing and environment of deposition as a function of the pristane/n-C<sub>17</sub> versus phytane/n-C<sub>18</sub> for samples from Woodleigh 2A. See Table 10.2 to relate sample number to sample depth**



AJM347

01.05.01

**Figure 10.10. Environment of deposition as a function of C<sub>27</sub>/C<sub>29</sub> steranes versus diasteranes of a sample from Woodleigh 2A. See Table 10.2 to relate sample number to sample depth**



## Source-rock maturity

The levels and timing of thermal maturation in Woodleigh 2 and 2A are indicated from organic petrology, Rock-Eval pyrolysis, and AFTA.

**Organic petrology:** The organic petrology of the seven samples analysed is summarized in Table 10.13. Mean vitrinite reflectance (% Ro) values in the Cretaceous Birdrong Sandstone and Jurassic Woodleigh Formation range from 0.24 to 0.45% Ro, indicating these units are immature for oil generation (Table 10.13). Two samples with mean % Ro values of 0.50 and 0.52 from the unnamed breccia indicate that the underlying section is marginally mature (Table 10.13). Figure 10.11 illustrates maturity as percent reflectance histograms for these samples.

**Rock-Eval pyrolysis:**  $T_{\max}$  is a maturation parameter, measured in °C, at which the pyrolytic yield of hydrocarbons (from a rock sample) reaches its maximum. Values in the range 435–470°C commonly characterize the oil generative window.  $T_{\max}$  values between 418 and 428°C for the Cretaceous Birdrong Sandstone and Jurassic Woodleigh Formation imply these units are immature for oil generation. Two clasts of the Coburn Formation within the unnamed breccia yielded values of 431 and 436°C, indicating that the Silurian is marginally mature (Table 10.2). These results are consistent with those from the organic petrology.

**Apatite fission-track analysis (AFTA):** Fission-track annealing in apatite is a function of temperature, time, and the chlorine content of apatite — tracks in chlorapatite are more resistant to annealing than in fluorapatite (Green et al., 1986). The fission-track age is largely a function of fission-track annealing in response to increasing temperature commonly between 70 and 120°C, whereas fission-track length reflects the style of cooling. Therefore, AFTA is useful in understanding the burial history of the host rocks, as it provides data complementary to thermal maturity measurements, such as vitrinite reflectance and  $T_{\max}$ . The basic analytical data for the AFTA of the sample (498.35 – 499.05 m) from Woodleigh 2A is given in Table 10.14, and the interpretation is summarized in Table 10.15. Figures 10.12a to 10.12c show the distribution of chlorine weight percent, fission-track lengths, and fission-track ages respectively. The AFTA data indicate that the sample reached higher temperatures than the present level after deposition. At least one cooling event between 180 and 60 Ma is required by the AFTA results and constraints on the maximum palaeotemperature reached prior to cooling depending on the actual time of cooling. Three possible timing and temperature regimes are suggested, but only one of these regimes is required by the AFTA results (Table 10.15; Figure 10.13). These regimes are between 208 and 180 Ma when the sample may have cooled from 90 to 105°C; between 180 and 120 Ma when the sample may have cooled from 75 to 95°C; or between 120 and 60 Ma when the sample may have cooled from 75 to 90°C (Gibson et al., 2000). The last two timing and temperature regimes encompass two previously recognized regional cooling events: during the Jurassic and Early Cretaceous. A cooling event after 60 Ma is not required by the AFTA data, but is indirectly indicated by vitrinite reflectance data because the inferred temperature from vitrinite reflectance is higher than the present-day temperature, and so requires additional cooling as recognized in Gibson et al. (1988) and Ghori (1999).

**Subsurface temperatures:** The present-day geothermal gradient of the Woodleigh area was determined from bottomhole temperatures (BHTs) recorded during wireline logging of Woodleigh 1 and 2A. Woodleigh 1 is 14 km to the east of 2A and both were logged on the same very hot day. The actual surface temperature is not available, thus an arbitrary value for mean surface temperature of 30°C was assumed in summarizing the present-day subsurface temperatures (Table 10.16). A temperature gradient of 3.5°C was determined from the gradient between the deepest temperatures recorded while logging Woodleigh 1 (34.5°C at 93 m) and 2A (58.3°C at 618.5 m). These temperatures are compared with palaeotemperatures determined from AFTA and vitrinite reflectance in Figure 10.14, which shows that only three of the eight palaeotemperatures inferred from the vitrinite reflectance data are close to those from AFTA.

**Thermal conductivity:** Thermal conductivity measurements on 17 core samples from Woodleigh 2A were undertaken in the Earth Science Department of Monash University by Graeme Beardsmore; the analytical results provided are listed in Table 10.17. Of the 17 samples, nine were from the Woodleigh Formation, five from the unnamed paraconglomerate, one from the unnamed breccia, and two from the Coburn Formation.

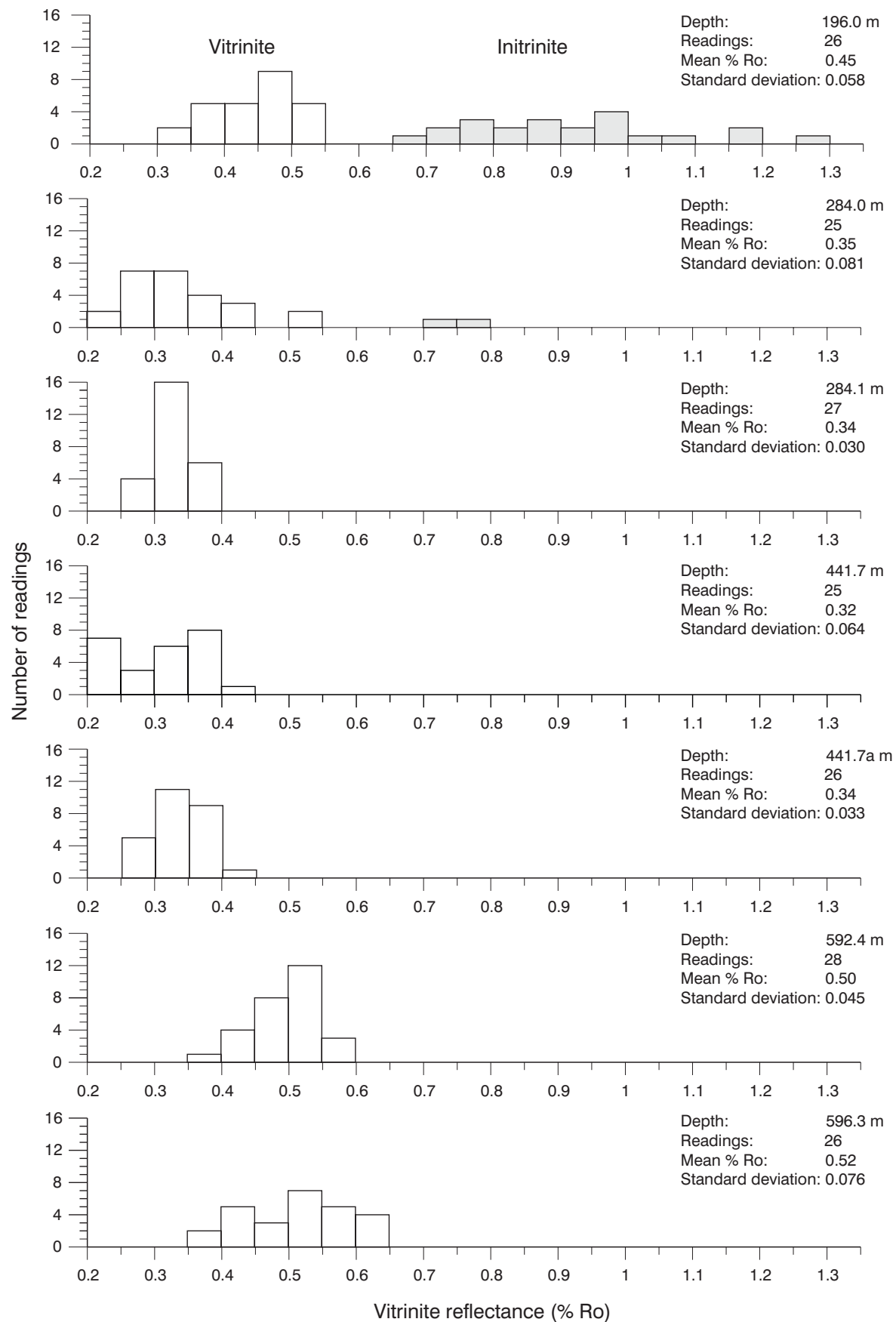
Table 10.13. Organic petrologic data for samples from Woodleigh 2 and 2A

Depth (m)	VR mean (%Ro)	VR min (%Ro)	VR max (%Ro)	No. of readings	Comments
196	0.45 (V) 0.92 (I)	0.33 0.68	0.54 1.26	26 22	Rare liptodetrinite, rare sporinite, orange to dull orange, rare resinite orange. (Siltstone highly argillaceous. DOM abundant, I>V>L. Inertinite abundant, vitrinite and liptinite sparse. Some telovitrinite is present. Mineral fluorescence pervasive, very weak dull orange to absent, anomalously low, possibly due to incipient weathering. Iron oxides sparse. Pyrite rare)
284	0.35 (V) 0.76 (I)	0.245 0.74	0.55 0.78	25 2	Abundant lamalginite, initially non-fluorescing but developing dull-orange fluorescence on prolonged irradiation, common sporinite, orange to dull orange, sparse resinite, orange to non-fluorescing. (Claystone. DOM abundant, I<V<L. Liptinite and inertinite common, vitrinite sparse. Lamalginite appears to be diffuse humic matter until irradiated for about 5 minutes. Although not apparent on initial examination, a possible bitumen phase associated with larger pyrite framboids commenced to fluoresce on prolonged irradiation. The sporinite show moderate positive alteration. Mineral fluorescence pervasive, very weak dull orange, anomalously low, high pyrite content may be the cause for some grains, but even where pyrite is less abundant, mineral fluorescence is very weak. Pyrite major)
284.1	0.34	0.26	0.40	27	Common resinite, bright orange, sparse suberinite, dull orange to dull brown. (Coal. Coal 100% but may represent a single large log rather than a true bed of peat. Telovitrinite with some resinite and suberinite. Some of the resinite appears to have mobilized during setting of the mounting resin so that it resembles fluid hydrocarbons. Telovitrinite having some open cell lumens, texto-ulminite tending to ulminite. Pyrite sparse)
441.7	0.32	0.21	0.45	25	Abundant lamalginite, yellow to yellowish orange, sparse sporinite, yellowish orange, rare indeterminate origin telalginite, bright yellow. (Claystone. DOM abundant, L>>V, I absent. Liptinite abundant, vitrinite sparse, and inertinite absent. Host grains can be considered as lacostic shale, but lamalginite ranges from major to common. In parallel section, the lamalginite shows dull-orange fluorescence probably due to overlying minerals, and can be seen to be derived largely from small tests mostly less than 0.01 mm in diameter, very little can be distinguished of the morphology of the phytoplankton. Mineral fluorescence pervasive moderate orange. Pyrite abundant)
441.7a	0.24	0.26	0.41	26	Sparse resinite, bright orange. (Coal. Coal and pyritized coal 100% but may represent a single large log rather than a bed of peat, most of the tissues are xylem. Pyrite ranges from a minor component to dominant within some fragments. Telovitrinite having same open cell lumens, texto-ulminite tending to ulminite. Pyrite major)
592.4	0.50	0.40	0.58	28	Sparse telalginite, bright yellow to dull orange, sparse lamalginite, yellow to yellowish orange. (Claystone, silty. DOM common, L>V, I absent. Liptinite common, vitrinite sparse and inertinite absent. The material referred to vitrinite could be derived from graptolite tests — see comments below. Only one population could be distinguished, which could represent graptolites rather than chitinozoans on the basis of the length and thickness in some instances. The telalginite is derived from tasmanitids, these are relatively small, and the walls are generally relatively thin. Mineral fluorescence is weakly patchy, moderate orange but with local weak-orange areas. Pyrite abundant)
596.3	0.52	0.38	0.64	26	Rare lamalginite as isolated, bright-yellow tests and weak, yellowish-orange to dull-orange lamellae, rare possible resinite, dull orange. (Claystone, silty calcareous. DOM rare to sparse, V>L. Vitrinite and liptinite rare, the vitrinite is concentrated on the margins of the grains but appears to be part of the sample and not a contaminant. The morphology of some of the larger phytoclasts is more consistent with a higher plant origin than from graptolites or chitinozoans. One occurrence contains a possible resin body. This would be more consistent with a Devonian rather than Silurian age, which could explain the presence of tasmanitids in the sample from 592.4 m. Mineral fluorescence is patchy moderate to bright orange. Pyrite common)

**NOTES:** The Jurassic section is very immature, although the abundance of lamalginite in two of the samples may have resulted in unusually low reflectances. The two deeper samples appear to be distinctly higher in rank, although they are still marginally to early mature. The organic matter assemblage appears more consistent with a Devonian rather than a Silurian age

V: vitrinite  
L: liptinite

I: inertinite  
DOM: dispersed organic matter



AJM348

31.05.01

Figure 10.11. Percent vitrinite reflectance histograms for seven samples from Woodleigh 2 and 2A

Table 10.14. Basic AFTA data for a core sample (298.35 – 499.05 m) from Woodleigh 2A (Gibson et al., 2000)

Depth (m) From	Depth (m) To	Grain	Ns	Ni	Na	RHOs (10 <sup>6</sup> )	RHOi (10 <sup>6</sup> )	Ratio	U (ppm)	Cl (wt%)	Fission-track age (Ma)	+/- (Ma)
498.35	499.05	9	77	95	80	1.5290	1.8870	0.811	18.1	0.08	183.8	28.7
		10	11	26	30	0.5827	1.3770	0.423	13.2	0.00	96.6	34.9
		11	81	69	32	4.0220	3.4260	1.174	32.8	0.00	264.5	44.0
		12	19	21	20	1.5100	1.6690	0.905	16.0	0.25	204.8	65.1
		15	0	1	16	0.0000	0.0993	0.000	1.0	0.00	0.0	0.0
		19	44	36	40	1.7480	1.4300	1.222	13.7	0.31	275.2	62.4
		23	44	39	16	4.3700	3.8730	1.128	37.1	0.45	254.4	56.4
		26	70	45	40	2.7810	1.7880	1.556	17.1	0.19	348.2	67.3
		28	26	24	40	1.0330	0.9534	1.083	9.1	0.37	244.5	69.6
		34	6	5	30	0.3178	0.2648	1.200	2.5	0.06	270.3	163.9
		35	31	43	30	1.6420	2.2780	0.721	21.8	0.02	163.7	38.9
		36	24	46	30	1.2710	2.4370	0.522	23.4	0.00	118.9	30.1
		37	28	24	30	1.4830	1.2710	1.167	12.2	0.00	262.9	73.5
		38	19	15	12	2.5160	1.9860	1.267	19.0	0.05	285.0	98.8
		39	43	38	40	1.7080	1.5100	1.132	14.5	0.24	255.2	57.3
		44	10	8	50	0.3178	0.2542	1.250	2.4	0.09	281.3	133.7
		45	80	75	20	6.3560	5.9590	1.067	57.1	0.02	240.8	39.9
		47	8	11	20	0.6350	0.8740	0.727	8.4	0.23	165.2	76.9
		48	3	9	40	0.1192	0.3575	0.333	3.4	0.00	76.2	50.9
		49	22	42	20	1.7480	3.3370	0.524	32.0	0.18	119.4	31.6

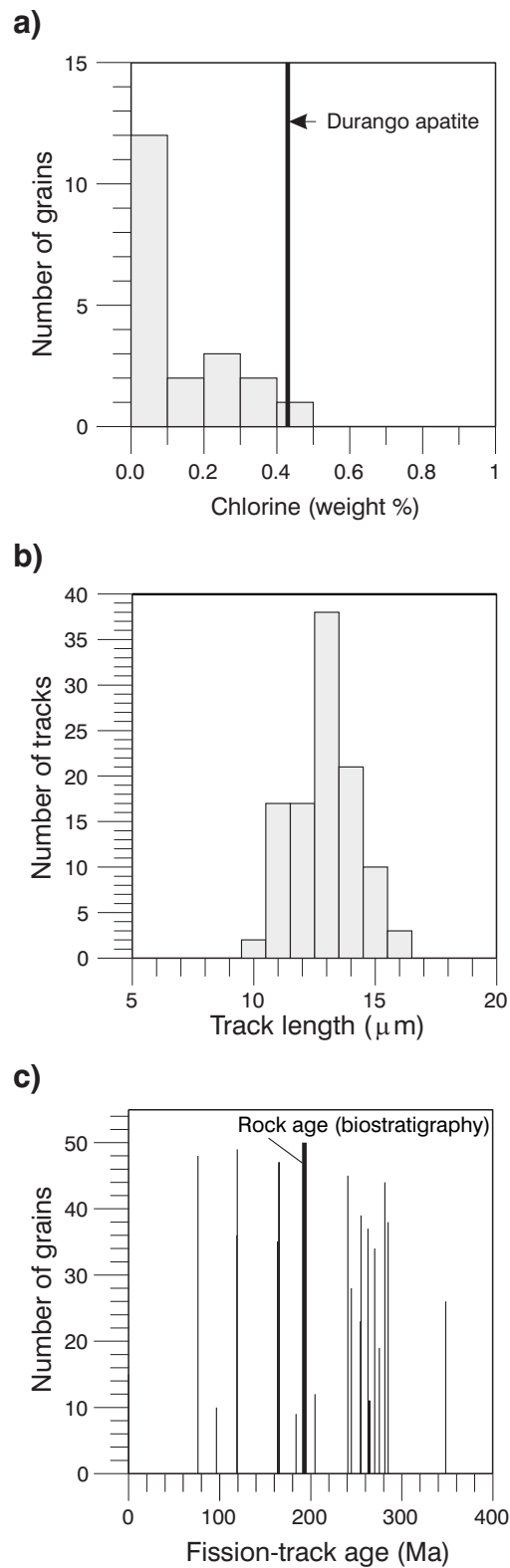
NOTES: Ns: number of spontaneous tracks  
 Ni: number of induced tracks  
 Na: number of grid squares counted in each grain  
 RHOs: spontaneous track density  
 RHOi: spontaneous induced track density

U: uranium  
 Cl: chlorine  
 Ma: million years before present  
 ppm: parts per million  
 wt%: weight percent

Table 10.15. Summary of AFTA of a core sample from Woodleigh 2A (Gibson et al., 2000)

Parameter	Unit	Sample
Depth	m	498.35 – 499.05
Formation		Woodleigh Formation
Stratigraphic age		Early Jurassic
Age	Ma	206–180
Present-day temperature	°C	52
Chi squared (freedom)	$\chi^2$	36.287 (19°)
P(chi squared)	P ( $\chi^2$ )%	1.0
Age dispersion	%	23.292
Number of grains		20
Ns/Ni		0.961 ± 0.053
Mean ratio		0.911 ± 0.087
RHOd (ND)	×10 <sup>6</sup> /cm <sup>2</sup>	1.189 (1858)
RHOs (Ns)	×10 <sup>6</sup> /cm <sup>2</sup>	1.614 (646)
RHOi (Ni)	×10 <sup>6</sup> /cm <sup>2</sup>	1.679 (672)
Uranium content	ppm	16
Pooled age	Ma	217.4 ± 13.6
Central age	Ma	211.3 ± 18.2
Mean track length	µm	12.43 ± 0.13
Standard deviation	µm	1.33
Number of tracks	N	108
Predicted mean track length	µm	13.0
Fission-track age	Ma	211.3 ± 18.2
Predicted fission-track age	Ma	169.4
Maximum palaeotemperature <sup>(a)</sup>	°C	90–105
Onset of cooling <sup>(a)</sup> or	Ma	206–180
Maximum palaeotemperature <sup>(a)</sup>	°C	75–95
Onset of cooling <sup>(a)</sup> or	Ma	180–120
Maximum palaeotemperature <sup>(a)</sup>	°C	75–90
Onset of cooling <sup>(a)</sup>	Ma	120–60
Maximum palaeotemperature <sup>(b)</sup>	°C	75
Onset of cooling <sup>(b)</sup>	Ma	60–0

NOTES: (a) first episode  
 (b) second episode  
 d: density from standard  
 Ma: million years before present  
 Mean ratio: mean of (Ns/Ni) for individual grains  
 ND: total number of tracks counted  
 Ni: number of induced tracks  
 Ns: number of spontaneous tracks  
 P(chi squared): probability of obtaining observed chi squared values  
 RHOd: track density from uranium standard glass  
 RHOi: induced track density  
 RHOs: spontaneous track density  
 SQR: square root

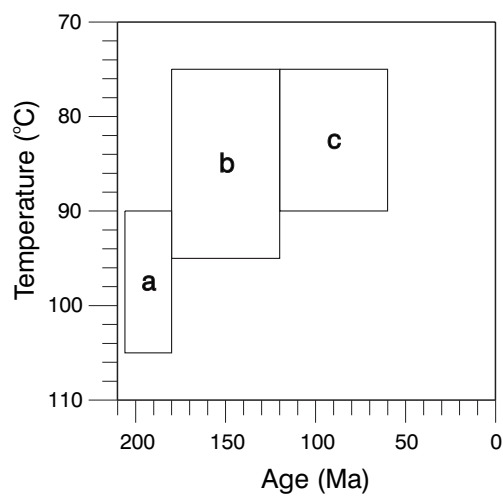


AJM349

01.05.01

**Figure 10.12. Results of AFTA for a core sample (498.35 – 499.05 m) from Woodleigh 2A: a) distribution of chlorine compared to Durango apatite; b) distribution of fission-track length; c) distribution of fission-track age compared to stratigraphic age**

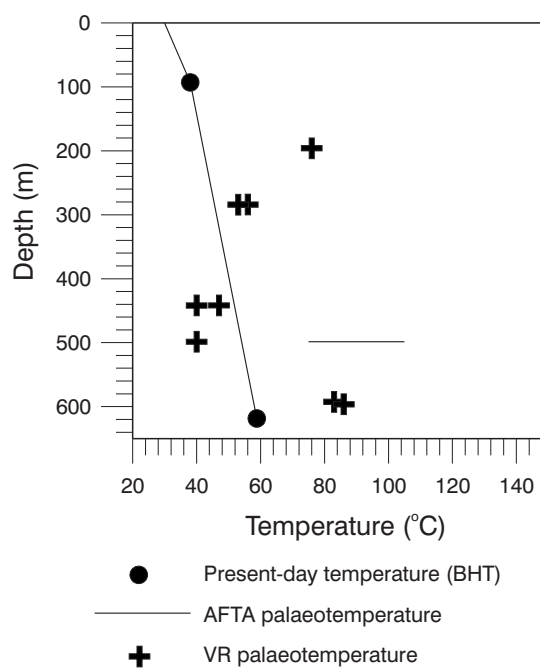




AJM350

01.05.01

**Figure 10.13. Magnitude and timing of a single palaeothermal episode based on AFTA data with three possible timings and temperatures**



AJM351

30.05.01

**Figure 10.14. Comparison of present-day temperature from BHT with palaeotemperatures from AFTA and vitrinite reflectance**

**Table 10.16. Present-day temperature data, Woodleigh 1 and 2A**

<i>Well</i>	<i>Depth (mKB)</i>	<i>Depth (mGL)</i>	<i>Recorded BHT (°C)</i>	<i>Estimated BHT (°C + 10%)</i>	<i>Surface Temperature (°C applied)</i>	<i>Recorded gradient (°C/100 m)</i>	<i>Estimated gradient (°C/100 m)</i>	<i>BHT data source</i>	<i>Date of recording</i>
Woodleigh 1	93.0	93.0	34.5	38.0	30	4.8	8.5	Gamma ray	27/3/99
Woodleigh 2A	618.5	618.5	53	58.3	30	3.7	4.6	Gamma ray	27/3/99

**NOTES:** GL: ground level  
KB: kelly bushing  
BHT: bottomhole temperature

**Table 10.17. Thermal conductivity measurements, Woodleigh 2A**

<i>GSWA number</i>	<i>Depth (m)</i>	<i>Plug length (mm)</i>	<i>Porosity (%)</i>	<i>Matrix density (g/cm<sup>3</sup>)</i>	<i><math>\lambda_{total}</math> (W/mK)</i>	<i><math>\lambda_m</math> sq.rt mean (W/mK)</i>	<i><math>\lambda_m</math> geom. mean (W/mK)</i>	<i>Comments</i>
149180	292.80	25.75	22.9	2.64	1.55	1.91	2.04	Sample destroyed in preparation
149181	317.09	36.65	4.2	2.68	5.58	5.91	6.15	
149182	347.75	—	24.7	—	—	—	—	
149183	387.26	32.30	24.2	2.63	4.06	5.79	7.40	
149184	421.90	31.75	13.5	2.67	4.23	5.08	5.71	
149185	456.94	29.60	22.5	2.68	2.67	3.53	4.06	Held together with epoxy Held together with epoxy Cell method, matrix $\lambda$ only
149186	472.36	36.45	12.6	2.69	3.87	5.57	5.04	
149187	496.05	14.60	21.0	2.65	4.31	5.85	7.22	
149188	500.95	32.50	22.8	2.64	3.72	5.14	6.33	
149189	521.96	24.90	22.5	2.63	2.24	2.91	3.27	
149190	529.93	26.70	19.6	2.63	2.59	3.28	3.68	
149191	544.05	—	19.7	2.63	3.76	7.49	13.14	
149192	563.15	37.6	18.5	2.63	4.16	5.40	6.41	
149193	582.49	36.4	18.1	2.63	4.51	5.85	7.00	
149194	589.00	39.65	24.6	2.83	3.88	5.55	7.07	
149195	608.25	32.40	13.9	2.84	4.52	5.49	6.23	
149196	617.75	35.30	8.0	2.87	5.24	5.86	6.31	

**SOURCE:** Graeme Beardsmore, Monash University

**NOTES:**  $\lambda$ : thermal conductivity  
sq.rt: square root  
geom.: geometric

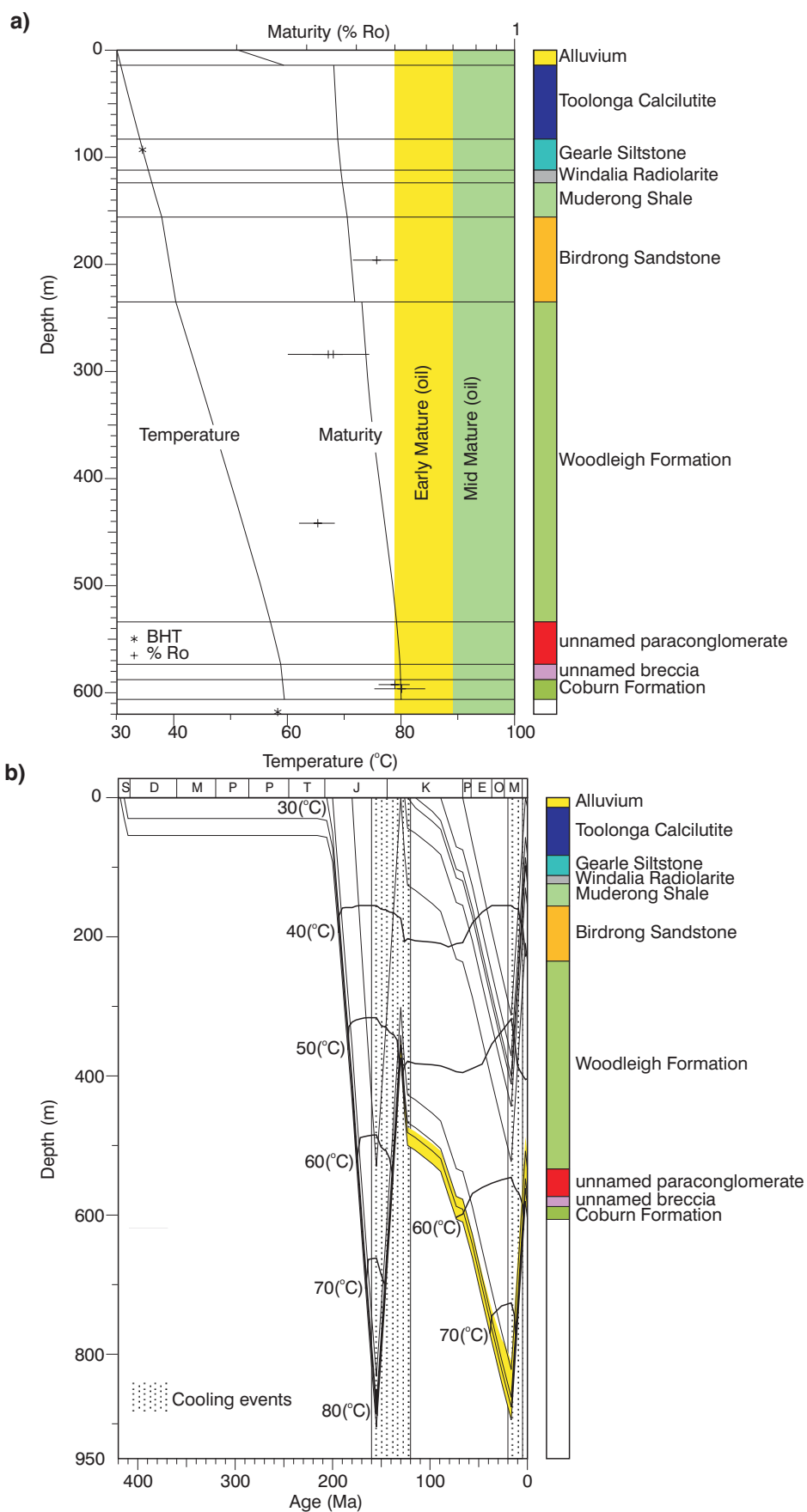


**Figure 10.15. Basin modelling of Woodleigh 2A: a) calibration of maturity model, measured versus calculated temperature and maturity; b) burial and maturation history**

## Basin modelling

The geological, structural, geochemical, temperature, and thermal conductivity data available from the Woodleigh wells and regional geology were integrated to simulate burial and maturation history of the section in Woodleigh 2A, utilizing BasinMod of Platte River Associates. The modelled present-day and palaeotemperatures were calibrated against measured BHTs, % Ro,  $T_{max}$ , AFTA, and thermal conductivities. Predicted maturity is based on Lawrence Livermore National Laboratory (LLNL) vitrinite kinetics.

Figure 10.15a shows the calibration of the maturity model and compares measured with calculated temperatures and maturity, whereas Figure 10.15b shows the burial and maturation history and the timing of cooling events. The AFTA temperature from one core sample (498.35 – 499.05 m) in Woodleigh 2A is from the Gibson et al. (2000) study of onshore Carnarvon Basin wells, and indicates one palaeothermal episode, with the onset of cooling some time between the earliest Jurassic (206 Ma) and early Tertiary (60 Ma), but with three different likely possibilities for its magnitude and timing (Fig. 10.13). This palaeothermal episode encompasses Jurassic and Early Cretaceous, regional thermal-episodes recognized from the previous AFTA study (Gibson et al., 1998; Ghori, 1999). The AFTA data did not require a discrete second thermal episode, but the vitrinite reflectance value from the Birdrong Sandstone indicates a higher palaeotemperature than present day, and thus suggests an additional cooling event during the late Tertiary, consistent with the Tertiary regional thermal-episode. Maturity modelling, as constrained by vitrinite reflectance and AFTA data, implies that about 500–700 m may have been eroded from the top of the Jurassic during the first cooling event and 300–400 m from the top of the Cretaceous during the latter cooling event. The geothermal history modelling indicates that the Woodleigh and older formations are marginally mature (0.5 – 0.7% Ro) and are within the initial stages of the oil-generative window.

## Conclusions

TOC, Rock-Eval, PGC, GC-MS, and organic petrology indicated that the Cretaceous Birdrong Sandstone has fair hydrocarbon-generating potential, but is immature for oil generation.

The Jurassic Woodleigh Formation was deposited in a highly reducing, lacustrine environment and has excellent oil-generating potential, but is immature in relation to the oil-generative window.

Clasts from the Silurian Coburn Formation within the unnamed breccia have good oil- and gas-generating potential and lie within the initial stages of the oil-generative window.

The present-day geothermal gradient of the Woodleigh area is at least 3.5°C/100 m.

AFTA and vitrinite reflectance data indicate at least one discrete palaeothermal episode and cooling some time between the Jurassic and early Tertiary (206–60 Ma); a time interval that encompasses regional Jurassic and Early Cretaceous palaeothermal episodes. Vitrinite reflectance data indicate higher palaeotemperatures than at present for the Cretaceous, and indirectly suggest a palaeothermal episode during the Tertiary.

Geothermal history modelling indicates that in Woodleigh 2A the Cretaceous and Jurassic formations are immature, whereas the Silurian Coburn Formation is marginally mature for oil generation. Modelling also suggests that two cooling events may be related to the erosion of about 500–700 m between the preserved Woodleigh Formation and overlying Cretaceous section, and 300–400 m from the top of the preserved Cretaceous section.

## References

- GHORI, K. A. R., 1999, Silurian–Devonian petroleum source-rock potential and thermal history, Carnarvon Basin, Western Australia: Western Australia Geological Survey, Report 72, 88p.
- GIBSON, H. J., MARSHALLSEA, S. J., and WATSON, P. G. F., 1998, Thermal history reconstruction in Carnarvon Basin wells: Barrabiddy 1A, Yaringa East 1, Coburn 1 and an outcrop sample using apatite fission track analysis and vitrinite reflectance; Geotrack International Pty Ltd (Geotrack), Report 670: Western Australia Geological Survey, Statutory petroleum exploration report, S31321 A1 (unpublished).
- GIBSON, H. J., O'BRIEN, C., and WATSON, P. G., 2000, Thermal history reconstruction in Carnarvon Basin wells Candace 1, Pendock 1, Wandagee 1, Woodleigh 2A and Echo Bluff 1 using apatite fission track analysis and vitrinite reflectance; Geotrack International Pty Ltd (Geotrack), Report 764: Western Australia Geological Survey, Statutory petroleum exploration report, S31450 A1 (unpublished).
- GREEN, P. F., DUDDY, I. R., GLEADOW, A. J. W., TINGATE, P. R., and LASLETT, G. M., 1986, Thermal annealing of fission tracks in apatite, 1. A quantitative description: *Chemical Geology (Isotope Geoscience Section)*, v. 59, p. 237–253.



## Appendix 11

### Core analyses

#### Permeability, porosity, and density measurements

Porosity and permeability measurements were made on 17 samples from Woodleigh 2A: nine core samples from the Woodleigh Formation, five from the unnamed paraconglomerate, one from the unnamed breccia, and two from the Coburn Formation. Helium porosity and air and Klinkenberg (liquid equivalent) permeabilities were determined for each core sample at a confining pressure of 1000 psi (Core Laboratories, 1999).

The core samples of the Woodleigh Formation had porosities up to 24.7% (average 18.7%) and Klinkenberg permeabilities up to 71.7 mD (average 15.4 mD). In the unnamed breccia, core porosities range up to 22.5% (average 19.7%) with Klinkenberg permeabilities ranging up to 15.4 mD (average 4.5 mD). The core sample from the unnamed breccia had a porosity of 24.6% and a Klinkenberg permeability 0.197 mD. In the Coburn Formation, the two core porosities are 8.0 and 13.9%, with corresponding Klinkenberg permeabilities of 0.241 and 7.94 mD (Table 11.1).

Bulk density measurements were also made on eight gneiss and granite core samples from Woodleigh 1 as an aid to gravity modelling. Approximate porosities were calculated of up to 8% (average 5.6%; Table 11.2).

**Table 11.1. Core porosity and permeability, Woodleigh 2A**

GSWA number	Corelab sample number	Depth (m)	800psi NOB pressure		Porosity (%)	Grain density (g/cc)	Dry density (g/cc)
			Kinf (mD)	Kair (mD)			
149180	1	292.80	4.36	5.41	22.9	2.64	2.04
149181	2	317.10	0.003	0.006	4.2	2.68	2.57
149182	3	347.75	22.7	25.4	24.7	2.64	1.99
149183	4	387.25	66.7	71.7	24.2	2.63	1.99
149184	5	421.90	14.1	15.4	13.5	2.67	2.31
149185	6	456.95	0.042	0.094	22.5	2.68	2.08
149186	7	472.35	0.124	0.206	12.6	2.67	2.33
149187	8	496.05	0.198	0.350	21.0	2.65	2.09
149188	9	500.95	17.1	19.8	22.8	2.64	2.04
149189	10	521.95	13.3	15.4	22.5	2.63	2.04
149190	11	529.95	1.58	2.21	19.6	2.63	2.11
149191	12	544.05	1.14	1.67	19.7	2.63	2.11
149192	13	563.15	1.37	1.98	18.5	2.63	2.14
149193	14	582.50	0.894	1.38	18.1	2.63	2.15
149194	15	589.00	0.104 <sup>(a)</sup>	0.197 <sup>(a)</sup>	24.6	2.83	2.13
149195	16	608.25	6.90	7.94	13.9	2.84	2.45
149196	17	617.75	0.185	0.241	8.0	2.87	2.64

**NOTES:** (a) This permeability was determined by probe permeametry and predominantly reflects the permeability of the matrix. The sample was extremely vuggy. Permeability determined on the entire plug by steady-state flow through varied between 800 and 1300 mD depending on the direction of flow

Kinf: Klinkenberg permeability  
Kair: Permeability to air

Table 11.2. Density measurements, Woodleigh 1 and 2A

<i>Depth (m)</i>	<i>Dry density (g/cc)</i>	<i>Water-saturated density (g/cc)</i>	<i>Lithology</i>	<i>Calculated porosity (%)</i>
<b>Woodleigh 1</b>				
192.1	2.43	2.45	granitoid	2
201.3	2.39	2.45	granitoid	6
225.9	2.34	2.42	granitoid	8
245.4	2.47	2.52	granitoid	5
266.7	2.72	2.76	biotite gneiss	4
289.3	2.46	2.52	granitoid	6
311.9	2.45	2.52	granitoid	7
333.0	2.43	2.50	granitoid	7
<b>Woodleigh 2A</b>				
289.00	1.90	–	siltstone <sup>(a)</sup>	–
292.80	2.04	2.26	sandstone	–
317.10	2.57	2.61	sandstone	–
326.85	1.98	–	siltstone <sup>(a)</sup>	–
347.75	1.99	2.24	sandstone	–
387.25	1.99	2.24	sandstone	–
421.90	2.31	2.44	sandstone	–
456.95	2.08	2.30	sandstone	–
457.90	2.13	–	siltstone <sup>(a)</sup>	–
472.35	2.33	2.48	sandstone	–
486.00	1.99	–	siltstone <sup>(a)</sup>	–
496.05	2.09	2.30	sandstone	–
500.95	2.04	2.27	sandstone	–
521.95	2.04	2.26	diamictite	–
529.95	2.11	2.31	diamictite	–
544.05	2.11	2.31	diamictite	–
563.15	2.14	2.33	diamictite	–
582.50	2.15	2.34	diamictite	–
589.00	2.13	2.38	dolomite breccia	–
608.25	2.45	2.58	dolomite	–
617.75	2.64	2.72	dolomite (gypsiferous)	–

NOTE: (a) siltstone samples disintegrated in water after several hours

## Core gamma

Core gamma was run on the intervals 498–505 m (basal Woodleigh Formation) and 582–595 m (basal unnamed paraconglomerate to unnamed breccia) to precisely locate the high-gamma zones seen on the down-hole log at 502 m and 585–590 m. The high-gamma zone at 502 m probably corresponds to a zone of fragments that do not fit together marked on the core at 501.4 m. Ground core at 502.9, 504.7, 504.8, 504.9, and 505.0 m indicate recovery problems over this interval. By comparison, recovery over the interval 582–595 m was good and the wireline gamma peaks at 585.5 and 589.5 m correspond to zones at 587.0 and 591.0 m as marked on the core, indicating a 1.5 m discrepancy (Fig. 11.1; Table 11.3).

Spectral core gamma was run over the highest core-gamma intervals 502.50 – 503.50 and 590.0 – 590.9 m (Fig. 11.1; Table 11.4).

Table 11.3. Core gamma, Woodleigh 2A, 498–506 m and 582–595 m

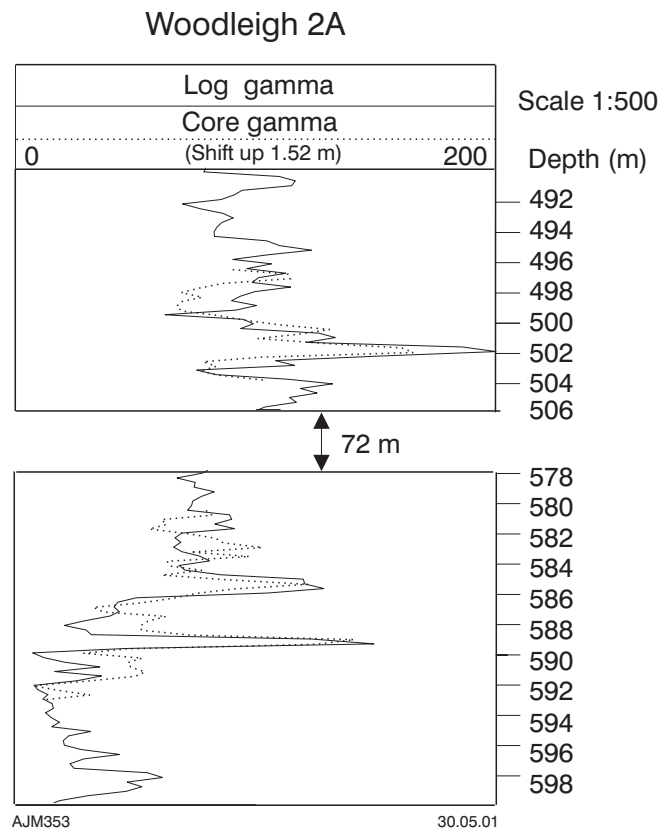
Depth (m)	Gamma (API)	Depth (m)	Gamma (API)	Depth (m)	Gamma (API)	Depth (m)	Gamma (API)
498.00	73.01	501.54	85.8	505.08	74.11	585.00	77.89
498.06	83.93	501.60	92.25	505.14	74.11	585.06	100.11
498.12	92.91	501.66	94.89	505.20	76.49	585.12	96.26
498.18	98.94	501.72	113.06	505.26	95.48	585.18	94.64
498.24	87.09	501.78	111.11	505.32	74.7	585.24	99
498.30	72.42	501.84	123.11	505.38	98.84	585.30	97.89
498.36	98.25	501.90	106.33	505.44	98.84	585.36	89.36
498.42	118.53	501.96	94.89	505.50	108.16	585.42	68.61
498.48	127.8	502.02	106.81	505.56	108.16	585.48	77.41
498.54	123.11	502.08	117.94	582.00	74.6	585.54	68.61
498.60	128.87	502.14	133.62	582.06	68.19	585.60	58.24
498.66	117.52	502.20	143.07	582.12	80.33	585.66	57
498.72	120.04	502.26	133.08	582.18	90.43	585.72	58.66
498.78	111.61	502.32	139.69	582.24	78.88	585.78	62.04
498.84	108.22	502.38	125.1	582.30	85.79	585.84	70.41
498.90	103.05	502.44	107.68	582.36	83.78	585.90	76.92
498.96	100.97	502.50	96.83	582.42	85.79	585.96	87.81
499.02	83.91	502.56	96.14	582.48	80.33	586.02	83.26
499.08	61.09	502.62	88.92	582.54	66.41	586.08	93.57
499.14	77.16	502.68	99.53	582.60	64.66	586.14	85.78
499.20	70.67	502.74	110.55	582.66	61.21	586.20	62.04
499.26	88.99	502.80	101.59	582.72	50.99	586.26	53.35
499.32	77.76	502.86	96.83	582.78	57.02	586.32	54.55
499.38	74.18	502.92	98.18	582.84	60.78	586.38	66.83
499.44	74.77	502.98	135.25	582.90	60.37	586.44	68.16
499.50	80.2	503.04	152.4	582.96	72.74	586.50	87.3
499.56	80.8	503.10	148.86	583.02	60.78	586.56	101.22
499.62	68.93	503.16	157.23	583.08	59.1	586.62	85.27
499.68	56.25	503.22	162.17	583.14	53.77	586.68	81.28
499.74	68.35	503.28	171.73	583.20	52.17	586.74	77.41
499.80	82.67	503.34	175.67	583.26	60.78	586.80	92.5
499.86	85.17	503.40	149.44	583.32	61.64	586.86	105.21
499.92	89.64	503.46	158.44	583.38	58.27	586.92	119.88
499.98	78.37	503.52	177.01	583.44	51.38	586.98	125.87
500.04	64.97	503.58	154.2	583.50	72.74	587.04	121.99
500.10	64.97	503.64	160.29	583.56	72.74	587.10	124.57
500.16	68.35	503.70	176.34	583.62	73.19	587.16	117.37
500.22	73.59	503.76	143.65	583.68	74.6	587.22	110.48
500.28	70.08	503.82	142.51	583.74	69.54	587.28	90.93
500.34	63.85	503.88	113.47	583.80	84.79	587.34	71.33
500.40	64.41	503.94	94.81	583.86	83.78	587.40	72.24
500.46	73.59	504.00	91.52	583.92	82.8	587.46	65.5
500.52	75.96	504.06	90.21	583.98	77.43	587.52	70.41
500.58	80.8	504.12	98.84	584.04	78.88	587.58	70.41
500.64	74.77	504.18	90.21	584.10	83.29	587.64	76.92
500.70	52.57	504.24	80.74	584.16	82.3	587.70	80.79
500.76	72.41	504.30	65.47	584.22	83.78	587.76	71.79
500.82	69.5	504.36	71.18	584.28	83.29	587.82	72.71
500.88	67.8	504.42	81.36	584.34	89.88	587.88	68.61
500.94	68.35	504.48	96.14	584.40	99	587.94	56.22
501.00	63.29	504.54	92.82	584.46	108.7	588.00	61.22
501.06	69.5	504.60	81.36	584.52	85.78	588.06	59.95
501.12	72.41	504.66	73.52	584.58	94.64	588.12	41.54
501.18	81.43	504.72	75.9	584.64	104.06	588.18	48.67
501.24	88.99	504.78	75.29	584.70	97.35	588.24	41.9
501.30	86.44	504.84	81.98	584.76	91.45	588.30	57.04
501.36	90.94	504.90	77.7	584.82	86.78	588.36	59.54
501.42	98.24	504.96	78.91	584.88	70.41	588.42	37.94
501.48	95.55	505.02	75.9	584.94	59.5	588.48	26.45

Table 11.3. (continued)

Depth (m)	Gamma (API)	Depth (m)	Gamma (API)	Depth (m)	Gamma (API)	Depth (m)	Gamma (API)
588.54	20.49	590.16	59.12	591.78	34.34	593.40	30.61
588.60	15.41	590.22	59.12	591.84	27.32	593.46	29.29
588.66	27.42	590.28	58.28	591.90	36.43	593.52	17.96
588.72	31.05	590.34	68.65	591.96	40.33	593.58	16.48
588.78	38.65	590.40	86.82	592.02	41.43	593.64	0.05
588.84	37.94	590.46	98.48	592.08	49.33	593.70	4.2
588.90	35.13	590.52	120.33	592.14	37.83	593.76	14.72
588.96	53.39	590.58	130.78	592.20	49.72	593.82	15.02
589.02	70.45	590.64	135.79	592.26	56.12	593.88	18.56
589.08	64.67	590.70	146.28	592.32	51.3	593.94	19.78
589.14	66.87	590.76	146.76	592.38	39.97	594.00	17.96
589.20	61.22	590.82	147.75	592.44	47.8	594.06	20.38
589.26	64.67	590.88	156.38	592.50	55.7	594.12	17.37
589.32	64.23	590.94	134.87	592.56	50.11	594.18	19.78
589.38	59.12	591.00	120.33	592.62	56.53	594.24	24.75
589.44	51.39	591.06	94.68	592.68	54.48	594.30	37.49
589.50	52.2	591.12	78.41	592.74	54.08	594.36	37.83
589.56	51.8	591.18	54.19	592.80	55.7	594.42	30.95
589.62	52.99	591.24	32.74	592.86	54.08	594.48	33.31
589.68	51.39	591.30	50.22	592.92	42.53	594.54	21.92
589.74	55.81	591.36	38.29	592.98	57.76	594.60	20.38
589.80	52.99	591.42	42.27	593.04	65	594.66	17.37
589.86	51.39	591.48	37.23	593.10	56.93	594.72	5.79
589.92	51.8	591.54	28.62	593.16	35.37	594.78	4.72
589.98	38.29	591.60	34.34	593.22	24.75		
590.04	46.37	591.66	28.62	593.28	30.95		
590.10	51.8	591.72	32.3	593.34	42.17		

Table 11.4. Spectral core gamma, Woodleigh 2A,  
502.50 – 503.50 m and  
590.0 – 590.9 m

Depth (m)	Total equiv. U (ppm)	K (%)	Th (ppm)
502.50	25	22	33
502.60	34	27	41
502.70	31	35	34
502.80	29	28	37
502.90	30	31	43
503.10	34	31	39
503.20	37	38	51
503.30	35	40	47
503.40	36	37	38
503.50	32	36	51
590.0	51	32	58
590.1	38	23	50
590.2	36	31	46
590.3	37	34	55
590.4	39	30	43
590.5	40	34	55
590.6	44	30	63
590.7	60	45	81
590.8	39	25	59
590.9	44	30	65



**Figure 11.1.** Comparison of core gamma (dashed line) and downhole gamma logs between 480 and 600 m in Woodleigh 2A. The two logs have been depth matched by shifting the core gamma up by 1.5 m

## Reference

CORE LABORATORIES, 1999, Routine core analysis, well Woodleigh no. 2A, Western Australia: Western Australia Geological Survey, Statutory petroleum exploration report, S20566 A1 (unpublished).



## Appendix 12

# Palaeomagnetism

by P. W. Schmidt  
(CSIRO Exploration and Mining)

## Introduction

Initially, five granitoid samples from Woodleigh 1 were sent to the Commonwealth Scientific and Industrial Research Organisation (CSIRO) Rock Magnetism Laboratory in June 2000 to determine if any lithologies were suitable for a palaeomagnetic study to constrain the age of the Woodleigh impact structure. The felsic samples (255.5, 230.25, 309.3, and 332.3 m) were found to be extremely weakly magnetic and the remanence present was not stable, and could easily be attributed to the drilling process. However, the one mafic sample from 197.2 m proved to retain a reverse remanent magnetization, which was resistant to alternating field demagnetization, implying that the remanence may be quite ancient, and perhaps dating from the time of impact. Before undertaking a fuller investigation, more mafic samples from around that depth were investigated to ensure that the first sample had not been inadvertently marked upside-down or inverted in the core tray. In August 2000, the presence of a reverse remanence component was confirmed from a further five samples from 194.85, 196.2, 196.6, 197.2, and 197.6 m. This indicated a fuller study could provide a palaeolatitude for the impact event, thereby allowing the age of the event to be estimated from the calibrated apparent polar wander path for Australia.

## Methods and procedures

Standard palaeomagnetic procedures (Collinson, 1983) were followed throughout this study. As the core samples could not be oriented azimuthally, only the inclinations are meaningful.

The cores were subsampled in the laboratory to yield one or two specimens approximately 25 mm in diameter and 20 mm high. In total, 25 specimens were processed. Magnetic susceptibilities were measured using the instrument described by Ridley and Brown (1980). Magnetic remanence was measured using a 2G 755R cryogenic magnetometer.

Specimens were subjected to both thermal and alternating field demagnetization. Alternating field demagnetization is most effective at removing drilling-induced magnetization and was carried out using the built-in 2G AF demagnetization system. Thermal demagnetization was carried out using the CSIRO three-stage carousel furnace, which is housed inside multiple Helmholtz coils fitted with automatic feed-back to compensate for stray fields due to diurnal changes and vehicular traffic.

## Units

The convention of expressing magnetic survey measurements in induction units clearly complicates calculations of the Koenigsberger ratio ( $Q$ ) in SI units. For this reason, most rock magnetic properties are still expressed in centimetre-gram-second (cgs) units:

- Susceptibility ( $k$ ): the cgs unit is Gauss/Oersted (G/Oe) and all susceptibilities here are given in  $\mu\text{G/Oe}$ , i.e.  $\times 10^{-6}$  G/Oe. As in SI, this is dimensionless but 1 cgs unit is greater than a SI unit by a factor of  $4\pi$ , i.e.  $k_{\text{cgs}} = 4\pi \times k_{\text{SI}}$  (cf. 1" = 25.4 mm).
- Remanent magnetization: the cgs unit of the intensity of magnetization is the Gauss (G), which is also commonly given as electromagnetic units per cubic centimetre ( $\text{emu/cm}^3$ ). In SI, the unit of magnetization is the ampere/metre ( $\text{Am}^{-1}$ ), which is equivalent to  $10^{-3}$  G,

i.e.  $1 \text{ Am}^{-1} = 10^{-3} \text{ G} = 10^{-3} \text{ emu/cm}^3$ . Some commercial modelling packages avoid using remanent magnetization units by making use of  $Q$ . The appealing simplicity of this approach is deceptive though, since calculating  $Q$  requires familiarity with magnetization units.

- $Q$  is a measure of the relative importance of remanent magnetization compared to induced magnetization, and as such is fundamental to the interpretation of magnetic surveys in terms of the magnetic properties of rocks. The ratio  $Q$  is calculated by dividing the natural remanent magnetization (NRM) intensity by the induced magnetization intensity. The induced magnetization is given by multiplying the susceptibility by the magnetizing field — in this case, the magnetizing field is the geomagnetic field,  $55\,000 \text{ nT} = 0.55 \text{ Oe}$ . It is emphasized that the SI value of  $55\,000 \text{ nT}$  is magnetic induction, or flux density, and the equivalent SI magnetic field value, in vacuo, is equal to  $43.8 \text{ Am}^{-1}$ .

In cgs units,  $Q$  is simply derived by dividing the cgs remanent magnetization by the cgs induced magnetization:  $0.85 \mu\text{G} / (36.6 \mu\text{G} / \text{Oe} \times 0.55 \text{ Oe}) = 0.042$ . However, in SI units this calculation must be performed after first converting magnetic induction (measured in Tesla) to units of magnetic field (measured in  $\text{Am}^{-1}$ ), and expressing NRM and susceptibility in SI units. As an example, again using the results from Woodleigh 1, the NRM intensity becomes  $0.85 \times 10^{-3} \text{ Am}^{-1}$ , susceptibility becomes  $4\pi \times 36.6 \times 10^{-6} = 0.00046 \text{ SI}$ , and the field is given by the induction in nT divided by the magnetic permeability of free space ( $\mu_0$ ) or  $55\,000 / (4\pi \times 10^{-7}) = 43.8 \text{ Am}^{-1}$ . Thus  $Q_{\text{SI}} = 0.00085 / (0.00046 \times 43.8) = 0.042 = Q_{\text{cgs}}$ .

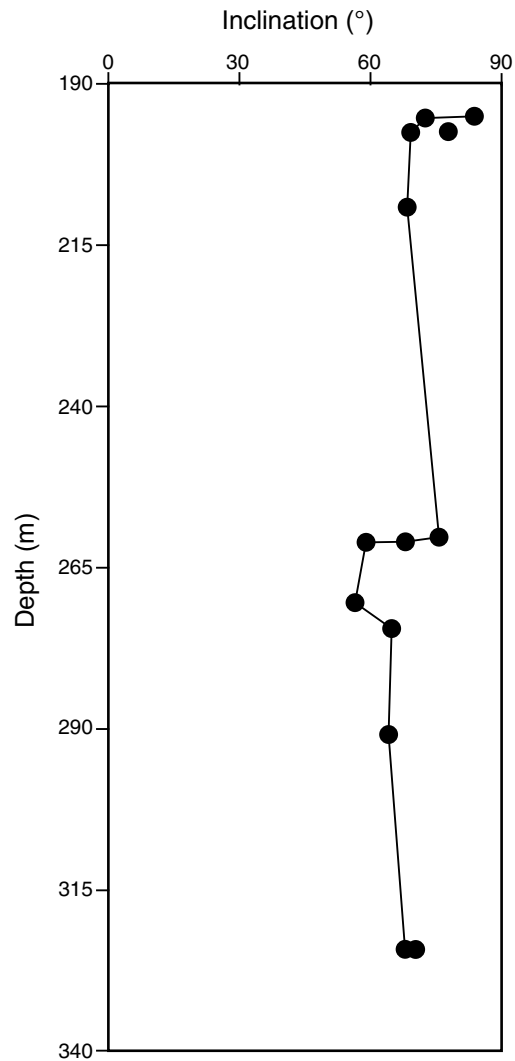
## Results

The intensity of natural remanent magnetization for these samples is very weak at  $0.085 \pm 0.18 \text{ Jgamma}$  (ranging for  $0.001 \text{ Jgamma}$  to  $0.77 \text{ Jgamma}$  —  $0.01 \text{ mAm}^{-1}$  to  $7.7 \text{ mAm}^{-1}$  in SI). Magnetic susceptibility is also low at  $36.6 \pm 2.7 \mu\text{G/Oe}$  ( $460 \mu\text{SI}$ ). Therefore,  $Q$  for these rocks is very low (0.042), and would not be expected to show a magnetic anomaly reflecting remanent magnetization.

Following magnetic cleaning, 15 specimens were found to retain a stable reverse polarity remanence. As only the magnetic inclination is meaningful, the statistical analysis of the data was performed using techniques developed especially for ‘inclination-only’ data (see Enkin and Watson, 1996, for a full discussion). The inclinations versus depth from Table 12.1 are plotted in Figure 12.1. The mean inclination assuming a Gaussian distribution is  $70.2^\circ \pm 3.7^\circ$ , as compared with  $70.0^\circ +5.6^\circ / -4.5^\circ$  using an iterative numerical estimate. The errors are 95% confidence limits. The latter estimate is preferred even though the confidence limits are greater.

**Table 12.1. Cleaned palaeomagnetic inclinations versus depth for mafic lithologies from Woodleigh 1**

<i>Depth (m)</i>	<i>Inclination (°)</i>
195	71.9
195	83.4
196.6	68.8
197.05	77.4
197.5	68.6
197.5	69.3
209.2	68.5
260.45	75.6
261.2	67.9
261.2	58.4
270.7	56.4
274.4	65.1
291.2	64.2
324.6	68.2
324.6	70.4

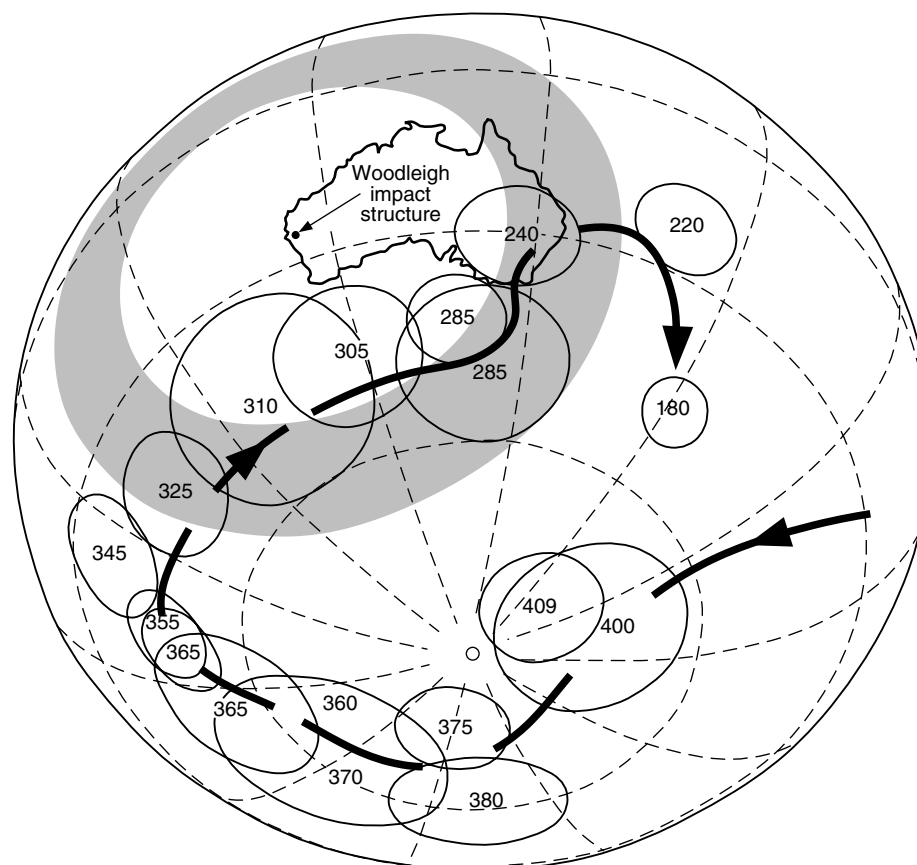


AJM327

23.03.01

**Figure 12.1. Cleaned palaeomagnetic inclinations versus depth for mafic lithologies from Woodleigh 1**

Assuming that the magnetic remanence dates from the time of impact, the palaeo-inclination estimate translates to a palaeolatitude band for the Woodleigh impact structure of 48°S to 63°S. This is shown in Figure 12.2 where selected poles from Schmidt and Clark (2000) have been plotted to compare with the palaeolatitude band shown in bold. Poles and their 95% confidence ovals ranging in age from 425 to 180 Ma are shown. The age of the Woodleigh impact structure accords best with poles from 325 to 240 Ma. However, the polarity of the geomagnetic field was continuously reversed from about 318 Ma until 265 Ma (see Opdyke et al. (2000) for lower boundary, and Gallet et al. (2000) for the upper boundary). Therefore, the palaeomagnetic data favour an age in this range. However, the field is also known to have been reversed at various times during the Early Triassic, so it is not possible to emphatically rule out an Early Triassic age.



AJM328

30.05.01

**Figure 12.2. Selected mid-Palaeozoic to Early Mesozoic poles from Australia. The circles centred on the Woodleigh impact structure represent 95% confidence limits on the palaeomagnetic pole position calculated from 'inclination-only' data**

A tilt of  $5\text{--}303^\circ$  TN (estimated by Iasky et al., 2001) of the region superficially appears to add to the uncertainty of the palaeomagnetic age. However, the effect of such a tilt on the estimation of inclination (Inc.) depends on the declination (Dec.), which is not known here because the core samples were not azimuthally oriented. Therefore, it is instructive to consider what the tilting effect may be for various notional declinations. For the oldest age estimates ( $\sim 320$  Ma), a declination of about  $230^\circ$  is implied. Correcting the direction of Dec. =  $230^\circ$ , Inc. =  $+70^\circ$  for the  $5^\circ$  tilt to  $303^\circ$  yields a direction of Dec. =  $241^\circ$ , Inc. =  $+66^\circ$ . The corresponding pole is moved to the northwest more or less along the permissible palaeolatitude band (Fig. 12.2), that is, the effect is mainly on the declination. For this part of the pole path, the effect is therefore inconsequential. For the younger ages of 280–240 Ma, a similar analysis shows that the palaeolatitude band is also pushed to the northwest by about  $10^\circ$ . The overall effect then, would be to anchor the 325 Ma end of the band shown in Figure 12.2, but move the younger end to the northwest. Such a 'tilt' corrected band agrees better with known poles than the 'untilted' band. The tilt would move the band further away from the Late Triassic and Jurassic poles, however, and would have no substantial effect on the palaeomagnetic age limits.

## Conclusions

Preliminary palaeomagnetic investigations of a range of material from Woodleigh 1 identified biotite–hornblende granitoid that, although very weakly magnetic and not oriented azimuthally, appears to retain an ancient magnetic remanence of reverse polarity. A fuller palaeomagnetic investigation has confirmed the reverse remanence and, if a direct consequence of the Woodleigh impact structure, implies the age of impact was between 318 and 265 Ma (mid-Carboniferous to early Late Permian).

## References

- COLLINSON, D. W., 1983, *Methods in rock magnetism and palaeomagnetism*: London, Chapman and Hall, 503p.
- ENKIN, R. J., and WATSON, G. S., 1996, Statistical analysis of palaeomagnetic inclination data: *International Geophysical Journal*, v. 126, p. 495–504.
- GALLET, Y., KRYSTYN, L., BESSE, J., SAIDI, A., and RICO, L.-E., 2000, New constraints on the Upper Permian and Lower Triassic geomagnetic polarity timescale from the Abadeh section (central Iran): *Journal of Geophysical Research*, v. 105B2, p. 2805–2815.
- IASKY, R. P., MORY, A. J., and BLUNDELL, K. B., 2001, The geophysical interpretation of the Woodleigh impact structure, Southern Carnarvon Basin, Western Australia: Western Australia Geological Survey, Report 79, 41p.
- OPDYKE, N. D., ROBERTS, J., CLAOUÉ-LONG, J., IRVING, E., and JONES, P. J., 2000, Base of the Kiaman: Its definition and global stratigraphic significance: *Geological Society of America, Bulletin* 112, p. 1315–1341.
- RIDLEY, B. H., and BROWN, H. E., 1980, The transformer bridge and magnetic susceptibility measurements: *Australian Society of Exploration Geophysics, Bulletin*, v. 11, p. 110–114.
- SCHMIDT, P. W., and CLARK, D. A., 2000, Paleomagnetism, apparent polar-wander path, and paleolatitude, *in* Billion-year earth history of Australia and neighbours in Gondwanaland *edited by* J. J. VEEVERS: Sydney, GEMOC Press, Macquarie University, p. 12–17.



## Appendix 13

### Well index sheets

<b>ORGANIZATION:</b> Geological Survey of Western Australia <b>WELL:</b> GSWA Woodleigh 1 <b>SPUDED:</b> 9 March 1999 <b>COMPLETED:</b> 15 March 1999 <b>TD:</b> 333.1 m <b>STATUS:</b> Abandoned			<b>S no.:</b> 20565 <b>TYPE:</b> Stratigraphic
<b>BASIN:</b> Southern Carnarvon Basin <b>SUB-BASIN:</b> Gascoyne <b>ELEV. GL:</b> 108 m AHD <b>LAT.:</b> 26°03'19.3"S; <b>LONG:</b> 114°39'56.3"E <b>NORTHING:</b> 71116095; <b>EASTING:</b> 266452 (MGA Zone 50)			
FORMATION	TOPS (m)		LITHOLOGICAL SUMMARY
	DRILL	SUBSEA	
Alluvium	Surface	+108	Light-brown, fine- to coarse-grained sand; granules, pebbles
Toolonga Calcilutite	17	+91	Pale-yellow to grey, soft marl and calcareous siltstone, fossiliferous, glauconitic
Gearle Siltstone	35	+72	Dark-grey to black siltstone, pyritic, soft
Windalia Radiolarite	60	+48	Dark-grey siltstone, hard; bedded chert
Muderong Shale	79	+24	Medium- to dark-grey shale
Birdrong Sandstone	92	+16	Medium-grey, fine- to coarse-grained sandstone with minor glauconite, minor carbonaceous siltstone
Granitoid and gneiss	171	63	Granite gneiss, brecciated, impact shocked, and with pseudotachylite veinlets
<b>CORES</b>	Continuously cored:		NQ: 190.5 – 333.1 m (97.9% recovery)
<b>LOGS</b>	Gamma ray-temperature-caliper from Woodleigh 1981/1: Gamma and density:		1–92 m 2 – 187.5 m
<b>CASING</b>	HW (OD 114.3 mm, ID 101.6 mm): HQ (OD 88.9 mm, ID 77.8 mm): HQ casing pulled out before abandonment		0–26 m (left by Layton and Associates) 0 – 190.5 m

<b>ORGANIZATION:</b> Geological Survey of Western Australia <b>WELL:</b> GSWA Woodleigh 2 <b>SPUDED:</b> 16 March 1999 <b>COMPLETED:</b> 20 March 1999 <b>TD:</b> 198 m <b>STATUS:</b> Abandoned			<b>S no.:</b> 20566 <b>TYPE:</b> Stratigraphic
<b>BASIN:</b> Carnarvon Basin <b>SUB-BASIN:</b> Gascoyne Platform <b>ELEV. GL:</b> 67 m AHD <b>LAT.:</b> 26°03'28"S; <b>LONG:</b> 114°31'34"E <b>NORTHING:</b> 7115587; <b>EASTING:</b> 252493 (MGA Zone 50)			
FORMATION	TOPS (m)		LITHOLOGICAL SUMMARY
	DRILL	SUBSEA	
Alluvium	Surface	+67	Light-brown, fine- to coarse-grained sand; granules, pebbles
Toolonga Calcilutite	14	+53	Pale-yellow to grey, soft marl and calcareous siltstone, fossiliferous, glauconitic
Gearle Siltstone	79	12	Dark-grey to black siltstone, pyritic, soft
Windalia Radiolarite	106	39	Dark-grey siltstone, hard; bedded chert
Muderong Shale	134	67	Medium- to dark-grey shale
Birdrong Sandstone	148	81	Medium-grey, fine- to coarse-grained sandstone, minor glauconite
<b>CORES</b>	Continuously cored:		NQ: 192–198 m (46% recovery)
<b>LOGS</b>	None		
<b>CASING</b>	NQ: HQ (OD 88.9 mm, ID 77.8 mm): Casing pulled out before abandonment		0–193 m 0 – 190.5 m

<b>ORGANIZATION:</b> Geological Survey of Western Australia <b>WELL:</b> GSWA Woodleigh 2A <b>SPUDED:</b> 21 March 1999 <b>COMPLETED:</b> 28 March 1999 <b>TD:</b> 618.3 m <b>STATUS:</b> Abandoned			<b>S no.:</b> 20566 <b>TYPE:</b> Stratigraphic
<b>BASIN:</b> Carnarvon Basin <b>SUB-BASIN:</b> Gascoyne Platform <b>ELEV. GL:</b> 67 m AHD <b>LAT.:</b> 26°03'28"S; <b>LONG:</b> 114°31'33"E <b>NORTHING:</b> 7115587; <b>EASTING:</b> 252468 (MGA Zone 50)			
FORMATION	TOPS (m)		LITHOLOGICAL SUMMARY
	DRILL	SUBSEA	
Alluvium	Surface	+67	Light-brown, fine- to coarse-grained sand; granules, pebbles
Toolonga Calcilutite	14	+53	Pale-yellow to grey, soft marl and calcareous siltstone, fossiliferous, glauconitic
Gearle Siltstone	79	12	Dark-grey to black siltstone, pyritic, soft
Windalia Radiolarite	106	39	Dark-grey siltstone, hard; bedded chert
Muderong Shale	134	67	Medium- to dark-grey shale
Birdrong Sandstone	148	81	Medium-grey, fine- to coarse-grained sandstone, minor glauconite, carbonaceous siltstone
Woolleigh Formation	223	166	Laminated siltstone and mudstone interbedded with fine-grained silty sandstone, woody material common
Unnamed paraconglomerate	521.3	454.3	Massive, red to pink, oxidized, medium- to fine-grained sandstone supporting subangular to rounded clasts of sandstone, minor granite, and siltstone
Unnamed breccia	587.2	520.2	Dolomite and siltstone breccia
Coburn Formation	600.85	533.85	Light-grey dolostone, with skeletal debris and ooids, gypsiferous, gypsum veins, and beds
<b>CORES</b>	Continuously cored:		NQ: 270 – 618.3 m (91.2% recovery)
<b>LOGS</b>	Gamma-density: Gamma-neutron-neutron-caliper:		2–612 m 2–612 m
<b>CASING</b>	HQ (OD 88.9 mm, ID 77.8 mm): Casing pulled out to 130 m before abandonment		0–270 m





